MULTIVALENT MONOCLONAL ANTIBODIES AS IMPROVED CANCER THERAPIES:

PROOF-OF-CONCEPT AND MECHANISTIC STUDIES USING RITUXIMAB-LIPID NANOPARTICLES

by

Jesse Popov

B.Sc., B.Mus., The University of Western Ontario, 2004

A THESIS SUBMITTED IN PARTIAL FULFILLMENT OF
THE REQUIREMENTS FOR THE DEGREE OF

DOCTOR OF PHILOSOPHY

in

THE FACULTY OF GRADUATE STUDIES
(Interdisciplinary Oncology)

THE UNIVERSITY OF BRITISH COLUMBIA
(Vancouver)

March 2012

Abstract

This body of work describes a novel methodology for discovering and developing new cancer drugs based on therapeutic monoclonal antibodies. Such antibodies generally contain two sites where they bind to their target, but interesting improvements are often observed when the valence (number of target-binding sites) is increased above two. The methodology outlined in this dissertation involves using liposomes to prepare multivalent antibody-lipid nanoparticle formulations of different valence that can be utilized for preclinical drug development.

As a proof-of-concept, we applied the methodology to rituximab, a therapeutic antibody used to treat lymphomas and leukemias. For the same dose of rituximab, multivalent rituximab-lipid nanoparticles with valences up to ~250 showed significantly elevated anticancer activity from enhanced complement-dependent cytotoxicity, antibody-dependent cell-mediated cytotoxicity, and direct induction of apoptosis. A valence-dependent improvement in apoptosis in lymphoma cells was observed up to levels that were 21-fold higher than those observed after treatment with bivalent rituximab.

We subsequently employed the different valences of multivalent rituximab to investigate its poorly defined direct mechanism of action. We uncovered a novel mechanism consisting of upregulation and activation of CD120a which led to ensuing apoptosis. Effector cells of the immune system were capable of hypercrosslinking rituximab on lymphoma cells and reproducing this mechanism, suggesting that it contributes to the *in vivo* cytotoxicity of regular bivalent rituximab therapy.

The methodology described in this dissertation can therefore serve to identify antibodies that are more active as multivalent rather than bivalent molecules, define the optimal valence of such antibodies, and elucidate the mechanism of action of the new multivalent drugs. Furthermore, we illustrate that this information applies to other types of constructs with similar valences, enabling use of the methodology for advancing both liposomal and non-liposomal multivalent antibody formulations to preclinical maturity.

Finally, this work suggests that every therapeutic antibody may have a different valence where it shows optimal therapeutic activity. For example, antibodies directed against targets that exert therapeutic effects upon clustering may show maximum activity at valences above two. This methodology can easily be applied to other antibodies in an effort to develop superior therapies against nearly any type of cancer.

Preface

A version of Chapter 2 has been published [Popov J, Kapanen AI, Turner C, Ng R, Tucker C, Chiu G, Klasa R, Bally MB, Chikh G. Multivalent rituximab lipid nanoparticles as improved lymphoma therapies: Indirect mechanisms of action and *in vivo* activity. Nanomedicine 2011 Nov;6(9):1575-91]. I collaborated primarily with Dr. Ghania Chikh for collection of data in this article, and I wrote the manuscript based on a preliminary draft by Dr. Chikh. I obtained the content in Chapters 3–6 independently; I planned and carried out all experiments, performed data analysis, prepared figures, and wrote manuscripts for future publication.

A separate article resulting from collaboration with the laboratory of Dr. Ruth Signorell (Department of Chemistry, University of British Columbia) was also published and referenced in this dissertation [Weiss A, Preston TC, Popov J, Li Q, Wu S, Chou KC, Burt HM, Bally MB, Signorell R. Selective recognition of rituximab-functionalized gold nanoparticles by lymphoma cells studied with 3D imaging. J Phys Chem C 2009 Oct 21;113(47):20252-8].

All experiments involving the use of animals were completed in accordance with the current guidelines of the Canadian Council of Animal Care. The University of British Columbia Animal Care Committee reviewed and approved certificate numbers A05-1582 and A06-1537 for the animal studies carried out in Chapter 2 (*in vivo* efficacy of rituximab and rituximab-lipid nanoparticles, and pharmacokinetics of rituximab-lipid nanoparticles).

This document is written using United States English spelling.

Table of Contents

List of Tables

List of Figures

List of Abbreviations

2^{o}Ab	secondary antibody
[^{3}H]CHE	[^{3}H]cholesteryl hexadecyl ether
A###-τ	Alexa Fluor ###-labeled antibody against antigen τ e.g. A647-CD120a = Alexa Fluor 647 labeled anti-CD120a antibody
Ab	antibody
ADCC	antibody-dependent cell-mediated cytotoxicity
AF	ammonium ferrothiocyanate
AFC	7-amino-4-trifluoromethyl coumarin
BB	binding buffer
BCA	bicinchoninic acid
CBQCA	3-(4-carboxybenzoyl)quinoline-2-carboxaldehyde
CDC	complement-dependent cytotoxicity
CFSE	carboxyfluorescein diacetate succinimidyl ester
Chol	cholesterol
CLL	chronic lymphocytic leukemia
CTX	cholera toxin B subunit
D649	DyLight 649
DISC	death-inducing signaling complex
DLBCL	diffuse large B-cell lymphoma
DMSO	dimethyl sulfoxide
DR	detergent resistance
DSPC	1,2-distearoyl-*sn*-glycero-3-phosphocholine
DSPE-PEG	1,2-distearoyl-*sn*-glycero-3-phosphoethanolamine-*N*-[methoxy(polyethylene glycol)-2000]
DSPE-PEG-biotin	1,2-distearoyl-*sn*-glycero-3-phosphoethanolamine-*N*-[biotinyl(polyethylene glycol)-2000]
DSPE-PEG-Mal	1,2-distearoyl-*sn*-glycero-3-phosphoethanolamine-*N*-[maleimide(polyethylene glycol)-2000]
DTT	dithiothreitol
EB	elution buffer
EDTA	ethylene diamine tetraacetic acid
ELISA	enzyme-linked immunosorbent assay
FAM	carboxyfluorescein
FcγR	IgG Fc receptor
FcεRI	IgE Fc receptor I
FITC	fluorescein isothiocyanate
FL	follicular lymphoma
FLICA	fluorescent inhibitor of caspase
FMK	fluoromethyl ketone
FSC	forward scatter
HABA	4-hydroxyazobenzene-2-carboxylic acid
HEPES	2-[4-(2-hydroxyethyl)piperazin-1-yl]ethanesulfonic acid
HBS	HEPES buffered saline
HMG-CoA	3-hydroxy-3-methylglutaryl coenzyme A
IgE/IgG	immunoglobulin E/immunoglobulin G
IL	interleukin
IP	intraperitoneally

IV	intravenous/intravenously
LNP	lipid nanoparticle
Luc	luciferase
LV	lentivirus
Mal	maleimide
MCL	mantle cell lymphoma
MS	microsphere
Neut	NeutrAvidin
NHL	non-Hodgkin's lymphoma
NHS-PEG-biotin	*N*-Hydroxysuccinimide ester-dPEG$_4$-biotin
NIMAC	nickel immobilized metal affinity chromatography
NK	natural killer
NP	nanoparticle
PBMC	peripheral blood mononuclear cell
PBS	phosphate buffered saline
PE	phycoerythrin
PEG	polyethylene glycol
PI	propidium iodide
Prz	pertuzumab
QLS	quasi-elastic light scattering
Rtx	rituximab
Rtx-LNP(α)	rituximab-lipid nanoparticle of valence α
ROI	region of interest
SB	stripping buffer
SC	subcutaneous/subcutaneously
SCID	severe combined immunodeficiency
SD	standard deviation
SPDP	N-Succinimidyl 3-(2-pyridyldithio)propionate
SSC	side scatter
SUV	small unilamellar vesicle
TNFα	tumor necrosis factor α
TNFR	tumor necrosis factor receptor
TRAPS	TNFR-associated periodic syndrome
Trz	trastuzumab
TX100	Triton X-100
wrt	with respect to

Acknowledgements

I would like to offer my gratitude to my supervisor, Dr. Marcel Bally, for his support and guidance in my graduate studies, and for encouraging my growth as a scientist. I would also like to acknowledge the other members of my supervisory committee, Dr. Pieter Cullis and Dr. I. Robert Nabi for their scientific direction.

I would like to give special thanks to the members of the Department of Experimental Therapeutics at the British Columbia Cancer Research Centre, both the laboratory and administrative groups, who provided assistance and encouragement with my work. I would also like to thank the Interdisciplinary Oncology Program (College for Interdisciplinary Studies), who provided support as well as financial assistance in the form of travel awards.

I would also like to thank Dr. Gert Storm, my supervisor during a six-month work term at the Utrecht Institute for Pharmaceutical Sciences at Utrecht University, The Netherlands. Some data found in Chapter 4 was obtained during this time, including confocal laser-scanning fluorescence microscopy images which were obtained at the Center for Cellular Imaging in the Faculty of Veterinary Medicine, and I would like to thank Dr. Richard Wubboltz and Esther van 't Veld for help and technical advice.

I would also like to acknowledge the generous financial support from the following sources:

- Canadian Institutes of Health Research
- Michael Smith Foundation for Health Research
- British Columbia Innovation Council
- Natural Sciences and Engineering Research Council

Finally, a heartfelt thank you to my friends, family, and partner Sébastien for their love, encouragement, and enduring support.

To my father

1 Introduction: Developing novel therapies for treating cancer

1.1 Overview

The goal of the work presented in this dissertation is to create new drug technologies for the treatment of cancer. It involves a novel methodology for discovering and developing new treatments based on therapeutic monoclonal antibodies (Abs), a class of drugs that hold great promise in cancer treatment[1, 2]. The methodology makes use of a drug formulation based on liposomes, a type of lipid nanoparticle (LNP) that normally serves to enhance the delivery of an encapsulated chemotherapeutic drug to the site of disease and therefore increase its efficacy[3]. One common way to further improve this favorable targeting effect is by attaching tumor-specific proteins or peptides to the liposome surface[4-6]. We generated such Ab-LNP constructs by attaching several copies of the therapeutic Abs rituximab (Rtx) or trastuzumab (Trz) to the exterior surface of the liposome, with the exception that the liposome interior was devoid of chemotherapy. Strikingly, these Ab-LNPs exhibited much higher efficacy *in vitro* and *in vivo* than Ab or bare liposomes alone[7].

Given the absence of encapsulated drug, the mechanism by which Ab-LNPs exert their effects is distinct from the changes in drug pharmacokinetics and biodistribution normally attributed to liposomal formulations[3, 8]. Because of this entirely abnormal behavior, the mechanism of action of these promising Ab-LNP constructs was completely elusive, but the mechanism of action is a critical element for further preclinical and clinical development of such drug technologies. The work presented in this dissertation began with efforts to uncover the unique mechanism of action of these constructs. The outcomes were not only the uncovering of a novel mechanism of action explaining the enhanced efficacy of Rtx-LNPs and Rtx itself, but also the creation of a novel methodology with clear potential in the pharmaceutical industry for discovering, studying, and developing new cancer treatments based on therapeutic monoclonal Abs.

1.2 Liposomal formulations

1.2.1 Liposomes in cancer treatment

Liposomes are nanometer-scale particles made up of one or more hydrophobic lipid bilayers that enclose an internal aqueous compartment. There are currently four approved liposomal formulations for the treatment of cancer, and at least 14 in Phase I clinical trials or later stages of development[9]. In cancer treatment, liposomes are traditionally used as drug delivery vehicles, where a chemotherapeutic agent is encapsulated within the liposome and the drug-liposome complex accumulates at the tumor site[8]. The main mechanism by which this occurs is the enhanced permeability and retention effect, also referred to as passive targeting. It results from the passage of liposomes through tumor vasculature, which unlike normal vasculature, is permeable to liposomes and macromolecules. Because tumors exhibit poor lymphatic drainage, liposomes subsequently accumulate at the site of the tumor[10]. Compared to administration of the same dose of free drug, concentrations of drug at the tumor site can be 10-fold or higher[3]. Such enhanced delivery to target cell populations at the site of disease, without an associated increase in toxicity, is instrumental in achieving therapeutic improvement of the encapsulated drug[8].

As a method to further refine the specificity of targeting, the attachment of target-specific proteins or peptides to the drug carrier surface has received considerable attention[4-6]. This results in active targeting of the liposome and its contents to the tumor site. The targeting protein is most commonly a tumor-specific Ab, and such constructs are therefore termed immunoliposomes. Abs are selected on the basis of their ability to bind to target molecules at the disease site; when these Abs are coupled to liposomes containing chemotherapy, liposome targeting is regularly enhanced[6, 11, 12]. It has been shown, however, that the chemical modification of the protein required for conjugation to liposomes impairs the function of the Ab[13-15]. With the advent of monoclonal Abs such as Rtx and Trz (Section 1.3), the targeting Ab itself can exhibit a therapeutic response in

addition to encapsulated drug (Section 1.3). Surprisingly, previous work from our laboratory using "empty immunoliposomes" containing a therapeutic Ab (rather than simply a targeting Ab) indicated that coupling the Ab to the liposome actually *benefited* its therapeutic activity[7]. These special constructs have been termed Ab-LNPs.

1.2.2 What are Ab-LNPs?

Ab-LNPs consist of many therapeutic Ab molecules tethered to the outer surface of a small unilamellar vesicle (SUV), creating a construct with a diameter of approximately 130 nm. An SUV is a type of liposome that contains one lipid bilayer surrounding an aqueous interior, and in the current application, the bilayer contains a mixture of phospholipids, cholesterol (Chol), and polyethylene glycol (PEG) (see Section 2.3.2 and Chapter 3 for more detail)[16, 17]. The PEG serves specifically to block the binding of plasma proteins to the Ab-LNPs; in the absence of PEG, such binding results in uptake by the reticuloendothelial system and results in significantly decreased circulation lifetime of the formulation[18, 19].

Ab-LNPs employ liposomes strictly as scaffolds to bridge many Ab molecules together, which is distinct from the traditional use of liposomes, which actively or passively target an encapsulated drug. In fact, due to the lack of encapsulated drug, the advantages normally associated with liposomal formulations discussed in Section 1.2.1 (improvements in pharmacokinetics and biodistribution of an encapsulated drug) are not applicable to Ab-LNPs[3, 8]. In order to emphasize this distinction in liposome function and mechanism of action, the term "Ab-LNP" is employed rather than other terms such as "liposomal antibody" or "empty immunoliposome."

Previous studies from our laboratory made use of Ab-LNPs prepared with two different therapeutic Abs, Rtx and Trz[7]. As shown in **Figure 1.1**, these studies demonstrated that even though cells were given the same dose of Rtx or Trz, the Abs exhibited significantly higher activities against different cancer cell lines when the Abs were attached to the liposome as Ab-LNPs.

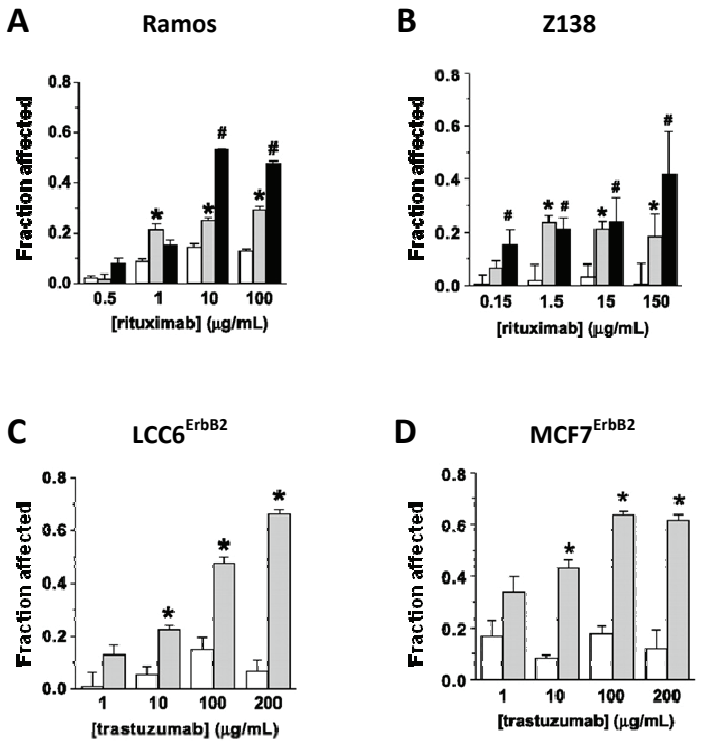

Figure 1.1 Ab-LNPs exhibit enhanced therapeutic responses *in vitro* compared to equal doses of Ab[†].

(A & B) Two different lymphoma cell lines (Ramos and Z138) were treated for 3 days with Rtx (*white columns*), Rtx-LNP (*gray columns*), or Rtx and a crosslinking secondary Ab (2^{o}Ab) (*black columns*). **(C & D)** Two different breast cancer cell lines ($LCC6^{ErbB2}$ and $MCF7^{ErbB2}$) were treated for 5 days with Trz (*white columns*) or Trz-LNP (*gray columns*) in the presence of heregulin. "Fraction affected" was calculated by determining the fraction of remaining viable cells using the 3-(4,5-dimethylthiazol-2-yl)-2,5-diphenyltetrazolium bromide assay, and subtracting this value from 1. *Columns*: mean of three independent experiments; *bars*: standard error; $*p < 0.05$, $^{\#}p < 0.05$, compared with the free Ab treatment.

The *in vivo* efficacy and pharmacokinetics of Trz-LNPs were also examined to determine if these favorable effects were observed *in vivo*. As shown in **Figure 1.2**, the *in vivo* efficacy of Trz-LNP was shown to be significantly higher than that of Trz. The pharmacokinetics of Trz-LNP were also studied and compared to those of Trz; as shown in **Table 1.1**, Trz-LNP exhibited significantly elevated Trz plasma levels after 24 h compared to free Trz, as well as enhanced tumor localization of Trz, explaining the increased efficacy that was observed[7].

[†]Adapted and reprinted by permission from the American Association for Cancer Research: Chiu, G.N.C. *et al.*, Modulation of Cancer Cell Survival Pathways Using Multivalent Liposomal Therapeutic Antibody Constructs, Molecular Cancer Therapeutics, 2007, vol. 6(3), 844–55.

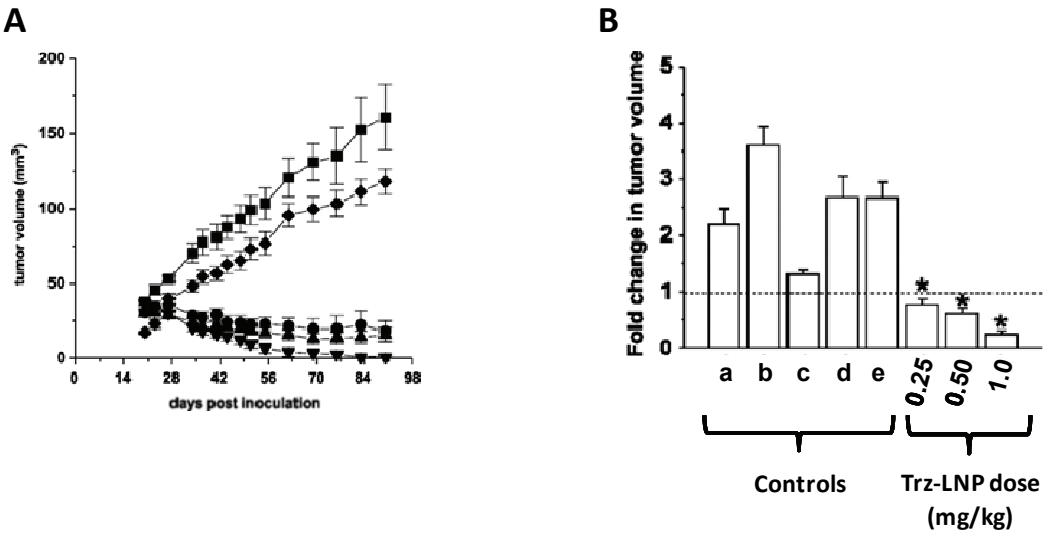

Figure 1.2 Trz-LNP exhibits improved *in vivo* efficacy in an LCC6^{ErbB2} breast cancer model compared to Trz†.
(A) *In vivo* efficacy of Trz-LNP in the LCC6^{ErbB2} breast cancer model. Trz-LNP was administered at 0.25 mg/kg (●), 0.5 mg/kg (▲), and 1 mg/kg (▼) IV twice weekly for 5 weeks starting on day 18 after inoculation of tumor cells. Ab-LNP containing an irrelevant Ab (◆) was administered at 1 mg/kg according to the same dosing schedule, and saline (■) was used as the vehicle control. **(B)** Fold-change in tumor volume after 5 weeks of various treatments (controls and Trz-LNP) according to the same dosing schedule. Controls: *a*, saline; *b*, irrelevant Ab; *c*, Trz (1.0 mg/kg); *d*, irrelevant Ab-LNP; *e*, bare liposomes. *$p < 0.05$ compared with Trz. Data represent means obtained from using six mice in each study group. *Bars*: standard error.

This was the first report describing enhanced activity of drugs attached to the outside of liposomes, where the liposomes serve a purely structural role. These studies therefore established that Ab-LNPs exhibited novel therapeutic activity that could not be explained by passive or active targeting of an encapsulated drug, so the improvements in Ab efficacy resulted from an unknown mechanism of action that remained elusive. The complications in understanding this mechanistic puzzle were due, wholly or in part, to the fact that the mechanisms of the therapeutic Abs themselves are not clearly delineated.

Table 1.1 Pharmacokinetic variables and tumor localization of Trz-LNP[†].

Pharmacokinetic comparison[a]:	Trz	Trz-LNP
Plasma levels at 24 h (μg/mL)	2.91 ± 0.13	27.7 ± 1.3
$AUC_{0\text{-}24\ h}$ ($\mu g \cdot h \cdot mL^{-1}$)[b]	88.7	883
Total body clearance ($mL \cdot h^{-1}$)	4.04	0.386
Volume of distribution at steady state (mL)	277	29.7
MRT_{last} (h)	9.64	10.3

Tumor localization[a]:	Control liposome	Trz-LNP
% Injected dose/g tumor at 24 h	3.84 ± 2.4	13.9 ± 3.4

Abbreviations: $AUC_{0\text{-}24\ h}$: Area under the curve from time of dosing (t = 0 h) up to the last measured plasma concentration (t = 24 h); MRT_{last}: Mean residence time, calculated using values up to the last measured plasma concentration (t = 24 h).
[a] For plasma elimination studies, 12 animals were used for each study group, with four animals used for each time point of blood collection (at 1, 4, and 24 h). For tumor localization study, four animals were used for each study group, and tumors were harvested at 24 h.
[b] Noncompartmental analysis based on the linear trapezoidal rule was done using the software WinNonlin version 1.5 to estimate the values of various pharmacokinetic variables.

1.3 Therapeutic monoclonal Abs

Therapeutic monoclonal Abs are a class of drugs that hold great promise in cancer treatment due to their ability to target and kill cancer cells while leaving healthy cells in the body unaffected. This concept of using "magic bullets" to treat disease was proposed as early as 1897 by Paul Ehrlich[20]. It was not until 1975, however, that the development of therapeutic Abs as targeted drugs became possible with the invention of hybridoma technology, allowing for the production of monoclonal Abs of predefined antigen specificity[21]. Monoclonal Abs were thought to be ideal candidates for administration in humans because of their specificity to a single epitope on their corresponding antigen, but early therapeutic Abs were antigenic in humans due to their origins in mice, limiting their clinical potential[22, 23].

Starting in the early 1980s, protein engineering techniques allowed for replacement of mouse regions of the Ab molecules with corresponding regions of human origin, reducing the

mouse-specific immunogenic response when administered in humans. Chimeric Abs refer to Abs with antigen-binding regions coded by genes of mouse origin and constant regions from human genes. Humanized Abs refer to a genetically engineered mouse Ab where the protein sequence has been modified to increase the similarity of the Ab to human Abs[22, 23]. Subsequent technological advances have allowed fully human therapeutic Abs to also be produced[24-26].

The first monoclonal Ab to be approved for use in oncology was Rtx in 1997[27, 28], and over the past decade, the market for therapeutic monoclonal Abs has grown exponentially[29-31]. Over 30 Abs and their derivatives have been approved for use in various indications, including 10 in oncology, and there are hundreds in the late stages of preclinical and clinical development[31]. **Table 1.2** shows a selection of therapeutic monoclonal Abs that are currently approved for use in treating cancer, or at late stages of clinical trials.

Table 1.2 Selected therapeutic monoclonal Abs approved or under development in oncology.

Generic name	Trade name	Target	Ab format	Cancer indication	Status	Refs.
Rituximab (**Rtx**)	Rituxan/Mabthera	CD20	Chimeric IgG1	NHL	Approved	27, 28
Trastuzumab (**Trz**)	Herceptin	ErbB2	Humanized IgG1	Breast	Approved	32, 33
Alemtuzumab	Campath/MabCampath	CD52	Humanized IgG1	CLL	Approved	34
Cetuximab	Erbitux	EGFR	Chimeric IgG1	Colorectal	Approved	35
Bevacizumab	Avastin	VEGFA	Humanized IgG1	Colorectal, breast, lung	Approved	36
Panitumumab	Vectibix	EGFR	Human IgG2	Colorectal	Approved	24
Ofatumumab	Arzerra	CD20	Human IgG1	CLL	Approved	25, 37
Pertuzumab (**Prz**)	Omnitarg	ErbB2	Humanized IgG1	Breast, ovarian	Phase III	38, 39
Veltuzumab	N/A	CD20	Humanized IgG1	NHL, CLL	Phase III	40, 41

Abbreviations: CLL: Chronic lymphocytic leukemia; N/A: Not applicable; NHL: Non-Hodgkin lymphoma.

Even though in humans there are five classes of immunoglobulin (IgM, IgD, IgG, IgA, and IgE) as well as four IgG subclasses (IgG1, IgG2, IgG3, and IgG4), by far most therapeutic Abs are of the IgG1 subtype (Table 1.2). This is because IgG1 exhibits a long half-life in blood (~21 days) and it elicits more favorable indirect mechanisms of action (see Sections 1.4.1 & 1.4.2) compared to the

other Ig classes and subclasses[42]. Cancer patients treated with therapeutic Abs typically need to receive weekly doses of several hundred milligrams over several months to maintain an effective serum concentration of over 10 μg/mL[43]. The 150 kDa Y-shaped structure of IgGs can be divided into two distinct functional units: the fragment of antigen binding (Fab; the v-shaped upper part of the molecule) and the constant fragment (Fc), which are connected at a site called the hinge region. The Fab region contains two identical sites where the Ab (drug) binds its antigen (target), while the Fc region interacts with specific effector cells of the immune system[1]. The Fab and Fc regions each are responsible for different mechanisms of action of therapeutic Abs, as described in Section 1.4.

1.3.1 Rituximab and CD20

Rtx is often heralded as a "blockbuster" Ab given its widespread success in significantly improving the survival statistics for B-cell non-Hodgkin lymphomas (NHLs), as well as other malignancies such as chronic lymphocytic leukemia (CLL) and autoimmune disorders such as rheumatoid arthritis[31, 44]. As opposed to more recently developed Abs, which are often humanized or fully human molecules, Rtx is a chimeric Ab containing a murine variable region attached to a human IgG1 constant region.

The target of Rtx is CD20, a 33 to 37 kD membrane-associated phosphoprotein that is highly expressed on all normal and most malignant B cells, but not other cells in the body, making it an attractive target for B cell-based therapy. CD20 is not detected on embryonic stem or pro-B cells, but is expressed on the surface of mature B cells; expression ceases upon differentiation into plasma cells. The protein spans the plasma membrane four times and there is some evidence that it may function in calcium entry[45, 46]. It has been shown to form tetramers which associate with the B cell antigen receptor in unstimulated cells, and upon antigen binding, CD20 is released and it associates transiently with phosphoproteins and calmodulin-binding proteins, which regulate calcium entry[47].

Most anti-CD20 therapeutic Abs do not internalize upon binding to CD20[40]. Despite its proven success as a target for Ab therapy, the precise function of CD20 is still elusive.

1.4 The mechanisms of action of therapeutic monoclonal Abs

In general, the precise mechanisms of action of therapeutic Abs are not completely clear, and they vary from Ab to Ab. The activity of a given therapeutic Ab is commonly viewed as resulting from a combination of indirect and direct effects that occur after the Ab binds to its target[44]. The indirect and direct mechanisms are mediated by the Fc and Fab regions of the Ab molecule, respectively.

The indirect mechanisms are related to the action of the immune system on target cells that are coated with therapeutic Ab. They involve the interaction of specific cell-surface or plasma proteins with the Fc region of the therapeutic Ab molecule; since the Fc region is common to most therapeutic Abs, it is not surprising that the indirect mechanisms are common to all therapeutic Abs. Specifically, the two indirect mechanisms are known as complement-dependent cytotoxicity (CDC; Section 1.4.1) and Ab-dependent cell-mediated cytotoxicity (ADCC; Section 1.4.2). The Fc region possesses interaction sites for ligands which can induce effector functions, including three structurally homologous cellular IgG Fc receptor types (FcγRI, FcγRII, FcγRIII) as well as the C1q component of the complement[48]. Even though every therapeutic Ab elicits CDC and ADCC, the relative contributions of the two mechanisms vary from one Ab to the next[44, 49, 50].

As opposed to the Fc region-mediated indirect mechanisms, the direct mechanism of action of a therapeutic Ab results from the physical interaction of its two identical Fab regions with the target on the cell surface[48] (Section 1.4.3). The direct mechanism is therefore Ab-specific, and highly variable between different Abs; for example, the direct mechanism of action can result in therapeutic effects such as growth inhibition, chemosensitization, or induction of apoptosis[51].

1.4.1 Complement-dependent cytotoxicity

As part of the innate immune system, complement is one of the main mechanisms of Ab-mediated immunity and is responsible for protecting the host from attack by intruding pathogens. It was first identified as a serum component that "complemented" Abs in order to kill bacteria, but we now know today that it consists of more than 30 proteins found in the plasma and on the surfaces of cells[52, 53]. Activation of complement occurs after distinct events that trigger different protease cascades known as the classical, mannose-binding lectin, and alternative pathways. For example, the classical pathway is activated by the binding of the complement protein C1q to the Fc region of the Ab on the surface of an invading pathogen or on a cancer cell coated with therapeutic Ab. The final result of all three complement pathways is the assembly of a 5–10 nm diameter membrane-attack complex on the foreign cell, which causes cell death by disrupting the plasma membrane[53, 54]. Complement is finely regulated so that it is activated on foreign Ab-coated cells (resulting in their elimination) but not on normal cells[52].

For the induction of strong CDC activity during monoclonal Ab therapy, relatively high expression of target antigen is required in order to attain sufficiently high Ab levels on the tumor-cell surface to initiate CDC. It is also clear that higher amounts of bound C1q to the Fc region of the Ab correlate with elevated levels of CDC[43, 54]. Moreover, given the importance of CDC in the mechanism of action of therapeutic Abs, several strategies have been employed to enhance CDC in new Abs under development, such as amino acid mutations that enhance CDC through improved C1q binding[55, 56]. Another strategy involves shuffling IgG1 and IgG3 sequences within a heavy chain constant region, since IgG3 exhibits superior CDC compared to the other IgG isotypes, while IgG1 exhibits higher ADCC, the other principal indirect mechanism of action[57]. A discussion of CDC relating specifically to Rtx is provided in Section 2.2.1.

1.4.2 Ab-dependent cell-mediated cytotoxicity

ADCC results from the interaction between effector cells of the immune system and a foreign cell coated with Ab. Effector cells contain IgG Fc receptors (FcγRs) that bind to the Fc region of IgG molecules, and they consist of macrophages, natural killer (NK) cells, granulocytes, and other types of leukocytes[43, 58]. FcγRs can be classified as activating or inhibitory; for example, FcγRIa, FcγRIIa, FcγRIIc and FcγRIIIa, are activating receptors, while FcγRIIb is an inhibitory receptor. NK cells and granulocytes contain only activating FcγRs, and are therefore better inducers of ADCC compared to macrophages, which contain both activating and inhibitory FcγRs[54]. When activating FcγRs on effector cells are crosslinked by IgG bound to its target, activation of the effector cell occurs and results in phagocytosis of the target cell or cell lysis through the release of cytotoxic granules by the effector cell[43, 54, 58].

When studied *in vitro*, ADCC resulting from therapeutic Ab treatment can be achieved at Ab concentrations below 10 ng/mL, which is several orders of magnitude lower than the required *in vivo* serum concentrations mentioned in Section 1.3 (ref. 43). This discrepancy results from competition between endogenous human serum IgG and therapeutic Abs for binding to activating FcγR on effector cells (such as FcγRIIIa on NK cells), which leads to the requirement of a significant amount of drug, contributing to the very high costs associated with such therapies[58].

Different Abs against the same target show variable levels of ADCC, and the magnitude of induced ADCC does not correlate with the density of the target on the cell surface, underscoring the complexity of this mechanism of action[59]. Since increased ADCC has been shown to enhance the efficacy of therapeutic Abs, strategies for improving ADCC activity occupy an important role in the development of the next generation of therapeutic Abs[58]. Some approaches include modifications of glycosylation of the Ab that result in enhanced ADCC[58, 60, 61] as well as amino acid mutations that result in enhanced binding to FcγRIIIa[62-64]. Properties relating to the ability of Rtx to induce ADCC are described in further detail in Section 2.2.2.

1.4.3 Direct mechanisms of action of Rtx and other therapeutic Abs

Because the direct mechanism of a therapeutic Ab is highly Ab-specific, it depends on a multitude of factors. These include the molecular biology of the target, the nature of the interaction between Ab and target, and the specific characteristics of the target cell, such as mutation status, target expression levels, and expression of proteins that regulate activation of the target[51]. The direct mechanisms of therapeutic Abs are therefore far less well-defined and more variable than the indirect ones, even when looking at direct mechanisms of different Abs directed against the same target.

One such example is two therapeutic Abs used in the treatment of breast cancer, Trz and pertuzumab (Prz)[32, 65]. Both of these Abs are directed against ErbB2 (also known as Her2 or EGFR2), which is overexpressed in 15-30% of invasive breast carcinomas, and which is predictive of poor prognosis[66]. The ErbB family includes four receptor tyrosine kinases with a common extracellular ligand-binding domain. Upon ligand binding, various homodimers and heterodimers are formed among the four family members, resulting in the activation of intracellular pathways that control survival and cell cycle progression. Dysregulation of this kinase pathway, resulting in constitutive activation, has been shown to regulate tumor growth in a variety of cancers[67].

Trz acts by binding to the extracellular juxtamembrane domain of ErbB2. This causes dimerization of ErbB2 and subsequent internalization and downmodulation of the protein on the tumor surface. Downstream signaling from ErbB2 overexpression therefore ceases, resulting disruption of cell-cycle progression and inhibition of the growth of metastases[68-70]. Prz, on the other hand, binds to an epitope on the extracellular domain of ErbB2 that sterically inhibits the ability of ErbB2 to form ligand-activated dimer complexes. This does not result in downmodulation like with Trz, but instead it causes inhibition of ErbB signaling by disrupting the vast array of different ligand-dependent receptor combinations that exist in the ErbB kinase pathway[71].

Because of the differences in direct mechanisms of action, Trz requires overexpression of ErbB2 on the cell surface in order to have therapeutic activity, and it shows low activity when ErbB2 is not overexpressed. Prz, however, is highly effective at inhibiting tumor growth when ErbB2 is overexpressed or when ErbB2 expression is low[71]. Moreover, the two Abs together have also been shown to show synergistic effects against breast cancer cells *in vitro*[72] and against *in vivo* breast cancer xenografts[73], and the combination exhibited favorable response rates in patients who had progressed following previous Trz therapy[38].

The direct mechanism of action of Rtx involves a different mechanism: it is known to consist of induction of apoptosis in target cells. Generally, in the absence of ADCC and CDC *in vitro*, Rtx exhibits low levels of cytotoxicity in neoplastic cells unless it is crosslinked with a reagent such as an anti-human-IgG secondary Ab (2^{o}Ab). This has been demonstrated with established cell lines[7, 74, 75] as well as primary cells[76]. This direct effect is generally thought to result from clustering of CD20 in the plasma membrane, and since it has been shown to occur in the absence of ADCC or CDC, the direct mechanism also plays a role in the overall mechanism of action of Rtx.

It has been postulated that *in vivo*, such a direct mechanism may occur as a result of FcγR-mediated hypercrosslinking of Rtx by NK cells and other effector cells, since it is known that Rtx and other therapeutic Abs mediate FcγR crosslinking in the induction of ADCC[43, 54, 58]. Such direct effects may be responsible for a substantial proportion of the cytotoxic effects of Rtx therapy, although this has not been definitively shown[77]. Moreover, a direct mechanistic link between Rtx crosslinking and apoptosis has not been established, so it is not understood how crosslinking can result in apoptosis. The crosslinking of therapeutic Abs is further discussed in Section 1.6.

Taken together, the complex nature of the mechanism of action of therapeutic Abs makes it difficult to define features of specific Abs that, upon modulation, would increase or decrease the efficacy of the Ab. Several strategies for improving the activity of therapeutic Abs by increasing CDC

or ADCC were mentioned above, and equivalent strategies can also be employed for enhancing the Ab-specific direct mechanisms of action. In the case of Abs such as Rtx whose direct mechanism consists of induction of apoptosis, methods to enhance levels of apoptosis would have clear benefit in improving these drugs.

1.5 Apoptosis as a target in cancer therapy

Evasion of apoptosis is one of the hallmarks of cancer[78], and a large and promising focus in cancer research involves inducing apoptosis specifically in cancer cells but not in normal cells[79-82]. Apoptosis is the process of programmed cell death, and is conserved across all metazoans; it is necessary under normal physiological conditions at all stages of life. During embryonic development, apoptosis is essential for organogenesis and the formation of multicellular tissues, where it ensures the proper balance of each differentiated cell lineage, and in adult organisms, apoptosis maintains normal cellular homeostasis[83].

In multicellular organisms, the total number of cells is a balance between new cells created through mitosis and cells that die through apoptosis[80]. Different studies have shown that disruptions in this balance due to altered apoptotic signaling can be primary pathogenic events resulting in disease. Accelerated cell death is evident in acute and chronic degenerative diseases, immunodeficiency, and infertility, while insufficient apoptosis can manifest as autoimmunity or cancer[80, 83].

Apoptosis can be contrasted to necrosis, which is traumatic cell death following acute cellular injury such as rupture of the plasma membrane, and which may lead to an inflammatory response. Apoptosis, on the other hand, is a controlled process that leads to characteristic changes in biochemistry and morphology before death. Morphological changes include condensation of the chromatin and DNA fragmentation, reduction of cell volume, cytoskeletal rearrangement, plasma membrane blebbing, and eventual formation of small vesicles known as apoptotic bodies. These

apoptotic bodies are rapidly phagocytosed by macrophages so the dead cell is removed without any inflammatory response[81].

One early biochemical change in apoptosis is the loss of plasma membrane lipid asymmetry. This results in the exposure of phosphatidylserine in the outer leaflet of the plasma membrane, which under normal conditions is present almost exclusively in the inner leaflet[84]. The appearance of phosphatidylserine in the extracellular leaflet can be used to identify cells in early apoptosis using fluorescently-labeled conjugates of Annexin-V, a protein that interacts strongly and specifically with phosphatidylserine. Using appropriate protocols, labeled Annexin-V conjugates can be employed in applications such as flow cytometry and fluorescence microscopy[85].

Apoptosis signaling most often results from activation of the caspases, a family of cysteine proteases that also plays a role in inflammation. To date, 12 human caspases have been discovered, and each is activated by cleavage of its procaspase precursor. Cleavage is often performed by other activated caspases, resulting in different proteolytic cascades[82, 86, 87]. When a cell receives a stimulus to die, caspase signaling begins with the cleavage of one or more specific initiator caspases; this early event corresponds to the loss of plasma membrane asymmetry and appearance of phosphatidylserine in the outer leaflet of the plasma membrane[84, 85]. Specific molecular mechanisms related to the direct induction of apoptosis by Rtx and Rtx-LNP are discussed in greater detail in Sections 5.2 and 6.2.

1.6 Multivalent Abs as improved therapies

1.6.1 Characteristics of multivalent Ab constructs and a definition of valence

As mentioned in Section 1.4.3, Rtx induces low levels of apoptosis in target cells unless it is crosslinked with a 2^{o}Ab[7, 74-76]. The importance of this mechanism *in vivo* was provided by studies showing that cross-linked Rtx induced apoptosis in a dose- and time-dependent manner in freshly

isolated clinical samples of B-CLL cells, in the absence of ADCC and CDC[76]. To make use of this effect *in vivo* is a challenge because clearly, administration of a 2^{o}Ab is not feasible. A different method that has been shown to result in induction of apoptosis is the use of multivalent Rtx constructs[75, 88-90].

The valence of a multivalent ligand is defined as the number of target-binding sites it contains. For example, normal therapeutic Abs are bivalent molecules because they are IgGs (Table 1.2), which contain two identical sites where they bind to their target. Multivalent Ab constructs possess valences of three or higher, and consist of two or more Ab molecules and/or Fab fragments bound together in a stable configuration. In general, the valence of a multivalent Ab prepared using whole IgG will be equal to twice the number of IgG molecules per construct; for example, an IgG dimer produced by chemically crosslinking two IgG molecules has a valence of four. Rtx, as well as a variety of other Abs, have been shown in some cases to be more efficacious as multivalent rather than bivalent constructs (see Section 1.6.3).

Multivalent Abs of low valence (<10) can be Ab or Ab-like molecules produced by protein engineering and/or recombination techniques[89, 91], or can involve coupling Ab or fragments together using crosslinking chemistry with or without molecular scaffolds[92]. Higher valences can achieved by coupling Abs to nanostructures consisting of different types of polymers[93], dendrimers[94, 95], rotaxanes[92], or gold nanoparticles[96]. Regardless of the type of construct, multivalent Abs are able to crosslink their target in the plasma membrane without the need for a crosslinking 2^{o}Ab. When the crosslinking involves more than two proteins being bridged, creating an extensive network of crosslinked target due to the numerous binding sites on the multivalent Ab, the term "hypercrosslinking" is employed.

The increased efficacy of many multivalent Abs is related to the fact that they exhibit different properties compared to their bivalent counterparts. Conversion of Abs into multivalent formats has been shown to result in increased functional affinity toward the cell-surface target,

decreased dissociation rates, enhanced biodistribution, and longer *in vivo* half-life[97, 98]. These characteristics provide the basis for mechanisms of enhancements (or inhibitions) of therapeutic activity that are fundamentally different in the multivalent case compared to the bivalent one[99].

1.6.2 Examples of multivalent interactions in biology and their physical basis

Multivalent interactions are found throughout biology and are necessary for processes such as adhesion of viruses or bacteria to the surface of cells, binding of transcription factors to multiple sites on DNA, and Abs interacting with macrophages and other immune effector cells through their Fc regions[99]. In nature, examples of biological molecules with clustered and repeated epitopes include biopolymers such as polysaccharides, proteoglycans, filamentous proteins, and DNA[100]. Besides Abs, other types of multivalent ligands include carbohydrates, peptides, and small molecules, all of which demonstrate enhanced binding affinity to targeted tissue[15].

A multivalent interaction consists, in theory, of a complex created by an initial univalent interaction where the local concentrations of the remaining free binding sites on both species become greatly enhanced due to their close proximity[15]. Due to this increase in effective ligand and target concentrations, there is a significantly higher probability that subsequent ligand-target interactions will result after the first univalent interaction. This increased probability translates into a higher avidity of the multivalent ligand. Avidity refers to the association constant of a polyvalent interaction, as opposed to affinity, which refers to the association constant of a univalent interaction; avidity is usually greater than the sum of constituent affinities for a multivalent ligand[99, 100].

Kinetic studies have shown that enhanced avidity results from decreases in the rate of dissociation of the multivalent ligand from its target, rather than increases in the rate of association; a greater number of univalent interactions must be broken[99]. While some are being broken, others continue to form, resulting in recapture of the ligand before the ligand-target complex dissociates

completely[100]. From a molecular point of view, the avidity of a multivalent interaction results from the length and flexibility of the linker(s), the strength of the noncovalent forces involved, the number of binding elements, and the conformational freedom of the multivalent construct[101]. On top of an enormous diversity of constructs in terms of the materials employed, significant work has also been described on the configuration, architecture, and spacing of the target-binding sites[102, 103].

The effects of multivalency can result in many biological consequences; for example, multivalent ligands can be strong inhibitors, particularly if they bind to a receptor whose agonistic ligand is monovalent; there is significant therapeutic interest in creating such multivalent ligands[104]. Multivalent interactions can also serve to induce specific geometric shapes in the plasma membrane such as clathrin-coated pits[99]. They may also play a role in the grading of biological responses; for example, macrophages cannot ingest a pathogen based on recognizing a single Ab Fc region with its FcγRs, but more Fc-FcγR associations strengthen the interaction between pathogen and macrophage, increasing the likelihood that the pathogen will be cleared[99].

Interactions between Fc regions on antibody-coated cells with FcγRs in general constitute multivalent interactions; FcγR crosslinking, a multivalent interaction, is required for the initiation of ADCC by NK cells and other types of effector cells (Section 1.4.2). Moreover, initiation of the classical complement cascade requires a multivalent interaction; C1q is a hexavalent ligand and requires binding to many Fc regions of Ab molecules on the surface of a pathogen or cancer cell in order for CDC to result[105, 106] (Section 1.4.1). In cell signaling processes, there are innumerable examples of multivalent ligands that cause receptor activation due to oligomerization. Clustering of the receptor results in signal amplification because many receptors become activated by a single ligand, which creates high local concentrations of activated receptor and which also causes exclusion of negative modulators[107, 108]. For example, tumor necrosis factor α (TNF-α), the ligand to CD120a (Tumor necrosis factor receptor 1 (TNFR1)), is a trivalent ligand that is capable of binding and crosslinking three CD120a molecules; receptor clustering is required for the activation of CD120a

and the subsequent initiation of diverse signaling processes ranging from proliferation to apoptosis (see Section 6.2.1).

Taken together, these descriptions highlight that multivalent interactions are ubiquitous in nature. They also illustrate that even though a univalent and multivalent ligand may share the same target-binding site, they exhibit distinct physiochemical and biochemical properties that can result in remarkably different biological responses.

1.6.3 Descriptions of multivalent Abs that exhibit superior efficacies

Although all therapeutic Abs differ in terms of their direct mechanism of action (Section 1.4.3), the multimerization of many bivalent therapeutic Abs that are approved or under development has been shown to enhance their associated biological responses[7, 74, 89, 109-113]. For example, using two different breast cancer cell lines, one that responds to Trz and one that is Trz-resistant, it was shown that creating multivalent Trz by coupling it to magnetic microspheres resulted in therapeutic effects in both cell lines including the Trz-resistant one[110]. Another example illustrated that multivalent Trz constructs with valences up to four showed significantly higher levels of growth inhibition compared to Trz, and similarly constructed multivalent therapeutic anti-death receptor 5 (DR5) Abs showed equivalent levels of apoptosis to bivalent Ab at doses that were ~100-fold lower[89].

Consistent with the requirement of crosslinking of Rtx in order to induce apoptosis, many many multivalent anti-CD20 designs have been described, including tetravalent Rtx dimers[88], Rtx-dextran polymers (valence ~10) and nanoparticles (NPs) prepared by coupling Rtx to Dynabeads[75], trivalent and tetravalent Rtx constructs obtained through protein engineering[89], Rtx coupled to gold nanoparticles[96], anti-CD20 multivalent branched copolymer-Fab conjugates[15], and hexavalent anti-CD20 created using the Dock-and-Lock method[90]. In general, the multivalent constructs exhibited

superior binding to target cells along with elevated responses *in vitro* and *in vivo*; these responses are described in greater detail in Section 4.2.

One type of multivalent Ab not listed above is Ab-LNPs. In fact, before the experiments described in Section 1.2.2 (ref. 7) were carried out, the use of a liposome as a nanoscale scaffold for creating a multivalent therapeutic Ab had not been considered. This may be surprising in light of the interest surrounding immunoliposomes, but the focus of such work had always been to target encapsulated chemotherapy; the Abs employed therefore possessed targeting properties and not necessarily therapeutic activity (Section 1.2). Since the work in this dissertation began, only one report describing a similar application of liposomes has been published; Oliveira *et al.* describe a situation where anti-EGFR nanobodies coupled to empty liposomes resulted in enhanced anticancer activity through downregulation of EGFR[114]. The work presented herein shows that Ab-LNPs provide a convenient, useful, and promising means for the preclinical discovery and development of liposomal and non-liposomal therapeutic Abs.

1.7 Multivalent Ab-LNPs and the content of this dissertation

The work in this dissertation makes use of the therapeutic Ab Rtx in order to prove the concept that Ab-LNPs are multivalent therapeutic Ab constructs with enhanced activity compared to bivalent Ab. It also sets the groundwork for developing improved multivalent drugs based on other therapeutic Abs. Section 1.2.2 illustrated that the direct mechanism of action of Rtx (induction of apoptosis) is enhanced when cells are treated with equal doses of Rtx-LNP instead of Rtx. Chapter 2 serves to examine how the coupling of Ab to Ab-LNP affects the indirect mechanisms of action (CDC and ADCC), since the improved direct mechanism should not occur at the cost of decreased indirect mechanisms. This chapter also examines the *in vivo* efficacy and pharmacokinetics of Rtx-LNP. Next, to study the direct mechanism of action of Rtx-LNP, it was necessary to prepare many different valences of Rtx-LNP, but the available methods for coupling Abs to liposomes were found

to be unsuitable. Chapter 3 describes a superior methodology that was developed for creating numerous Ab-LNP constructs of different valence from the same Ab. This methodology shows significant improvements in terms of yield of coupled Ab, time required to produce many valences, and reproducibility.

Chapter 4 makes use of the new methodology to prepare many different Rtx-LNP valences in order to examine their novel physiochemical and biological properties. These include binding characteristics as well as improvements in their therapeutic activity in $CD20^+$ lymphoma cells. This chapter establishes a relationship between the valence of a multivalent Rtx-LNP construct and its ability to induce apoptosis. The work in Chapter 5 employs the different valences of Rtx-LNP to uncover a novel molecular mechanism of action of Rtx-LNP that explains its ability to induce apoptosis. This is extended into Chapter 6, where it is shown that conditions involving the interaction of immune effector cells with lymphoma cells coated with bivalent Rtx give rise to the same mechanism, suggesting that it is also a mechanism of action of bivalent Rtx under *in vivo* conditions. This provides compelling evidence of a defined direct mechanism of action of Rtx, which so far has not been described.

Overall, this proof-of-concept serves to illustrate that the methodology described in this dissertation would be invaluable in the development of multivalent therapeutic Abs. Because multivalent Abs show enhanced efficacies over bivalent ones, it is possible that some “discarded” Abs under development (due to low activity as bivalent molecules) may actually show significantly improved activity as multivalent Abs. This methodology can therefore be employed in the context of drug discovery to progress promising multivalent therapeutic Ab formulations to an advanced stage of preclinical development.

2 Indirect mechanisms and *in vivo* activity of multivalent rituximab-lipid nanoparticles‡

2.1 Synopsis

Although creating multivalent Ab-LNPs has been shown to enhance the direct mechanism of action (Section 1.2.2), the effects on the indirect mechanisms of action are unclear. The indirect mechanisms of therapeutic Abs consist of complement-dependent cytotoxicity (CDC; Section 1.4.1) and antibody-dependent cell-mediated cytotoxicity (ADCC; Section 1.4.2). This chapter examines how the indirect mechanisms of Rtx are affected by creating Rtx-LNPs, and it also examines the *in vivo* efficacy and pharmacokinetics of Rtx-LNP.

2.2 Background

2.2.1 Complement-dependent cytotoxicity of Rtx

Rtx activates the classical complement pathway by binding C1q[115], leading to generation of the membrane attack complex and ensuing tumor cell lysis[116]. Rtx has been shown to induce CDC in many different lymphoma cell lines *in vitro*[115, 117] and Rtx has been shown to be effective only in a mouse model expressing a full complement system, while its activity was ablated in C1q-deficient mice[118]. Infusion of Rtx in CLL patients has also been shown to deplete complement, and pre-Rtx complement levels do not return until several weeks after completion of therapy[119]. The complement cascade leading to CDC is regulated by proteins on the lymphoma cell surface such as CD55 and CD59. Blocking CD55 and/or CD59 has been shown to increase levels of CDC in NHL cell

‡ A version of Chapter 2 has been published[16]. Adapted and reprinted by permission from Future Medicine Ltd.

lines and primary cells treated with Rtx, indicating that these two proteins function in the mechanism of action of Rtx as important regulators of CDC[46, 120].

2.2.2 Ab-dependent cell-mediated cytotoxicity of Rtx

ADCC is also an established contributor to the mechanism of action of Rtx and therapeutic Abs in general. On Ab-coated tumor cells, it occurs upon binding of the Fc region of the Ab to activating Fcγ receptors (FcγR) such as FcγRIIIa which are present on effector cells such as natural killer (NK) cells, granulocytes, and macrophages. Rtx has been shown to induce ADCC in many human lymphoma cell lines[117] and ADCC was abolished in nude mice deficient in activating FcγR yet present in the wild-type mice[121], establishing a central role of ADCC in the therapeutic activity of Rtx.

The importance of Rtx-induced ADCC in humans was illustrated in studies on a FcγRIIIa dimorphism that influences the binding affinity of the receptor to Rtx, where enhanced binding corresponds to elevated ADCC. Patients homozygous for the high-affinity dimorphism showed enhanced clinical and molecular responses compared to the other patients[122, 123]. In terms of ADCC-regulating molecules on the tumor cells themselves, expression levels of ligands to NKG2D, a NK cell receptor, influence the susceptibility of the tumor cell to Rtx-induced ADCC[124]. Other molecules present on B cells which trigger NK cell activation include CD40[125], CD80, and CD86[126], but in general, the molecular determinants of whether a tumor cell will elicit ADCC upon Rtx binding are not well understood. Moreover, the relative contributions of CDC and ADCC that occur after Rtx treatment, as well as the relative contribution of the direct mechanism (Section 1.4.3), are unclear and have been shown to depend on the origin of the target cell[44, 49, 50].

2.2.3 Does the creation of Rtx-LNPs affect the indirect mechanisms and *in vivo* properties of Rtx?

We examined how the known indirect mechanisms of action of Rtx are affected by creating Rtx-LNPs. We have previously shown that cells treated with Rtx-LNP exhibit increased levels of apoptosis compared to those treated with equal doses of free Rtx (Section 1.2.2)[7]. These studies established that Rtx-LNP exhibits an improved direct mechanism of action compared to Rtx. The objective of the current study was to establish whether levels of ADCC and CDC are preserved, since under *in vivo* conditions, the favorable direct effects of Rtx-LNP should not occur at the cost of decreased indirect contributions to the efficacy.

To examine differences between Rtx and Rtx-LNPs in terms of their indirect mechanisms of action, we employed two mantle cell lymphoma cell lines, Z138 and JVM2, which exhibited different *in vivo* sensitivities to Rtx along with variable expression levels of cell-surface proteins that regulate ADCC and CDC. Rtx-LNPs were prepared which showed enhanced binding and which induced apoptosis in both cell lines. We demonstrate that multivalent Rtx-LNPs exhibited increased levels of CDC and ADCC compared to Rtx, alongside an increase in NK cell activation levels. Finally, in order to understand the manifestations of these mechanisms of action *in vivo*, we examined the efficacy and pharmacokinetics of Rtx and Rtx-LNP.

2.3 Materials and methods

2.3.1 Reagents and cell lines

The following lipids were obtained from Avanti Polar Lipids (Alabaster AL, USA): 1,2-distearoyl-*sn*-glycero-3-phosphocholine (DSPC), 1,2-distearoyl-*sn*-glycero-3-phosphoethanolamine-*N*-[methoxy(polyethylene glycol)-2000] (DSPE-PEG), and 1,2-distearoyl-*sn*-glycero-3-phosphoethanolamine-*N*-[maleimide(polyethylene glycol)-2000] (DSPE-PEG-Mal). [^{3}H]cholesteryl

hexadecyl ether ([^{3}H]CHE) was from Perkin-Elmer Life Sciences (Woodbridge ON, Canada). Cholesterol (Chol) was purchased from Sigma-Aldrich (St. Louis MO, USA). Pico-Fluor 15 and Pico-Fluor 40 scintillation cocktails were bought from PerkinElmer BioSignal (Montreal QC, Canada). *N*-Succinimidyl 3-(2-pyridyldithio)propionate (SPDP) and dithiothreitol (DTT) were obtained from Pierce/Thermo Fisher Scientific (Rockford IL, USA). Rituximab (Rtx) and trastuzumab (Trz) were obtained from the BC Cancer Agency pharmacy (Vancouver BC, Canada). Matrigel was purchased from Collaborative Biomedical Products Inc. (Chicago IL, USA). Carboxyfluorescein diacetate succinimidyl ester (CFSE) was obtained from Molecular Probes (Eugene OR, USA). Anti-human CD3-FITC, CD56-PE, CD54-APC, and FcγRIII/II (CD16/32) Abs were obtained from BD Biosciences (Mississauga ON, Canada). Anti-Rtx-FITC Ab was purchased from Serotec (Oxford, UK). Rabbit anti-human IgG Fc fragment was purchased from MP Biomedicals (Irvine CA, USA). Lympholyte-Mammal was obtained from Cedarlane (Burlington ON, Canada). Unless otherwise noted, all other reagents were from Sigma-Aldrich (St. Louis MO, USA).

Mantle cell lymphoma (MCL) cell lines Z138 and JVM2 were generously provided by Dr. Zeev Estrov (University of Texas) and previously characterized[127]. Cells were maintained in RPMI 1640 medium (Stem Cell Technologies) supplemented with 2 mM L-glutamine, 10% FBS, and 1% penicillin/streptomycin. All cells were maintained at 37 °C in a humidified atmosphere containing 5% CO_2.

For *in vivo* imaging studies, Z138 cells were transfected to express luciferase (Luc). Constructs for the lentivirus (LV) vector containing the Luc genes were obtained from Dr. Alice Mui (Jack Bell Research Centre, Vancouver General Hospital, Vancouver BC, Canada) who also assisted in the transfection of the cell line. Briefly, the Luc coding sequence was isolated from the pGL-3 vector (Promega, Madison, WI, USA) and cloned into the lentiviral vector FG9 behind the CMV – LTR and UBiC promoters. To generate Luc-expressing lentivirus (LV-Luc), this vector was cotransfected using calcium phosphate with packaging constructs pRSVREV, pMDLg/pRRE, and the VSV-G expression

plasmid pHCMVG into HEK-293T cells. Five million 293T HEK cells were plated on poly-L-lysine-coated tissue culture plates allowed to adhere for 24 hours. The following day, 10 μg of the transducing vector, 7.5 μg of the packaging vector, and 2.5 μg of the VSV envelope pMD.G were co-transfected by LipofectAMINE 2000 (Invitrogen, Burlington ON, Canada), according to the manufacturer's instructions. After 24 h, fresh medium was applied to cells, and cells were cultured for another 24 h. Conditioned medium was then collected and cleared of debris by low speed centrifugation, filtered, and stored at -70 °C. Supernatant was collected daily for 4 days, pooled and ultracentrifuged. The pellet was re-suspended in 500 μL of medium, and aliquots were stored at -70 °C. The Z138 cells were then infected with LV-Luc (25 μL viral supernatant/mL medium). Briefly, one million cells were add to each well of a 12-well plate in 500 μL of complete medium and these were then cultured for 24 h. Subsequently, LV-vector or LV-Luc constructs were added to the medium in the presence of Polybrene (8 μg/mL medium). After approximately 5 h of incubation, the cells were washed with phosphate-buffered saline (PBS, pH 7.4), fresh culture medium was added and cells were incubated for up to 6 days. To enrich for Luc-positive cells, cells were sorted by FACS for GFP expression (cells were cotransfected with LV-GFP constructs). GFP-positive cells were considered to be positive for Luc and this was confirmed by culturing the sorted cells in low concentrations in the wells of a 96-well plate. Luciferin was added to each well and plates were imaged using IVIS (see below) to confirm Luc expression. These Z138-Luc cells were expanded and used for the *in vivo* studies described below.

2.3.2 Preparation of multivalent Ab-LNPs

Small unilamellar vesicles composed of DSPC/Chol/DSPE-PEG/DSPE-PEG-Mal (mole ratio 48:45:5:2) were prepared by the extrusion procedure[128, 129]. A total of 200 μmol lipid were dissolved in $CHCl_3$ and an aliquot of [^{3}H]CHE (0.009 μCi/μmol liposomal lipid) was added. A lipid film was formed by drying the solution first with a stream of N_2 then under vacuum for 3 h. The film was

hydrated in 2.0 mL HEPES-buffered saline (HBS) at 65 ^{o}C for 1 h with stirring, then was subjected to five freeze-thaw cycles each consisting of five-minute treatments in liquid N_2 and a 65 ^{o}C water bath, respectively. The suspension was then extruded ten times through two stacked polycarbonate filters (100 nm and 80 nm pore size) using a Lipex extruder (Northern Lipids, Burnaby BC, Canada). The resulting mean vesicle diameter was 95–110 nm as determined by quasielastic light scattering (QLS) using a Nicomp submicron particle sizer (model 370/270). Liposomal lipid concentrations were measured by liquid scintillation counting with a Packard scintillation counter (model 1900 TR) using aliquots mixed with 5.0 mL Pico-Fluor 15 scintillation fluid.

Rtx was coupled to liposomes according to an established procedure[130]. Briefly, 80 µL of a 12.5 mM solution of SPDP in ethanol were diluted with 920 µL HBS (25 mM HEPES, 150 mM NaCl, pH 7.4) to give a final concentration of 1.0 nmol/µL. The Ab (8 – 9 mg) was reacted with a five-fold molar excess of SPDP for 25 min at room temperature, and was subsequently eluted by gravity through a Sephadex G-50 column equilibrated with sodium acetate buffer (100 mM sodium acetate, 150 mM NaCl, pH 4.5). Fractions containing the Ab were determined by diluting aliquots 50-fold in HBS and by measuring the absorbance at 280 nm. Ab-containing fractions were pooled and added to solid DTT to give a final concentration of 25 mM DTT. This solution was incubated at room temperature for 25 min with stirring. The thiolated Ab was then isolated using a Sephadex G-50 column equilibrated with HBS, and was immediately added to liposomes (10 mM final liposomal lipid concentration). The mixture was incubated at room temperature for 18 h with gentle mixing. At the end of the reaction, the mixture was eluted through a Sepharose CL-4B column equilibrated with HBS to separate the unreacted Ab from the Ab-LNPs. The diameter of the Ab-LNPs was ~130 nm, as determined using QLS. The amount of Ab conjugated to liposomes was determined using the Pierce Micro bicinchoninic acid (BCA) protein assay kit. This quantitation was carried out according to the manufacturer's instructions with 0.5% Triton X-100 added to the reagent solution and using

Ab solutions of known concentration as standards. The number of Ab molecules per liposome was calculated as described previously[7] and was found to be between 38 and 47.

2.3.3 Measurement of cell-surface protein expression levels

A total of 1×10^6 Z138 or JVM2 MCL cells in the exponential growth phase were washed with cold PBS containing 1% FBS, then incubated at 4 ^{o}C for 10 min with anti-FcγRIII/II Ab followed by 20 min with saturating amounts of FITC-labeled anti-human CD20, CD40, CD80, CD86, CD95 (Fas receptor), CD54, CD55 or CD59 Abs. Samples were then washed and analyzed on a FACSCalibur flow cytometer (Becton Dickinson, San Jose, CA) collecting 10,000 events for each sample. Data was analyzed using BD CellQuest software. In this and all subsequent experiments, data values are reported as mean ± standard deviation (SD) unless indicated otherwise. In all cases, two-tailed unpaired Student's *t*-tests were applied with a level of significance of 0.05.

2.3.4 *In vivo* xenograft models to assess Rtx efficacy

All *in vivo* studies were completed using protocols approved by the Animal Care Committee at the University of British Columbia, and were in accordance with the current guidelines of the Canadian Council of Animal Care. To assess response to Rtx treatment, 5×10^6 Z138 or JVM2 cells in the exponential growth phase were mixed with Matrigel to a final volume of 100 µL, then injected subcutaneously (SC) into the flank of male Rag-2M mice. Treatments with Rtx or control (PBS) were initiated when tumors were palpable (0.5 × 0.5 × 0.5 mm), typically 25 to 28 days after cell inoculation. Groups of 6 mice were treated with Rtx (2.5 or 10 mg/kg) given intraperitoneally (IP) every 3 days for a total of 6 treatments (Q3D × 6). Tumor size was measured using a calibrated caliper every 2–3 days.

2.3.5 Quantification of Ab-LNPs bound to cells

Z138 or JVM2 cells (1×10^6) were incubated for 4 h at 4 °C with Rtx, Rtx-LNP or Trz-LNP at different doses as indicated. All treatments were done in triplicate. At the end of the incubation time, cells were washed with cold PBS containing 1% FBS and labeled with anti-Rtx-FITC for 30 min at 4 °C, then analyzed on a FACSCalibur flow cytometer as described above (10,000 events per sample).

A parallel study was performed to measure Ab-LNP binding to cells through quantification of [^{3}H]CHE present in liposomes bound to cells. After the incubation, cells were centrifuged at 300*g* for 5 min at 4 °C, then washed three times with 1 mL of PBS to eliminate unbound Ab-LNP. Washed cells were resuspended and solubilized with 1 mL of 0.9% Triton-X 100 in PBS, and concentrations of [^{3}H]CHE were measured by liquid scintillation counting using Pico-Fluor 40 scintillation cocktail and a Canberra-Packard Scintillation β counter (1900 TR Tri Carb).

2.3.6 Annexin-V/PI flow cytometry-based apoptosis assay

Cells were seeded in 96-well plates (20,000 cells/well) and treatments were added on the same day the cells were seeded. Control treatments consisted of HBS and uncoupled liposomes, negative controls employed Trz instead of Rtx, and positive controls included campothecin-treated samples. For analysis 72 h later, samples were transferred to 1.5 mL Eppendorf tubes and spun at 7000 rpm for 15 s. Supernatants were removed and pellets were washed with 500 µL cold Hanks' balanced salt solution. Samples were spun again at 7000 rpm / 15 s and supernatants were removed. Positive control samples were unstained, stained with Annexin-V-FITC, stained with propidium iodide (PI), or double-stained with both; all other samples were double-stained. For Annexin-V-FITC staining, pellets were resuspended in a mixture of 5 µL Annexin-V-FITC and 40 µL Annexin-V binding buffer and incubated at room temperature for 20 min. For PI staining, 500 µL of a cold 0.5 µg/mL solution of PI in Hanks' were added to the samples. Analysis was performed on a

Becton Dickinson FACSCalibur flow cytometer. Compensation values were set with positive controls and quadrant placement in a plot of PI fluorescence intensity (FL3) versus Annexin-V-FITC fluorescence intensity (FL1) in each case was decided on the basis of data obtained with the negative controls. Early apoptotic cells were defined as PI negative and Annexin-V-FITC positive, necrotic cells were positive for both fluorophores, and viable cells were negative for both.

2.3.7 Assay for measuring levels of complement-dependent cytotoxicity

MCL target cells (1×10^6 cells/mL) were incubated with Rtx, Rtx-LNP or controls (including HBS, uncoupled liposomes, and Trz-NP) for 15 min at 37 °C, then a 25% volume of human serum (50 µL) was added and the sample was further incubated for 4 h. Informed consent was obtained from volunteers who provided the serum. Cells were washed and stained with PI, then analyzed by flow cytometry as described above. Cell lysis due to CDC was expressed as a percentage according to the following: % cell lysis = [1 − (fraction of viable treated cells in the presence of human serum) / (fraction of viable treated cells in the absence of human serum)] × 100%.

2.3.8 Assay for the quantification of Ab-dependent cell-mediated cytotoxicity

A fluorometric method described by Gomez-Roman *et al*. was used[131]. Briefly, 1×10^6 Z138 or JVM2 target cells were double-stained with 2.5 µM PKH26 (a membrane dye) and 2.5 µM CFSE (a viability dye). Cells were then treated with controls (as described in the CDC assay above) or 10 µg/mL of Rtx (either as free Rtx or Rtx-LNP) for 30 min. Next, cells were incubated with mouse splenocytes (at 5:1, 50:1, and 100:1 ratios of effector to target cells) previously stimulated overnight with 25 ng/mL of interleukin-12 (IL-12). After a 24 h incubation, cells were washed in cold PBS containing 1% FBS and resuspended in the same buffer before analysis by flow cytometry, acquiring 10,000 nongated events. Flow cytometry data was acquired by setting FL1 as the CFSE emission channel and FL2 as the PKH26 emission channel. Percent cell kill was obtained by back-gating on the

PKH26^{bright} population of targets and is reported as the percentage of membrane-labeled target cells having lost the viability dye, i.e. % CFSE^{-} within PKH26^{bright}. Non-stained and single-stained targets were included in every experiment to compensate for single-stained CFSE and PKH26 emissions, and double-stained targets incubated with Ab without effectors were used to define spontaneous cell death to exposure to the media and Ab alone. The percentage of cells undergoing ADCC was quantified as follows: % undergoing ADCC = [1 − (fraction of viable double-stained target cells) / (fraction of double-stained untreated control cells)] × 100%.

2.3.9 Quantification of activated natural killer cells

Fresh peripheral blood mononuclear cells (PBMCs; effector cells) were obtained from volunteers who provided informed consent. PBMCs were treated with Lympholyte-Mammal, then incubated with Z138 target cells in a 1:1 ratio, at a final concentration of 1×10^6 effector cells/mL and 1×10^6 target cells/mL. Cultures were treated with 10 μg/mL of Rtx either as: free Rtx, Rtx-LNP, a mixture of free Rtx and unconjugated liposomes, or Trz-LNP (negative control). Treated cells were incubated for 20 h at 37 °C in RPMI 1640 complete medium supplemented with 50 μM β-mercaptoethanol. Several control samples containing effector cells only (without target cells) were also included. After incubation, cells were washed and labeled with anti-human CD3-FITC, CD56-PE and CD54-APC Abs for 30 min at 4 °C before analysis by flow cytometry. Natural killer (NK) cells were identified as the CD3^{-}/CD56^{+} population, and the percentage of CD54^{bright} cells was determined within this population. A total of 50,000 events were collected per sample.

2.3.10 *In vivo* xenograft models for Rtx-LNP efficacy studies

For *in vivo* efficacy studies, female C.B-17 mice with severe combined immunodeficiency (SCID) weighing 20-25 g were inoculated intravenously (IV) with 5×10^6 Z138-Luc cells (see Section 2.3.1). On day 7 after cell inoculation, the presence of tumors was assessed using the IVIS optical

imaging system 200 Series (Xenogen) prior to treatment. At 10 min before imaging, mice were injected IP with 200 µl of 15 mg/mL firefly D-luciferin potassium salt, which emits photons in the presence of oxygen, adenosine triphosphate, and Luc. The animals were imaged and the total photon counts from captured images were quantified using the Living Image software package (version 2.50; Xenogen). A photograph was first obtained in the imaging chamber under dim illumination, then a luminescence image was acquired. The overlay of the pseudocolour images represents the spatial distribution of photon counts produced by active Luc, with red representing the most intense (saturated) luminescence and blue representing the least intense luminescence. Captured images were then quantified using Living Image. Bioluminescent signals from the regions of interest (ROI) expressed in pseudocolour are presented as the cumulative photon counts collected within each ROI. Uninfected animals were imaged to detect background signals. Starting on day 7 after Z138 cell inoculation, treatments consisting of either free Rtx or Rtx-LNP were administered Q3D × 6. Tumor measurements with the IVIS optical imaging system were made twice (early in the study) or once per week. Mice were monitored daily for extended time frames using both qualitative and quantitative health status indicators. When the health status of the animal was considered poor based on a predefined scale, the animals were killed and the following day was recorded as the time of death in order to generate Kaplan-Meier survival curves.

2.3.11 *In vivo* studies on the pharmacokinetics of Rtx-LNP

For studies of liposome and Rtx clearance from the plasma, BALB/c mice (17-19 g) and C.B-17 SCID mice (19-22 g) were injected IV with 5 mg/kg (in 200 µL) free Rtx or Rtx-LNP. At various time points post-injection, blood was collected by cardiac puncture and placed into EDTA-coated microtainer tubes. Plasma was isolated from blood samples by centrifugation at 1000*g* for 15 min. Aliquots of the plasma were used to determine Rtx levels by a colorimetric enzyme-linked immunosorbent assay (ELISA). Briefly, a rabbit anti-human IgG Fc fragment was used for coating and

capturing Rtx. A horseradish peroxidase-conjugated rabbit anti-human whole IgG was used for detection, with orthophenylenediamine added as substrate. To determine the levels of Rtx in plasma, absorbance at 405 nm was measured and compared to values from a standard curve constructed from known amounts of Rtx. For liposomal lipid concentrations, aliquots of plasma were counted in 5 mL of Pico-Fluor 40 scintillation fluid.

2.4 Results

2.4.1 Characterization of Z138 and JVM2 cell lines: surface protein expression levels and *in vivo* response to Rtx treatment

Two human MCL cell lines, JVM2 and Z138, were used in our studies on the indirect mechanisms of action of Rtx and Rtx-LNPs. These cell lines were selected based on previous studies that characterized several MCL cell lines in terms of their expression of the classic features of MCL, namely the t(11;14)(q13;q32) translocation and overexpression of cyclin D1[127]. The Z138 line was found to possess both traits of classic MCL, and while the JVM2 cells retained the translocation, they expressed cyclin D2 and did not overexpress cyclin D1, therefore representing a variant form of the disease[132, 133].

Given these phenotypic differences, the two cell lines were further characterized in terms of select cell-surface proteins involved in the direct and indirect mechanisms of action of Rtx. These molecules consist of the target of Rtx, CD20, as well as a number of proteins known to regulate CDC and ADCC. **Figure 2.1A** shows that while CD20 expression is similar in both cell lines, the JVM2 line expresses significantly higher levels of tumor necrosis factor receptor (TNFR) receptor family receptors (CD95 and CD40), as well as the costimulatory molecules CD80 and CD86 which are necessary for T-cell activation and survival. NK cells are also activated by CD40[125], CD80, and CD86[126]. Levels of CD55 are elevated in Z138 cells, whereas CD59 expression is relatively the same in

both lines; these proteins have been shown to inhibit Rtx-induced CDC[46, 120]. The intercellular adhesion molecule CD54 also shows similar expression in both cell lines. Overall, the differences in phenotype observed suggest that levels of ADCC and CDC may vary between the two cell lines in response to treatment with Rtx and Rtx-LNP[46, 49].

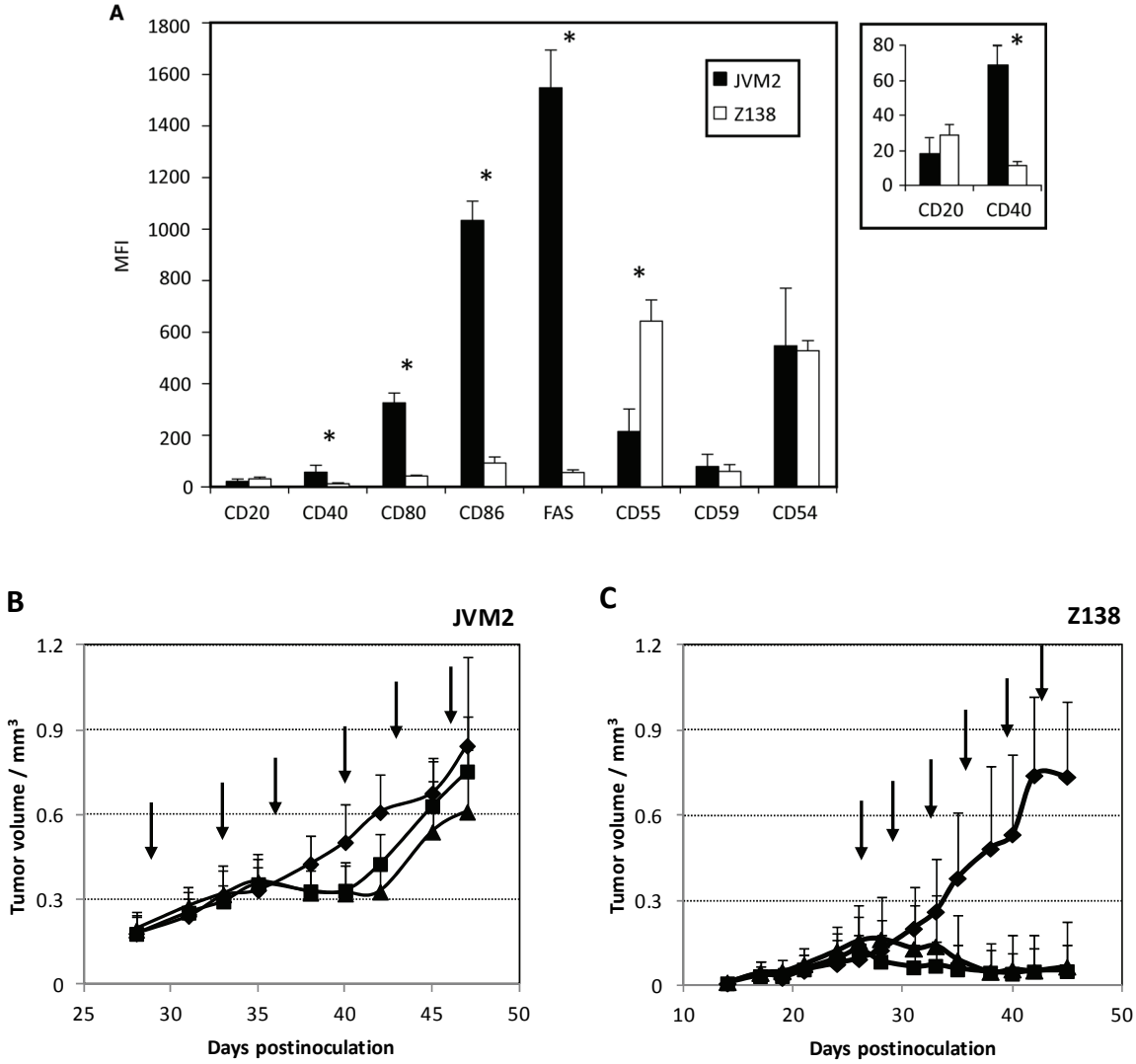

Figure 2.1 Phenotypic characterization of JVM2 and Z138 cell lines and *in vivo* response to Rtx treatment.

(A) Cell-surface marker expression on JVM2 and Z138 cells, assessed by flow cytometry. **p* < 0.05. MFI: mean fluorescence intensity. **(B & C)** To assess *in vivo* responses to treatment with Rtx, 5 × 10^6 JVM2 **(B)** or Z138 **(C)** cells were injected SC into Rag-2M mice. Once the tumors reached ~200 mm^3, mice were treated twice weekly for 3 weeks with either 2.5 mg/kg (■) or 10 mg/kg (▲) Rtx. Control mice (◆) were injected with PBS. Treatments are indicated by arrows. Data correspond to the average metastasis from 6 mice for each time point ± SD and are representative of two separate experiments.

The responses to Rtx treatment of Rag-2M mice inoculated subcutaneously (SC) with JVM2 and Z138 cells were also determined. As shown in **Figure 2.1B**, JVM2 tumors in mice treated with Rtx exhibited an initial growth delay (after day 35 postinoculation), but eventually the tumors progressed in a manner that was comparable to controls. On day 45 after JVM2 cell inoculation, the control animals possessed tumors that were approximately 600 mg in size. The animals treated with 2.5 or 10 mg/kg Rtx exhibited slightly smaller tumors, albeit the differences were not significant. **Figure 2.1C** shows that mice bearing established Z138 tumors were sensitive to treatment with Rtx. Control animals exhibited tumors that were approximately 500 mg in size 40 days after Z138 cell inoculation, while the tumors in mice treated with Rtx (2.5 or 10 mg/kg) were 50% smaller then the tumors measured prior to initiation of treatment. Based on these data, the JVM2 tumors were considered to be Rtx-insensitive and the Z138 tumors were considered Rtx-sensitive.

2.4.2 Rtx-LNPs bind specifically to JVM2 and Z138 cells and induce apoptosis

Multivalent Rtx-LNPs were prepared from bivalent Rtx as described in Section 2.3.2. To examine the behavior of these constructs when tested against the Z138 and JVM2 cell lines, cells were treated with Rtx and Rtx-LNP and the levels of bound Rtx were determined using flow cytometry. The results, summarized in **Figure 2.2A & B**, indicate that 4.9 and 3.2 times more Rtx became bound to JVM2 and Z138 cells, respectively, when added as multivalent Rtx-LNP compared with free Rtx at a dose of 100 μg/mL. Comparable increases in binding were also observed at lower Rtx doses, and these data agree with the general observation that multivalent constructs exhibit increased functional affinity and decreased dissociation rates when bound to cell-surface antigens[97]. Surprisingly, even though both cell lines had similar levels of CD20 expression (Figure 2.1A), JVM2 cells had the ability to bind more Rtx and Rtx-LNP. At doses of 25 μg/mL and above, the mean fluorescence intensities for both Rtx and Rtx-LNP in Figure 2.2A are between 1.8- and 2.5-fold higher than those of Figure 2.2B ($p < 0.05$ for all equivalent treatments). Using non-exchangeable

[^{3}H]cholesteryl hexadecyl ether ([^{3}H]CHE) incorporated in the liposomes as an alternative means to assess cell binding, the amount of bound lipid following addition of Rtx-LNP was approximately two-fold greater for JVM2 cells compared to Z138 cells ($p < 0.05$; data not shown). JVM2-derived tumors were less sensitive to Rtx treatment although they bound more Ab than Z138 cells, again suggesting that the JVM2 cells are more resistant to Rtx therapy.

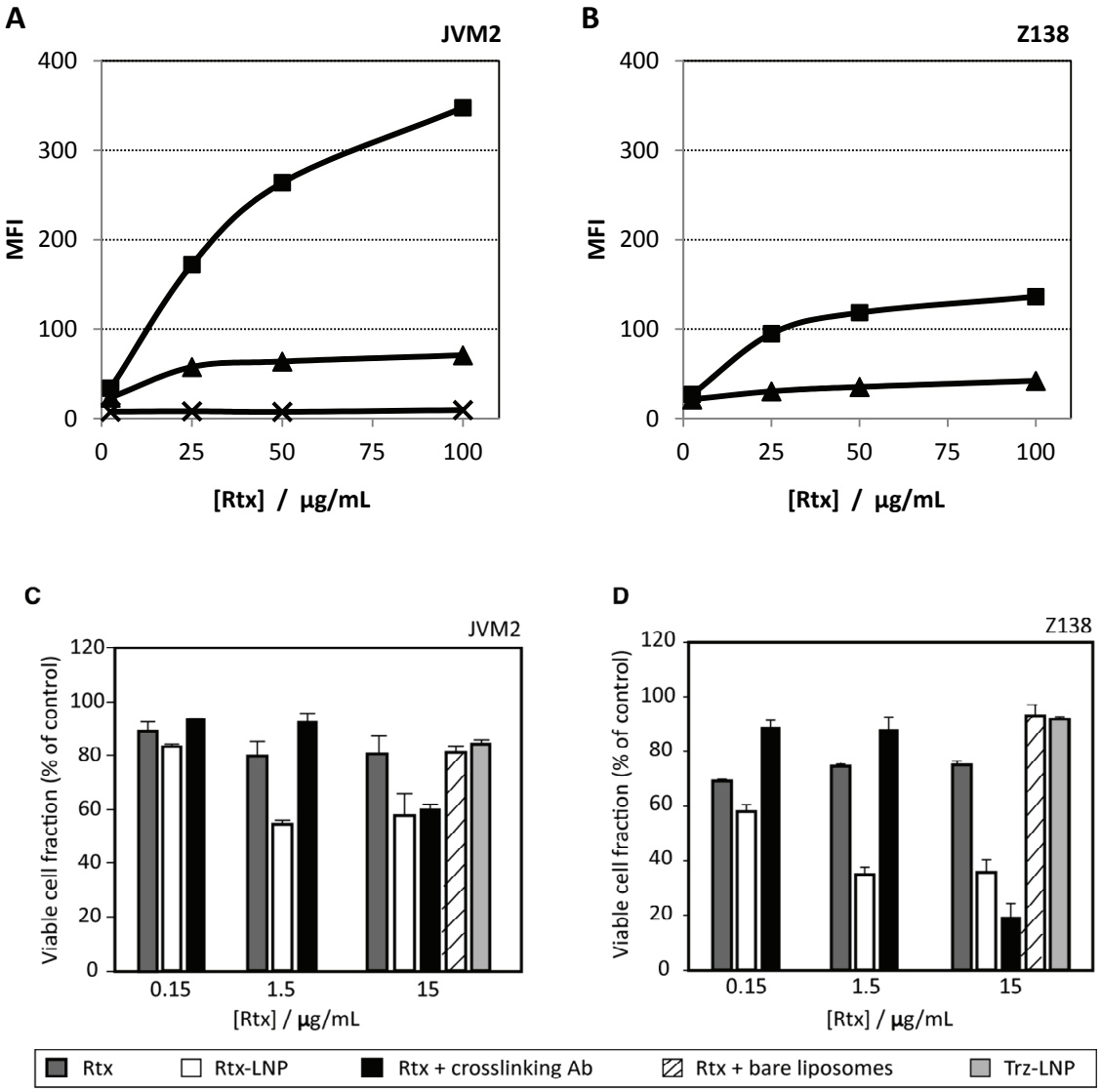

Figure 2.2 Binding of Rtx-LNPs to target cells and direct induction of apoptosis.

(A & B) Rtx binding to JVM2 **(A)** and Z138 **(B)** MCL cells when incubated with Rtx-LNP (■), free Rtx (▲), or Trz-LNP (×), as assessed by flow cytometry. Error bars are within the size of the data points. Data are the means of experiments performed in triplicate. MFI: mean fluorescence intensity. **(C & D)** Fraction of viable cells remaining after *in vitro*

treatment of JVM2 **(C)** or Z138 **(D)** cells with Rtx or Rtx-LNP at 37 ^{o}C for 72 h, as assessed by flow cytometry after Annexin-V-FITC and PI staining. Double-negatively stained cells were considered viable. The different treatments are indicated in the legend. Data correspond to means of triplicates, and are representative of three separate experiments.

The *in vitro* responses to treatment of JVM2 and Z138 cells with Rtx and Rtx-LNP were also assessed. Previous work has demonstrated that Rtx, on its own, has little therapeutic effect *in vitro* unless a crosslinking Ab is added[7, 74-76]. Using the AlamarBlue assay, we have previously observed that both crosslinked Rtx and multivalent Rtx-LNP decrease Z138 cell proliferation *in vitro* to an equivalent extent[7]. In this study, flow cytometry was used to measure the fraction of viable (nonapoptotic) JVM2 and Z138 cells remaining after treatment with free Rtx, crosslinked Rtx, and Rtx-LNP. The results, summarized in **Figure 2.2C & D**, suggest that when using Annexin-V and PI to identify nonviable cells, free Rtx was the least effective of the treatments (dark gray bars), with minimum cell viabilities of 80% in JVM2 cells (at 1.5 μg/mL) and 69% in Z138 cells (0.15 μg/mL). The percentages of viable cells were measured relative to untreated control cell populations in all cases. Compared to free Rtx, the multivalent Rtx-LNP (white bars) engenders significant therapeutic effects on both JVM2 and Z138 cells. At a treatment dose of 15 μg/mL of Rtx-LNP, 42% and 62% of JVM2 and Z138 cells, respectively, were considered non-viable (Figure 2.2C & D). These results suggest that Z138 cells are more sensitive to Rtx-LNP than JVM2 cells *in vitro*. The effects on the cell populations after Rtx treatment were equal in the absence or presence of bare uncoupled liposomes (hatched bars), indicating that the enhanced effects observed for Rtx-LNP result from Rtx being bound to the LNPs. As an additional control, LNPs formulated with Trz (an anti-ErbB2 therapeutic monoclonal Ab) instead of Rtx showed minimal activity (light gray bars), indicating that the therapeutic effects are specific to Rtx. The effects of Rtx-LNPs were comparable ($p > 0.05$) to 2^{o}Ab-crosslinked Rtx (black bars) when the dose of Rtx used was 15 μg/mL.

2.4.3 Multivalent Rtx-LNPs elicit superior complement-dependent cytotoxicity and Ab-dependent cell-mediated cytotoxicity compared with Rtx

Taken together, the data summarized above indicate that the multivalent Rtx-LNPs exhibit enhanced activity *in vitro* when compared to the effects achieved with equal doses of free Rtx, and these data are consistent with previous results[7]. The therapeutic activity of Rtx-LNP shown in Figure 2.2 occurred as a result of direct effects on the cells, yet it is understood that the *in vivo* activity of Rtx is largely dependent on indirect mechanisms of action involving CDC and ADCC[115-119, 121, 123]. Thus it was important to assess how the CDC and ADCC responses are affected when tumor cells are treated with Rtx-LNPs.

To measure levels of CDC, JVM2 and Z138 cells were given equivalent doses of Rtx and Rtx-LNP, then human serum was added and cell lysis was measured 4 h later using flow cytometry (see Section 2.3.7). These data have been summarized in **Figure 2.3A & B**. Rtx-LNP treatment resulted in more significant cell lysis than Rtx treatment in both cell lines, indicating that Rtx-LNP is better at inducing CDC than free Rtx. When comparing results obtained in the two cell lines, CDC activity was higher in JVM2 cells, where treatment with a 1 μg/mL dose of Rtx-LNP induced a 3.4-fold increase in CDC activity (relative to control), compared with a 2.0-fold increase in Z138 cells. This effect was even more pronounced when the dose increased to 10 μg/mL, where the values increased to 5.3-fold (JVM2) and 3.9-fold (Z138). The level of CDC observed following treatment with free Rtx was comparable to controls, which included Trz-LNP as well as a mixture of free Rtx and uncoupled liposomes (Rtx + lip) (Figure 2.3A & B). The level of cell lysis obtained for Rtx plus crosslinking secondary Ab (2^{o}Ab) was identical to that obtained with Rtx alone (data not shown). These results suggest that indirect CDC-based mechanisms of activity would be enhanced *in vivo* when using Rtx-LNP, even when compared to situations where Rtx crosslinking is achieved by an anti-Rtx 2^{o}Ab.

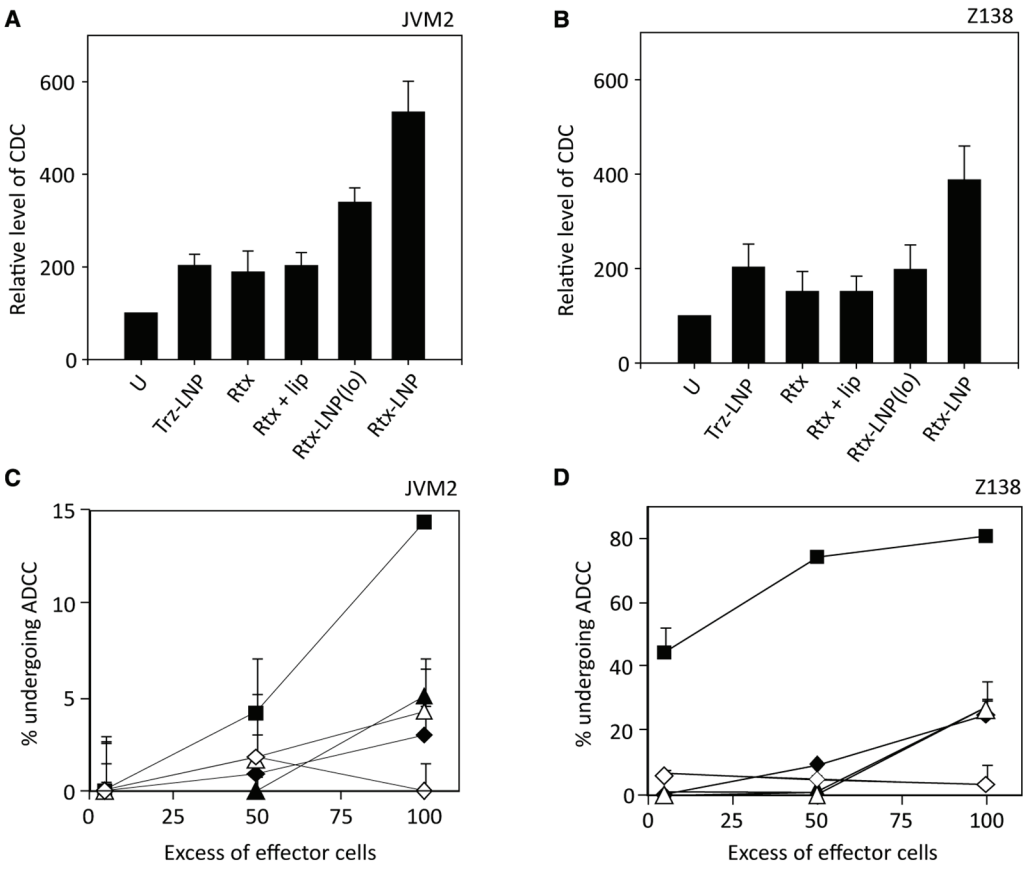

Figure 2.3 ***In vitro*** **levels of Rtx-mediated CDC and ADCC are augmented when Rtx is presented to cells as multivalent Rtx-LNP.**

(A & B) For measuring levels of CDC, JVM2 or Z138 cells were untreated (U) or treated with Trz-LNP, Rtx, Rtx + bare liposomes (Rtx + lip), or Rtx-LNP. All treatments consisted of 10 µg Ab except for Rtx-LNP(lo), which consisted of 1 µg. **(C & D)** For ADCC experiments, JVM2 or Z138 target cells were incubated for 30 min with 10 µg of Ab in the form of free Rtx (▲), Rtx + bare liposomes (Δ), Rtx + crosslinking 2^{o}Ab (◆), Trz-LNP (◇), or Rtx-LNP (■). Stimulated effector cells (mouse splenocytes) were then added in excess of target cells at effector-to-target cell ratios of 5:1, 50:1, and 100:1. After a 24 h incubation, ADCC was measured as described in Section 2.3.8. Data represent the means of triplicates, and are representative of three separate experiments.

To assess ADCC, a fluorometric method described by Gomez-Roman *et al*. was used[131]. Cells were first dual-labeled with PKH26, a membrane-associating lipid dye, and carboxyfluorescein diacetate succinimidyl ester (CFSE), which stains viable cells. Cells were then incubated with Rtx-LNP or other treatments for 30 min, followed by the addition of mouse splenocytes (effector cells). After 24 h, the JVM2 and Z138 target cells that were lysed as a result of ADCC retained the PKH26 signal but lost that of CFSE. The percentage of lysed cells was therefore determined using flow cytometry

as the fraction of CFSE-negative cells within the PKH26^{bright} population. The results, shown in **Figure 2.3C & D**, indicate that free Rtx (filled triangles) elicits an ADCC response at levels comparable to those observed when using secondary-antibody crosslinked Rtx (filled diamonds) or a mixture of Rtx and uncoupled liposomes (open triangles). The extent of ADCC resulting from Rtx-LNP treatment (filled squares) was significantly enhanced in both cell lines, but it was particularly notable when using Z138 cells, where at a 100-fold excess of effector cells, 81% of cells were undergoing ADCC after treatment with Rtx-LNP, compared to 26% for free Rtx ($p < 0.05$ at all target/effector cell ratios tested). Overall levels of ADCC were significantly lower in JVM2 cells, where at the same excess of effector cells, Rtx-LNP treatment resulted in an ADCC response of 14%, compared to 5% after treatment with Rtx ($p < 0.05$ only at this target cell/effector cell ratio).

2.4.4 Rtx-LNP induces the activation of natural killer cells

In order to corroborate the results suggesting that Rtx-LNP elicits a superior ADCC response compared with free Rtx, the extent to which NK cells were activated after exposure to Rtx or Rtx-LNP was determined. Bowles and Weiner demonstrated a correlation between ADCC activity after treatment with Rtx and CD54 upregulation on NK cells[134], and therefore the activation state of human NK cells was quantified here in terms of their CD54 expression levels. The NK cells used were a subpopulation within a sample of human peripheral blood mononuclear cells (PBMCs). These effector cells were mixed with Z138 cells as the target cells; only Z138 cells were used since the ADCC response was most robust with these cells, as shown in Figure 2.3D. Samples of effector cells or combined effector and target cells were treated with Rtx, Rtx-LNP, and controls (U or T-NP). The results, shown in **Figure 2.4**, compare the activation state of the NK cells in terms of the fraction of CD54^{bright} cells contained within the NK cell population (CD3^{-}/CD56^{+}). Open bars indicate control samples that contained only effector cells, while black bars correspond to samples containing both effector and target (Z138) cells. In general, a greater fraction of NK cells are activated in the

presence of Z138 target cells, as illustrated by the elevated CD54 expression levels (black bars compared to the white ones). NK cell activation was greatest when the target Z138 cells were treated with Rtx or Rtx-LNP, with the highest level of CD54 expression found after treatment with Rtx-LNP (rightmost black bar). Among the samples containing both effector and target cells (black bars), the only significant difference ($p < 0.05$) occurred between the untreated (34% activated) and Rtx-LNP treated (62%) samples. This study confirms that the elevated levels of ADCC resulting from Rtx-LNP treatment are associated with enhanced NK cell activation.

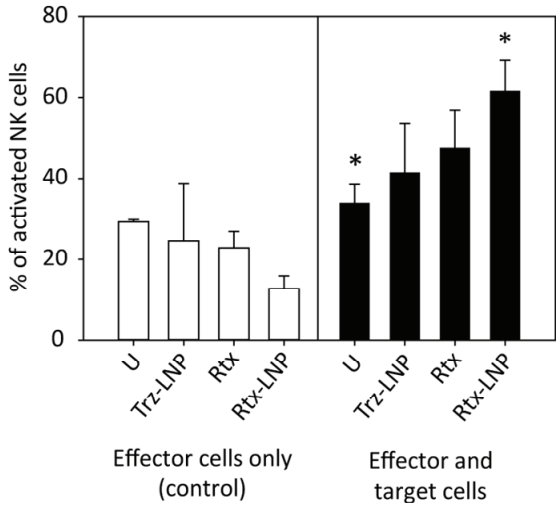

Figure 2.4 NK cell activation upon treatment of Z138 cells with different forms of Rtx.
Human PBMCs (effector cells) were incubated overnight with or without Z138 target cells that were untreated (U) or treated with Trz-LNP, Rtx, or Rtx-LNP. Cells were then labeled with anti-human-CD3, CD56 and CD54 Abs conjugated to different fluorophores. Flow cytometric analysis was performed and NK cells were identified as the $CD3^{-}/CD56^{+}$ population. Within this population, the percentage of $CD54^{bright}$ cells was determined, corresponding to the fraction of activated NK cells. $*p < 0.05$.

2.4.5 *In vivo* efficacy of multivalent Rtx-LNP

The ability of Rtx-LNP to induce ADCC and CDC is enhanced compared to that of free Rtx, and when this is considered alongside the increased direct activity leading to cell death, one would

expect that Rtx-LNP would exhibit significantly improved therapeutic effects compared with free Rtx when used *in vivo*. We therefore completed *in vivo* efficacy studies on Rtx-LNP in C.B-17 SCID mice. Although these mice lack functional B and T cells (similar to the Rag-2M mice used to generate the data in Figure 2.1), they have a well-defined NK cell population and should therefore be capable of eliciting ADCC responses[135]. The Z138 cell line was used for these studies since it was the most responsive to Rtx treatment, and a systemic tumor model was employed, where the cells were inoculated IV. This model is considered to be more aggressive and less sensitive to treatment compared to the SC model.

In order to follow disease development non-invasively, Z138 cells were transfected to express Luc, and tumor-bearing mice (as confirmed by bioluminescent imaging) were treated with HBS, Rtx, or Rtx-LNP. At specified time points after the start of treatment, the animals were imaged and representative images are provided in **Figure 2.5A**. Mice treated with Rtx and Rtx-LNP exhibited a significantly lower tumor burden compared to control animals and this was readily apparent 14 days after initiation of treatment. The imaging data also highlighted that following IV injection of Z138-Luc cells, disease development was throughout the body. Notably, there was significant disease burden in the brain, which would partially explain why this model may be considered more aggressive. As highlighted in the Rtx-treated examples, disease development within the brain was unaffected by treatment with Rtx or Rtx-LNP. Tumor burden was quantified by measuring the total number of emitted photons from each mouse, and the average photon counts determined for each treatment are summarized in **Figure 2.5B**. These data show that the tumor burden in mice treated with Rtx and Rtx-LNP are not significantly different, but both treatment groups exhibited significantly lower tumor burden when compared with control (HBS-treated) mice.

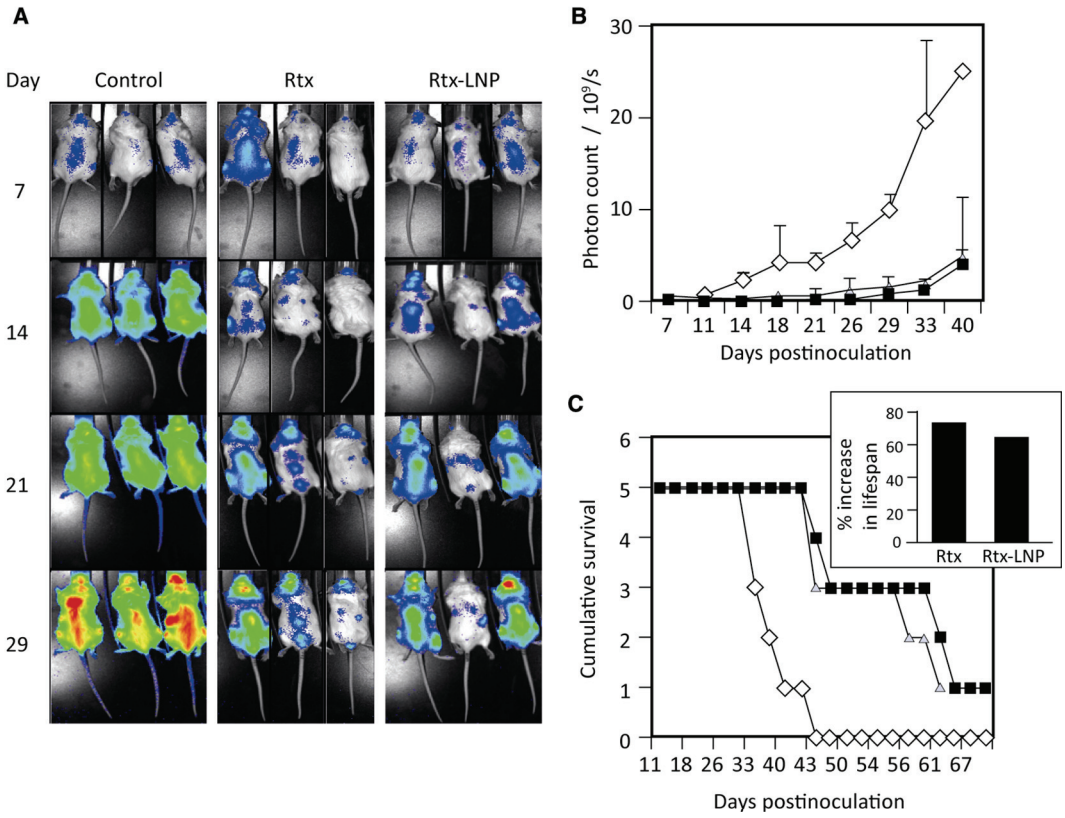

Figure 2.5 **Efficacy study for Rtx-LNP.**

C.B-17 SCID mice were injected with Z138-Luc cells and were monitored for tumor growth with the IVIS 200 optical imaging system. A total of 10 days after visible tumor growth appeared, mice were treated twice per week for 3 weeks with either HBS or 1 mg/kg of free Rtx or multivalent Rtx-LNP (R-NP). Tumors were scanned once or twice per week. **(A)** Images of three out of five mice are presented. Red and blue regions represent the highest and lowest luminescence, respectively. **(B)** Assessment of tumor growth, as measured by the total amount of light emitted by Luc-expressing tumor cells from the entire body of control mice (◆), and mice treated with Rtx (■) or Rtx-LNP (▲). **(C)** Kaplan-Meier survival curve for the mice in this study; symbols are the same as in (B). *Inset*: Increase in lifespan with respect to control. Data is representative of two separate studies.

Kaplan-Meier survival curves were also generated as described in Section 2.3.10, and are provided in **Figure 2.5C**. They are consistent with the imaging data and indicate that treatment with Rtx and Rtx-LNP provided equivalent survival benefits. The median survival time for the Rtx and Rtx-LNP treated animals was 56 and 61 days, respectively, while the median survival time for control animals was 35 days. These data were somewhat surprising given that the *in vitro* studies suggested that the Rtx-LNP would exhibit improved treatment effects when compared with Rtx. In an effort to

understand why these expectations were not realized, pharmacokinetic studies were completed to compare the Rtx levels in the plasma compartment over time following IV injection of Rtx or Rtx-LNP.

2.4.6 Pharmacokinetics of Rtx and Rtx-LNP

Pharmacokinetic studies were completed in immunocompromised mice (C.B-17 SCID) as well as immunocompetent BALB/c mice, and the data obtained are summarized in **Figure 2.6**. The black symbols in Figure 2.6A (C.B-17 SCID mice) and Figure 2.6C (BALB/c mice) represent the plasma concentration of Rtx in the different mouse strains, and in general, the elimination rate of Rtx was comparable in both strains. The percentage of the initial Rtx dose remaining after 72 h was 27% for C.B-17 SCID mice and 24% for BALB/c mice. These values are comparable to those reported elsewhere[136] and highlight that Rtx is slowly eliminated from the circulation following IV administration in mice. The open symbols in Figure 2.6A & C represent plasma concentrations of Rtx following IV injection of Rtx-LNP, and it is obvious that these values are considerably reduced. In both mouse strains, the injected dose was reduced by as much as 80% within the first hour after administration, and at 72 h postinjection, the remaining percentages of the initial dose were 0.3% (C.B-17 SCID) and 2.8% (BALB/c).

The plasma concentration of liposomal lipids was also monitored after administration of Rtx-LNP. As highlighted in Figure 2.6B & D, the time-dependent LNP concentration curves mirror those of Rtx for the same treatments; after 72 h, 0.7% of the initial dose remained in the C.B-17 SCID mice, while 0.5% remained in the BALB/c animals. The observation that the plasma concentrations of Rtx and LNPs decrease at approximately the same rate suggests that Rtx does not dissociate from LNPs in the circulation and that both are cleared together. Since the detected levels of Rtx-LNP are similar in both mouse strains, the data also indicate that Rtx-LNP is not cleared *via* an immunogenic

mechanism. Nevertheless, the plasma levels of Rtx-LNP are so low compared to free Rtx that its full therapeutic potential, as illustrated *in vitro* in Figures 2-4, is compromised in mice as a result.

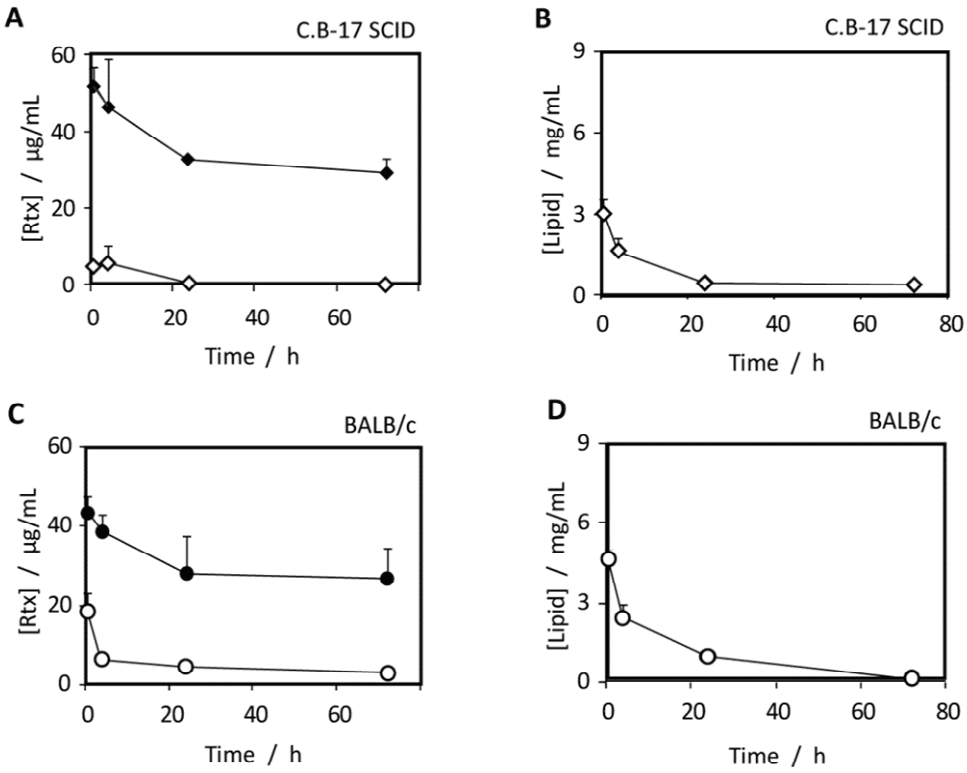

Figure 2.6 Pharmacokinetics of Rtx-LNP in two mouse models.

C.B-17 SCID mice **(A & B)** and BALB/c mice **(C & D)** were injected IV with 5 mg/kg of Rtx in free form (black symbols) or in Rtx-LNP (open symbols). At time points of 0.5, 4, 24 and 72 h after the injection, circulating Rtx **(A & C)** and lipid **(B & D)** were quantified by ELISA and liquid scintillation counting, respectively. Data is representative of two separate experiments.

2.5 Discussion and conclusions

2.5.1 Discussion

In spite of the fact that nearly all therapeutic Abs are bivalent IgG molecules, it has been demonstrated in numerous cases that equivalent doses of multivalent Abs have more therapeutic

potency. A number of multivalent anti-CD20 designs have been reported which exhibit enhanced binding to target cells[15, 96] and/or elevated levels of cell kill *in vitro*[7, 75, 88-90] and enhanced *in vivo* efficacy[75, 90]. The Rtx-LNPs studied here represent the only liposomal formulation of a multivalent therapeutic IgG that has been described[137]. These constructs have a valence of ~90, which is much higher than the other types of reported multivalent constructs, whose valences generally do not exceed 10.

The favorable effects related to the direct mechanism of action following treatment with Rtx-LNPs[7] were confirmed in the experiments described above. Figure 2.2 shows that the Z138 cell line was substantially more sensitive to Rtx-LNP-induced apoptosis in spite of the fact that it bound only half as much Rtx-LNP, indicating that higher levels of apoptosis do not result from more Rtx being bound to the cells. These results may be explained, in part, by the fact that the JVM2 line (and not the Z138 line) is Epstein-Barr virus positive, and latently infected Epstein-Barr virus-positive B-cell lymphomas are often protected from death-receptor induced apoptosis such as that triggered by CD95 (Fas receptor)[138]. This may justify why the high levels of CD95 observed in the JVM2 line (Figure 2.1) did not correlate with lower cell viability levels following treatment with crosslinked Rtx or Rtx-LNP (Figure 2.2C & D).

There has been a lack of studies on the indirect mechanisms of multivalent therapeutic Abs (ADCC and CDC), even though the indirect mechanisms are known to be essential to the *in vivo* efficacy of Rtx[118, 119, 121, 123] and this information would be critical for developing such constructs for clinical use. In the current study, the JVM2 cell line was expected to induce higher levels of CDC than the Z138 line since, as shown in Figure 2.1, it exhibited lower expression of CD55, a CDC inhibitor[46]. It was also expected that the JVM2 line would exhibit enhanced ADCC since its expression levels of CD40, CD80, and CD86 were elevated, and these proteins activate NK cells[125, 126]. As expected, the JVM2 cell line induced a more robust CDC response, but Z138 cells were substantially better at inducing ADCC (Figure 2.3). This illustrates the poor understanding of how

different types of lymphoma cells induce ADCC to various extents[49]. Together with the apoptosis data from Figure 2.2C & D, however, the observations in Figure 2.3 support the results in Figure 2.1B & C, which show that animals bearing established Z138 tumors are Rtx-sensitive whereas those bearing JVM2 tumors are not. This is of particular interest since these models may provide a framework for the future elucidation of molecular markers of Rtx resistance or response in MCL, which are currently poorly defined[139, 140].

Figure 2.3 also demonstrates that multivalent Rtx-LNP elicits superior CDC and ADCC responses compared with bivalent Rtx. In fact, bivalent Rtx did not induce specific CDC activity *in vitro*. A multivalent interaction consists, in theory, of a complex created by an initial univalent interaction where the local concentrations of the remaining free binding sites on both species are greatly enhanced[15]. This may help explain the increased CDC and ADCC observed in Rtx-LNP-treated cells. The elevated CDC may result from the fact that C1q is itself a hexavalent ligand that requires binding to several IgG Fc regions in order to activate a CDC response[105, 106]. Multivalent Rtx-LNP provides significantly higher local concentrations of exposed Fc available to bind C1q after the initial univalent Fc – C1q interaction. Similarly, ADCC requires binding of the Fc region of Rtx to FcγR on effector cells such as NK cells. Following the initial interaction between an Fc region on Rtx-LNP and a FcγR on a NK cell, the remaining Fc and FcγR are at significantly elevated local concentrations with respect to one another. This facilitates subsequent Fc – FcγR interactions leading to ADCC, and this effect is absent with bivalent Rtx.

Despite the fact that Rtx-LNPs appear to be therapeutically superior *in vitro*, we unexpectedly found that Rtx and Rtx-LNP exhibited equivalent activity when used to treat a systemic Z138 tumor model (Figure 2.5). This could be explained by the rapid elimination of Rtx-LNP following IV injection (Figure 2.6). The observed removal of Rtx-LNP from the circulation was surprising in light of previous studies from our laboratory on Trz-LNP (Section 1.2.2), which is identical to Rtx-LNP in every way except for the Ab employed. These studies showed that the

pharmacokinetics (plasma concentrations and area under the curve) and efficacy (decrease in tumor volume) of Trz-LNP were both significantly enhanced with respect to free Trz in breast tumor xenograft mouse models[7]. Thus, the rapid clearance of Rtx-LNP does not appear to result from the binding of plasma proteins such as albumin or lipoproteins to the LNPs, which would result in uptake by the reticuloendothelial system[18, 19]. This is expected since Rtx-LNP contains PEG for this purpose, and Trz did not interfere with PEG function in Trz-LNP[7]. As shown in Figure 2.6, the rapid elimination of Rtx-LNP involved neither dissociation of Rtx from the liposomes nor an immunogenic reaction, but when compared with Trz-LNP, the pharmacokinetic behavior of Rtx-LNP appears to arise from the Ab used and not from the liposomal component of the formulation. The issue of rapid clearance is discussed further in Section 7.3.1.

2.5.2 Conclusions

The studies in this chapter demonstrate that multivalency can be an effective strategy for improving the efficacy of therapeutic Abs. The greatest barrier to developing multivalent Abs for clinical use is their poorly understood mechanism of action, but we have shown that both the direct and indirect modes of action of multivalent Rtx-LNPs are significantly improved compared with Rtx. This chapter focused on the enhanced indirect mechanisms (CDC and ADCC), and we further showed that elevated ADCC occurred alongside higher levels of activated NK cells. In spite of more favorable direct and indirect cytotoxicity, we found that the *in vivo* efficacy of Rtx and Rtx-LNP were equivalent, and pharmacokinetic studies revealed that Rtx-LNP was very rapidly cleared from the circulation compared to Rtx. This not only indicates the need to create multivalent Rtx constructs with more extended circulation lifetimes (using a different type of NP formulation and/or a different anti-CD20 Ab) if they are to be developed for clinical use, but it also highlights the therapeutic potency of Rtx-LNP compared to Rtx.

Part of this potency results from the direct mechanism of action, which in the case of Rtx, is undefined from a molecular point of view. The next chapter describes an alternative, more versatile methodology that we developed for producing Ab-LNPs of differing valence for use in studies on the direct mechanisms of action of therapeutic Abs[51]. Applying this methodology to Rtx-LNPs will add to the current results on the indirect factors and will help to delineate the overall mechanism of action of multivalent Rtx. This understanding will further define cases where it might be more efficacious to employ a multivalent Ab rather than a bivalent IgG in order to treat cancer.

3 Improved methodology for preparing multivalent antibody-lipid nanoparticles

3.1 Synopsis

Previous methods of coupling Abs to liposomes were unsuitable for creating many different valences of (Ab-LNPs). An improved methodology developed for this purpose is described in this chapter. It exhibits significant improvements over previous methods in terms of reproducibility, length of time required to produce many valences, and yields of coupled Ab.

3.2 Background

3.2.1 The need to produce a new method for creating many valences of Ab-LNPs

An updated methodology was required to produce many different valences of Ab-LNP because previous methods, which have been described largely in light of immunoliposomes, were inadequate in terms of reproducibility, time required, and overall yields of coupled Ab. These problems stem from the method of chemical coupling, which normally involves thiolation of the Ab followed by reaction with maleimide (Mal)-containing liposomes or micelles[3, 5, 141, 142]. Between three and seven thiol groups are required per Ab molecule[7, 143], resulting in a very heterogeneous reaction product that varies from preparation to preparation. Such heavy chemical modification may also pose a problem particularly for therapeutic Abs, which after thiolation have shown decreased binding to target[144] and whose indirect mechanisms depend on a native Fc fragment[44].

One common coupling strategy, described in Section 2.3.2, involves the preparation of small unilamellar vesicles (SUVs) containing surface Mal moieties, followed by the addition of thiol-modified Ab[7, 144]. In the current application, where smaller amounts of several different

formulations are required, this method is impractical since a different SUV composition would need to be prepared, by extrusion or other means, for every desired valence.

A more recent variation is the coupling of Abs to DSPE-PEG micelles using thiol-maleimide chemistry, followed by heating in the presence of SUVs, enabling the "post-insertion" of the micellar lipids and Ab into the preformed SUVs[142, 145]. Although this method may be useful for preparing immunoliposomes, it is unsuitable for preparing many precise valences of Ab-LNPs because the Ab undergoes substantial heterogeneous chemical modification as described above. This results in variable valences from one preparation to the next as well as potentially reduced therapeutic activity of the Ab. Moreover, low yields of Ab in the final product are obtained (59%) compared to the amount of Ab that was initially modified. This is particularly a problem when using therapeutic Abs since they are generally available in limited quantities, especially novel drugs under development.

3.2.2 How the new methodology overcomes previous limitations

The improved methodology described in this chapter overcomes the above limitations by drawing on desirable features from earlier methods, including the post-insertion technique[142, 145], while replacing thiol-maleimide chemistry with high-affinity biotin-NeutrAvidin (Neut) interactions[146, 147]. In doing so, a novel feature concerning the kinetics of biotin-Neut interactions on liposomes was discovered and incorporated in the methodology. Specifically, it involves surprisingly slow kinetics of association between biotinylated protein and Neut on the surface of PEG-containing liposomes, attributed to a steric blocking effect by PEG[148]. Since Ab addition is slow (coupled Ab levels continued to increase over 72 h), to make a series of different valences, it was only necessary to stop fractions of the same coupling reaction at different times. To improve yields, a solid-support Ab biotinylation technique was employed[149] that provides high recovery (96%), and to aid with reproducibility, relevant analytical assays were developed for the characterization of preparation

intermediates, including fluorescence-based protein quantitation[150] and an assay for PEG content in liposomes[151]. This chapter details this new methodology and the significant improvements it brings to the preparation of multivalent Ab-LNPs of different valence.

3.3 Materials and methods

3.3.1 Materials

The following lipids were obtained from Avanti Polar Lipids (Alabaster AL, USA): 1,2-distearoyl-*sn*-glycero-3-phosphocholine (DSPC), 1,2-distearoyl-*sn*-glycero-3-phosphoethanolamine-*N*-[methoxy(polyethylene glycol)-2000] (DSPE-PEG), and 1,2-distearoyl-*sn*-glycero-3-phosphoethanolamine-*N*-[biotinyl(polyethylene glycol)-2000] (DSPE-PEG-biotin). [^{3}H]cholesteryl hexadecyl ether ([^{3}H]CHE) and Pico-Fluor 15 scintillation fluid were from Perkin-Elmer Life Sciences (Woodbridge ON, Canada). NeutrAvidin (Neut) and immobilized iminodiacetic acid gel were obtained from Pierce/Thermo Fisher Scientific (Rockford IL, USA). Rituximab (Rtx) and trastuzumab (Trz) were obtained from the BC Cancer Agency pharmacy (Vancouver BC, Canada). *N*-Hydroxysuccinimide ester-dPEG$_4$-biotin (NHS-PEG-biotin) was purchased from TimTec (Newark DE, USA). Disposable PD-10 columns (which contain Sephadex G-25 medium) were obtained from GE Healthcare Life Sciences (Piscataway NJ, USA). 4-Hydroxyazobenzene-2-carboxylic acid (HABA)/avidin reagent was purchased from Sigma-Aldrich (St. Louis MO, USA) as a lyophilized powder. ATTO-TAG 3-(4-carboxybenzoyl)quinoline-2-carboxaldehyde (CBQCA) was from Invitrogen (Burlington ON, Canada). Unless noted otherwise, all other reagents were obtained from Sigma-Aldrich and were of the highest quality available.

3.3.2 Preparation of Neut-micelles

Separate micellar suspensions of DSPE-PEG and DSPE-PEG-biotin were prepared by gently dissolving the lipids in HBS (25 mM HEPES, 150 mM NaCl, pH 7.4). The two suspensions were then mixed in different mole ratios of DSPE-PEG to DSPE-PEG-biotin corresponding to different desired Neut-LNP formulations. Separately, with vortexing, the micellar suspension was slowly added to a threefold mole excess of Neut over DSPE-PEG-biotin. Suspensions were vortexed for 30 s longer, then incubated for 30 min at room temperature with stirring.

3.3.3 Preparation of Neut-LNP

Using the same procedure as described in Section 2.3.2, SUVs composed of DSPC and cholesterol (Chol) in a mole ratio of 2:1 and labeled with [^{3}H]CHE (0.009 μCi/μmol liposomal lipid) were prepared by extrusion. In all cases when producing Neut-LNPs, the total number of added moles of DSPE-PEG + DSPE-PEG-biotin (in Neut-micelles) was 4 % of the number of moles of DSPC (in SUV). SUV and Neut-micelles were heated separately in a 65 ^{o}C water bath for 10 min with stirring, then were combined with vortexing and incubated for 60 min with stirring. After being allowed to return to room temperature (with stirring), Neut-LNP preparations were purified on Sepharose CL-4B columns pre-equilibrated with HBS. Lipid concentrations were determined with liquid scintillation counting, and Neut concentrations were determined using CBQCA (see below).

The number of Neut molecules per SUV was calculated by dividing the number of Neut molecules per liter by the number of SUV per liter. This latter quantity was calculated assuming that each DSPC molecule occupies 0.815 nm^2 of surface area in the bilayer of DSPC/Chol (mole ratio 2:1) SUV[144] and that the bilayer thickness in these SUV is 4.9 nm[152]. For a 100-nm diameter SUV, this corresponds to 6.98×10^4 DSPC molecules per SUV. The number of SUV per liter was calculated by dividing the number of DSPC molecules per liter by the number of DSPC molecules per SUV.

3.3.4 CBQCA assay for measuring protein concentration in solution or Ab-LNP suspension

Solutions of borate (100 mM $Na_2B_4O_7 \bullet 10H_2O$, pH 9.3) and KCN (20 mM) were prepared in ultrapure water. A KCN/borate solution was then prepared by mixing 25 volumes of borate and 1 volume of KCN. A 96-well plate layout was prepared for each assay, which included separate Rtx and Neut standards over appropriate concentration ranges, as well as triplicates of unknowns. To each sample-containing well, 130 µL of KCN/borate were added, followed by 10 µL of standard or unknown sample. Finally, a 40 mM stock solution of ATTO-TAG CBQCA in dimethyl sulfoxide (DMSO) was diluted tenfold in borate, and 10 µL of the resulting solution were added to the wells. The plate was covered with aluminum foil and incubated for 1 h at room temperature with shaking. Fluorescence emission intensities were then measured in triplicate at 550 nm with an excitation wavelength of 465 nm using a BMG Labtechnologies Fluorstar plate reader. Unknown concentrations of Rtx and Neut were calculated from their respective standard curves.

3.3.5 Ammonium ferrothiocyanate assay for measuring polyethylene glycol content in LNPs

Ammonium ferrothiocyanate (AF) was prepared by dissolving 30.4 g of NH_4SCN and 27.0 g of $FeCl_3 \bullet 6H_2O$ in ultrapure water to a final volume of 1.0 L. Standard solutions of DSPE-PEG (0 to 500 µM) and DSPC (0 to 4.5 mM) were prepared from DSPE-PEG micelles and DSPC/Chol (2:1) SUV. In 1.5 mL Eppendorf tubes, 500 µL of $CHCl_3$ were added, followed by 500 µL of AF and 50 µL of standard or unknown solution (assayed in triplicate). Tubes were closed and mixed vigorously on a plate shaker for 30 min, then tubes were spun in a microcentrifuge at 13000 rpm for 2 min, and the lower $CHCl_3$ layers (495 µL) were pipetted into separate Eppendorf tubes. The absorbances of these $CHCl_3$ solutions were measured at 530 nm. The expected absorbances of the unknown samples in the absence of DSPE-PEG were calculated based on their known DSPC concentrations from

scintillation counting, and excess absorbances at 530 nm in each case were attributed to the presence of PEG. PEG concentrations of the unknowns were calculated from the excess absorbance values.

3.3.6 Ab biotinylation on a nickel immobilized metal affinity chromatography column

Immobilized iminodiacetic acid gel was transferred into a 1.5 mL polypropylene column to a final gel bed volume of 500 µL then rinsed with 5.0 mL of ultrapure water. The gel was then chelated with nickel by adding 5.0 mL of 50 mM ammonium nickel(II) sulfate and washed with an additional 5.0 mL of water. If not used immediately, the resultant nickel immobilized metal affinity chromatography (NIMAC) columns were stored at 4 ^{o}C in 0.02 % sodium azide. Otherwise, columns were equilibrated with 5.0 mL binding buffer (BB; 25 mM HEPES, 1 M NaCl, pH 7.4). Separately, 500 µL of 10 mg/mL Rtx were added to 1250 µL of 2x BB and 750 µL of ultrapure water. For future analysis, 100 µL of this solution were set aside, and the remaining 2400 µL were loaded onto the column by eluting the solution through the gel bed twice. The column was then washed with 4 x 500 µL BB. For biotinylation, the desired mole excess of NHS-PEG-biotin with respect to Ab was measured from a stock DMSO solution and was diluted to 1.0 mL in cold BB. The concentration of NHS-PEG-biotin was equilibrated across the column by adding 500 µL of the solution to the column, allowing the eluent to drain into the NHS-PEG-biotin solution, vortexing briefly, then another 500 µL aliquot was added to the column. After five such aliquots, the entire 1.0 mL was added and allowed to drain from the column by gravity for 45 min, with the column being refilled as necessary with the drained solution. Next, the column was washed with 5 x 500 µL BB to remove NHS-PEG-biotin. Rtx was either eluted with imidazole or ethylene diamine tetraacetic acid (EDTA). For imidazole elution, the column was treated with 3 x 500 µL elution buffer (EB; 25 mM HEPES, 1 M NaCl, 200 mM imidazole, pH 7.4). A final 500 µL aliquot of EB was passed through the column three times, and the

four resulting fractions were pooled. For elution with EDTA, the column was treated with 4 x 500 µL stripping buffer (SB; 25 mM HEPES, 1 M NaCl, 50 mM EDTA, pH 7.4) and all four fractions were pooled. The concentration of Rtx was measured using the CBQCA assay and the number of biotin groups per Rtx molecule was calculated using HABA/avidin (see below) and CBQCA assay data. Columns were stripped of Ni^{2+} by treating with a total volume of 5.0 mL SB, then re-chelated with nickel and stored as described above.

3.3.7 Ab biotinylation in solution

As in the NIMAC procedure above, 500 µL of 10 mg/mL Rtx were added to 1250 µL of 2x BB and 750 µL of ultrapure water. Depending on the mole excess of NHS-PEG-biotin to Ab, the appropriate volume of a stock solution of NHS-PEG-biotin in DMSO was measured and diluted to 1.0 mL in cold BB. The Rtx and NHS-PEG-biotin solutions were combined and incubated at room temperature for 1 h with stirring. Biotinylated Rtx was purified on a PD-10 column pre-equilibrated with BB. Fractions (500 µL) were obtained and Rtx-containing fractions (as determined by measuring absorbances at 280 nm) were pooled. The number of biotin groups per Rtx molecule was calculated as per the NIMAC method.

3.3.8 HABA/avidin assay for measuring the extent of Ab biotinylation

HABA/avidin reagent was reconstituted with ultrapure water according to the instructions of the manufacturer. Biotin standards ranging from 0 to 150 µM were prepared in BB, EB, or SB depending on the method of biotinylation and elution (see above). In a 96-well plate, 140 µL of HABA/avidin solution were added to wells as required, and the absorbances of all wells were read at 500 nm in triplicate using a Thermo Scientific absorbance microplate reader. Next, 10 µL of each standard or unknown sample (assayed in triplicate) were added to the wells. The plate was shaken on a plate shaker for 3 min and the absorbances were read again at 500 nm in triplicate. The

average absorbance of each well after sample addition was subtracted from the absorbance before to obtain ΔA, which was plotted against biotin concentration to generate a standard curve. The number of biotin groups per Rtx molecule was obtained by dividing the biotin concentration by the Rtx concentration obtained from the CBQCA assay.

3.3.9 Coupling of Rtx-biotin to Neut-LNP to create Rtx-LNP

Based on the desired mole ratio of Rtx-biotin to Neut (in Neut-LNP), the necessary volume of Neut-LNP was added dropwise with vortexing to a solution of Rtx-biotin prepared using the NIMAC procedure above. The coupling reaction was allowed to proceed at 4 ^{o}C with stirring for 1 to 72 h. The resulting Rtx-LNPs were purified over Sepharose CL-4B columns pre-equilibrated with HBS. The mean vesicle diameter of Rtx-LNP was between 125 and 140 nm as determined by QLS. Lipid concentrations in Rtx-LNPs were determined with respect to Neut-LNP by liquid scintillation counting, and protein concentrations were measured using CBQCA. The concentration of Neut in Rtx-LNP was calculated from lipid concentrations by assuming no change in the Neut-to-DSPC ratio as a result of coupling. The expected contribution to the CBQCA signal by Neut was determined based on the Neut standard curve, and the excess signal was attributed to Rtx, whose concentration was calculated from this excess signal. The number of Rtx molecules per Rtx-LNP was determined using the same assumptions as for Neut-LNP above (Section 3.3.3).

3.4 Results

3.4.1 Overview of the improved methodology for creating Ab-LNPs of different valence

Given the considerations outlined in Section 3.2, we have developed and optimized an improved methodology for producing smaller amounts of several different Ab-LNP valences in a

manner that is time-efficient, reproducible, and that results in high yields of coupled Ab. **Table 3.1** shows that the new methodology provides yields of coupled Ab as high as 80% with far less Ab modification compared to the previous post-insertion method, which produces overall yields of 59%.

Table 3.1 Comparison of Ab yields between current and previous methods of Ab-LNP production[a].

Improved biotin-Neut methodology (Figure 3.1)	Recovered Ab / %	Cumulative yield / %	Notes
Ab biotinylation (NIMAC)	96 ± 6	96 ± 6	1-2 biotin groups per Ab
Coupling to Neut-LNP[b]	84 ± 6	**80 ± 7**	Ab loss from purification only
Previous thiol-Mal post-insertion method	**Recovered Ab / %**	**Cumulative yield / %**	**Notes**
Ab thiolation[c]	80 ± 4	80 ± 4	3-7 thiol groups per Ab
Coupling to micelles and post-insertion of Ab[d]	74 ± 6	**59 ± 6**	Ab loss from incomplete coupling, post-insertion, and purification

[a]All values are averaged over three experiments and are ± SD.
[b]Mole ratio of Rtx-biotin to Neut = 0.5; coupling time = 72 h.
[c]Using Traut's reagent followed by purification over a PD-10 column; information from the manufacturer states that 70-95% recovery is typical.
[d]Ab-to-DSPC ratio after purification was ~88% of the input amount, consistent with Ishida *et al.*[142], representing incomplete coupling and post-insertion. Ab (coupled to liposomes) was also subsequently lost during purification on a Sepharose CL-4B column.

Figure 3.1 summarizes the five major steps of methodology, and the ensuing sections describe them in greater detail. First, [1] DSPE-PEG and DSPE-PEG-biotin are dissolved in HBS, producing a suspension of micelles. [2] Biotin present on the micelles is saturated with an excess of Neut, a deglycosylated analog of streptavidin with low nonspecific binding. [3] Micellar lipids and Neut-lipid complexes become post-inserted into the outer leaflet of SUVs to produce Neut-LNP. SUVs are composed of DSPC/Chol (mole ratio 2:1; Chol not shown), and Neut is post-inserted rather than Ab, which eliminates Ab wastage during post-insertion. [4] Separately, Ab is biotinylated on a NIMAC support to produce Ab-biotin, resulting in well-controlled and reproducible Ab modification with very high Ab recovery. [5] Ab-biotin and Neut-LNP are combined, producing Ab-LNPs of defined valence.

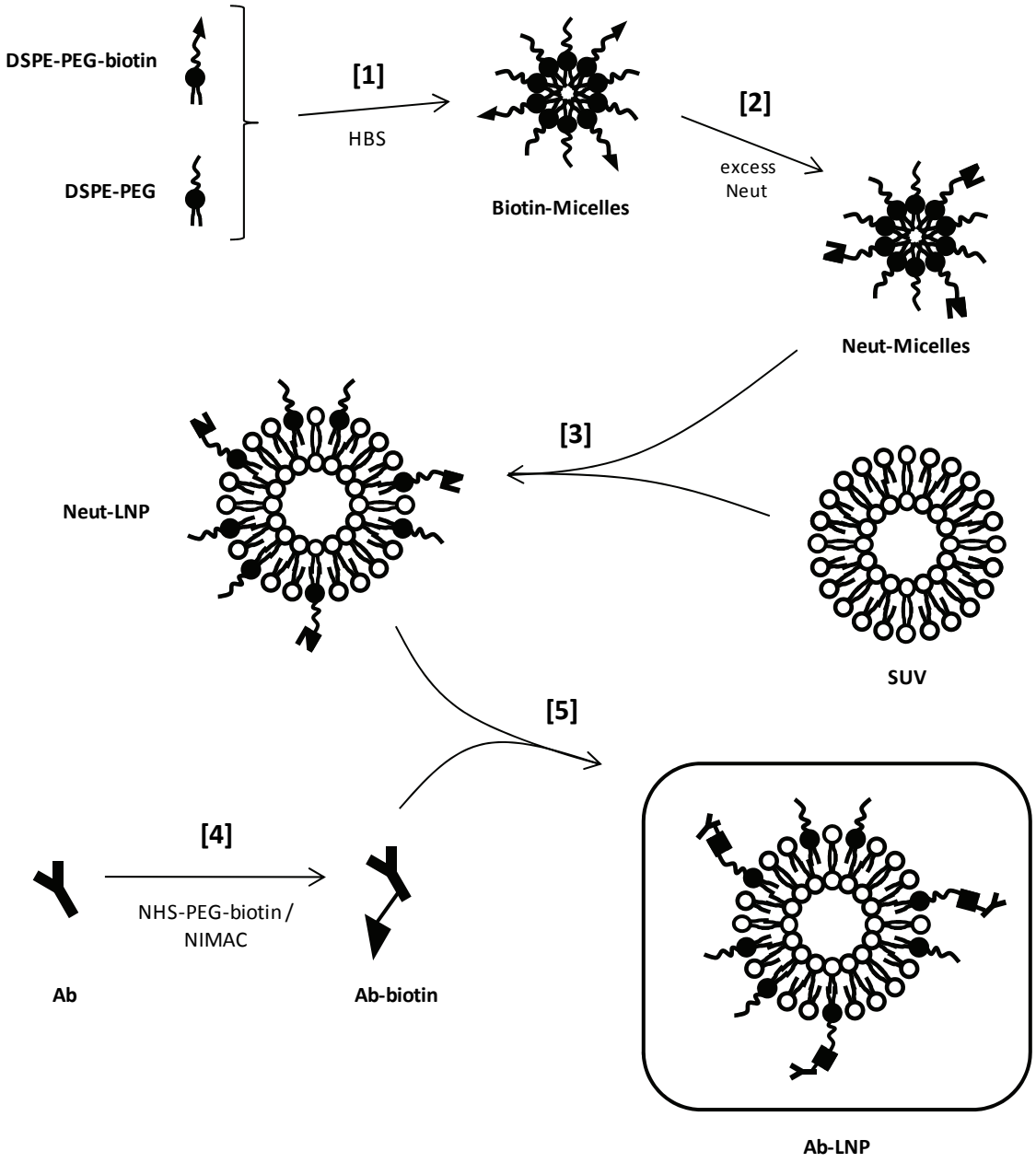

Figure 3.1 Overview of the improved methodology for preparing multivalent Ab-LNPs.

Please see text for details.

3.4.2 Preparation of Neut-LNP and measurement of protein content

Initially, a mixture of DSPE-PEG and DSPE-PEG-biotin was post-inserted into SUVs to create biotin-LNPs with different numbers of biotin groups per LNP. Separately, Ab was biotinylated and

saturated with Neut to make Ab-Neut, which was then coupled to the various biotin-LNPs to create Ab-LNPs of different valence. This approach was problematic, however, since each Neut molecule contains four biotin-binding sites, and adding Neut to Ab-biotin resulted in a mixture of Ab-Neut species containing between 0 and 4 Ab molecules per Neut. Yields were reduced because $(Ab)_4$-Neut could not bind to biotin-LNP, and separation of $(Ab)_4$-Neut and free Neut from the desired species was inefficient. Moreover, some Ab molecules contained more than one biotin group and thus bound more than one Neut molecule, resulting in a complex mixture of adducts (data not shown).

It was therefore more efficient to couple Neut to DSPE-PEG-biotin. Before post-insertion, biotin-micelles were saturated with a threefold excess of Neut, forming Neut-micelles (reaction [2] in Figure 3.1). For post-insertion, a total of 4 mol % PEGylated lipid was added with respect to DSPC; this percentage was selected on the basis that higher amounts of DSPE-PEG (above ~7 %) are known to result in unwanted effects such as dissociation back to DSPE-PEG micelles[153]. The number of Neut molecules added per SUV was controlled by preparing Neut-micelles containing different fractions of DSPE-PEG-Neut with respect to DSPE-PEG (reaction [3] in Figure 3.1) and several different post-insertion reactions were carried out simultaneously. Using this strategy, **Figure 3.2A** shows that the number of added Neut molecules per SUV can be controlled in a precise manner. The number of Neut molecules per Neut-LNP depended on the initial mole percent of DSPE-PEG-biotin used; 11 Neut per Neut-LNP were obtained using 0.5 mole % DSPE-PEG-biotin, while the number of Neut per Neut-LNP increased to 130 when 20 mole % DSPE-PEG-biotin was used ($p < 0.05$ between all pairs of shown conditions).

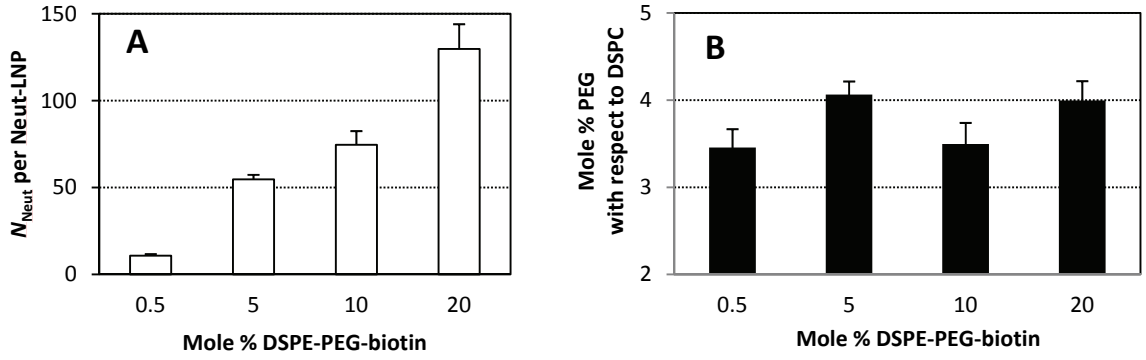

Figure 3.2 Control over Neut and PEG content during the preparation of Neut-LNPs.

(A) The number of Neut molecules per Neut-LNP (product of step [3] in Figure 3.1) can be controlled by varying the mole percent of DSPE-PEG-biotin present in biotin-micelles (step [1]). **(B)** The Neut content of Neut-micelles does not significantly influence the total amount of post-inserted PEGylated lipid in Neut-LNP; in all cases, approximately 4 % PEGylated lipid was added with respect to DSPC. Values for mole % DSPE-PEG-biotin in (A) and (B) are with respect to the total number of moles of PEGylated lipid (DSPE-PEG + DSPE-PEG-biotin).

Protein content in Neut-LNP and in all other cases was measured with the CBQCA assay (see Section 3.3.5). The direct advantage of employing this fluorescence-based assay is that there is no interference from liposomes or micelles. To verify the lack of interference, mixtures of known amounts of DSPC/Chol SUV, DSPE-PEG, and Ab were created in various combinations, and it was found that Ab concentrations obtained were equivalent regardless of the presence of lipids (data not shown). This is in contrast to other protein assays such as the bicinchoninic acid (BCA) assay (see Section 2.3.2), an absorbance-based assay which is commonly employed to measure protein content in liposomes[154, 155], although variable levels of interference from lipids are commonly observed, even in the presence of detergents[156, 157].

3.4.3 Direct measurement of levels of post-inserted polyethylene glycol in Neut-LNP

To enhance the reproducibility of the procedure by thoroughly characterizing intermediate products, the PEG content of Neut-LNP was also quantified following post-insertion. For this, we developed an assay for the direct measurement of PEG content in Neut-LNP or Ab-LNP based on a

method originally described for quantifying PEG in PEGylated proteins[151] (see Section 3.3.6). **Table 3.2** shows the PEG content during a sample purification of Neut-LNP, and as expected, the fractions with the largest mean diameter (those containing the most PEG) were eluted first from the Sepharose CL-4B column. The pooled fraction contained close to the amount of PEGylated lipid that was input (4 % with respect to DSPC). As shown in **Figure 3.2B**, analysis of other samples indicated that the PEG content was consistently in this range (3.5–4.1 mole % PEG with respect to DSPC), regardless of the mole % of DSPE-PEG-biotin initially used ($p > 0.05$ for all pairs of shown conditions in Figure 3.2B, except between 0.5 and 5 mole % DSPE-PEG-biotin, where $p < 0.05$). This assay was also verified by mixing different known quantities of DSPC/Chol SUV and DSPE-PEG micelles, and excellent agreement (within 5 %) was found between the measured and known values for PEG concentrations with respect to DSPC (data not shown).

Table 3.2 PEG content of 0.5 mL fractions during purification of Neut-SUV[a].

Column fraction	[DSPC] / mM	Mole % PEG wrt DSPC[b]
1	3.5 ± 0.3	4.4 ± 0.4
2	9.0 ± 0.7	4.4 ± 0.4
3	9.8 ± 0.7	3.9 ± 0.4
4	6.2 ± 0.5	3.8 ± 0.4
5	5.0 ± 0.4	3.7 ± 0.4
6	3.2 ± 0.3	3.7 ± 0.4
pooled	6.7 ± 0.4	3.8 ± 0.4

[a] All values are ± SD.
[b] wrt: with respect to.

3.4.4 Ab biotinylation on a nickel immobilized metal affinity chromatography support

A major drawback of thiol-maleimide chemistry is the need to extensively thiolate the Ab, as outlined above. To minimally biotinylate the Ab in a well-controlled manner before coupling it to Neut-LNP, the water-soluble compound NHS-PEG-biotin was employed. When the biotinylation reaction was carried out in solution, variable results were obtained in terms of the number of biotin

groups per Ab molecule, so to enhance yields and reproducibility, an alternative strategy was employed which made use of a NIMAC support[149] (reaction [4] in Figure 3.1).

A schematic of the biotinylation process using the NIMAC column is shown in **Figure 3.3A & B**. Loading takes place by eluting the Ab solution through the NIMAC support, and the Ab contains a highly conserved cluster of histidine residues that binds specifically to Ni^{2+} on the column[158, 159]. Biotinylation of the immobilized Ab then occurs by eluting an NHS-PEG-biotin solution through the column, and purification consists of simply washing the column. Ab can be eluted either by treatment with a solution containing imidazole (the side chain of histidine), which competes with Ab binding to Ni^{2+}, or through treatment with EDTA, which removes Ni^{2+} along with the bound Ab. No differences were found between imidazole and EDTA elution in terms of yield of recovered Ab-biotin or in terms of the ability of Ab-biotin to bind to Neut-LNP (data not shown). Imidazole elution was therefore employed to avoid contamination with Ni^{2+}, whose toxicity is well documented[160]. It was also found that imidazole does not interfere with the CBQCA or HABA/avidin assays (data not shown). Overall, imidazole elution resulted in very high recovery of Ab (96 %; Table 3.1) and the entire biotinylation scheme takes place under very mild conditions (room temperature, pH 7.4), important for the conservation of Ab structure and function.

Figure 3.3C compares the number of biotin groups added per Rtx molecule under conditions of different excesses of NHS-PEG-biotin, using either the NIMAC support (black bars) or by carrying out the reaction in solution (white bars). In general, the degree of Rtx biotinylation in solution increased substantially with the excess of NHS-PEG-biotin, whereas biotinylation on the NIMAC column resulted in more mild increases. When biotinylation was carried out in solution, the number of biotin groups per Rtx increased from 0.23 to 16 (~70-fold) from a 5-fold molar excess of NHS-PEG-biotin to a 50-fold excess ($p < 0.05$ between all pairs of conditions in solution). When the NIMAC column was employed instead over the same range of NHS-PEG-biotin concentrations, the number of biotin groups per Rtx molecule increased from 0.90 to 3.8 (~4-fold; $p > 0.05$ between 5- and 10-

fold excesses, and $p < 0.05$ between the 10-fold and higher excesses). Greater control over the biotinylation process was therefore achieved using the NIMAC column compared to reaction in solution, since small unavoidable variations in reagent concentrations do not produce large fluctuations in the degree of biotinylation using NIMAC, resulting in a more reproducible procedure.

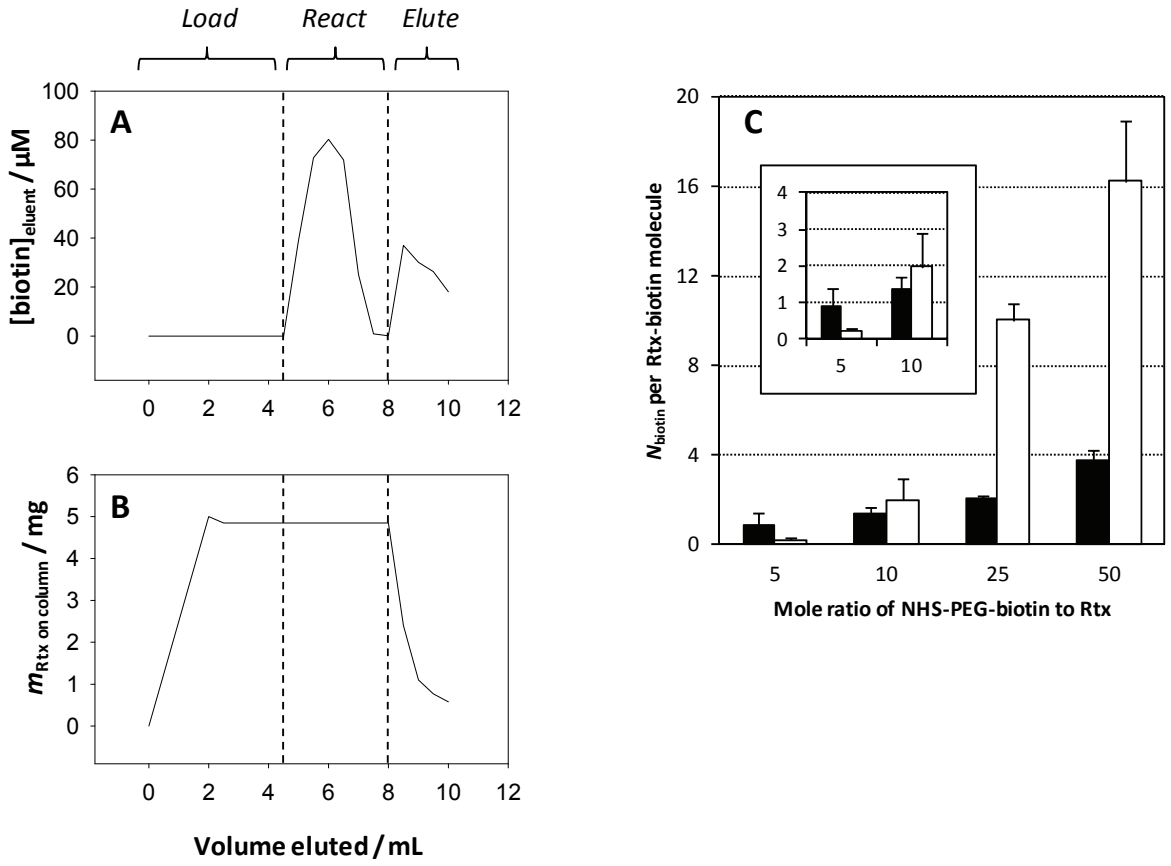

Figure 3.3 Ab biotinylation on a NIMAC column allows for easy purification, high recovery, and precise degree of biotinylation.

(A) Schematic representation of biotin concentration in the eluent and **(B)** mass of immobilized Rtx on the NIMAC column as a function of the total volume eluted through the column during biotinylation. During loading, Rtx in solution binds to immobilized Ni^{2+} on the column. Reaction with Rtx takes place by allowing a solution of NHS-PEG-biotin to flow through the column, then it is washed away. Finally, Rtx elution is performed with a solution containing imidazole, which releases biotinylated Rtx from the column. **(C)** The number of biotin groups added per Rtx molecule is shown for different excesses of NHS-PEG-biotin. *Black bars*: NIMAC column; *white bars*: biotinylation in solution.

In order to minimize the overall modification of Rtx and to obtain the most homogeneous Rtx-biotin preparation, biotinylation on the NIMAC support was henceforth performed with a 10-fold molar excess of NHS-PEG-biotin with respect to Rtx. This resulted in high yields of samples of Rtx-biotin containing, on average, between 1 and 2 biotin groups per Rtx molecule (Figure 3.3C).

3.4.5 Different Ab-LNP valences are achieved by taking advantage of the slow association dynamics between Ab-biotin and Neut-LNP

The final step in creating Ab-LNPs involved coupling Ab-biotin to Neut-LNP. In carrying out this coupling reaction, it was uncovered that the association of Rtx-biotin and Neut-LNP is actually a relatively slow process; the amount of bound Rtx-biotin continued to increase up to 72 h after the start of coupling. This was surprising since the interaction between biotin and Neut is one of the strongest noncovalent interactions known ($K_D = 10^{-15}$ M)[161], and mixing Rtx-biotin and free Neut in solution often causes the immediate formation of a precipitate, indicating very rapid association.

This significant reduction in coupling dynamics has not been previously described in a parallel application, and it is a key feature of the methodology described here. It provides a practical way of obtaining different valences of Ab-LNPs: fractions of the same coupling reaction can be stopped at consecutively longer time points, resulting in successively higher valences. **Figure 3.4** shows three different sets of reaction conditions (mole ratios of added Rtx-biotin to Neut), and in all cases, the number of moles of Rtx-biotin associated to Neut-LNP increased from an incubation time of 1 h to 72 h. For example, when the added mole ratio of Rtx-biotin to Neut (in Neut-LNP) was 0.5, the mole ratio of coupled Rtx to Neut (in Rtx-LNP) was 0.25 after 1 h and 0.47 after 72 h ($p < 0.05$); when the added Rtx-biotin to Neut mole ratio was increased to 2.0, the coupled mole ratio of Rtx to Neut was 0.28 after 1 h and 1.4 after 72 h ($p < 0.005$). The slow kinetic of association therefore provide great versatility to the methodology since many different Ab-LNP valences can be prepared from one or two Neut-LNP preparations and one sample of Ab-biotin.

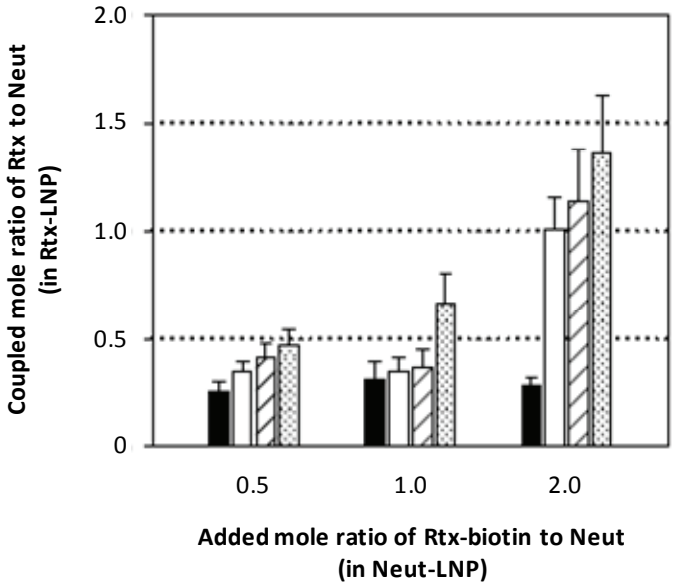

Figure 3.4 Control over the valence of Rtx-LNP when coupling Rtx-biotin to Neut-LNP.

The final valence of Rtx-LNP can be controlled by both the added mole ratio of Rtx-biotin with respect to Neut (in Neut-LNP) and the length of time that the coupling reaction is allowed to proceed. Note that for each value on the horizontal axis, a 100 % coupling efficiency is represented by the same value on the vertical axis. Reaction times: *black bars*: 1 h; *white bars*: 24 h; *hatched bars*: 48 h; *dotted bars*: 72 h.

Figure 3.4 indicates that in general, for equivalent reaction times of 24 h or longer, the amount of associated Rtx-biotin increases when higher excesses of Rtx-biotin (with respect to Neut) are added. Using these higher mole excesses, however, had the disadvantage of lower yields; in general, the coupling efficiency increased as less Rtx-biotin was added with respect to Neut. Importantly, coupling efficiencies close to 100% (represented by equal values on the horizontal and vertical axes) were obtained at a mole ratio of Rtx-biotin to Neut of 0.5 and by allowing the reaction to proceed for 72 h. (A 100% coupling efficiency does not represent a 100% yield since Ab, coupled to Ab-LNP, will invariably be lost during ensuing purification.)

Figure 3.4 also shows that although Neut has four biotin-binding sites (three available to bind to Rtx-biotin), Neut-LNP bound a maximum of 1.4 Rtx-biotin molecules per Neut. Although this stoichiometry likely resulted from PEG blocking the biotin-binding sites on Neut[148], one concern was

that aggregation might occur over time from unbound biotin groups on Rtx-biotin and free biotin-binding sites on Neut. Thus in an effort to reduce the available biotin-biding sites, some samples were prepared where excess free biotin was added at the end of coupling and incubated for 1h before purification. Over the course of one month, the sizes of Rtx-LNPs prepared with or without addition of biotin were measured at regular intervals and were found to remain constant at ~130 nm (data not shown). The ability of both types of preparations to induce apoptosis in lymphoma cells was also found to be similar and we therefore concluded that Rtx-LNPs were stable without the addition of excess biotin.

3.5 Discussion and conclusions

3.5.1 Discussion

The work described in this chapter has uncovered that the kinetics of the association between biotinylated protein and PEGylated liposomes containing an avidin analog are surprisingly slow. The slow association kinetics comprise a central feature of the improved methodology for preparing Ab-LNPs described here. The use of avidin-biotin interactions to couple proteins to liposomes is not a new concept, but one reason why the slow kinetics have not been previously described may be that, by and large, this type of coupling has been performed using liposomes lacking PEG[147, 162, 163]. In aqueous solution, however, a similar phenomenon involving biotinylated PEG and avidin has been attributed to a steric effect where the PEG chains effectively block the biotin-binding sites on the avidin molecules[148]. One unanswered question is how the presence of PEG on the liposome affects the kinetics of other types of coupling reactions, such as those that employ thiol-maleimide chemistry.

The effect of PEG blocking lends significant efficiency to the methodology because many different valences can be produced from single batches of Neut-LNP and Ab-biotin; the two reagents need only be mixed in different proportions and incubated for different times between 1 h and 72 h to produce different valences (Figure 3.4). This is in contrast to having to prepare a different Neut-LNP for every desired valence, which would be significantly more cumbersome and time-consuming. It should be noted that one case where this more time-consuming strategy would be desirable is a situation of severely limited Ab availability; this is because the reaction conditions leading to 100% coupling efficiencies could be employed for every valence (mole ratio of Ab-biotin to Neut = 0.5; Figure 3.4). Overall, the methodology is therefore versatile and easily adaptable to different circumstances of time and Ab availability.

Two other features of the methodology also served to improve the yields of coupled Ab (Table 3.1) and the reproducibility of the procedure: elimination of thiol-maleimide chemistry, and use of the NIMAC support to biotinylate the Ab. The NIMAC column enabled a very high yield of recovered biotinylated Ab (96 %) as well as a more homogeneous product with only 1 to 2 modified amine groups per Ab (using a 10-fold excess of NHS-PEG-biotin; Figure 3.3) compared to 3-7 thiol groups per Ab using thiol-maleimide coupling. The NIMAC method also has the advantage of very mild reaction and elution conditions; unlike the thiol-maleimide method, all steps take place at pH 7.4 at room temperature, which may aid in the conservation of native Ab structure.

As shown in Table 3.1, thiol-maleimide coupling followed by post-insertion of Ab may exhibit a high coupling efficiency, but the start-to-finish yield of Ab is much lower. Replacing thiol-maleimide chemistry also improved reproducibility due to the inherent problem that only one DSPE-PEG-maleimide molecule is required per Ab, but higher-order adducts inevitably result since the reaction must be carried out under an excess of DSPE-PEG-maleimide[142]. Exposed thiol groups on the Ab are also known to undergo oxidation into disulfide bonds[164], which along with the higher-order adducts, not only affect Ab structure and function but also constitute mechanisms of

interliposomal crosslinking. A further problem is that maleimide groups are particularly prone to hydrolysis at elevated temperatures (such as 65 ^{o}C, used for extrusion) and at pH levels above 7 (ref. 165). With the improved methodology, the issues of nonhomogeneous thiolation and adduct stoichiometry, disulfide bond formation, and maleimide hydrolysis have been eliminated and reproducibility has been improved.

The improved Ab-LNP preparation methodology may serve to identify therapeutic Abs that are more efficacious in a multivalent configuration and to identify the optimal valence of such Abs; it has been estimated that valences up to ~400 (200 IgG) can theoretically be achieved on a 100 nm-diameter liposome[141] although the highest valence achieved in sufficient yield with the current improved methodology was 250. Optimal valence information can be translated into non-liposomal multivalent Ab constructs where it might otherwise be more difficult or time-consuming to produce many different valences. These alternative multivalent Ab constructs may include Ab-coupled gold nanoshells[96], Ab-dendrimer conjugates[95], polymeric nanoparticles[166], or different types of multifunctional nanoparticles[167]. Using liposomes to create multivalent Abs also does not necessarily exclude the possibility of their application to immunoliposomes that contain encapsulated drug. Indeed, it should be noted that the methodology would be very useful in the development of targeted liposomal formulations where the effects of varying the protein-to-lipid ratio are being studied.

3.5.2 Conclusions

The methodology described above provides a means of studying therapeutic Ab multivalency in order to determine whether Abs under development may be more efficacious as multivalent rather than bivalent molecules. Compared to previous methods, the improved methodology described here is more time-efficient and reproducible, and also results in higher yields of coupled Ab. With this optimized methodology, studies which examine how the valence of a

therapeutic Ab affects its efficacy can now be carried out. For example, the different valences of Ab-LNP can be employed to identify the optimal valence of the Ab and to probe the mechanism of action of the multivalent drug. The resulting information could potentially be applied to the development of different liposomal and non-liposomal multivalent therapeutic Abs.

4 Unique biological properties of rituximab-lipid nanoparticles

4.1 Synopsis

This chapter examines the properties of different valences of Rtx-LNPs prepared using the improved methodology described in Chapter 3. These properties include binding characteristics to $CD20^+$ lymphoma cells, distribution of Rtx-LNPs on the cell surface, modulation of CD20 expression, cytotoxicity of the constructs, and ability of the different valences to directly induce apoptosis.

4.2 Background

4.2.1 Properties of different types of multivalent anti-CD20 Abs

Various designs of multivalent anti-CD20 Abs have been described, and in general, these constructs exhibit superior binding to target cells as well as elevated therapeutic activity *in vitro* and in some cases *in vivo*. Evidence of superior binding to $CD20^+$ lymphoma cells has been provided by multivalent Rtx constructs such as multivalent Rtx-gold nanoshells[96] and anti-CD20 multivalent branched copolymer-Fab conjugates[15]. Enhanced binding is consistent with the increased avidity of multivalent ligands that is usually observed, as described in Section 1.6. In spite of observations of improved binding, studies are scarce regarding the specific interaction of the multivalent Ab with the target on the cell surface. For example, when the multivalent Ab is bound to the cell, it is not known whether all Ab molecules in the construct are bound to CD20, or if there is a fraction that remains unbound.

Several studies have described therapeutic improvements in multivalent Rtx constructs compared to bivalent Rtx, and it is generally understood that this results from hypercrosslinking of CD20 in the plasma membrane. Ghetie *et al.* created tetravalent Rtx and $F(ab')_2$ homodimers, which

inhibited the growth of several different B-lymphoma cell lines *in vitro* through the induction of apoptosis, while monomeric Rtx had no such effect. Apoptosis did not depend on the presence of Fc receptors nor on the density of cell-surface CD20 on the target cells, and Rtx homodimers sensitized drug-resistant $CD20^+$ B-lymphoma cells to chemotherapy[88]. Zhang and colleagues prepared Rtx-dextran polymers (valence ~10) which induced significantly elevated apoptosis in several $CD20^+$ cell lines but not in $CD20^-$ lymphoma cell lines. This polymer also showed an extended circulation half-life compared to bivalent Rtx as well as producing a marked regression in $CD20^+$ lymphoma xenografts, while Rtx dimer and monomer showed little effect *in vivo*[75]. Trivalent and tetravalent Rtx constructs obtained through protein engineering were prepared by Miller *et al.*; many configurations of constructs were prepared with tandem Fab repeats (with or without Fc regions) in order to mimic crosslinked Rtx. Bivalent Rtx induced low levels of apoptosis while many of the multivalent constructs induced elevated apoptosis without crosslinking[89]. A final example from Rossi and colleagues involves the use of a technique known as the Dock-and-Lock method for creating hexavalent anti-CD20 constructs that comprise six Fab fragments and one Fc fragment. These constructs inhibited proliferation in $CD20^+$ lymphoma cells without a crosslinking Ab, and they induced ADCC although CDC was completely abolished[90].

These studies demonstrate clear benefits to employing multivalent Rtx constructs as opposed to bivalent Rtx. Importantly, nearly all reports on multivalent Rtx have employed constructs with valences that generally do not exceed 10. Higher valences are occasionally employed when different types of nanoparticle formulations are saturated with Ab, but the valences of such constructs are undefined and/or quite heterogeneous. Multivalent Rtx-LNPs, on the other hand, represent constructs of defined valence, and valences as high as 250 have been obtained in sufficient quantities for *in vitro* experiments.

4.2.2 Hypotheses concerning the observed increases in apoptosis induced by Rtx-LNP

Previous work has shown that Rtx-LNPs of valence ~90 induce significantly elevated levels of apoptosis in target lymphoma cells compared to bivalent Rtx (Fig. 2.2C & D)[7, 16]. There are two possible scenarios with respect to this observed enhancement of the direct mechanism of action: (1) the chemical modification imparted on the Ab and coupling to liposomes induces an increase in the apoptotic potency of the Ab itself, or (2) the multivalent Ab, through hypercrosslinking of its target in the plasma membrane, is responsible for the enhanced apoptosis through an undefined mechanism. For equivalent doses of Rtx, scenario (1) would result in equal amounts of apoptosis induced by Rtx-LNPs of different valence because the effect is due specifically to the Ab; this would result in valence-independent levels of apoptosis. On the other hand, scenario (2) would show valence-dependent apoptosis levels because the valence is correlated with the degree of crosslinking that the Ab is able to impart; higher valences can hypercrosslink more appreciably than lower valences.

These scenarios can be tested by creating Rtx-LNPs of different valence using the methodology described in Chapter 3 and adding them to $CD20^+$ lymphoma cells to determine whether the resulting levels of apoptosis are valence-independent or -dependent. With the ability to reproducibly prepare specific valences over a wide range (2 to 250), we are able to carry out one of the first studies that systematically examines the effects of increasing degrees of target hypercrosslinking brought about by different valences of multivalent Abs.

4.3 Materials and methods

4.3.1 Materials

Rituximab (Rtx) and trastuzumab (Trz) were obtained from the BC Cancer Agency pharmacy (Vancouver BC, Canada). Hanks' balanced salt solution (modified, without phenol red) was purchased from Stemcell Technologies (Vancouver BC, Canada). AlamarBlue, Annexin-V binding buffer, recombinant human Annexin-V labelled with fluorescein isothiocyanate (Annexin-V-FITC), and an Alexa Fluor 647 (A647) monoclonal antibody labeling kit were from Invitrogen (Burlington ON, Canada). FITC-labeled anti-Rtx Ab (FITC-anti-Rtx), A647-labeled monoclonal anti-CD20 Ab (A647-mCD20), and A647-labeled mouse IgG2a negative control Ab (A647-neg) were from AbD Serotec (Kidlington, UK). Glass cover slips (8 mm) and paraformaldehyde were purchased from Electron Microscopy Sciences. Phycoerythrin-conjugated anti-human-IgG Ab (PE-anti-IgG) and polyclonal anti-CD20 Ab were purchased from Santa Cruz Biotechnology (Santa Cruz CA, USA). FluorSave reagent was obtained from Calbiochem (Billerica MA, USA). Unless noted otherwise, all other reagents were obtained from Sigma-Aldrich and were of the highest quality available.

4.3.2 Cell lines

Ramos cells (a Burkitt's lymphoma cell line) were a kind gift from Dr. Robert Kay (Terry Fox Laboratory, Vancouver BC, Canada), and Z138 mantle cell lymphoma cells were generously provided by Dr. Zeev Estrov (University of Texas) and previously characterized[127]. Both cell lines were maintained in RPMI 1640 medium from Stemcell Technologies (Vancouver BC, Canada) supplemented with 10 % (v/v) fetal bovine serum and 2 mM L-glutamine from Invitrogen, as well as penicillin-streptomysin from Stemcell Technologies. Cells were maintained at 37 °C in a humidified atmosphere containing 5% CO_2.

4.3.3 Preparation of Rtx-LNPs

Rtx-LNPs were prepared using the methodology described in Chapter 3 and summarized in Figure 3.1. Three separate batches of four valences each were prepared over the course of approximately six weeks and the resulting valences ranged from 13 to 165. The valences and Rtx concentrations in each preparation were quantified as described in the previous chapter.

4.3.4 Measurement of levels of bound Rtx and free CD20 after treatment with Rtx or Rtx-LNP

To examine the relationship between the amount of Rtx bound to $CD20^+$ B-cell lymphoma cells and the levels of CD20 on the cell surface that are free from Rtx, 1.25×10^5 Ramos or Z138 cells in 250 µL medium were treated with doses of Rtx or Rtx-LNP ranging from 0–30 µg. After a 1 h incubation at 37 ^{o}C, the cells were transferred to Eppendorf tubes, washed with cold PBSB (phosphate-buffered saline (PBS) + 0.1% bovine serum albumin, pH 7.4), resuspended in 20 µL PBSB, and stained with 1 µL each of FITC-anti-Rtx and A647-mCD20. The latter Ab is blocked from binding to CD20 if Rtx is already bound, and the former one measures levels of Rtx. After staining for 1 h on ice, cells were washed with PBSB, then resuspended in 300 µL PBSB, filtered through 35 µm strainers, and analyzed on a FACSCalibur flow cytometer (Becton Dickinson, San Jose, CA) collecting 10,000 events for each sample. Fluorescence intensities were obtained from analysis using FlowJo software, and triplicates were averaged to obtain mean fluorescence intensities (MFIs). For each dose, the MFI from the appropriate negative control was subtracted from each measured MFI value before being scaled relative to the maximum value for each stain. Data values are reported in all cases as mean ± standard deviation (SD).

4.3.5 Confocal laser-scanning fluorescence microscopy of treated cells

Ramos and Z138 cells were divided in 48-well plates with 2.5×10^5 cells in 500 µL medium per well. Rtx-LNPs and free Rtx were diluted to obtain equal Rtx concentrations across all samples, and the required volume of Rtx-LNP or free Rtx was calculated. Generally, the treatment volume was between 100 and 200 µL for a 10 µg dose of Rtx. After treatment times of up to 48 h, cells were spun in a microcentrifuge at 7000 rpm for 15 s, washed with serum-free medium (also free of L-glutamine and penicillin-streptomysin), then resuspended in 500 µL of cold serum-free medium. In a cold room, a 50 µL volume of this suspension (5×10^4 cells) was transferred to an Eppendorf tube and 1 µL of PE-anti-IgG was added. The suspension was mixed and transferred onto an 8 mm poly-L-lysine glass cover slip onto which cells were allowed to adhere for 1 h on ice. Liquid was then removed from the cover slip, it was gently washed with HBS, then cells were fixed by applying a 75 µL drop of 4% paraformaldehyde for 20 min at room temperature. After fixing, the cover slip was washed with HBS before mounting onto a glass slide using 10 µL of FluorSave. Samples were allowed to dry overnight in closed Petri dishes protected from light, and were imaged within two days on a Bio-Rad 2100MP confocal and multiphoton microscope controlled by Zeiss/Biorad Lasersharp 2000 software. Negligible staining was observed in fluorescence images of control samples consisting of Ramos cells not treated with Rtx (data not shown).

4.3.6 Measurement of total CD20 levels in treated cells

A polyclonal anti-CD20 Ab was labeled with A647 using an antibody labeling kit according to the manufacturer's instructions. Unlike the monoclonal A647-mCD20 described in Section 4.3.4, the resulting A647-labeled polyclonal anti-CD20 Ab (A647-pCD20) exhibited equivalent staining of CD20 in the presence and absence of Rtx (data not shown). Ramos and Z138 cells were divided in 48-well plates with 2.5×10^5 cells in 500 µL medium per well, and were treated with a 10 µg dose of Rtx or Rtx-LNP. After an incubation of up to 48 h, cells were stained with PI and A647-pCD20, and were

analyzed using flow cytometry, as described in Section 4.3.4. Before analysis, cells were resuspended in PBSB containing 0.5 μg/mL propidium iodide (PI), and A647-pCD20 MFI values in all cases were calculated based on data from the viable (PI^-) populations. Here and in all subsequent cases, two-tailed unpaired Student's *t*-tests were applied with a level of significance of 0.05.

4.3.7 Measurement of mitochondrial activity using AlamarBlue

To evaluate the cytotoxicity of Rtx and Rtx-LNPs, AlamarBlue was employed to measure mitochondrial activity in samples of treated cells. In a 96-well plate, 5×10^3 Ramos or Z138 cells in 100 μL medium were added to the wells, followed by 50 μL/well of Rtx or Rtx-LNP at doses ranging from 0.2 to 2000 ng/well. After a 96 h incubation, 10 μL of AlamarBlue were added per well, and plates were incubated for a further 6 h before fluorescence measurements were obtained in a Fluorstar plate reader with excitation and emission wavelengths of 544 nm and 590 nm, respectively. Larger emission intensities corresponded to higher mitochondrial activities and greater fractions of viable cells.

4.3.8 Annexin-V/PI apoptosis assay using flow cytometry

This assay was also described in Section 2.3.6, but the modifications described here apply to this and all subsequent chapters. A total of 2.5×10^5 cells in 500 μL medium were treated with a 10 μg dose of Rtx. For time-course experiments, cells were incubated at 37 ^oC for 4 to 72 h, and all other experiments involved a 24 h incubation at 37 ^oC. Cells treated with an equivalent mass of Trz were used as negative controls, and for positive controls, cells were treated with 4.0 μM camptothecin at 37 ^oC for 4 h. For analysis, samples were transferred to 1.5 mL Eppendorf tubes and spun in a microcentrifuge at 7000 rpm for 15 s. Pellets were washed with 500 μL cold Hanks' balanced salt solution. Different positive control samples were unstained, single-stained, or double-stained with Annexin-V-FITC and/or propidium iodide (PI); all other samples were double-stained.

Double staining consisted of resuspending the pellets in Annexin-V-FITC (5 µL) and binding buffer (40 µL), incubating at room temperature for 20 min, then adding 500 µL of a cold 0.5 µg/mL solution of PI in Hanks'. Samples were strained through 50 µM strainers, kept on ice, and analyzed within 1 h on a Becton Dickinson FACSCalibur flow cytometer. Compensation values were set with positive controls and at least 10,000 events were recorded for each sample. Early apoptotic cells were defined as PI negative and Annexin-V-FITC positive, necrotic cells were positive for both fluorophores, and viable cells were negative for both.

4.4 Results

4.4.1 Rtx-LNPs exhibit unique binding properties to CD20$^+$ target lymphoma cells

In order to assess differences in binding properties of multivalent Rtx-LNPs compared to bivalent Rtx, two different CD20$^+$ cell lines were employed: Ramos, a Burkitt's lymphoma cell line, and Z138, a mantle cell lymphoma cell line. Two values were measured using flow cytometry: the amount of Rtx that became bound to the cells, using a FITC-anti-Rtx Ab, and the amount of CD20 on the cell surface free from bound Rtx, using the A647-mCD20 Ab (see Section 4.3.4). The binding of Rtx to CD20 completely inhibits the binding of A647-mCD20, thereby providing a practical way of measuring unbound CD20. A titration of bivalent Rtx was first performed across a 0–30 µg dose range given to 1.25×10^5 Ramos cells. As shown in **Figure 4.1A**, the amount of unbound CD20 (white bars) began to decrease at doses of 0.03 µg and above ($p < 0.05$ between the 0.01 and 0.03 µg doses), and at doses above 0.3 µg, essentially all cell-surface CD20 molecules were saturated with Rtx as reflected by the relative MFI values of zero (within error), which represent MFI values roughly equal to those of negative isotype controls. In terms of the amount of bound Rtx (black bars),

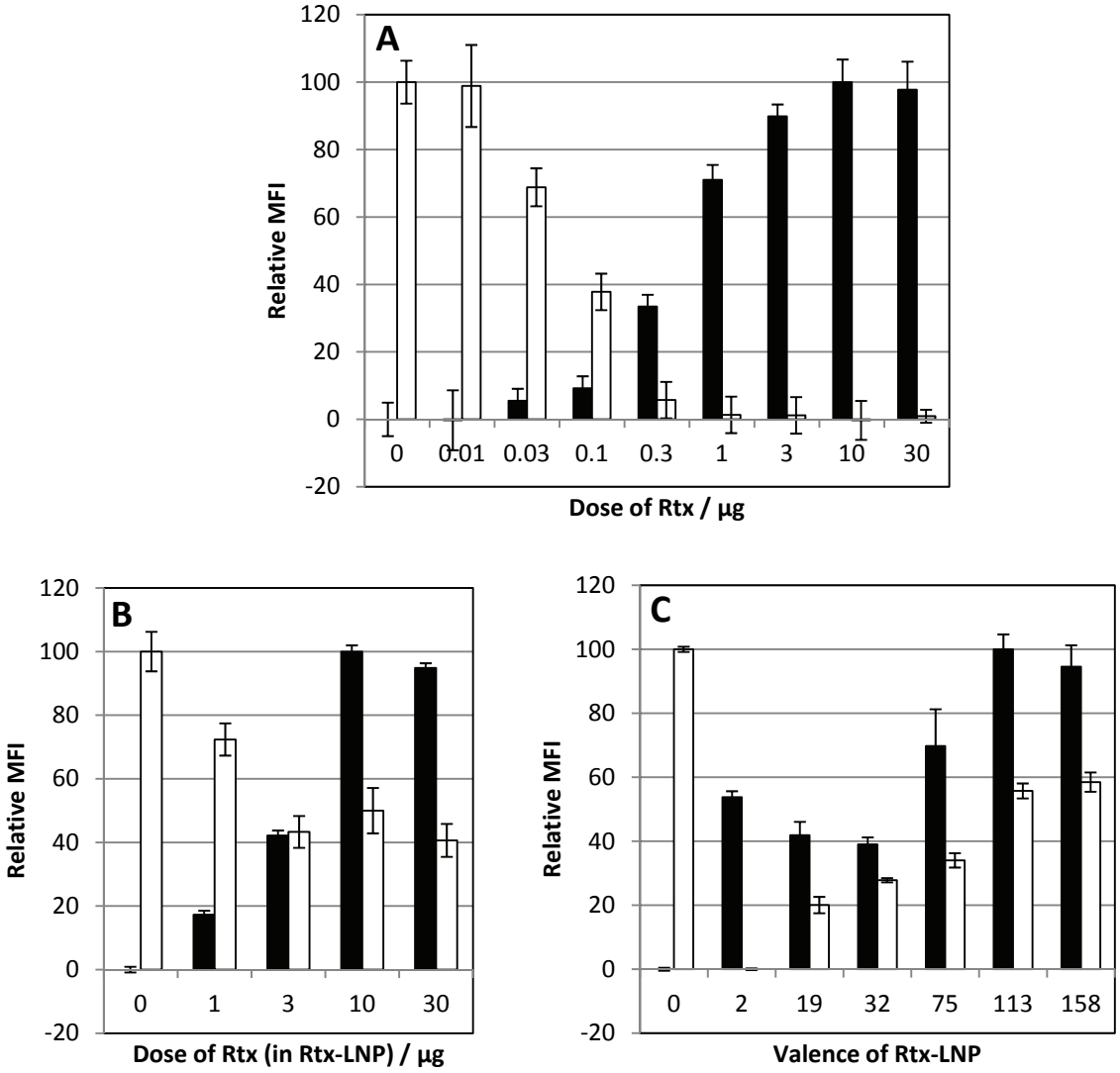

<u>Figure 4.1</u> Levels of bound Rtx and unbound CD20 show an inverse correlation when cells are treated with bivalent Rtx but not with Rtx-LNP.

In all cases, 1.25×10^5 Ramos cells in 250 µL medium were treated with Rtx or Rtx-LNP, then analyzed for levels of bound Rtx (*black bars*) and unbound CD20 (*white bars*). **(A)** The indicated doses of bivalent Rtx were given, and the results show an inverse correlation between the amount of bound Rtx and the level of unbound CD20. **(B)** Cells were treated with Rtx-LNP(158), and although the same relationship was observed compared to cells treated with Rtx, there was still a significant proportion of unbound CD20 at the highest dose. **(C)** Rtx-LNPs of different valence were administered to Ramos cells at the 3 µg dose. Lower valences showed similar levels of bound Rtx to bivalent Rtx, but as the valence was increased at the same dose, the amount of unbound CD20 also increased. Higher valences also showed more elevated levels of bound Rtx. *Black bars*: FITC-anti-Rtx staining; *white bars*: A647-mCD20 staining. *MFI*: mean fluorescence intensity.

measurable amounts appeared at doses of 0.03 μg and above, and the cells were saturated with Rtx at doses of 3 μg and above ($p < 0.005$ between 1 and 3 μg doses; $p > 0.05$ for the 3, 10, and 30 μg doses). At doses between 0.1–0.3 μg, there were measurable amounts of both bound Rtx and free CD20, indicated that the cells were only partially saturated at these doses, and suggesting that the point where the cells were half-saturated (equal values of white and black bars) lied between these two doses. Apart from Rtx saturation data in Ramos cells, this figure illustrates that the Abs employed in this assay function as expected, given the excellent inverse correlation observed between the data reported from the two Abs. Similar data was observed using the Z138 cell line (data not shown).

A similar titration was next carried out using Rtx-LNP of valence 158 (Rtx-LNP(158)), and the data that was obtained is shown in **Figure 4.1B**. As with the data shown for bivalent Rtx, the measured amount of bound Rtx detected using FITC-anti-Rtx increased as the dose of Rtx-LNP(158) increased, but the dose at which Rtx-LNP(158) saturated the cells was found to be 10 μg, which is higher than that of Rtx. Moreover, the unscaled MFI measured when cells were saturated with Rtx-LNP(158) (10 μg dose) was 984 after subtracting negative isotype control; this value is 10.0 times higher than the same value for bound bivalent Rtx at the same dose in Figure 4.1A (98.7). This shows that the Ramos cells are able to bind significantly more multivalent Rtx-LNP compared to bivalent Rtx.

In spite of the higher levels of bound Rtx, Figure 4.1B shows a significant fraction of CD20 on the cell surface that does not have Rtx bound to it at doses of 3 μg and above ($p > 0.05$ for 3, 10, and 30 μg doses), which includes saturating doses. For example, at the 30 μg dose of Rtx-LNP(158), 41% of the CD20 on the cell surface is free of Rtx. Therefore, at saturating doses, although significantly higher levels of Rtx are bound to cells after treatment with Rtx-LNP compared to bivalent Rtx, only a fraction of the Rtx in Rtx-LNP physically binds to CD20, since under one half of the CD20 molecules on the cell surface are free of Rtx when cells are saturated with Rtx-LNP. Note that the scaling of

black bars is different between Figures 4.1A–C, but the scaling of white bars is roughly the same; the white bars are scaled according to cells in the absence of Rtx, but the black bars are scaled according to the maximum measured levels of bound Rtx.

Finally, Ramos cells were treated with equivalent doses (3 μg) of Rtx-LNPs of different valence, and the binding properties were examined in the same way. The 3 μg dose was selected because as shown in Figure 4.1B, the cells were not saturated with Rtx-LNP(158) at this dose, but cells treated with bivalent Rtx were just saturated, as indicated in Figure 4.1A. **Figure 4.1C** summarizes the data for the treatment with the different valences. The first feature worth noting is that at the same dose of Rtx-LNP, the lower valences (19 and 32) show equal levels of bound Rtx ($p > 0.05$) that are roughly equivalent to those measured for bivalent Rtx (albeit $p < 0.05$ between these valences and valence 2). Valences 2, 19, and 32, however, show increasing levels of unbound CD20 as the valence increases ($p < 0.05$ for all pairs of valences). As with the Rtx-LNP titration in Figure 4.1B, this suggests that not all Rtx in Rtx-LNP is bound to CD20 on the cell surface at the same time, but that at any given time there is a fraction of Rtx associated to the LNP that is not bound to CD20.

At this same dose, as the valence increased above 32, more and more bound Rtx was measured; for example, the unscaled MFI for Rtx-LNP(32) was 133, while that for Rtx-LNP(113) was 343, representing a 2.6-fold increase in the Rtx signal ($p < 0.0001$) even though cells were given the same dose of Rtx. Because the dose that was employed is below saturating levels, this suggests a greater avidity of the Rtx-LNPs of higher valence. Finally, even though the measured amount of bound Rtx increased with the valence, so did the measured amount of unbound CD20, which was as high as 58% unbound CD20 at the highest valence of 158. Valences of 113 and 158 showed equivalent levels of bound Rtx and unbound CD20 ($p > 0.05$ for both parameters). This further suggests that as opposed to bivalent Rtx, which is spread evenly across the cell surface, the binding of Rtx-LNP causes some plasma-membrane CD20 to be present in very high local concentrations, while some CD20 is not bound to Rtx. In other words, this supports the existence of Rtx/CD20

clusters that form between a fraction of Rtx in Rtx-LNP and a fraction of CD20 present in the plasma membrane.

4.4.2 Rtx-enriched domains are found on cells treated with Rtx-LNP but not on those treated with bivalent Rtx

To examine the organization of Rtx/CD20 in the plasma membrane, the distribution of Rtx on the cell surface was investigated using confocal laser-scanning fluorescence microscopy. Cells were treated with Rtx or Rtx-LNP for different times then stained with an anti-Rtx Ab to label Rtx on the cell surface. The images that were obtained, as shown in **Figure 4.2**, indicate that Rtx and Rtx-LNP became bound to Ramos cells as soon as 15 min after treatment, and remained associated 24 h later. Rtx remained associated up to 48 h post-treatment, and no staining was observed in the absence of Rtx (not shown). Cells that were treated with free Rtx showed a relatively uniform distribution of Rtx over the surface of the cell, but cells treated with Rtx-LNP exhibited Rtx-enriched domains with significantly elevated fluorescence intensities on the cell surface (arrows in Figure 4.2). The size of the domains was < 500 nm and they were visible at all time points between 15 min and 24 h after treatment with Rtx-LNP, although they were most prevalent after 45 min. At this time point, there were between 0 and ~15 domains per cell, as found by counting the domains observed in *z*-stacked images (on average, 10 slices per cell). No domains were present on Rtx-treated cells at any time, but a qualitative rise in the number of domains per cell was observed as the valence increased: on average, valence 53 showed ~5 domains/cell and valence 121 showed ~15 domains/cell. Overall, these images support the binding data in Figure 4.1 which showed that for equivalent doses, cells treated with the higher valences of Rtx-LNP bound more Rtx but had more unbound CD20. The result is the formation of Rtx-enriched domains on the cell surface after treatment with Rtx-LNP, with a greater number of domains being formed as the valence increases.

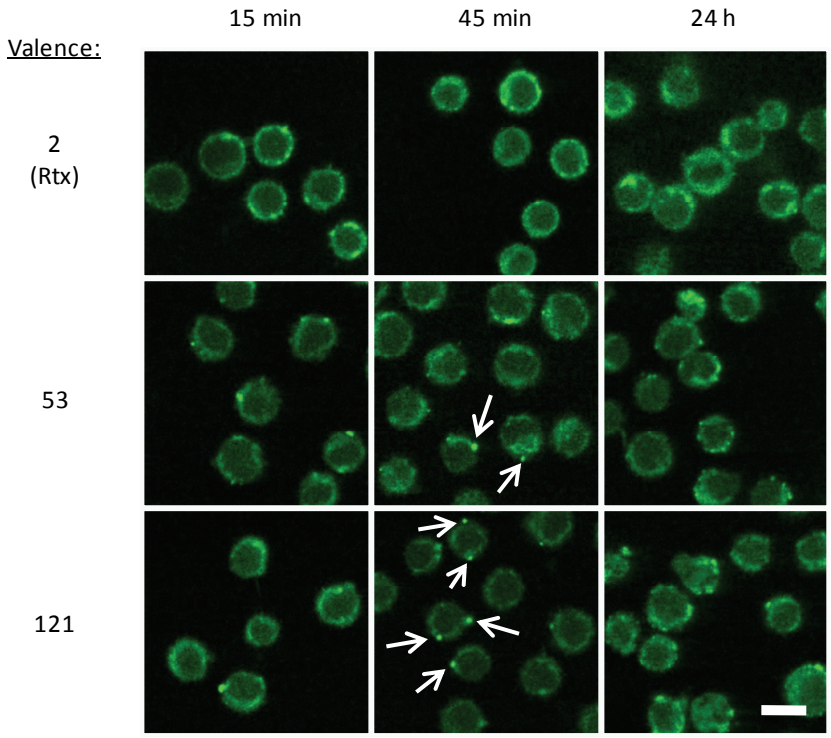

Figure 4.2 Representative confocal fluorescence microscopy images of Rtx distribution on Ramos cells treated with Rtx or Rtx-LNP.

The distribution of Rtx on the cell surface is shown at the indicated time points after treatment with Rtx or Rtx-LNP. As early as 15 min after treatment, and more pronouncedly at 45 min, Rtx-enriched domains appeared on the surface of the cells treated with Rtx-LNP (arrows) but not those treated with Rtx. *Bar*: 5 μm.

4.4.3 Expression of CD20 does not change substantially after treatment with Rtx-LNP

The previous two sections showed that at the same dose of Rtx, $CD20^+$ lymphoma cells bound more Rtx as the valence of Rtx-LNP increased. The increased levels of bound Rtx occurred although a significant fraction of CD20 on the cell surface was free from any bound Rtx, resulting in the formation of Rtx/CD20-enriched clusters in the plasma membrane. One important possibility that could be responsible for this effect is that Rtx-LNPs may cause an upregulation of CD20 to the cell surface after binding, which would not only help explain the increased binding capacity of Rtx

but also the large fraction of unbound CD20. Note, however, that the data in Figure 4.1 was obtained at a time point of 1 h post-treatment.

The total expression of CD20 in the plasma membrane was therefore measured after treatment with Rtx and Rtx-LNP at time points up to 48 h after treatment. This was done using an A647-labeled polyclonal anti-CD20 Ab (A647-pCD20; see Section 4.3.6). Unlike the monoclonal A647-mCD20 used in Section 4.4.1, no measurable interference was observed in the A647-pCD20 signal when cells were pretreated with Rtx or Rtx-LNP (data not shown). The time course of CD20 expression in the plasma membrane after treatment with Rtx or Rtx-LNPs is summarized in **Figure 4.3**. At all time points, levels of CD20 in the plasma membrane of cells treated with Rtx (light gray bars) were roughly equivalent to those in cells treated with HBS, as indicated by the relative MFI values of ~1. At the 8 h time point, CD20 expression after Rtx-LNP(52) and Rtx-LNP(170) treatment was maximal; measured MFI values were 1.7 and 1.9 times those measured in HBS-treated cells, respectively. These elevated levels of CD20 in PI^- cells were sustained up to 48 h post-treatment. Between all treatments up to and including 8 h, there was no significant difference between any of the treatments ($p > 0.05$ between all possible pairs of treatments). With the exception of the 16 h time point, there was no significant difference between the measured CD20 expression after Rtx-LNP(52) and Rtx-LNP(170) treatment ($p < 0.05$ only at 16 h). At 16 h and longer, however, the differences between Rtx and either Rtx-LNP treatment were significant ($p < 0.05$ between Rtx and Rtx-LNP(52) and $p < 0.01$ between Rtx and Rtx-LNP(170) in all cases).

It is unlikely, however, that the increases in CD20 expression after Rtx-LNP treatment (~1.5 times those measured in cells treated with Rtx) explain the data in Figure 4.1 showing up to 10.0-fold higher levels of bound Rtx-LNP compared to bivalent Rtx. Moreover, such a modest increase in CD20 expression cannot account for the high levels of unbound CD20 (up to 58%) that were also measured after treatment with Rtx-LNP. These data therefore do not support the hypothesis that the results shown in Figures 4.1 & 4.2 were an effect of CD20 upregulation. They suggest instead

that a reorganization of CD20 in the plasma membrane occurred following Rtx-LNP treatment, forming CD20/Rtx-enriched microdomains that may play a role in the therapeutic activity of these constructs.

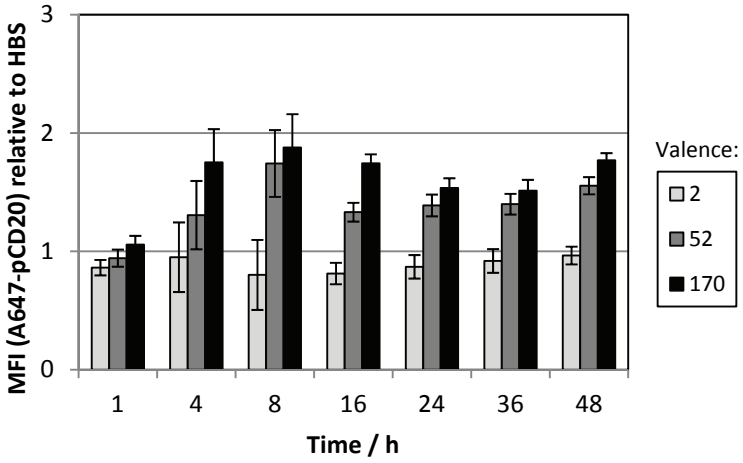

Figure 4.3 Time course of plasma-membrane CD20 expression in Ramos cells treated with Rtx or Rtx-LNP.
Using a polyclonal anti-CD20 Ab (A647-pCD20), the total CD20 expression in the plasma membrane of PI^- cells was measured at different times after treatment with Rtx or Rtx-LNP. *MFI*: mean fluorescence intensity.

4.4.4 Cytotoxicity of Rtx-LNPs in two lymphoma cell lines

To assess the cytotoxicity of Rtx-LNP, a range of valences were added to Ramos and Z138 lymphoma cells. Five doses of Rtx were selected (0.2–2000 ng; see Section 4.3.7) based on the binding data in Figure 4.1 as well as on doses employed in previous studies[74, 168, 169]. Cells were incubated for 96 h with the various Rtx-LNP preparations or with free Rtx (valence 2) at each dose. **Figure 4.4** shows that in both cell lines at the highest dose (2.0 μg), all Rtx-LNP valences were significantly more cytotoxic than free Rtx ($p < 0.0005$ for all valences). At this dose, 39% of Ramos cells were viable after treatment with Rtx with respect to control cells, compared to ≤ 1% viable cells for all Rtx-LNPs. At the same dose, Z138 cells showed 86% viability with respect to control after Rtx treatment, compared to 25–42% viability after treatment with Rtx-LNPs.

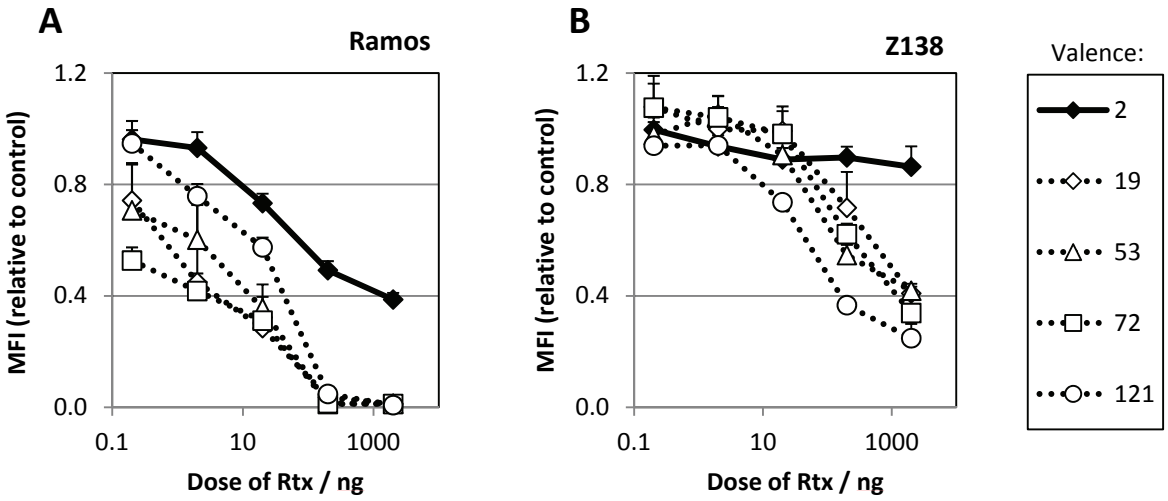

Figure 4.4 Particularly at higher doses, Rtx-LNPs are significantly more cytotoxic than equivalent doses of free Rtx.
To each well of a 96-well plate, 5×10^3 cells in 100 µL medium were added followed by 50 µL medium containing the dose of Rtx indicated above. The control consisted of medium only. Plates were incubated for 96 h and cell viability was measured using AlamarBlue.

Overall, Ramos cells were more sensitive to the cytotoxic effects of Rtx-LNP, and for doses of 2.0 ng and above, all Rtx-LNP valences were significantly more cytotoxic than free Rtx ($p < 0.025$ for all valences). At the 200 ng dose, there were 49% viable cells after Rtx treatment, compared to ≤ 5% for Rtx-LNPs ($p < 0.0005$ for all valences). In Z138 cells, significant differences between Rtx and Rtx-LNP treatment began to appear at 20 ng for the valence of 121: 89% for Rtx, 74% for Rtx-LNP(121) ($p < 0.005$). At the 200 ng dose, all valences showed significant difference compared to free Rtx ($p < 0.05$). These data demonstrate that regardless of the fact that equal doses of Rtx were administered, Rtx-LNPs are significantly more cytotoxic than Rtx.

4.4.5 Time dependence of apoptosis induced in lymphoma cells by Rtx-LNP

It is well-documented that Rtx induces direct apoptosis in lymphoma cells when it is crosslinked on the cell surface using a reagent such as an anti-human-IgG secondary antibody[7, 74-76]. To determine if the cytotoxicity observed above could be due to Rtx-LNPs directly inducing

apoptosis on their own without hypercrosslinking, the ability of Rtx and Rtx-LNPs to induce apoptosis in the same two cell lines was examined. **Figure 4.5A** illustrates the flow cytometric Annexin-V-FITC/PI assay that was employed. This figure shows that levels of apoptosis after treating Ramos cells with Rtx were similar to those after treatment with HBS, confirming that Rtx, in the absence of crosslinking, does not elicit apoptosis *in vitro*. Figure 4.5A also demonstrates that the precursors to Rtx-LNP (Rtx-biotin and Neut-LNP) did not induce apoptosis on their own, and neither did a mixture of unbiotinylated Rtx and Neut-LNP. On the other hand, treating cells with Rtx-LNP resulted in the onset of significant levels of apoptosis (bottom rightmost plot in Figure 4.5A). This indicates that as opposed to bivalent Rtx, Rtx-LNP induces apoptosis on its own in target cells, and the induction of apoptosis depends on many Rtx molecules being associated together in a multivalent Rtx construct.

The time course of the induction of apoptosis was also measured by analyzing cells treated with Rtx or two different valences of Rtx-LNP at time points up to 48 h after treatment. As shown in **Figure 4.5B**, the percentage of Ramos cells in early apoptosis (Annexin-V-FITC$^+$ / PI$^-$) after treatment with Rtx-LNP(63) and Rtx-LNP(158) increased sharply up to 16 h after treatment, and after 24 h, the levels of early apoptosis subsequently decreased ($p > 0.05$ between the 16 and 24 h time points for both treatments). The decrease after 24 h was associated with an increased fraction of necrotic cells (Annexin-V-FITC$^+$ / PI$^+$; not shown). Cells treated with HBS (valence 0) and bivalent Rtx did not show peak levels at 24 h post-treatment; the levels of apoptosis for both HBS and Rtx at 16 h were equivalent to those at 0 h ($p > 0.05$ in both cases), but slight increases in apoptosis after treatment with HBS or Rtx were observed at time points of 24 h and longer (from 2.9% at 0 h to 8.2% at 48 h). However, at all time points, HBS and Rtx treatment resulted in equivalent levels of apoptosis ($p > 0.05$). A separate experiment revealed that Z138 cells also exhibited maximum levels of apoptosis at a time point 24 h after treatment (data not shown). Based on these data, the 24 h time point was

considered to be the time point when early apoptosis was considered maximal after treatment with Rtx-LNPs.

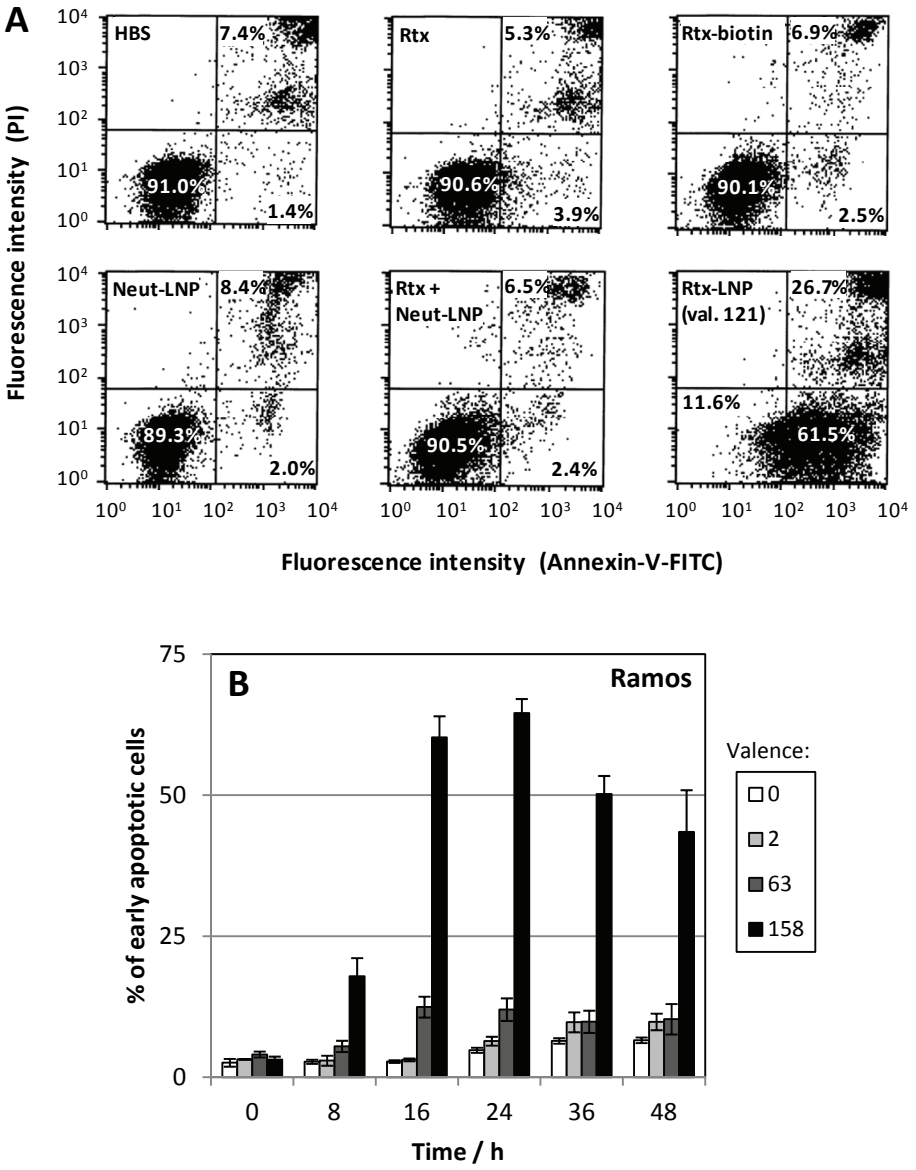

Figure 4.5 **Rtx-LNPs directly induce apoptosis in lymphoma cells while the individual precursors to Rtx-LNP do not.**
(A) To measure apoptosis levels, cells were stained with Annexin-V-FITC and PI and analyzed using flow cytometry. Viable cells were negative for both dyes (lower left quadrant), early apoptotic cells were Annexin-V-FITC^{+} and PI^{-} (lower right quadrant), and necrotic cells were positive for both dyes (upper right quadrant). In this example, 5×10^5 Ramos cells were treated with a 20 µg Rtx dose (or amount of Neut-LNP equivalent to that given in the Rtx-LNP treatment) for 24 h. The Rtx-LNP treatment exhibited a significant increase in the fraction of early apoptotic and necrotic cells compared to all other treatments. **(B)** Ramos cells were treated with HBS, Rtx, or Rtx-LNP (10 µg Rtx dose given to 2.5×10^5 cells in 500 µL medium) and percentages of early apoptotic cells were measured at different times post-treatment. Maximum levels of

apoptosis occurred approximately 24 h after treatment with Rtx-LNP, regardless of valence, while free Rtx showed low levels of apoptosis at all time points.

4.4.6 Levels of apoptosis in lymphoma cells depend on the valence of Rtx-LNP

At the time point where maximum apoptosis occurred (24 h), the apoptotic potency of the various Rtx-LNP valences was measured. A total of 2.5×10^5 Ramos or Z138 cells were treated with a 10 µg dose of Rtx, either in its bivalent form or in the different Rtx-LNP valences. Cells were also treated with HBS (valence 0). After an incubation of 24 h, the viable and early apoptotic fractions were measured as in the previous section, and are shown in **Figure 4.6**. This figure clearly illustrates that higher valences of Rtx-LNPs have a much stronger ability to directly induce apoptosis in lymphoma cells, even though the same dose of Rtx is given in all cases. The figure also shows an inverse correlation between the viable and apoptotic populations (black and white symbols) in both cell lines, indicating a shift from the viable population to the early apoptotic population due to exposure to Rtx-LNP.

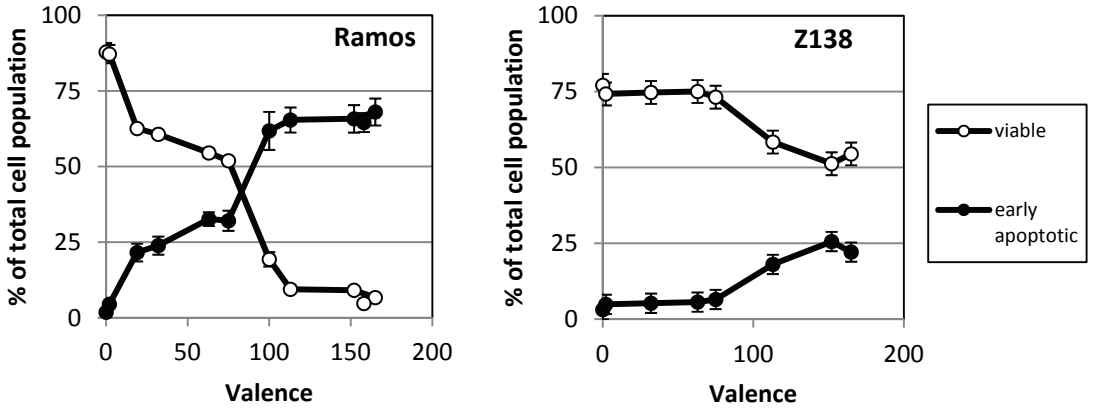

Figure 4.6 A valence-dependent increase in the level of apoptosis is observed in Rtx-LNP-treated lymphoma cells even though all cells are given equal doses of Rtx.

A total of 2.5×10^5 Ramos **(A)** or Z138 **(B)** cells were treated with a 10 µg dose of free Rtx (valence 2) or different valences of Rtx-LNP. Valence 0 refers to treatment with HBS. Percentages of early apoptotic and viable cells were measured as in Figure 4.5. At 24 h post-treatment, the higher valences of Rtx-LNP induced elevated apoptosis compared to the lower valences, indicating that induction of apoptosis by Rtx-LNP is valence-dependent. In Ramos cells, maximum levels of apoptosis occurred at valences of approximately 100 and higher.

The Ramos cell line (Figure 4.6A) was more sensitive to direct induction of apoptosis by Rtx-LNPs than the Z138 line (Figure 4.6B). In Ramos cells, treatment with Rtx (valence 2) resulted in 4.5% early apoptotic cells after 24 h, and this value increased to 21% for Rtx-LNP(19) ($p < 0.001$), while in the Z138 line, low equivalent levels of apoptosis were observed up to a valence of 75 ($p > 0.05$ for all valences up to and including 75), and it was not until a valence of 113 when higher levels of apoptosis were observed (18%, compared to 6.5% for Rtx-LNP(75); $p < 0.05$). In Ramos cells, maximum levels of apoptosis (65%) occurred at valences of 100 and above ($p > 0.05$ for all pairs of these valences), but it is unclear whether such a plateau was also observed in Z138 cells, although $p > 0.05$ between valences of 113, 152, and 165. These valences show levels of early apoptosis of 22%, which is significantly lower than those observed in Ramos cells, further indicating that the Z138 cell line is less sensitive to the direct induction of apoptosis compared to the Ramos line.

Overall, these data confirm that the apoptotic activity of Rtx-LNP is significantly elevated compared to bivalent Rtx, and the levels of apoptosis are valence-dependent in two different lymphoma cell lines. Increasing the valence is therefore a method of improving the therapeutic activity of Rtx by enhancing its direct mechanism of action. The data in the Ramos cell line also show that the optimal valence of Rtx-LNP is 100, since no further increase in apoptosis occurred at higher valences. This implies that, in terms of the direct mechanism of action, there would be no additional therapeutic benefit of using valences higher than 100.

4.5 Discussion and conclusions

4.5.1 Discussion

This chapter has demonstrated that the methodology described in Chapter 3 can be employed to create multivalent Ab-LNP constructs that possess unique biological properties (Figures 4.1–4.3) and significantly improved therapeutic activity (Figures 4.4–4.6). This chapter also proves

the concept that the methodology can be employed to identify Abs that show enhanced responses when they are multivalent, such as Rtx, and also to identify the optimal valence of such multivalent constructs (valence of 100 for multivalent Rtx; Figure 4.6A). These constructs warrant further study due to their potential in improving therapeutic antibody-based cancer treatments.

The nature of the interaction between Rtx-LNPs and $CD20^+$ lymphoma cells uncovered here provides interesting clues regarding the direct induction of apoptosis by Rtx-LNP. Figure 4.1A shows that increased doses of bivalent Rtx correlated with decreased levels of unbound CD20, until all CD20 became saturated with Rtx. Saturating cells with Rtx-LNP(158) in Figure 4.1B, however, showed that 10-fold more Rtx was bound to the cells although 41% of CD20 was unoccupied, indicating that a significant proportion of Rtx bound to the cells was not associated with CD20. This could be due to the spherical structure of Rtx-LNP interacting with CD20 in the plasma membrane. When Rtx-LNP is bound to the cell, the Rtx molecules closest to the cell surface are more accessible to CD20 compared to those on the opposite side of the Rtx-LNP. The Rtx molecules on the opposite side may therefore not bind directly to CD20 although they remain associated to the cell through the Rtx-LNP construct.

Moreover, Figure 4.1C showed that at the same dose of Rtx-LNP, treatment with the higher valences results in elevated levels of both bound Rtx and unbound CD20. Although this may seem counterintuitive, it can be explained by the fact that for Rtx-LNPs, equal doses of Rtx do not represent the same number of Rtx-LNPs given to the cells. Because the higher valences have more Rtx molecules per Rtx-LNP, the number of Rtx-LNPs administered deceases as the valence increases, when the dose of Rtx is held constant.

The data in Figure 4.1C, when compared to that in Figure 4.6, show that bivalent Rtx saturates all CD20 on the cell surface and induces low levels of apoptosis, while multivalent Rtx-LNP engages only a fraction of available CD20 and induces significantly higher apoptosis. It is therefore not simply the number of Rtx/CD20 interactions that provides the stimulus for induction of

apoptosis. These data imply that instead, high local concentrations of Rtx/CD20 in the plasma membrane, such as in the microdomains shown in Figure 4.2, elicit the apoptotic signal. Higher local concentrations of Rtx/CD20 are provided by more extensive hypercrosslinking of CD20, which is facilitated by higher valences of Rtx-LNP.

The Rtx-LNP valences of 113 and 158 exhibited equivalent levels of bound Rtx and unbound CD20 (Figure 4.1C), and in Figure 4.6A & B, they were shown to induce equivalent levels of apoptosis in lymphoma cells ($p > 0.05$ for all parameters). This suggests that the maximum levels of apoptosis observed above the optimal valence of 100 in Figure 4.6 are related to equivalent levels of bound Rtx and unengaged CD20; in other words, it suggests that maximum hypercrosslinking of CD20 achievable by Rtx-LNP is correlated with maximum apoptosis observed in lymphoma cells.

We showed specifically that multivalent Rtx-LNPs are considerably more cytotoxic than bivalent Rtx in two lymphoma cell lines (Figure 4.4) and that they induce apoptosis in these cells while none of their individual constituents do (Figure 4.5A). Moreover, at 24 h post-treatment, when levels of apoptosis were maximal (Figure 4.5B), the level of apoptosis induced in both cell lines was directly related to the valence of Rtx-LNP even though all cells were given equivalent doses of Rtx (Figure 4.6). This clearly shows that by increasing the valence of Rtx, its efficacy is improved through an augmentation of the direct mechanism of action. This has not been previously demonstrated for Rtx, likely because until now there has not been a precise methodology for creating defined valences of multivalent Abs as high as those employed here.

The observation of valence-dependent levels of apoptosis supports hypothesis (2) in Section 4.2.2, where different levels of hypercrosslinking resulting from multivalency are responsible for the induction of apoptosis. The different valences can therefore be used to study the direct mechanism of action since one would also expect concomitant valence-dependent signaling events that precede apoptosis. The direct mechanism of action of Rtx-LNP is further explored in Chapters 5 and 6.

4.5.2 Conclusions

The methodology in Chapter 3 can be successfully used to create many Ab-LNPs that differ in terms of valence. Multivalent Rtx-LNPs prepared with this methodology exhibit unique binding properties to $CD20^+$ lymphoma cells, where more Rtx is associated to cells as the valence is increased although there is a significant fraction of CD20 on the cell surface that remains unassociated with Rtx. This is consistent with the formation of Rtx/CD20-enriched domains observed on cells treated with Rtx-LNP. Bivalent Rtx saturates all CD20 on the cell and results in low cytotoxicity and low levels of apoptosis, while multivalent Rtx-LNPs do not saturate all CD20 and result in higher cytotoxicity and high levels of apoptosis. This indicates that the number of Rtx/CD20 interactions does not determine the therapeutic efficacy of multivalent Rtx; the clustering of CD20 in the plasma membrane does instead, which is facilitated by multivalent Rtx. These results suggest that it may be beneficial to apply the methodology in Chapter 3 to other therapeutic Abs such as Trz, which has also shown benefits associated with multivalency[7, 89, 109, 110].

Moreover, the Rtx-LNP constructs of higher valence are capable of greater hypercrosslinking, and levels of apoptosis were observed to depend on the valence even though all cells were given the same dose of Rtx. This valence-dependent relationship opens the door to studies on the poorly defined direct mechanism of action of Rtx because signaling events that precede and cause apoptosis would also be expected to be valence-dependent. The methodology therefore provides a framework for probing the direct mechanism of action from a molecular point of view.

5 A novel direct mechanism of action of multivalent rituximab

5.1 Synopsis

The previous chapter showed that even though lymphoma cells can be given Rtx-LNPs at equivalent doses of Rtx, higher level of apoptosis are induced by the constructs of higher valence. This chapter describes studies undertaken to understand the mechanism of action of the direct induction of apoptosis by Rtx-LNP.

5.2 Background

5.2.1 Extrinsic and intrinsic apoptosis pathways

Apoptosis occurs primarily through two distinct pathways, the intrinsic pathway (also known as the mitochondrial or Bcl-2 family regulated pathway) and the extrinsic pathway[82, 86, 87]. The two pathways involve distinct initiator caspases that set each pathway in motion, while they both converge on the activation of effector caspases such as caspase-3, -6, and -7. The intrinsic pathway depends on the activation of caspase-9, which occurs after perturbation of mitochondria due to cellular stress, growth factor withdrawal, or cytotoxic stimuli. Death stimuli activate pro-apoptotic Bcl-2 family members, leading to disruption of the outer mitochondrial membrane and release of cytochrome c and other apoptosis-inducing proteins into the cytosol. Cytochrome c, along with the adaptor protein APAF1, forms a complex termed the apoptosome, which activates caspase-9, which in turn leads to activation of effector caspases. Additional caspase-independent cell death processes regulated by the Bcl-2 family have also been described[86].

In cancer treatment, apoptosis is usually triggered in oncogenic cells by chemotherapy and irradiation through the intrinsic pathway, since these agents cause cellular damage. This pathway

usually involves requires p53 function, but mutations or inhibiting proteins impair p53 function in many human cancers. In this way, tumour cells evade apoptosis and continue to proliferate even though the treatment caused genetic instabilities[82]. This has been demonstrated in lymphoma specifically; for example, the inhibition of the intrinsic apoptosis pathway downstream of caspase-9 activation has been shown to cause resistance to chemotherapy in diffuse large B-cell lymphomas[170].

In the extrinsic apoptosis pathway, caspase-8 is the critical initiator caspase. The cleavage of procaspase-8 occurs in the death-inducing signaling complex (DISC), a plasma membrane-associated complex of specific proteins that is responsible for initiating the extrinsic pathway. Activated caspase-8 is released into the cytosol from the DISC and goes on to activate the effector caspases[87, 171]. Crosstalk between the two apoptosis pathways is also well-documented, such as caspase-8-mediated activation of proapoptotic Bcl-2 family members, resulting in cytochrome c release. Such amplification of the extrinsic pathway through the intrinsic pathway is required in some cell types but not in others[82]. This highlights that the intrinsic and extrinsic pathways are not distinct, but interdependent.

5.2.2 The death-inducing signaling complex and the tumor necrosis factor receptor superfamily

Besides procaspase-8, there are two other essential components of the DISC: an adaptor protein (either Fas-associated death domain (FADD) or TNFR-associated death domain (TRADD)), and a death receptor[171, 172]. Death receptors constitute specific members of the tumor necrosis factor receptor (TNFR) superfamily. Discovery of the TNFR superfamily was made possible by observations in 1868 where tumors in some patients showed regression following acute bacterial infection, but it was not until 1975 that the term “tumor-necrosis factor” (TNF) was coined[82, 173].

The members of the TNFR superfamily are critically involved in maintenance of homeostasis of the immune system. They are type-I transmembrane proteins with a C-terminal intracellular tail,

a membrane-spanning region, and an extracellular ligand-binding N-terminal domain. The hallmark of TNFR superfamily members is the presence of cysteine-rich extracellular domains, the number of which can vary from one to six, and which define ligand specificity. Over 40 members of the TNFR superfamily have been identified to date[172, 174].

5.2.3 Death receptors

Death receptors are members of the TNFR superfamily characterized by an ~80 amino-acid cytoplasmic "death domain" which is essential for the induction of apoptosis. When the cell receives a proapoptotic signal, the death domain is responsible for recruiting FADD or TRADD, which in turn recruits procaspase-8, forming the DISC which leads to caspase-8 activation[175]. There are six death receptors that have been identified to date; the four most extensively studied are CD120a (also known as TNFR1 or TNFRSF1A), CD95 (Fas receptor, APO-1, or TNFRSF6), DR4 (TRAILR1 or TNFRSF10A), and DR5 (TRAILR2, APO-2, or TNFRSF10B)[174, 176]. The ligands to these receptors, respectively, are TNF-α, Fas ligand (FasL), and Apo2L/TRAIL (for both DR4 and DR5). These ligands comprise a group of complementary cytokines that are mainly type-II transmembrane proteins, although some can be released as soluble cytokines upon proteolytic cleavage[174, 176].

Almost all of the TNF ligands are expressed only by cells of the immune system, including B cells, T cells, NK cells, monocytes and dendritic cells, but the TNFRs are expressed by a wide variety of cells. For example, no cell type in the body has yet been found that does not express CD120a[177]. There is also another subset of TNFR superfamily members known as decoy receptors, which lack the death domain and therefore have a nonsignaling role; they compete with death receptors for ligand binding, thereby inhibiting death receptor function[172]. Finally, the other two death receptors that have not been mentioned, which in general are not as effective at inducing apoptosis, are DR3 (TNFRSF12) and DR6 (TNFRSF21)[174, 178].

A common requirement to form the DISC is the oligomerization of death receptors in the plasma membrane, which is facilitated with ligand binding and which results in receptor trimerization[172, 174]. Although ligand binding was originally thought to be required for DISC formation, there is substantial evidence showing the formation of preassembled death receptor complexes (such as ones containing CD95 and CD120a) on the cell surface in the absence of ligand[179]. This has been shown to occur due to interaction of the membrane-distal extracellular cysteine-rich domain termed the preligand assembly domain[180]. The ligand-independent activation of death receptors resulting in apoptosis is well-documented in a variety of cases[181-186].

5.2.4 Deciphering the direct mechanism of action of multivalent Rtx

Rtx-LNP was shown to induce apoptosis in target lymphoma cells in Figure 2.2, and the levels of apoptosis were also shown to be valence-dependent in Figure 4.6. The aims of the experiments outlined in this chapter were to first determine whether the observed apoptosis was caspase-dependent, and if so, to determine the pattern of caspase activation to discern whether Rtx-LNP was inducing apoptosis through the intrinsic or extrinsic apoptosis pathway. Based on the known mechanisms of apoptosis described, further experiments were performed to determine the specific proteins involved in the mechanism of action of this apoptosis. Because the level of apoptosis was valence-dependent, signaling events directly preceding apoptosis (such as concentrations of activated proteins that induce apoptosis) were also valence-dependent. Finally, the role of the liposomal component in the induction of apoptosis by multivalent Rtx-LNP was also examined.

5.3 Materials and methods

5.3.1 Materials and cell lines

The Vybrant FAM Caspase-8 Assay Kit, Alexa Fluor 488-labeled cholera toxin subunit B (A488-CTX), Annexin-V binding buffer, recombinant human Annexin-V labelled with fluorescein isothiocyanate (Annexin-V-FITC), and the Alexa Fluor 647 (A647) monoclonal Ab labeling kit were obtained from Invitrogen (Burlington ON, Canada). The SensoLyte AFC (7-amino-4-trifluoromethyl coumarin) Caspase Profiling Kit was purchased from AnaSpec (Fremont CA, USA). The caspse-8 inhibitor Z-IETD-FMK was obtained from R&D Systems (Minneapolis MN, USA). The negative control peptide Z-FA-FMK was obtained from Santa Cruz Biotechnology (Santa Cruz CA, USA). The death domain receptor antibody detection set was purchased from ProSci (Poway CA, USA). A647-labeled Abs against CD120a (A647-CD120a) and CD95 (A647-CD95) as well as an A488-labeled anti-DR4 Ab (A488-DR4), an A488-labeled mouse IgG1 negative control, an A647-labeled mouse IgG2a negative control, and a FITC-labeled anti-Rtx Ab (FITC-anti-Rtx) were obtained from AbD Serotec (Kidlington, UK). Streptavidin-coated polystyrene microspheres with a diameter of 100 nm (streptavidin-MS) were purchased from Bangs Laboratories (Fishers IN, USA). DyLight 649-conjugated goat anti-rabbit-IgG $F(ab')_2$ fragment (D649-anti-rabbit-IgG) was purchased from Jackson ImmunoResearch (West Grove PA, USA). Disposable PD-10 columns (which contain Sephadex G-25 medium) were obtained from GE Healthcare Life Sciences (Piscataway NJ, USA). Unless noted otherwise, all other reagents were obtained from Sigma-Aldrich and were of the highest quality available.

Ramos and Z138 cell lines were acquired and maintained as described in Section 4.3.2.

5.3.2 Preparation of Rtx-LNPs

The methodology described in Chapter 3 and summarized in Figure 3.1 was used to prepare and characterize two separate batches (four valences each) of Rtx-LNPs with valences up to 204.

5.3.3 Assay for quantifying caspase-8 levels in treated cells

The Vybrant FAM Caspase-8 Assay Kit was employed to quantify levels of caspase-8 in treated cells. The kit contains the cell-permeable and noncytotoxic peptide reagent FAM-LETD-FMK, which contains an affinity peptide sequence specific to activated caspase-8 (leucine-glutamic acid-threonine-aspartic acid (LETD)). Upon association with the peptide sequence, the probe covalently binds to cleaved caspase-8 through the fluoromethyl ketone (FMK) moiety, while the FAM (carboxyfluorescein) reporter has excitation and emission wavelengths of approximately 488 nm and 530 nm, respectively. Bound FAM-LETD-FMK remains within the cell, while unbound reagent diffuses out and is washed away. In each well of a 48-well plate, 2.5×10^5 Ramos cells in 250 μL medium were added and treated with HBS, Rtx, or Rtx-LNP (10 μg dose). For the time-course study, Rtx-LNP(165) was employed and incubation was allowed to proceed for different times at 6 h intervals up to 48 h after treatment. For the valence-dependence study, different valences of Rtx-LNP were employed and analysis was performed 24 h post-treatment. After the treatment time, 8.3 μL of a 30x FAM-LETD-FMK solution (prepared according to kit instructions) was added to each well and the plate was gently shaken on a plate shaker for 3 min. The plate was then incubated at 37 ^{o}C and 5 % CO_2 for 60 min, and the plate was mixed every 20 min during the incubation. Cells were resuspended and transferred to Eppendorf tubes, spun in a microcentrifuge at 7000 rpm for 15 s, washed twice with wash buffer (500 μL and 300 μL), then resuspended in 350 μL wash buffer containing 0.2 μg/mL propidium iodide (PI) before analysis on a FACSCalibur flow cytometer (Becton Dickinson, San Jose, CA). FAM fluorescence was measured in the FL1 channel. Using a sample where caspase-8 was irreversibly inhibited using Z-IETD-FMK (cells were treated with 200 μM for 4 h at 37 ^{o}C), a fluorescence intensity threshold in the FL1 channel was defined above which cells were considered caspase-8 positive. Treatments were performed in triplicate, and data here and in all subsequent figures is shown as mean ± standard deviation (SD) unless noted otherwise. Two-tailed unpaired Student's *t*-tests were performed in all cases with a level of significance of 0.05.

5.3.4 Profiling of caspases and inhibition of caspase-8

The SensoLyte AFC Caspase Profiling Kit was used according to the manufacturer's instructions to measure levels of cleaved caspases 1, 2, 3 and 7 (3/7), 6, 8, and 9 in response to different treatments. The kit contains a substrates specific to each caspase that contains an AFC that when cleaved from the substrate by the caspase, has emission and excitation wavelengths of approximately 380 nm and 500 nm, respectively.

A total of 2×10^6 Ramos cells in 2.0 mL medium were treated with HBS or an 80 µg dose of Rtx or Rtx-LNP(150) for 24 h. For experiments involving inhibition of caspase-8 using Z-IETD-FMK or Z-FA-FMK (negative control), 200 µL of a 2.0 mM solution in cell culture medium were added to the cells which were then incubated for 4 h at 37 ^{o}C before treatment with Rtx-LNP(150) as described above. A positive control consisted of treatment with 4.0 µM camptothecin for 4 h. After the incubation, cells were collected by centrifugation at 500*g* for 5 min, and the pellet was resuspended in 1.3 mL of lysis buffer (provided with the kit). The suspension was rotated on a rotating apparatus for 30 min at 4 ^{o}C, then centrifuged at 2500*g* for 10 min at 4 ^{o}C. A total of 50 µL of the resulting caspase-containing supernatant were added to the wells of a 96-well plate containing the various substrates dissolved in assay buffer and dithiothreitol (DTT). Samples were in triplicate for every caspase for each treatment. Plates were shaken and read every 30 min for up to 3 h. Average fluorescence intensities were calculated after subtracting averages of blanks, and were scaled relative to HBS for each caspase.

The Fluorstar fluorescence plate reader was calibrated using free AFC, and fluorescence readings were obtained in the linear range of an emission intensity versus AFC concentration plot.

5.3.5 Measurement of levels of death receptors using flow cytometry

To quantify levels of death receptors in treated cells, 2.5×10^5 Ramos or Z138 cells in 500 µL medium were treated with a 10 µg dose of Rtx, Rtx-LNP, or an equivalent volume of HBS, and

analyzed at different times after treatment. For analysis using flow cytometry, cells were transferred to 1.5 mL Eppendorf tubes and spun in a microcentrifuge at 7000 rpm for 15 s. Pellets were washed with cold PBSB (phosphate-buffered saline (PBS) + 0.1% bovine serum albumin, pH 7.4) and resuspended in 20 µL PBSB. An appropriate volume of each Ab was added and cells were stained for 1 h on ice. A titration was performed on each Ab to determine levels of saturation in each cell line and appropriate volumes of Ab required to be added (generally between 0.5 – 3.0 µL). Primary labeled Abs consisted of A647-CD95, A488-DR4, and A647-CD120a, and nonlabeled primary Abs included anti-DR3, DR4, DR5, and DR6 Abs from the death domain receptor Ab detection set (see Section 5.3.1).

After staining for 1 h on ice, cells were washed with cold PBSB. For staining with a secondary Ab (if required), pellets were resuspended in 20 µL cold PBSB containing 0.5 µL D649-anti-rabbit-IgG, incubated for an additional 1 h on ice, then washed again with cold PBSB. Pellets were then resuspended in 300 µL PBSB containing 0.5 µg/mL propidium iodide (PI), filtered through 35 µm strainers, and analyzed on a FACSCalibur flow cytometer (Becton Dickinson, San Jose, CA) collecting 10,000 events for each sample. Appropriate single-stained controls were run in all cases to set compensation. Fluorescence intensities were obtained from analysis with FlowJo software, and triplicates were averaged to obtain mean fluorescence intensities (MFIs). For each dose, the MFI from the appropriate negative control was subtracted from each measured MFI value before being scaled to obtain relative MFIs.

5.3.6 Annexin-V/PI apoptosis assay and measurement of CD120a levels within apoptotic subpopulations

The Annexin-V-FITC apoptosis assay was performed as described in Section 4.3.8 using 2.5×10^5 Ramos cells in 500 µL medium and a 10 µg Rtx dose, and cells were co-stained with A647-CD120a (2 µL / sample) during Annexin-V-FITC staining. Quadrants were set as described on the

plots of PI versus Annexin-V-FITC fluorescence intensity, and the quadrants were set as separate gates in order to measure the expression of CD120a within the early apoptotic (PI^-/Annexin-V-$FITC^+$), necrotic (PI^+/Annexin-V-$FITC^+$), and viable (PI^-/Annexin-V-$FITC^-$) populations. Appropriate single-stained and double-stained positive controls (cells treated with 4.0 µM camptothecin at 37 ^oC for 4 h) were run to set compensation, and A647-labeled IgG2a negative control was used to set the FL4 detector voltage (for A647 emission detection) such that the negative signal occurred within the first decade. Analysis of percentages within each population and mean fluorescence intensities were performed using FlowJo software.

5.3.7 Confocal laser-scanning fluorescence microscopy

Samples were prepared using the same procedure as described in Section 4.3.5, with the exception of staining and the microscope used. For staining of caspase-8 using FAM-LETD-FMK, the same procedure as described in Section 5.3.4 was used; for CD120a staining (either on its own or after caspase-8 staining), cells were resuspended in 20 µL cold PBSB containing an appropriate volume (determined by titration – Section 5.3.6) of A647-CD120a and incubated on ice for 30 min, then 5×10^4 cells were suspended in a total of 50 µL of cold serum-free medium and allowed to adhere on each 8 mm poly-L-lysine glass cover slip for 1 h on ice before washing the cover slips with HBS and fixing with paraformaldehyde as described in Section 4.3.5. Sample preparation proceeded as described in Section 4.3.5.

Samples were imaged on a confocal Eclipse TE2000-E microscope (Nikon Instruments, Melville NY, USA) controlled with EZ-C1 software. Acquired images were converted to TIFF format for presentation.

5.3.8 Preparation of Rtx-MS

To prepare Rtx-MS, Rtx was biotinylated using the nickel immobilized metal affinity chromatography (NIMAC) method described in Section 3.3.6 with a 10-fold molar excess of NHS-PEG-biotin with respect to Rtx, yielding between 1 and 2 biotin groups per Rtx molecule. Streptavidin-MS were exchanged into HBS using a PD-10 column in order to remove surfactants and EDTA. Based on the certificate of analysis provided by the manufacturer, a fivefold molar excess of Rtx-biotin was added with respect to streptavidin present in the streptavidin-MS suspension in order to produce Rtx-MS. The suspension was incubated with stirring at room temperature for 30 min, then at 4 ^{o}C for 12 h. Unbound Rtx-biotin was purified from Rtx-MS using Sepharose CL-4B columns pre-equilibrated with HBS.

5.4 Results

5.4.1 Caspase dependence of Rtx-LNP-induced apoptosis

To determine whether Rtx-LNP-induced apoptosis proceeds *via* a caspase-dependent mechanism, the caspase-8-specific peptide reagent FAM-LETD-FMK was employed (Section 5.3.3). Time-course experiments were performed to determine the activation state of this caspase in treated Ramos cells at different points after treatment. As shown in **Figure 5.1A**, caspase-8 was not activated in Ramos cells after treatment with HBS or Rtx, but it was activated after treatment with Rtx-LNP(165). The fraction of caspase-8 positive cells increased until 30 h after treatment, after which point levels of caspase-8 began to drop. At the 30 h time point, 83 % of cells were found to be caspase-8-positive compared to 19 % and 18 % for HBS and Rtx, respectively ($p < 0.005$ between both Rtx-LNP(165) and HBS/Rtx). These data correlate with the apoptosis data in Figure 4.5B, which shows a similar time course to the one observed here. Moreover, the percentage of caspase-8-

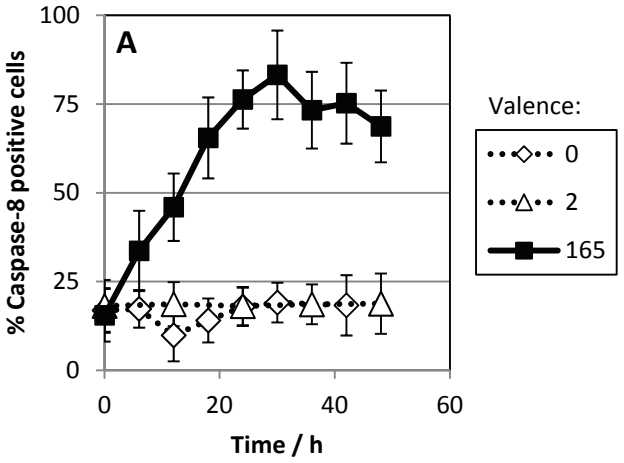

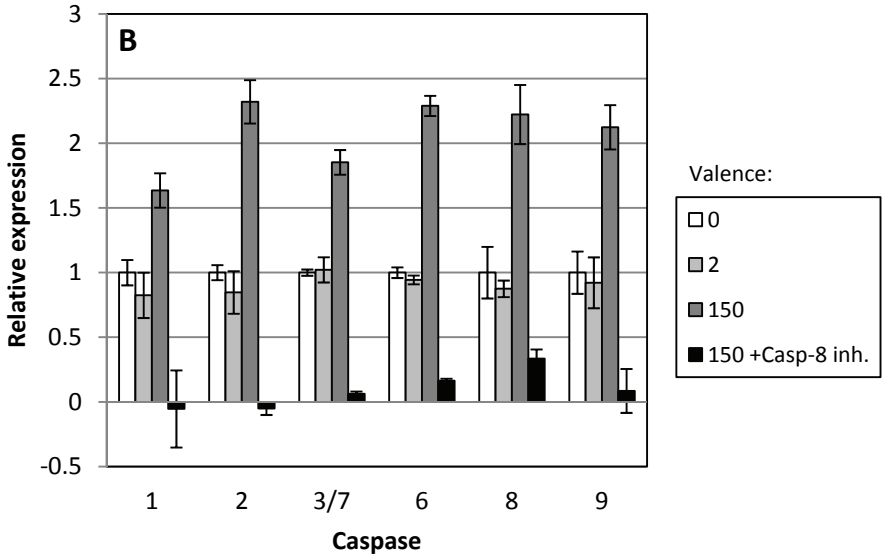

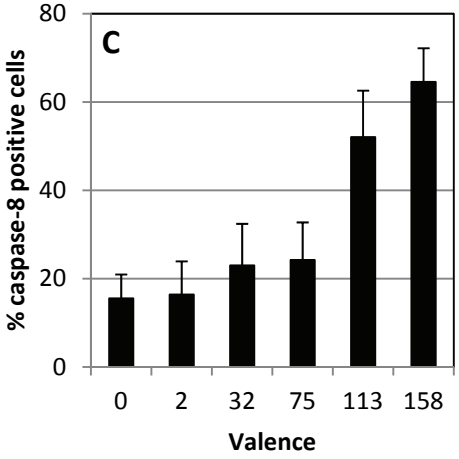

Figure 5.1 Rtx-LNP-induced apoptosis is dependent on the activation of caspase-8.

(A) Levels of cleaved caspase-8 are shown with respect to time in Ramos cells after different treatments. **(B)** Expression levels of each activated caspase are shown for the various treatments as the measured fluorescence values after subtracting blanks and normalizing to HBS-treated samples. By treating cells with a peptide inhibitor specific for caspase-8 (Casp-8 inh.) for 4 h and then treating the cells with Rtx-LNP(150), levels of nearly all activated caspases were reduced to levels similar to blanks. **(C)** Levels of cleaved caspase-8 measured after treating Ramos cells with different valences of Rtx-LNP for 24 h.

positive cells in Figure 5.1A is roughly equal to the sum of the percentages of early apoptotic and necrotic cells in Figure 4.6A.

The elevated levels of caspase-8 suggest that apoptosis occurred *via* the extrinsic apoptosis pathway, which involves formation of the DISC. Next, to determine the pattern of activation of other caspases, the levels of activated caspases 1, 2, 3, 6, 7, 8, and 9 were profiled 24 h after treatment. These data are shown in **Figure 5.1B** and they indicate that treatment of Ramos cells with Rtx resulted in similar levels of caspase activation as treatment with HBS (no drug), but treatment with Rtx-LNP(150) resulted in an approximately two-fold higher level of detected cleaved caspase levels for all caspases tested ($p < 0.005$ for every caspase between valences 0 or 2 and 150). A positive control was also carried out by treating cells with 4.0 μM camptothecin for 4 h, and these samples showed elevated levels of all caspases compared to HBS, particularly the reading from the caspase 3/7 substrate, which was at least 10-fold higher than all other caspases (data not shown). This is expected since camptothecin inhibits topoisomerase I, causing DNA damage that results in apoptosis through the intrinsic pathway, which does not involve caspase-8-dependent initiation[82, 187].

To determine whether caspase-8 is responsible for the activation of the other caspases, cells were treated for 4 h with Z-IETD-FMK, a cell-permeable, irreversible peptide inhibitor specific to caspase-8, followed with a 24 h treatment with Rtx-LNP(150). Figure 5.1B shows that the inhibition of caspase-8 resulted in a dramatic reduction in the levels of activated caspases down to levels that were roughly one-tenth of those in HBS-treated cells (caspases 3/7 and 6) or similar to blanks (caspases 1, 2, and 9). The caspase with the highest level of activation was caspase-8 itself, which was 0.33 with respect to HBS ($p < 0.005$ for every caspase between valences 0 or 2 and 150(Casp-8 inh.)).

Ramos cells that were pretreated with equivalent amounts of Z-FA-FMK, a negative control peptide that does not inhibit caspases, showed levels of cleaved caspases after treatment with Rtx-

LNP(150) that were similar to those after treatment with Rtx-LNP(150) alone (data not shown). Apoptosis was also significantly reduced by inhibiting caspase-8; treatment of Ramos cells with Z-IETD-FMK followed by Rtx-LNP(165) resulted in 11% of cells in early apoptosis, compared to 61% for cells treated only with Rtx-LNP(165) ($p < 0.001$), as measured using flow cytometry (Section 5.3.6; data not shown). These data therefore indicate that the direct induction of apoptosis by Rtx-LNP is caspase-dependent, and they are consistent with the role of caspase-8 as the initiating caspase.

Since apoptosis induced by Rtx-LNP is valence-dependent as shown in Figure 4.6, one would also expect that levels of activated caspase-8 would show a valence-dependent relationship. Ramos cells were therefore treated with different valences of Rtx-LNP and caspase-8 levels were measured. **Figure 5.1C** confirms that the levels of activated caspase-8 are valence-dependent, with higher valences producing elevated levels compared to lower valences. Ramos cells treated with HBS or Rtx showed 16 % caspase-8-positive cells, while treatment with Rtx-LNP(158) resulted in 65 % caspase-8-positive cells ($p < 0.001$). These data, when taken together, reveal that Rtx-LNP induces apoptosis in lymphoma cells *via* the caspase-8-dependent extrinsic apoptosis pathway.

5.4.2 Dependence of tumor necrosis factor receptor superfamily member expression on apoptosis induced by Rtx-LNP

As described in Section 5.2, the extrinsic apoptosis pathway involves formation of the DISC, which normally contains specific members of the TNFR superfamily. In order to determine which receptor(s), if any, initiate the extrinsic apoptosis pathway after treatment with Rtx-LNP, the expression levels of death domain-containing death receptors were measured at different times following treatment with HBS, Rtx, or Rtx-LNP. The data summarized in **Figure 5.2** show the results for three key death receptors: CD95 (Fas receptor), death receptor 4 (DR4), and CD120a (TNFR-I). Figure 5.2A summarizes the fluorescence intensities measured in the total Ramos cell population after staining with fluorescently labeled primary Abs against the shown antigens. In the total cell

population, DR4 showed very low staining over all treatments, and the labeling of CD95 was also low and constant except at 24 h after treatment with Rtx-LNP(165), where the relative MFI was 5.7 compared to 0.96 for HBS at the same time point ($p < 0.05$). The most significant change was with CD120a, where the relative MFI after treatment with Rtx-LNP(165) was 9.2 after 4 h compared to 21 after 24 h ($p < 0.005$ in both cases compared to HBS at the same time point). The total staining levels of CD95, DR4, and CD120a were similar in Z138 cells (data not shown).

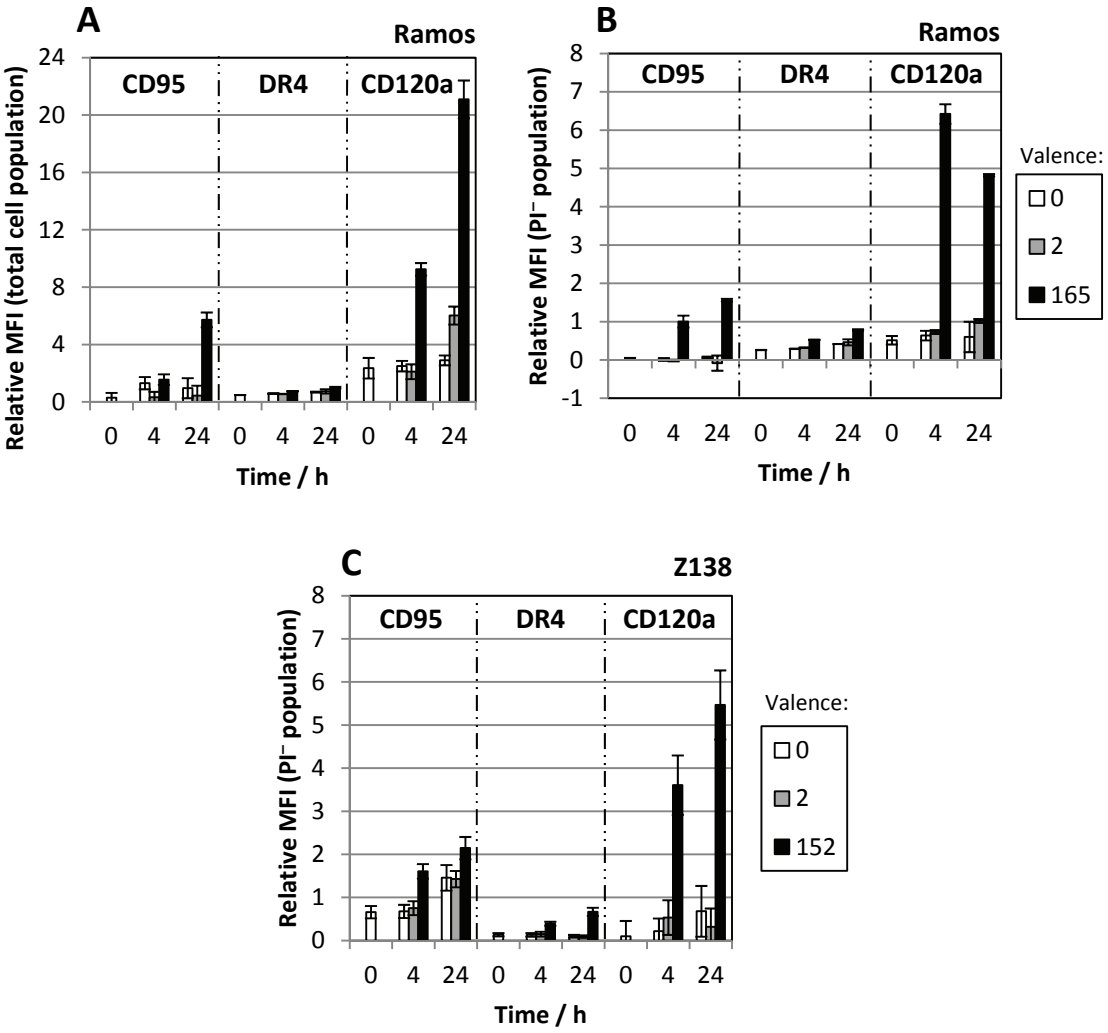

Figure 5.2 CD120a expression is dramatically elevated in lymphoma cells after treatment with Rtx-LNP.

Using flow cytometry, the relative expression levels of the indicated death receptors were measured in the total cell population of treated Ramos cells **(A)** as well as in the plasma membrane of Ramos **(B)** and Z138 **(C)** cells. Plasma membrane expression was obtained by measuring fluorescence intensities in the PI^- population. *MFI*, mean fluorescence intensity.

Figure 5.2B & C show the levels of each death receptor in the plasma membrane after the same treatments, obtained by gating for the cells that exclude PI. The same overall trends were observed in the PI^- populations as in the total cell populations, with the levels of CD120a being the highest of all the death receptors that were tested. In general, levels of all death receptors did not change after the start of treatment (0 h) in cells treated with HBS or Rtx. Comparing Figure 5.2A to Figure 5.2B, one notable observation was that most of the detected CD120a in Figure 5.2A after 4 h was associated with the plasma membrane (relative MFI of 9.2 in Figure 5.2A and 6.4 in Figure 5.2B, representing 70% of the signal), while the majority after 24 h was associated with intracellular staining (relative MFI of 21 in Figure 5.2A and 4.8 in Figure 5.2B; 23% of the signal). Also, levels of CD120a in Ramos cells at 4 h after treatment with Rtx-LNP(165) (relative MFI of 6.4) were higher than those at 24 h (relative MFI 4.8) ($p < 0.05$), but the other death receptors showed highest levels in the plasma membrane at 24 h (0.78 for DR4 ($p < 0.005$), 1.6 for CD95 ($p < 0.0005$; both compared to HBS)). Observations in Z138 cells (Figure 5.2C) paralleled those in Ramos cells, with the exception that the average CD120a levels in the plasma membrane at 24 h after treatment with Rtx-LNP(152) were higher than those after 4 h (5.5 compared to 3.6), albeit the difference is not significant ($p > 0.05$).

Levels of DR3, DR5, and DR6 in Ramos cells were also tested using fluorescently labeled secondary Ab detection after staining with primary Abs (not shown); at 4 h and 24 h post-treatment, DR3 and DR6 showed similar expression as DR4 (total and PI^- populations), and the expression levels of DR5 lied between those of DR3/DR4/DR6 and CD95, i.e. DR3 ≈ DR4 ≈ DR6 < DR5 < CD95 < CD120a. These data indicate a global upregulation of death receptors in the plasma membrane following treatment with Rtx-LNP but not Rtx, with CD120a undergoing by far the most significant upregulation. This indicates that CD120a may play a key role in the direct induction of apoptosis by Rtx-LNP.

5.4.3 CD120a is equally upregulated in viable and early apoptotic cells after treatment with Rtx-LNP

With CD120a being the member of the TNFR superfamily that is most upregulated in cells treated with Rtx-LNP, we further investigated which subpopulations (viable, apoptotic, or necrotic) expressed elevated levels of CD120a. As described in Section 5.3.6, analysis was performed using flow cytometry on HBS-, Rtx-, or Rtx-LNP-treated cells that were triple-stained with Annexin-V-FITC, PI, and Alexa Fluor 647 labeled anti-CD120a Ab (A647-CD120a). As shown in the leftmost plots in **Figure 5.3**, cell populations were gated according to whether they were viable (*V*), early apoptotic (*A*), or necrotic (*N*), and within each subpopulation, the expression of CD120a is shown in the corresponding dot plots.

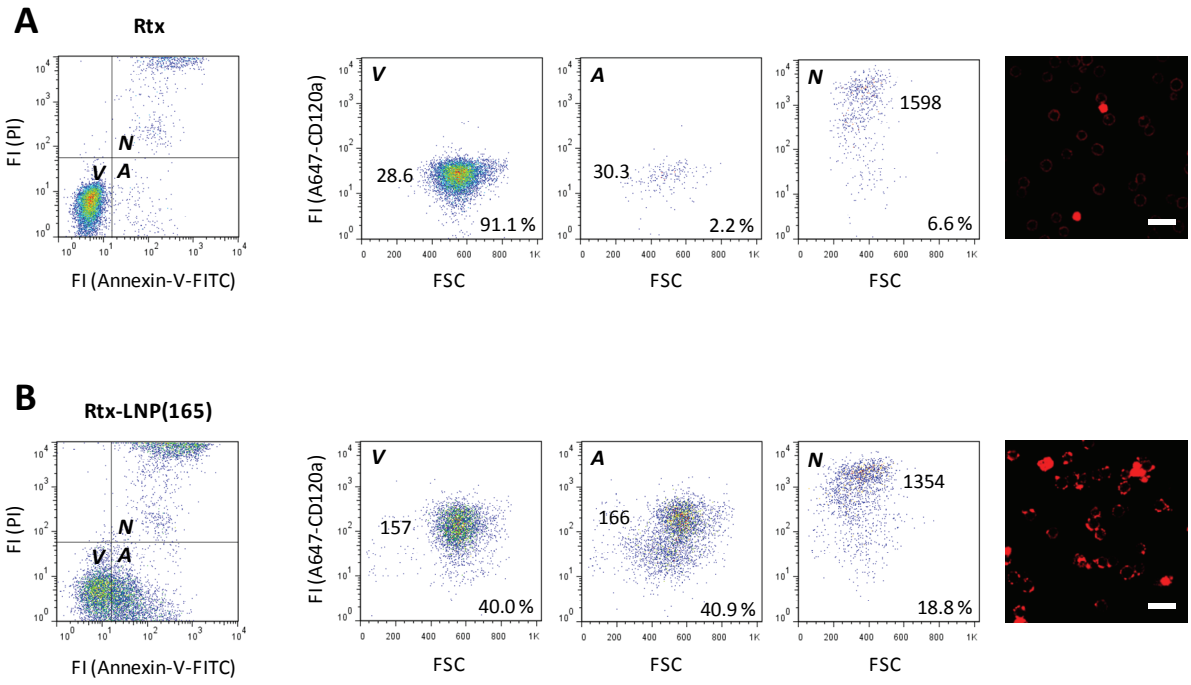

Figure 5.3 CD120a levels are elevated in the viable and apoptotic fractions of Rtx-LNP-treated cells 8 h after treatment. Ramos cells were treated with Rtx **(A)** or Rtx-LNP(165) **(B)** for 8 h, then triple-stained with Annexin-V-FITC, PI, and A647-CD120a. Gates were set for each quadrant on a plot of PI versus Annexin-V-FITC fluorescence intensities (shown at the left of the figure) using HBS-treated cells as a negative control (not shown). A647-CD120a expression within each of the three relevant quadrants is shown *(V*, viable; *A*, early apoptotic; *N*, necrotic). Mean fluorescence intensities and percentages of cells in each population are indicated on the dot plots. The fluorescence intensities in viable and apoptotic cells (PI^-)

represent the expression of plasma membrane-bound CD120a, while CD120a in necrotic cells is significantly elevated, presumably from intracellular, extracellular, and nonspecific staining. These data correlate with the confocal laser-scanning fluorescence microscopy images shown at the right of the figure, where elevated staining of A647-CD120a (*red*) is visible in Rtx-LNP(165)-treated cells, and necrotic cells are visible in both samples. *FI*, fluorescence intensity. *Scale bars*, 20 μm.

This experiment revealed that the expression of CD120a in viable and early apoptotic cells is low in cells treated with Rtx but higher in cells treated with Rtx-LNP(165). In both cases, the viable and early apoptotic fractions showed relatively equal levels of CD120a expression (shown directly on the dot plots). Since these fractions both constituted cells which excluded PI, these CD120a levels represent plasma membrane-bound (extracellular) CD120a. The mean fluorescence intensity (MFI) of an A647-labeled negative isotype control under the same conditions was 14.4 (not shown), and when this value is subtracted from the MFIs shown in Figure 5.3, the level of CD120a in the plasma membrane of viable and early apoptotic cells after treatment with Rtx-LNP(165) (Figure 5.3B) is 10-fold higher than that in Rtx-treated cells (Figure 5.3A). The data for HBS-treated cells was very similar to that for Rtx-treated cells and is therefore not shown. Regardless of treatment, necrotic cells showed much higher CD120a staining, possibly due to an internal pool of CD120a and/or nonspecific intracellular staining.

Confocal laser-scanning fluorescence microscopy images seen at the right of Figure 5.3 confirm the flow cytometry data since they show significantly higher levels of CD120a in the plasma membrane of cells treated with Rtx-LNP(165) compared to Rtx, and a few necrotic cells are visible in both cases with high staining throughout the cells. These data suggest that the direct mechanism of action of Rtx-LNP involves upregulation and activation of CD120a in the plasma membrane. This CD120a would subsequently form DISCs with caspase-8, leading to apoptosis. The upregulation of CD120a in the plasma membrane can only be responsible for apoptosis if it precedes apoptosis, and the observation that CD120a levels are equal in the viable and early apoptotic fractions of Rtx-LNP-treated cells does initially suggest that CD120a upregulation occurs before the onset of apoptosis.

5.4.4 Time course and valence dependence of CD120a upregulation

Having established that CD120a shows higher expression in the plasma membrane of Rtx-LNP-treated lymphoma cells, we next determined the time course of CD120a upregulation. At time points between 0 h and 48 h, plasma-membrane levels of CD120a were measured using flow cytometry by measuring the intensity of A647-CD120a staining within the PI^- cell population. As shown in **Figure 5.4A**, these experiments revealed that CD120a expression increased in the plasma membrane up to approximately 8 h post-treatment, then decreased to relatively stable levels by 24 h after treatment. This is contrasted to the A647-CD120a signal from the total cell population, which continued to increase up to 48 h post-treatment, consistent with Figure 5.2A & B (data not shown).

The maximum observed values were an 18-fold higher CD120a expression (relative to HBS) 8 h after treatment with Rtx-LNP(158) ($p < 0.001$ between this and other time points for the same treatment), and an 8.1-fold higher expression at 16 h after treatment with Rtx-LNP(63) ($p > 0.05$ for the 8 h time point, and $p < 0.05$ for the other time points). By 24 h post-treatment, these relative expression values decreased to 5.2 (valence 158) and 3.8 (valence 63) with respect to HBS at the same time point. Increases in plasma-membrane CD120a levels were not observed in cells treated with Rtx, which showed levels equal to HBS-treated cells (relative MFI = 1 in Figure 5.4A) at all time points ($p > 0.05$). A comparison of Figure 5.4A to Figure 4.5B shows that maximum apoptosis occurred approximately 16 h after peak plasma membrane CD120a levels (peak CD120a at 8h, apoptosis at 24 h post-treatment). This time course is consistent with the notion that Rtx-LNP treatment results in CD120a upregulation and activation leading to subsequent apoptosis.

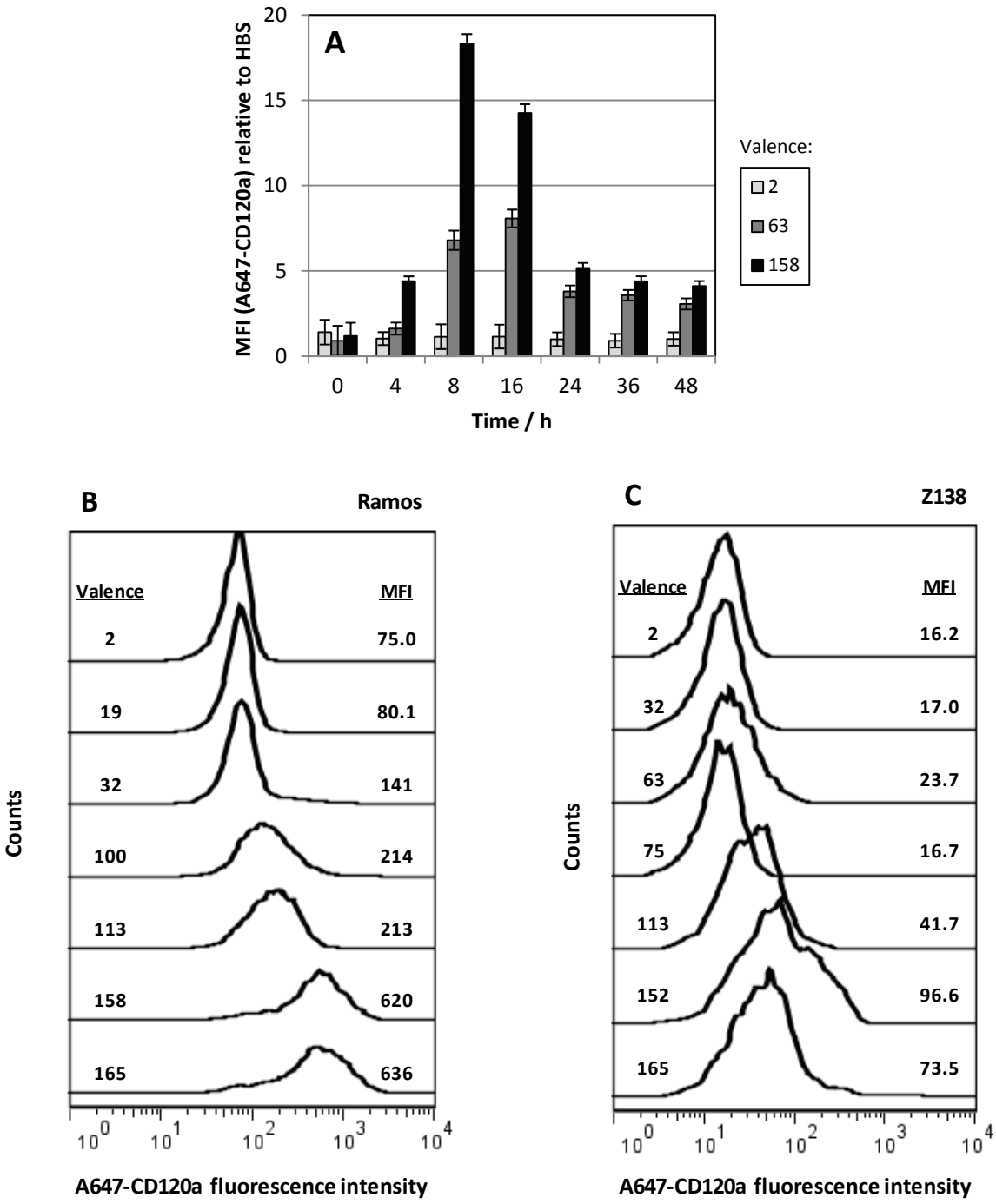

Figure 5.4 CD120a expression levels in the plasma membrane are highest at 8 h post-treatment and are valence-dependent.

(A) The expression of plasma membrane-bound CD120a in non-necrotic Ramos cells was significantly higher in cells treated with Rtx-LNP, suggesting that Rtx-LNP causes upregulation of CD120a in the plasma membrane. Peak CD120a levels in the plasma membrane were observed approximately 8 h post-treatment. **(B & C)** The treatment of Ramos **(B)** and Z138 **(C)** cells with Rtx-LNPs of higher valence resulted in enhanced upregulation of CD120a in the plasma membrane. This valence-dependent process mirrors the valence-dependent levels of apoptosis induced by Rtx-LNP shown in Figure 4.6. MFI values are shown on the histograms.

To determine if CD120a upregulation corresponds to the valence-dependent levels of apoptosis shown in Figure 4.6, the plasma membrane levels of CD120a were next measured after treating Ramos and Z138 cells with the various Rtx-LNP valences. **Figure 5.4B & C** illustrate that in all cases, treatment with the higher valences of Rtx-LNP resulted in more elevated CD120a expression, even though all cells were given the same dose of Rtx. Measured levels of CD120a also correlated with the percentages of apoptotic cells in Figure 4.6 insofar as different valences that induced relatively the same amount of apoptosis also resulted in equal expression of CD120a in the plasma membrane. Moreover, the Z138 lymphoma cell line was less sensitive to apoptosis induced by Rtx-LNP, and increases in the levels of CD120a in this cell line were more modest than in the Ramos cell line. Together, these data confirm that upregulation and activation of CD120a appears to play a central role in the direct mechanism of action of Rtx-LNP.

5.4.5 Colocalization of caspase-8 and CD120a

Next, confocal laser-scanning fluorescence microscopy images were obtained of Ramos cells treated with different valences of Rtx-LNP and dual-labeled with A647-CD120a and FAM-LETD-FMK, the latter of which labels cleaved caspsase-8 (Section 5.3.3). FAM-LETD-FMK is plasma-membrane permeable, but cells were not permeabilized prior to A647-CD120a staining in order to visualize CD120a only in the plasma membrane. Representative images are shown in **Figure 5.5** for cells treated with Rtx-LNP with valences of 32, 75, and 113.

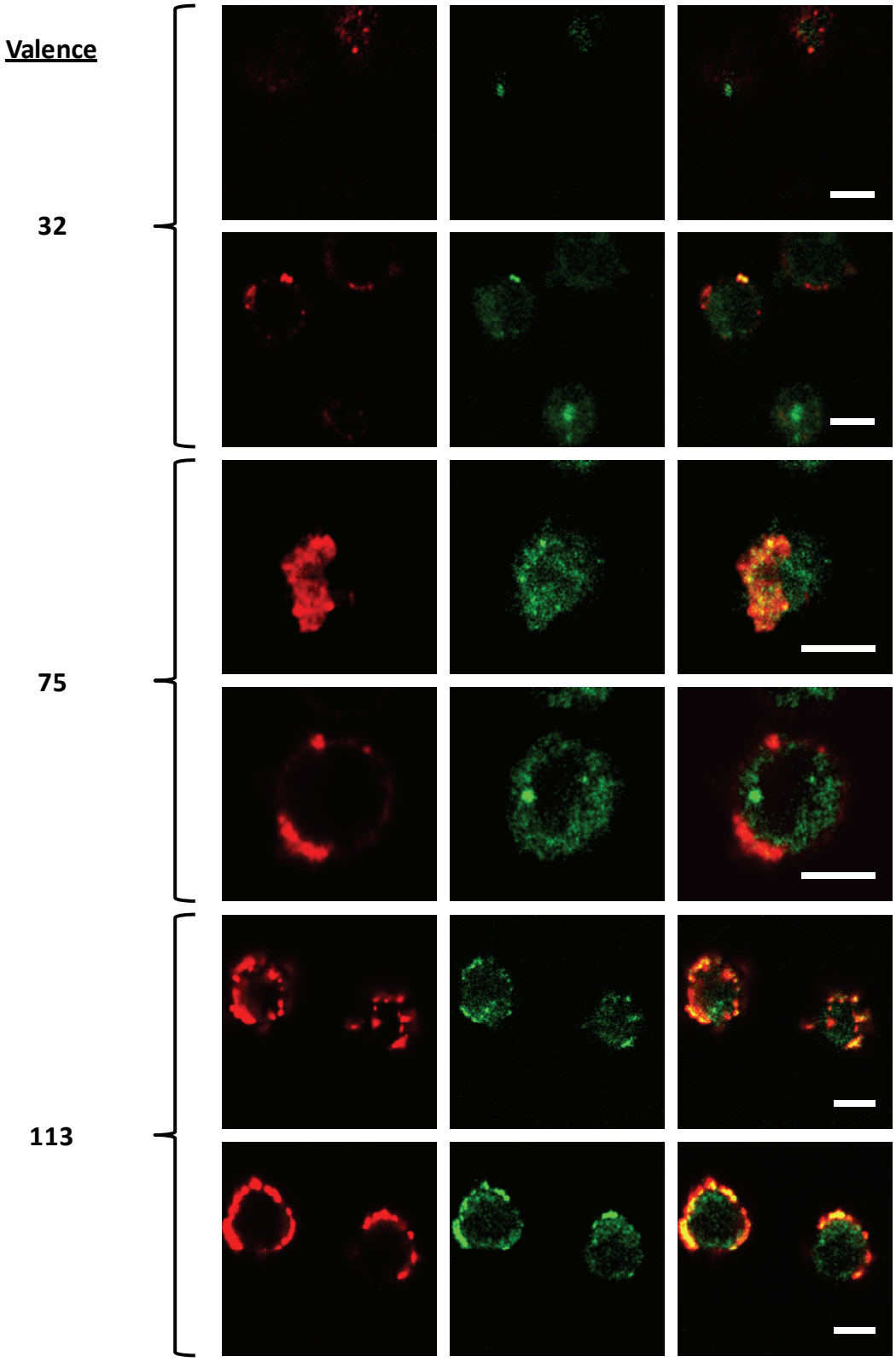

Figure 5.5 Two slices of the same representative non-necrotic Ramos cells 24 h after treatment with different valences of Rtx-LNP.

Activated caspase-8-rich regions (*green;* FAM-LETD-FMK emission) can be seen inside the cell colocalized with and directly adjacent to CD120a-enriched domains in the plasma membrane (*red*; A647-CD120a emission), suggesting that CD120a and

caspase-8 are both DISC constituents. As the valence increased, CD120a expression became higher, and caspase-8 activation became increasingly associated with plasma membrane CD120a. *Scale bars*, 5 μm.

These images visually confirm that greater CD120a upregulation occurred after treatment with Rtx-LNPs of higher valence, since levels of CD120a (*red*) became more intense as the valence increased. The images also show specific colocalization of CD120a and caspase-8, as well as caspase-8 staining in the intracellular region directly adjacent to CD120a-enriched domains in the plasma membrane; this is particularly the case at the higher valences. Procaspase-8 is cleaved to caspase-8 while it is bound to the plasma membrane-associated DISC; after cleavage, caspase-8 leaves the inner leaflet of the plasma membrane and enters the cytoplasm[87, 171]. This is illustrated in the images, which show an increasing degree of colocalized and adjacent caspase-8 and CD120a as the valence increased from 32 to 113. These experiments visually imply that Rtx-LNP treatment results in CD120a upregulation and DISC formation with procaspase-8, which is ultimately cleaved to caspase-8, resulting in the initiation of apoptosis.

5.4.6 CD120a upregulation and direct induction of apoptosis result from Rtx multivalency and not the liposomal component of Rtx-LNP

To more fully understand why multivalent Rtx-LNP induces CD120a upregulation, CD120a/procaspase-8 DISC formation, and significantly higher levels of apoptosis compared to equal doses of Rtx, it was important to examine the role of the liposome in Rtx-LNP. As described in Section 1.2.2, the liposome serves as a scaffold for bridging many Rtx molecules together into a multivalent configuration, which is distinct from traditional applications of liposome technology. If the liposome serves only a structural role without contributing to CD120a upregulation or induction of apoptosis, then the same effects should also be present when cells are treated with multivalent Rtx constructs that are not based on liposomes.

As an alternative to Rtx-LNPs, polystyrene microspheres (MS) with a diameter of 100 nm were employed to create multivalent Rtx; these MS have the same diameter as the SUV used to prepare Rtx-LNPs. To mirror the preparation of Rtx-LNPs employed in Chapter 3, Rtx was biotinylated on a NIMAC column under identical conditions (Section 3.3.6), and streptavidin-coupled MS (streptavidin-MS) were saturated with Rtx-biotin, as described in Section 5.3.8. The resulting Rtx-MS were added to Ramos cells, and a dose-response curve is shown in **Figure 5.6A**. This figure illustrates that Rtx-MS induced significantly elevated levels of apoptosis compared to equal doses of Rtx, which mirrors the behavior of Rtx-LNP. At a dose of 4.1 μg Rtx (in Rtx-MS), 43% of cells were undergoing early apoptosis after 24 h, while for doses of 20.6 μg and higher, equal levels of apoptosis were observed for all doses (~60%); this is in contrast to 3–4% early apoptosis induced by bivalent Rtx at all doses tested (not shown). Maximum levels of early apoptosis observed after treatment with Rtx-MS were similar to those measured after treatment with Rtx-LNP, as shown in Figure 4.6A. Another parallel between the two figures is the inverse relationship between the viable and apoptotic cell fractions, indicating that in both cases cells were dying *via* apoptosis and not another mechanism of cell death that would result in viable cells directly becoming necrotic. Treatment of cells with Rtx-biotin or streptavidin-MS resulted in levels of apoptosis equivalent to treatment with HBS (not shown).

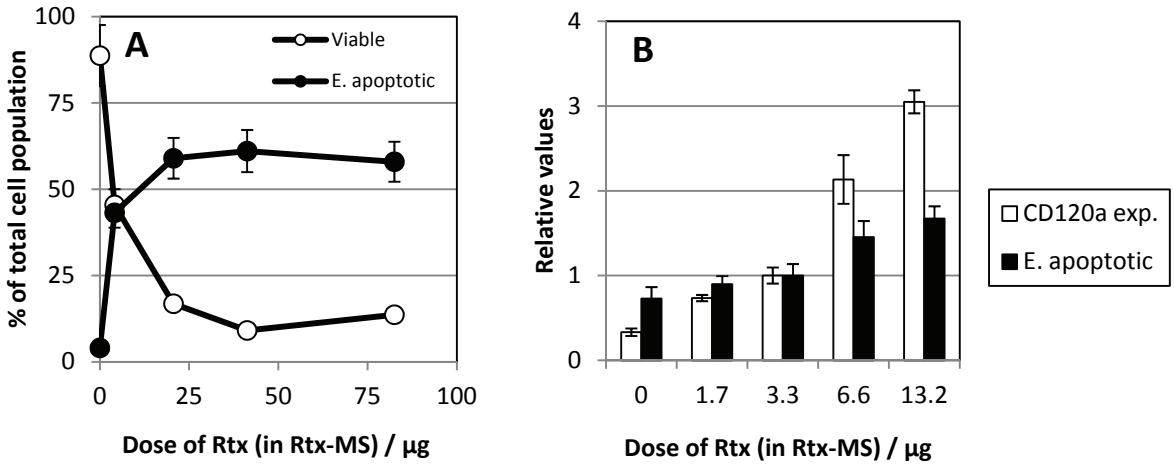

Figure 5.6 Apoptosis via upregulation of CD120a is not an effect of the liposomal component of the formulation of Rtx-LNP.

(A) Dose-response curve for the treatment of 1.25×10^5 Ramos cells in 250 µL medium with Rtx-MS for 24 h. **(B)** Similar to treatment with Rtx-LNP, Ramos cells treated with different doses of Rtx-MS exhibited increased apoptosis alongside elevated plasma membrane CD120a levels. Both CD120a expression and apoptosis were measured 12h after treatment (compared to 24h in **(A)**) in order to simultaneously measure CD120a expression and early apoptosis, which show maximum values at 8h and 24h, respectively.

Cells were next treated with amounts of Rtx-MS in the region where dose-dependent levels of apoptosis were observed (below a 25 µg Rtx dose). Levels of CD120a in the plasma membrane and apoptosis were measured simultaneously with flow cytometry 12 h after treatment. The resulting data, shown in **Figure 5.6B**, show that the dose-dependent increases in apoptosis correspond to elevated levels of CD120a in the plasma membrane. The fraction of cells in early apoptosis increased from 6.9 % to 16 % (2.3-fold; $p < 0.005$) from 0 to 13.2 µg Rtx (in Rtx-MS) while the MFI from A647-CD120a increased from 43.7 to 402 (9.2-fold; $p < 0.0001$) for the same dose difference. Each successively higher dose in this figure shows an elevated CD120a expression compared to the next lowest dose ($p < 0.05$ between all A647-CD120a MFIs). However, not all measured levels of apoptosis show differences that are statistically significant; $p > 0.05$ for doses of 0–3.3 µg and 6.6–13.2 µg, but $p < 0.05$ for pairs of doses when one dose is from each of these

groups. Note that apoptosis values in Figure 5.6B were measured at 12 h post-treatment compared to 24 h post-treatment in Figure 5.6A; this was necessary to simultaneously measure CD120a levels and apoptosis in the same cells, which show maximum values at 8 h and 24 h, respectively. Overall, these results demonstrate that a liposome specifically is not required to achieve beneficial effects from multivalent Rtx because the same mechanism of action and maximum levels of apoptosis were reproduced using a non-liposomal formulation.

5.5 Discussion and conclusions

5.5.1 Discussion

The molecular basis of the direct mechanism of action of Rtx is poorly defined, but the work in this chapter provides some of the first evidence explaining the direct induction of apoptosis that is observed when Rtx is hypercrosslinked but not when it is bivalent (Sections 1.4.3 and 1.6.1). After cells are treated with Rtx-LNP, the direct mechanism uncovered here consists of upregulation of CD120a in the plasma membrane followed by activation of caspase-8 (consistent with CD120a/procaspase-8 DISC formation) and subsequent apoptosis.

This mechanism of action is supported by the observation that of all the known death receptors, CD120a showed the highest upregulation after treatment with Rtx-LNP (Figure 5.2). It was upregulated equally in the plasma membrane of both viable and early apoptotic cells (Figure 5.3), suggesting that upregulation preceded apoptosis. This was confirmed with time-course experiments in Figure 5.4A which showed that peak plasma-membrane CD120a levels occurred 8 h after treatment with Rtx-LNP, while maximum apoptosis was observed 24 h after treatment, as indicated in Figure 4.5B. The time course of apoptosis was also consistent with the measured levels of activated caspase-8 over time shown in Figure 5.1A.

Moreover, the valence-dependent levels of CD120a expression in the plasma membrane (Figure 5.4B & C) corresponded to the valence-dependent levels of activated caspase-8 (Figure 5.1C) as well as the valence-dependent levels of apoptosis in Figure 4.6. Finally, the same CD120a-dependent mechanism was observed in two lymphoma cell lines (Ramos and Z138), and it was also the same regardless of the type of multivalent construct used (Rtx-LNP or Rtx-MS; Figure 5.6). Overall, this data supports a role of CD120a upregulation and activation in the direct mechanism of action of multivalent Rtx.

Given that CD120a is expressed in all human cell types (Section 5.2.3), there are innumerable reported instances of CD120a upregulation in the pathogenesis of a wide variety of diseases. For example, its upregulation has been associated with cardiovascular diseases in diabetic rats[188], ocular allergic inflammation[189], and response to treatment for chronic hepatitis C[190]. Various viruses, bacteria, and parasites also act by modulating the expression of CD120a, which may result in caspase-dependent apoptosis or NF-κB-induced expression of inflammatory or antiapoptotic genes[191]. In oncology specifically, CD120a has been shown to be upregulated by estrogen in human breast adipose fibroblasts, serving as a mechanism that supports breast tumor growth[192]. It was also upregulated on endothelial cells *in vitro* and *in vivo* by endothelial monocyte activating polypeptide-II, a tumor-derived inflammatory cytokine[193]. Finally, CD120a was shown to be upregulated after treating chronic lymphocytic leukemia (CLL) B-cells with fludarabine, resulting in apoptosis[194].

The molecular basis of CD120a upregulation in the plasma membrane has been described as a method of sensitizing cells to its ligand, TNF-α (refs. 172, 189, 193). To test whether cells showed increased sensitivity to TNF-α following treatment with Rtx-LNP, cells were treated with soluble TNF-α in the presence and absence of different valences of Rtx-LNP. In all cases, regardless of whether Rtx-LNP was added, the addition of TNF-α to cells from 0.01 ng/mL to 1 μg/mL resulted in levels of apoptosis equivalent to treatments in the absence of TNF-α (data not shown).

This strongly suggests that Rtx-LNP-induced apoptosis through CD120a is ligand-independent, consistent with other reports of ligand-independent death receptor activation[181-186]. Although previous reports have indicated that soluble TNF-α associates with CD120a while membrane-bound TNF-α associates with CD120b (which does not contain a death domain)[195], ultimately the levels of soluble and plasma membrane-bound TNF-α in treated and untreated samples of cells should be measured in order to firmly establish ligand independence of this signaling process.

Together, this chapter provides a proof-of-concept that the methodology in Chapter 3 can be used to prepare many valences for use in studying the mechanism of action of multivalent Ab-LNPs. It also shows that non-liposomal formulations exhibit equivalent therapeutic activity to Ab-LNPs through the same mechanism of action. This indicates that information obtained using Rtx-LNP in terms of the therapeutic activity of an Ab (for example, the valence at which optimal activity is observed) can be employed in the development of formulations of multivalent Abs that do not utilize liposomes. This may be useful in cases where preparing many different valences of specific non-liposomal multivalent Abs is difficult or not feasible.

The fact that multivalent therapeutic Abs can show enhanced efficacies regardless of the specific formulation (Figure 5.6) further supports the conclusions of Chapter 4 where the improved therapeutic effects were driven by hypercrosslinking of the target by the multivalent Ab. It can be envisioned that another method of hypercrosslinking would entail treatment with Ab followed by a reagent that hypercrosslinks the Ab. For example, as described in Section 1.4.3, Rtx elicits higher levels of apoptosis when bivalent crosslinking is achieved using a 2^{o}Ab. Another conceivable mechanism of hypercrosslinking may occur *in vivo* when the Fc region of Rtx present on lymphoma cells interacts with FcγR on effector cells of the immune system. This constitutes a multivalent interaction that is known to play a role in ADCC (Sections 1.4.2 & 2.2.2), but it has not been shown to contribute to the direct mechanism of action of therapeutic Abs. The results from this chapter

suggest that if effector cells can induce apoptosis in Rtx-treated cells by a CD120a-dependent mechanism, then they are capable of hypercrosslinking Rtx sufficiently to directly induce apoptosis *in vivo*. This would imply that a CD120a-dependent mechanism of action is not only applicable to Rtx-LNP, but also to regular bivalent Rtx therapy, shedding light on the poorly defined direct mechanism of action of this drug.

5.5.2 Conclusions

The direct mechanism of action of multivalent Rtx constructs, including Rtx-LNP and Rtx-MS, involves the induction of apoptosis resulting from CD120a upregulation in the plasma membrane and resultant activation of caspase-8. Inhibition of caspase-8 significantly decreased the levels of other activated caspases as well as Rtx-LNP-induced apoptosis. This is consistent with the formation of DISCs that include both CD120a and procaspase-8, and confocal fluorescence microscopy images showed CD120a/caspase-8 colocalization as well as caspase-8 present in intracellular regions adjacent to CD120a-enriched domains on the cell surface. Higher valences of Rtx-LNP, which induced greater levels of apoptosis, also caused more significant CD120a upregulation and caspase-8 activation, supporting earlier conclusions that more extensive hypercrosslinking of CD20 drives this direct mechanism of action. Overall, this work provides a proof-of-concept that the methodology in Chapter 3 can be used to prepare many valences of multivalent Ab-LNPs for use in mechanistic studies, and the results of such studies can be applied to the development of both liposomal and non-liposomal multivalent formulations.

6 *In vivo* relevance of a CD120a-dependent mechanism of action of rituximab

6.1 Synopsis

The previous chapter identified a novel mechanism of action of multivalent Rtx *in vitro* that involves the upregulation of CD120a and ensuing apoptosis. By considering recent work concerning the molecular biology of CD120a, this chapter examines whether such a mechanism is plausible *in vivo* after normal bivalent Rtx therapy. The results suggest a possible treatment strategy for improving the sensitivity of lymphoma cells to Rtx.

6.2 Background

6.2.1 The biology and function of CD120a

Unlike other death receptors (discussed in Section 5.2.3), CD120a is primarily involved in mediating inflammation and not cell death[174]. It is often activated by its ligand, TNF-α, which is a trivalent ligand found in two forms, a soluble form and a plasma membrane-bound form. TNF-α is also specific to another TNFR superfamily member, CD120b (also known as TNFR2), which is not a death receptor since it does not possess an intracellular death domain[172]. It has been suggested that the soluble form primarily activates CD120a while the membrane-bound form activates CD120b[195], but CD120a appears to dominate TNF-α signaling in most cell types[174, 175].

TNF-α plays a key role in inflammation and immunity, as well as the proliferation and differentiation of many different cell types[177]. Like almost all of the TNFR ligands, it is expressed by cells of the immune system, including B cells, T cells, NK cells, and macrophages. CD120a, on the other hand, is expressed by every cell type in the body (Section 5.2.3), and although the other TNFR family members are expressed by a wide variety of cells, they are not done so as ubiquitously as

CD120a[177]. It is almost exclusively expressed at constitutively low levels and is controlled by a noninducible promoter[174].

CD120a and other TNFRs contain cysteine-rich repeats in their extracellular domains that mediate homophilic interactions in the absence of ligand. The preligand assembly domain is the membrane-distal first cysteine-rich domain, and it enables TNFRs to form homotrimers[180]. Binding of the trivalent ligand to the preformed complexes induces intracellular signal transduction. Ligand binding is not always required for activation of the receptor, however, since signal transduction of CD120a and other death receptors has been reported in the absence of ligand[181-186].

Once activated, CD120a is capable of inducing both proapoptotic and antiapoptotic signals. As described in further detail below, the signal that is transmitted is ultimately dictated by the compartmentalization of CD120a in the plasma membrane[175]. Within minutes of CD120a engagement in response to TNF-α or independent of ligand, one of two complexes can be formed: Complex I, which regulates the expression of antiapoptotic proteins, or Complex II, which triggers cell death[196, 197].

Activation of CD120a induces the recruitment of specific proteins to the plasma membrane (TRADD, RIP1, TRAF2, and c-IAP1/2), resulting in the formation of Complex I. These proteins then undergo post-translational modifications that lead to the translocation of NF-κB to the nucleus and transcription of antiapoptotic target genes such as cFLIP, cIAP-1, cIAP-2, TRAF1, and TRAF2[174, 177]. Alternatively, Complex II can form, which contains the DISC as described in Section 5.2.2. It therefore contains procaspase-8, which upon cleavage to caspase-8, induces apoptosis by the extrinsic pathway. Complex II forms under conditions where Complex I activates JNK in a sustained manner. JNK inhibits cFLIP, which itself inhibits the cleavage of procaspase-8 in the DISC/Complex II[174, 177]. It has been shown that Complex I remains associated with the plasma membrane while clathrin-dependent endocytosis of Complex II is required for proapoptotic signaling, although endocytosis may be cell-type dependent[175].

Many reports have demonstrated that Complex I efficiently activates NF-κB only when present in plasma membrane rafts (see below). This is because the necessary post-translational modifications required for NF-κB activation can only take place in the raft microenvironment[174, 177]. Outside of rafts, Complex I therefore activates NF-κB poorly, and the proapoptotic Complex II is formed instead[198].

6.2.2 Plasma membrane rafts

The plasma membrane is an extremely heterogeneous environment. In contrast to the familiar "fluid mosaic" model of the plasma membrane[199], the local concentrations of proteins and other molecular constituents vary considerably across the membrane surface[200]. Normal cell signaling events depend on these variations in local protein concentrations, and disruption of this regulation is a factor in the pathogenesis of many diseases including cancer[201-204]. These non-random arrangements are maintained by the complex interplay that separates the plasma membrane into various types of domains such as clathrin-coated pits, caveolae, and membrane rafts[205].

Plasma membrane rafts are small (10–200 nm) domains, enriched in cholesterol (Chol) and sphingolipids, that compartmentalize cellular processes[206]. They are unstable and transient on their own, but if stabilizing interactions arise, they aggregate into larger platforms[207], and these platforms play significant roles in cell signaling[108, 208].

For example, rafts and platforms confine specific proteins to small regions of the plasma membrane, and only proteins within the same raft or platform may interact with each other. This limits the number of other proteins with which a raft-associated protein may interact[209]. In addition, membrane rafts are slightly thicker and more tightly packed than the contiguous fluid phase, which may impact protein conformation and thus function[210]. Such spatial and temporal modulations of local protein concentrations in the plasma membrane play key roles in signal transduction, including,

for example, those of IgE Fc receptor I (FcεRI) and the T-cell antigen receptor[211-213], as well as Rtx/CD20 (see below). Because the plasma membrane localization of a protein often dictates the signals it transmits, it is surprising that such information is usually not specified in traditional linear signaling pathways.

The protein composition of rafts and signaling platforms is highly dynamic[214-217]. The raft affinity of a given membrane protein is affected by (and affects) the formation of stabilized raft platforms as a result of lipid-lipid, protein-protein, and lipid-protein interactions[207]. One important example is that when a moderately raft-associating protein becomes oligomerized as a result of crosslinking, its raft affinity usually increases or decreases[108, 218-220]. This has been shown in model membrane systems[221, 222] as well as live cells[223, 224]. Clearly this has implications with multivalent Ab constructs, which hypercrosslink their target in the plasma membrane; it would be expected that hypercrosslinking would modulate the raft affinity of the target.

In terms of Rtx, many studies have documented that the raft affinity of CD20 increases as early as 15 min following Rtx treatment[74, 168, 169]. Rtx induces apoptosis in $CD20^+$ lymphoma cell lines in culture only when it is crosslinked with reagents such as a 2^oAb (Sections 1.4.3 and 1.6.1), and crosslinking may be related to the modulation of CD20 raft affinity; some reports have shown that apoptosis does not occur after Rtx/2^oAb treatment if membrane rafts are disrupted through Chol depletion[74].

With respect to the relationship between rafts and CD120a, disrupting rafts by depleting cells of Chol has been shown in numerous instances to switch antiapoptotic CD120a signaling (Complex I) to proapoptotic signaling (Complex II). The Chol content of the plasma membrane is therefore one factor that influences the dual nature of CD120a signaling[174, 175, 177, 196-198]. The signaling of CD95 (Fas) has also been shown to depend on rafts, but unlike CD120a, CD95 triggers apoptosis when it translocates into (rather than out of) rafts[186]. The interplay between CD20,

CD120a, and rafts after treatment with multivalent Rtx may therefore give clues to the mechanism of action of the direct induction of apoptosis.

6.2.3 Studying plasma membrane rafts

6.2.3.1 Detergent-resistant membranes

The predominant biochemical means to assess the potential affinity of a protein to plasma membrane rafts is through the analysis of detergent-resistant membranes (DRMs). It was originally observed that raft constituents were insoluble in cold nonionic detergents such as Triton X-100 (TX100), and that the resulting DRM fractions could be isolated by flotation using equilibrium density gradient centrifugation[225]. It was found that detergent resistance of proteins in DRMs was related to Chol content[226], so it was hypothesized that DRMs were equivalent to membrane rafts.

It became clear, however, that DRMs are in fact the result of an aggregation process that is not fully understood[227-229]. Model membrane studies have shown that although raft lipids resist solubilization by detergent[230, 231], the detergent can also artificially induce the formation of rafts[232]. DRM analysis has also been shown to be highly cell type-dependent[233]. Although useful as a tool to initially assess raft affinity, DRMs do not reflect membrane organization under physiological conditions and therefore cannot be equated with rafts[228].

Although detergent solubility and insolubility are not strict criteria in themselves, the usefulness of DRM analysis lies in observations of changes in DRM association upon induction of physiologically relevant stimuli[234]. One of the first such demonstrations was in studies on the allergic immune response, where the multivalent ligand IgE crosslinked the FcεRI receptor, which became detergent insoluble along with its downstream effectors[235]. The use of DRMs therefore represents a preliminary means of assessing raft affinity; differences in detergent solubility before and after biological stimuli can be used as a basis for raft affinity[234].

Alternative approaches to study rafts have been described including detergent resistance analysis on intact cells rather than cell lysate after ultracentrifugation[236] as well as the preparation of fractions enriched in raft constituents without the use of detergents[237]. A common way to support DRM data is with confocal laser-scanning fluorescence microscopy by observing the colocalization between a protein of interest and a constituent known to associate constitutively with rafts. A frequently employed raft marker is ganglioside GM1, which can be detected with fluorescently labeled cholera toxin B subunit (CTX)[224]. To further study the raft affinity of a protein, data obtained using DRMs and/or microscopy can be examined under conditions of modulated Chol content in the plasma membrane. Addition of Chol results in the formation of new rafts, while decreasing the Chol content disrupts raft integrity[238].

6.2.3.2 Manipulation of plasma membrane cholesterol content

MBCD is a reagent commonly used to remove Chol from the plasma membrane[201, 238]. It is a cyclic oligosaccharide with hydrophilic external faces and a hydrophobic internal cavity. The mechanism by which it efficiently removes Chol is related to its ability to lower the activation energy for Chol efflux; this is done by allowing the Chol molecule to incorporate directly into the hydrophobic cavity without having to pass through an intermediate aqueous phase. It is also this property that allows MBCD to be an efficient donor of Chol, so by employing MBCD complexed with Chol (MBCD/Chol), cellular Chol content can be enriched[239]. It is understood that MBCD disrupts plasma membrane rafts by removal of Chol, but some caution must be observed because other cellular effects have been observed due to MBCD treatment that are unrelated to raft disruption, such as disruption of exocytosis, blockage of clathrin-coated endocytic vesicles, and disruption of the actin cytoskeleton[210]. It is therefore important to use more than one method of Chol depletion to verify results obtained with MBCD.

Other methods of disrupting rafts by Chol interference include sequestration using filipin, nystatin or amphotericin, or inhibition of Chol synthesis using 3-hydroxy-3-methylglutaryl coenzyme A (HMG-CoA) reductase inhibitors, also known as statins[240]. For example, simvastatin is a drug prescribed for lowering total Chol levels in order to control hypercholesterolemia and to prevent atherosclerosis. It was originally marketed under the trade name Zocor but is now available generically in most countries[241]. Simvastatin is also used to inhibit Chol synthesis in cells *in vitro*. This results in the disruption of plasma membrane rafts by decreasing total plasma-membrane Chol levels[240, 242, 243].

6.2.4 Can the direct mechanism of action of bivalent Rtx involve CD120a *in vivo*?

Chapter 5 illustrated that the mechanism of action of Rtx-LNP involves apoptosis resulting from the upregulation of CD120a. This mechanism of action was observed for different types of multivalent Rtx constructs (Rtx-LNP and Rtx-MS), suggesting that CD20 hypercrosslinking was responsible for the enhanced therapeutic effects as opposed to the liposomal or MS component of the formulation. This chapter extends these findings to investigate whether a CD120a-dependent mechanism could occur *in vivo* after normal Rtx therapy due to hypercrosslinking of Rtx by FcγR-expressing effector cells of the immune system. Such a mechanism has not been demonstrated *in vivo*, and it is not clear whether FcγR on effector cells would be capable of producing sufficient hypercrosslinking to induce direct therapeutic effects. It is known, however, that adequate hypercrosslinking of FcγR is achieved by Rtx *in vivo* to induce ADCC (Sections 1.4.2 & 2.2.2).

Based on the known function and biology of CD120a (Section 6.2.1), the experiments in this chapter also examine how modulation of the plasma-membrane Chol content of lymphoma cells influences the therapeutic efficacy of multivalent Rtx. Under conditions of increased and decreased plasma-membrane Chol concentrations, levels of apoptosis as well as CD120a detergent resistance and membrane raft localization are characterized after treatment with multivalent Rtx. These

experiments help define cases where lymphoma cells may be more or less sensitive to Rtx treatment, which is of particular interest because clinical resistance to Rtx is not well understood[139, 140].

6.3 Materials and methods

6.3.1 Materials and cell lines

Alexa Fluor 488-labeled cholera toxin subunit B (A488-CTX), Texas Red-labeled phalloidin, Annexin-V binding buffer, recombinant human Annexin-V labelled with fluorescein isothiocyanate (Annexin-V-FITC), an Alexa Fluor 568 (A568) protein labeling kit, and an Alexa Fluor 647 (A647) monoclonal Ab labeling kit were obtained from Invitrogen (Burlington ON, Canada). Alexa Fluor 647 (A647)-labeled Abs against CD120a (A647-CD120a) and an A647-labeled mouse IgG2a negative control were obtained from AbD Serotec (Kidlington, UK). Streptavidin-coated polystyrene microspheres with a diameter of 100 nm (streptavidin-MS) were purchased from Bangs Laboratories (Fishers IN, USA). A goat anti-human-Fcγ-fragment secondary Ab (2^{o}Ab) with no reactivity toward the Fab region and minimal reactivity toward Fc regions of IgG of other species was purchased from Jackson ImmunoResearch (West Grove PA, USA). Human peripheral blood mononuclear cells (PBMCs) from healthy donors, CTL-Anti-Aggregate-Wash supplement, and CTL-Test medium were purchased from Cellular Technology Ltd. (Cleveland OH, USA). Unless noted otherwise, all other reagents were obtained from Sigma-Aldrich and were of the highest quality available.

Ramos and Z138 cell lines were acquired and maintained as described in Section 4.3.2.

6.3.2 Preparation of Rtx-LNP and Rtx-MS

The methodology described in Chapter 3 was used to prepare and characterize of Rtx-LNPs with valences up to 204. Two separate batches of four valences each were prepared. Please see Section 5.3.8 for the procedure used to prepare Rtx-MS.

6.3.3 Depletion and augmentation of plasma membrane cholesterol levels

To deplete the plasma membrane of cells of Chol using MBCD, cells were treated with different concentrations of MBCD for times up to 16 h to determine the toxicity of MBCD in each cell line used. In Ramos cells, a final concentration of 0.2% MBCD (w/v) was not toxic but concentrations of 0.3% and higher were. MBCD treatment at concentrations up to 0.3% was performed at the same time as treatment with Rtx, Rtx-LNP, or controls. To insert additional Chol into the plasma membrane, cells were treated with complexes consisting of Chol-loaded MBCD (MBCD/Chol). These complexes were prepared as previously described[239] using a stock solution containing 3.5 mM Chol and 3.4% MBCD, representing a 25:1 mass ratio of MBCD to Chol. MBCD/Chol was added to cells in the same way as MBCD. Reported values of MBCD/Chol added are with respect to the concentration of MBCD.

To reduce plasma membrane levels of Chol through inhibition of Chol synthesis using simvastatin, a titration of simvastatin was performed in each cell line used in order to determine its toxicity. In Ramos cells, simvastatin was not toxic up to doses of 10 μM, but at doses of 30 μM and above, it was found to be cytotoxic after a 16 h incubation time. In the same way as MBCD and MBCD/Chol, simvastatin was added with Rtx, Rtx-LNP, or controls, and incubated for up to 16 h. Analyses were performed as described in previous sections.

6.3.4 Use of flow cytometry to determine levels of apoptosis or expression levels of cell-surface proteins

Please see Sections 5.3.5–5.3.6; the same procedures were used.

6.3.5 Assay for quantifying the detergent resistance of plasma membrane-associated proteins

A previously described method was used to quantify the degree to which plasma membrane proteins are resistant to solubilization by the nonionic surfactant TX100[236]. Briefly, cells were treated with HBS, Rtx, or Rtx-LNP, and stained with a fluorescently tagged Ab directed against a plasma membrane constituent for which the detergent solubility was being measured (treatment and staining were performed as described in previous sections). Cells were resuspended in cold PBSB, and mean fluorescence intensities (MFIs) of labeled cells were measured in triplicate before (MFI_{lab}) and after ($MFI_{lab+TX100}$) treatment with cold TX100 at a concentration of 0.2% for 5 min. Autofluorescence of unlabeled cells was also measured before (MFI_{auto}) and after ($MFI_{auto+TX100}$) TX100 treatment. The quantity defined as detergent resistance (DR) was then calculated as follows:

$$DR = (MFI_{lab+TX100} - MFI_{auto+TX100}) / (MFI_{lab} - MFI_{auto})$$

The method was verified using GM1 as a positive control (using A488-CTX) and CD95 as a negative control (using A647-CD95). GM1 is generally regarded as constitutively raft-associated[201] while CD95 is non-raft-associated in unstimulated cells[198, 244]. The positive control showed DR values approximately equal to 1 while for the negative control, DR < 0.35 (data not shown). The same measurements were performed after Chol depletion using 0.2% MBCD for 16 h, and the DR of the positive control dropped to 0.54 or lower while the DR of the negative control was unaffected (not shown). These experiments verified that DR values close to 1 represent plasma membrane proteins (or lipids) that are detergent-resistant, while the detergent solubility increases as DR values decrease.

6.3.6 Confocal laser-scanning fluorescence microscopy

Samples were prepared and imaged using the same procedure as described in Section 5.3.7. The labeling of GM1/plasma membrane rafts with A488-CTX was carried out in the same way as A647-CD120a staining, but the staining of F-actin staining using Texas Red phalloidin, required additional steps. F-actin labeling was carried out immediately after the step where cells were fixed with paraformaldehyde. Cover slips were washed with HBS and cells were permeabilized with 75 µL of 0.5% Triton X-100 (TX100) in HBS for 5 min; samples were washed again with HBS, then a 25 µL drop of PBSB containing 0.25 µL of a 0.2 U/µL Texas Red phalloidin was added for 20 min in order to stain F-actin, then washed with HBS. Sample preparation, image acquisition, and analysis proceeded as described in Section 5.3.7.

6.3.7 Experiments using Ramos cells pretreated with Rtx or A568-Rtx followed by addition of 2^{o}Ab or 2^{o}Ab-MS

Samples of 2^{o}Ab-MS were prepared in the same way as Rtx-MS as described in Section 5.3.8, with Rtx being replaced with 2^{o}Ab.

A568-labeled Rtx (A568-Rtx) was prepared using an A568 protein labeling kit according to the manufacturer's instructions. For experiments involving 2^{o}Ab-MS, Ramos cells were pretreated with saturating levels (see Figure 4.1) of Rtx or A568-Rtx (20 µg per 2.5×10^{5} cells in 500 µL medium) for 1 h at 37 ^{o}C. Cells were washed with medium to remove unbound Rtx or A568-Rtx, and were subsequently treated with different amounts of 2^{o}Ab or 2^{o}Ab-MS for different times, depending on the experiment.

6.3.8 Coculture of treated Ramos cells and human peripheral blood mononuclear cells

A sample of Rtx was labeled with A647 using an A647 monoclonal Ab labeling kit according to the manufacturer's instructions to produce A647-Rtx. A647-Rtx induced apoptosis and elevated CD120a expression upon hypercrosslinking with 2^{o}Ab-MS to an equivalent extent as unlabeled Rtx (data not shown). Ramos cells at 5.0×10^5 cells/mL were treated with 20 μg/mL Rtx or A647-Rtx (see below) or an equivalent volume of HBS for 1 h at 37 ^{o}C. Cells were washed with CTL-Test medium to remove unbound Rtx or A647-Rtx, and were resuspended in CTL-Test medium at 2.0×10^6 cells/mL. Cryopreserved human PBMCs were thawed using CTL-Anti-Aggregate-Wash supplement according to the provider's instructions, and were resuspended in CTL-Test medium at 4.0×10^6 cells/mL. Viability was >98% as assessed by trypan blue exclusion.

Appropriate volumes of cells were combined to obtain different ratios of Ramos:PBMC cells from 1:0 to 1:8, and CTL-Test medium was added to bring the final cell concentration to 1.0×10^6 cells/mL. Co-incubation at 37 ^{o}C was allowed to proceed for 16 h for measurement of CD120a or apoptosis levels. Previous experiments showed that there were no differences between Ramos cells grown in complete culture medium (Section 4.3.2) or in CTL-Test Medium in terms of CD120a expression or apoptosis after 16 h (data not shown).

Different triple-staining strategies were employed for analysis, and in all cases, positive controls consisted of Ramos cells treated with Rtx-LNP(158) and single-stained with each fluorophore and dual-stained in every combination (to set compensation) and triple-stained. An additional positive control for apoptosis consisting of treatment of cells with 4.0 μM camptothecin for 4 h was also employed. Negative controls consisted of PBMCs only (no Rtx), Ramos cells only (with and without Rtx), and a combination stained with an A647-labeled negative isotype control (for A647-CD120a measurements).

To identify Ramos cells from the PBMCs, the following preliminary experiments were carried out. For apoptosis measurements, Ramos cells were pretreated with A647-Rtx, and after the 16 h co-incubation, cells were stained with Annexin-V-FITC and PI as described in Section 4.3.8. Ramos cells were identified as the A647-Rtx$^+$ population, and levels of apoptosis within this population were measured. On the basis of this population identified on the SSC versus FSC plot, apoptosis levels were measured in cells treated with Rtx instead of A647-Rtx, and excellent agreement was obtained between the two values (within 3%; data not shown). A negative control consisting of PBMCs only revealed that 97% of PBMCs were excluded from this area.

For levels of plasma membrane CD120a, cells were stained with FITC-anti-Rtx and A647-CD120a before being resuspended in PBSB containing PI (using the same procedure as in Section 5.3.6). Rtx-treated Ramos cells were identified as FITC-anti-Rtx$^+$, and within this population, A647-CD120a fluorescence intensity was measured in the PI$^-$ population to quantify levels of CD120a in the plasma membrane. Using the same strategy as in the apoptosis measurements, a sample of cells stained only with PI and A647-CD120a showed very similar levels of mean fluorescence intensities of A647-CD120a as the cells stained with FITC-anti-Rtx (within 5%; data not shown).

These experiments revealed that gating on the basis of a defined region on a side scatter (SSC) versus forward scatter (FSC) plot was an effective method of identifying Ramos cells from the mixture of cells. Ramos cells were therefore pretreated with Rtx and cocultured with PBMCs as described above for 16 h, then stained with Annexin-V-FITC, PI, and A647-CD120a. As before, 97% of PBMCs were excluded from the defined area. Apoptosis and CD120a levels were measured simultaneously in the same cells (similar to Section 5.3.7) that were either pretreated with HBS or with Rtx. Triplicates were prepared for every cocultured sample.

6.4 Results

6.4.1 Apoptosis induced by multivalent Rtx is cholesterol-dependent

The biology of CD120a is interesting in the sense that this receptor can serve either an anti-apoptotic role or a pro-apoptotic one, depending on whether it is localized in Chol-dependent plasma membrane rafts (Sections 6.2.1 & 6.2.2). Since CD120a was shown to be involved in the mechanism of action of multivalent Rtx, the ability of multivalent Rtx to induce apoptosis in cells was examined under conditions of decreased or increased concentrations of Chol in the plasma membrane. This is because a CD120a-dependent mechanism of action, such as that of Rtx-LNP as illustrated in the previous chapter, would be expected to be amplified or attenuated in response to decreased or increased concentrations of Chol in the plasma membrane.

Using an established procedure (Section 6.3.5), we measured the detergent resistance (DR) of CD120a and the levels of apoptosis after different treatments under conditions of decreased or increased Chol concentrations. Controls to verify the DR measurements were performed as described in Section 6.3.5. Ramos cells were incubated for 12 h with different concentrations of MBCD or MBCD/Chol along with HBS, Rtx, Rtx-LNP(152), or Rtx-MS, and these data are illustrated in **Figure 6.1**. In general, the DR data support the Chol manipulation that occurred; the DR of CD120a (gray bars) decreased as more Chol was removed from the membrane with MBCD, and the DR of CD120a increased or stayed the same when Chol was added.

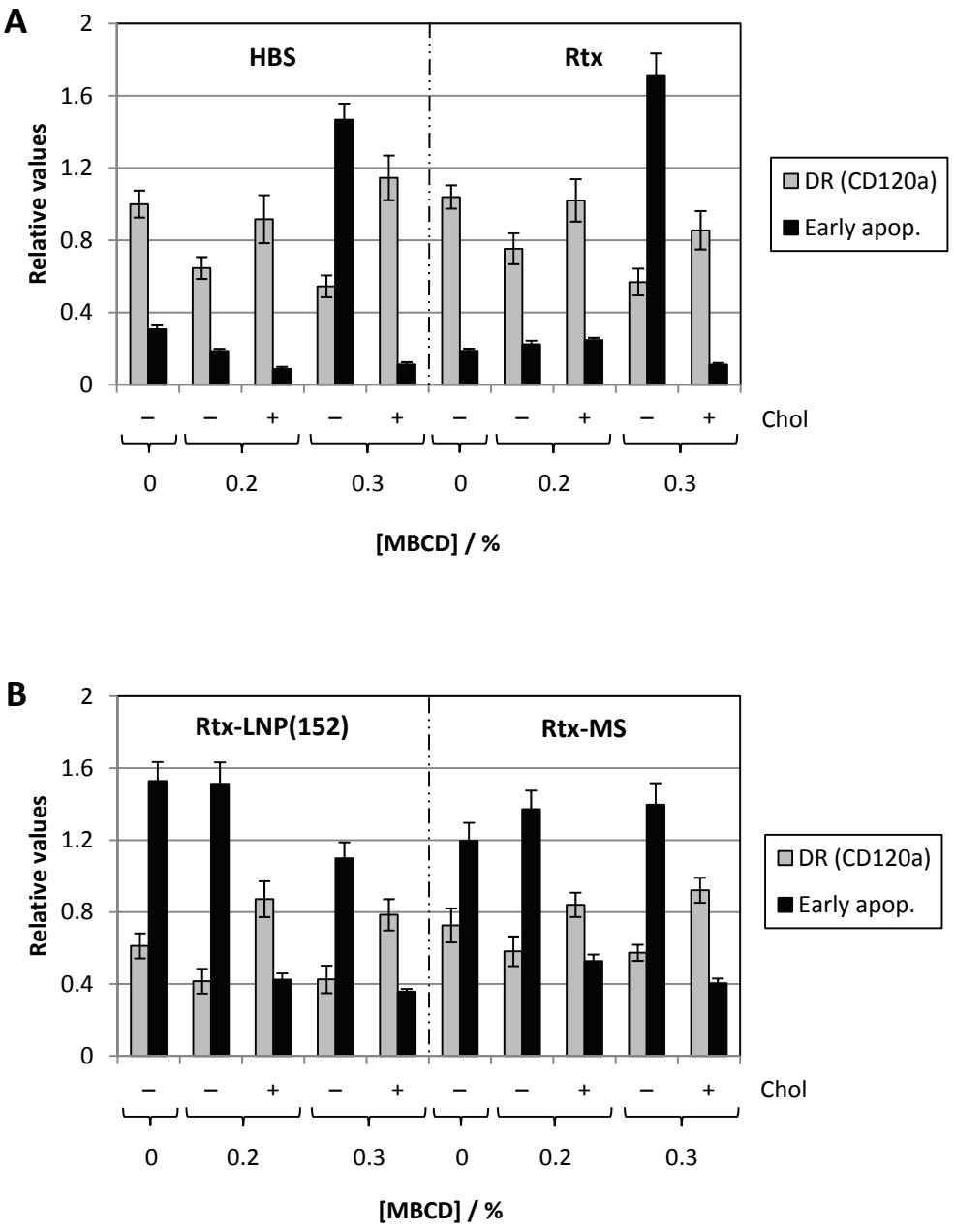

Figure 6.1 The manipulation of plasma membrane Chol content using MBCD or MBCD/Chol significantly impacts the ability of multivalent Rtx to induce apoptosis.

To modulate the Chol content of Ramos cells, the indicated doses of MBCD or MBCD/Chol were added simultaneously with HBS or Rtx **(A)**, or Rtx-LNP(152) or Rtx-MS **(B).** In all cases, a 10 µg Rtx dose was given to 2.5×10^5 cells in 500 µL medium, and the levels of early apoptosis and CD120a detergent resistance (*DR*) were measured after 12 h in samples obtained from the same population of treated cells. In samples treated with Rtx-LNP(152) and Rtx-MS, elevated plasma membrane Chol levels from added Chol/MBCD inhibited the multivalent Rtx-induced apoptosis that occurred under normal Chol levels. The same relative scales are used in (A) and (B).

Figure 6.1A shows that after treatment with HBS or Rtx, a concentration of 0.2% MBCD reduced the DR of CD120a to 65% (HBS) or 72% (Rtx) of the value measured under normal Chol concentrations ($p < 0.05$ in both cases). Note that the total levels of CD120a in the plasma membrane of HBS- and Rtx-treated cells are quite low, particularly when compared to multivalent Rtx-treated cells (Figure 5.2). Figure 6.1A also demonstrates that both HBS and bivalent Rtx showed similar profiles in terms of the relationship between levels of apoptosis and DR of CD120a under different Chol concentrations; specifically, that increased apoptosis occurred under conditions of decreased CD120a DR. Importantly, these data illustrate that a concentration of 0.3% MBCD was toxic to cells under the conditions of these experiments, as shown by the large increase in apoptosis observed from 0.2% to 0.3% MBCD in HBS-treated cells (6.8% to 33%; $p < 0.0001$). Insertion of additional Chol into the membrane, however, was not toxic under the conditions tested, since levels of apoptosis remained low (or were reduced) after all MBCD/Chol treatments.

Under equivalent conditions of Chol manipulation, Figure 6.1B shows the levels of apoptosis and CD120a DR measured after cells were treated with Rtx-LNP(152) and Rtx-MS. These data illustrate, like Figure 6.1A, that apoptosis was generally higher when the DR of CD120a was reduced. One exception involves the Rtx-LNP(152) treatment in Figure 6.1B. When comparing the data in the absence and presence of MBCD, the 0% and 0.2% MBCD treatments produced equivalent data ($p > 0.05$) but both the amount of apoptosis and the DR of CD120a were significantly reduced in the 0.3% MBCD sample compared to the 0% sample ($p < 0.05$ for both values). Separate experiments revealed that a pretreatment of Rtx-LNP with 0.3% MBCD resulted in an abolishment of the ability of the construct to induce apoptosis, most likely due to disruption of the structure of the LNP, which contains Chol. Pretreatment with 0.3% MBCD/Chol did not affect the apoptotic activity of Rtx-LNP (data not shown).

Equivalent experiments were therefore performed with Rtx-MS, a multivalent Rtx construct that does not contain Chol, and as opposed to Rtx-LNP(152) treatment, the data on the right-hand

side of Figure 6.1B show that 0%, 0.2%, and 0.3% MBCD treatment resulted in equivalent levels of apoptosis and DR of CD120a ($p > 0.05$ for all pairs of the same parameter). This shows that even though 0.3% MBCD was toxic to cells in the absence of multivalent Rtx, no further increase in apoptosis (or decrease in CD120a DR) was observed compared to treatment with the multivalent Rtx constructs tested.

The most important observation from Figure 6.1B is that under conditions of increased Chol content in the plasma membrane, the apoptotic activity of multivalent Rtx was strikingly reduced. For the Rtx-LNP(152) treatment, a comparison of the 0% and 0.3% MBCD/Chol concentrations shows that apoptosis was reduced from 34% to 7.9% ($p < 0.0001$) while the relative DR of CD120a increased from 0.61 to 0.79 ($p < 0.05$). The same MBCD/Cholreatments in the presence of Rtx-MS reduced apoptosis from 22% to 7.5% ($p < 0.0005$) and increased relative DR from 0.73 to 0.92 ($p < 0.05$). In both cases, the level of apoptosis after treatment with multivalent Rtx and 0.2% or 0.3% MBCD/Chol was equivalent to that which was measured in cells treated with HBS in the absence of MBCD ($p > 0.05$ in all cases).

To further investigate the phenomenon where increased Chol content in the plasma membrane rescues cells from the apoptosis induced by multivalent Rtx, confocal laser-scanning fluorescence microscopy images were obtained of cells treated with Rtx-LNP(165) under conditions of normal or increased plasma membrane Chol content. **Figure 6.2** shows representative images of Ramos cells obtained 12 h after treatment; cells were stained as described in Section 6.3.6. The blue signal represents staining by A488-CTX, which stains the plasma membrane raft marker ganglioside GM1, while the red signal represents A647-CD120a staining. These two signals are shown on their own (first and second panels on the left) and merged (third panels). Colocalization between the blue and red signals indicates CD120a that is associated with plasma membrane rafts.

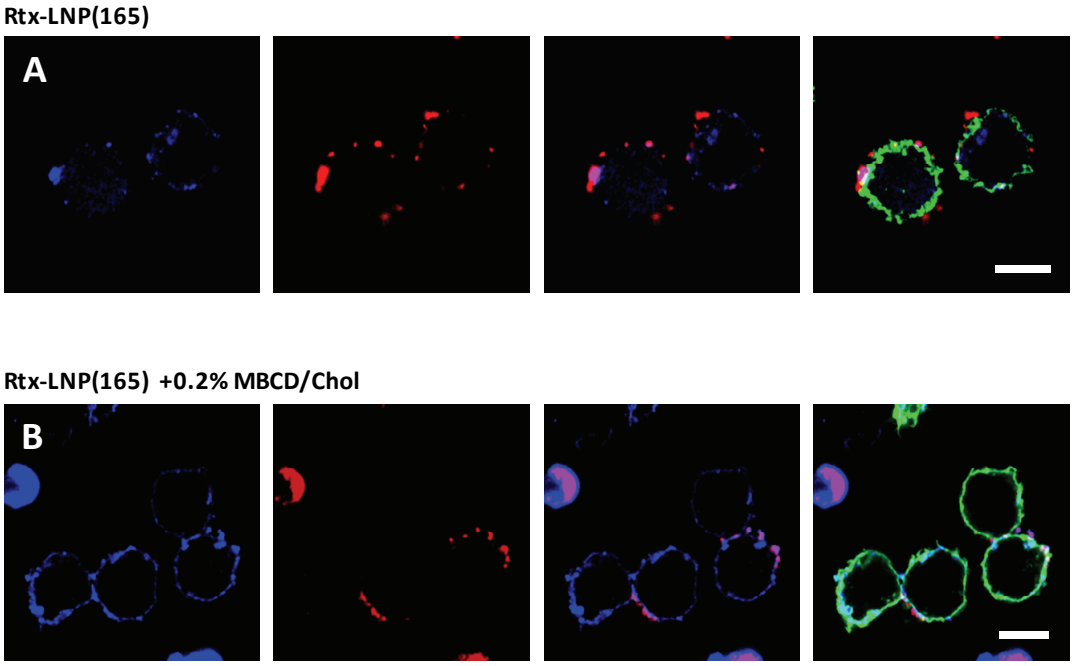

Figure 6.2 Cells that are rescued from apoptosis by increasing the plasma membrane Chol content show elevated levels of raft-associated CD120a.

Representative images of Ramos cells are shown that have been treated with either Rtx-LNP(165) **(A)** or Rtx-LNP(165) +0.2% MBCD/Chol **(B)** under the same conditions as in Figure 6.1. As described in Section 6.3.6, cells were stained before permeabilization with A488-CTX (*blue*; stains ganglioside GM1, a membrane raft marker) and A647-CD120a (*red*), and after permeabilization with Texas Red-labeled phalloidin (*green*; stains the actin cytoskeleton). Panels, from left to right, are: ganglioside GM1 staining only, CD120a staining only, a merge of the ganglioside GM1 and CD120a signals, and a merge of all three signals.

When comparing the membrane raft association of CD120a between Figure 6.2A and 6.2B, it is evident that CD120a was almost exclusively found in membrane rafts under conditions of increased Chol (Figure 6.2B), while a greater fraction of CD120a was found outside of membrane rafts under normal Chol concentrations (Figure 6.2A). The same result was observed across a large number of images. Evidence of higher plasma-membrane Chol concentrations in Figure 6.2B is provided by the greater fraction of the plasma membrane covered by rafts (blue signal) compared to Figure 6.2A.

The rightmost panels in Figure 6.2 show the A488-CTX and A647-CD120a signals merged with the signal from Texas Red phalloidin, which stains F-actin. The illustrated F-actin staining

pattern consisting of wavy ring-like structures on the outer rim of the cells is characteristic of the cortical actin cytoskeleton and is consistent with other reports[245]. F-actin staining was less intense and less uniform on the surface of cells treated with Rtx-LNP(165) in the absence of MBCD/Chol compared to in its presence. F-actin staining was also completely absent in necrotic cells, which only showed high intracellular staining of A488-CTX and A647-CD120a, consistent with Figure 5.3 (not shown). The F-actin staining in Figure 6.2 confirms that the observed CD120a and rafts are present on the cell surface, and that these cells would be considered either viable or early apoptotic using the Annexin-V/PI apoptosis assay.

6.4.2 Inhibition of cholesterol synthesis using simvastatin sensitizes cells to Rtx-LNP-induced apoptosis

MBCD is widely used to deplete Chol from the plasma membrane, resulting in the disruption of plasma membrane rafts, but MBCD is known to induce secondary effects on some cells, as described in Section 6.2.3. As an alternative means of reducing plasma membrane Chol levels, the HMG-CoA reductase inhibitor simvastatin was employed, which has been shown to disrupt plasma membrane rafts[240, 242, 243]. Unlike MBCD, which removes Chol from lipid bilayers, simvastatin is an inhibitor of Chol synthesis. As opposed to MBCD, therefore, pretreatment of Rtx-LNP with simvastatin in the absence of cells (30 μM for 16 h) had no effect on its apoptotic potency (data not shown). The behavior of Ramos cells treated with simvastatin along with Rtx or Rtx-LNP was therefore examined, and the resulting data is summarized in **Figure 6.3**. As was the case in Figure 6.1, the data obtained for HBS and Rtx treatment were very similar. Both of these treatments indicate that under the conditions of these experiments, a 10 μM dose of simvastatin was not toxic, while a dose of 30 μM resulted in the induction of apoptosis on its own. For example, in the HBS-treated samples, 5.3% early apoptosis was observed at the 10 μM dose of simvastatin, while this percentage increased to 12% at the 30 μM dose ($p < 0.05$). The DR of CD120a was also observed to

decrease from the 10 μM to the 30 μM dose of simvastatin, but as described above, the significance of this decrease is unclear given the very low levels of CD120a in the plasma membrane in HBS- and Rtx-treated cells (Figure 5.2).

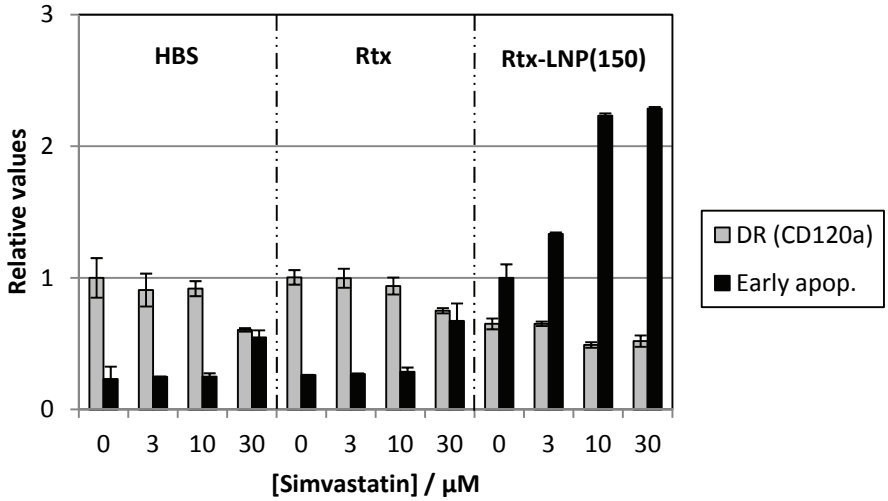

Figure 6.3 Simvastatin decreases the DR of CD120a and sensitizes cells to apoptosis induced by Rtx-LNP.
Ramos cells underwent incubation with simvastatin at different doses in order to study the effects of reduced plasma membrane Chol content on the ability of Rtx-LNP to induce apoptosis. The DR of CD120a (*gray bars*) and levels of early apoptosis (*black bars*) were measured after 12 h and are shown for each treatment.

When cells were treated with Rtx-LNP(150) in the presence of simvastatin at doses that were not toxic to Ramos cells, the right-hand side of Figure 6.3 shows a dose-dependent increase in early apoptosis alongside a decrease in the DR of CD120a (now present at elevated levels due to upregulation by Rtx-LNP(150)). At a dose of 3 μM simvastatin, early apoptosis was observed in 28% of cells, compared to 21% at 0 μM ($p < 0.05$); the CD120a DR values at these two doses were equivalent, however ($p > 0.05$). A significant decrease in DR of CD120a was observed at 10 μM simvastatin; the DR at 10 μM was 0.55, compared to 0.73 at 3 μM ($p < 0.001$), and the level of apoptosis at 10 μM simvastatin increased to 47% ($p < 0.0001$ compared to the 3 μM dose). In terms of both parameters, the 10 μM and 30 μM doses of simvastatin produced equivalent results in Rtx-LNP(150)-treated cells ($p > 0.05$). Overall, the simvastatin experiments corroborate the MBCD data

which indicate that increases in plasma membrane Chol inhibit apoptosis induced by multivalent Rtx, and decreases in plasma membrane Chol sensitize the cells to multivalent Rtx-induced apoptosis.

6.4.3 A model of Rtx hypercrosslinking that occurs *in vivo* after normal Rtx therapy

The data in Chapter 5 and in Sections 6.4.1 & 6.4.2 establish that the direct mechanism of action of multivalent Rtx involves CD120a upregulation and that Chol levels influence the ability of multivalent Rtx to induce apoptosis. These *in vitro* experiments would have more clinical relevance if evidence could be provided for this mechanism occurring *in vivo* upon hypercrosslinking of Rtx by FcγR-expressing effector cells (Section 6.2.4).

To first model the interaction between FcγR on effector cells and Rtx on lymphoma cells, a 2^{o}Ab specific to the Fc region of human IgGs was employed. The specificity of this 2^{o}Ab paralleled that of FcγR. To enable hypercrosslinking, the 2^{o}Ab was coupled to the surface of polystyrene MS to create 2^{o}Ab-MS (Section 6.3.7). Lymphoma cells were saturated with Rtx, and after washing the cells, the 2^{o}Ab was either added on its own, producing a low degree of crosslinking, or added as 2^{o}Ab-MS, enabling hypercrosslinking.

The ability of 2^{o}Ab-MS to induce apoptosis in Rtx-pretreated Ramos cells was first assessed in terms of the amount of 2^{o}Ab-MS added. This data is summarized in **Figure 6.4A**; Rtx-treated cells in the absence of 2^{o}Ab-MS showed low levels of early apoptosis (3.3%) 24 h after treatment, while maximum levels of early apoptosis (39%) occurred when masses of 8 μg of 2^{o}Ab (in 2^{o}Ab-MS) and above were given ($p < 0.0001$). From 8 μg to 16 μg 2^{o}Ab (in 2^{o}Ab-MS), the fraction of viable cells dropped from 39% to 14% ($p < 0.001$). The decreased viable fraction corresponded to an increase in the percentage of necrotic cells, and at doses above 16 μg, the necrotic fraction was so dominant that very few viable or early apoptotic cells were observed (not shown). These data parallel earlier

results from Rtx-LNP and Rtx-MS which showed low levels of apoptosis in the absence of Rtx hypercrosslinking, and significantly higher levels of apoptosis upon hypercrosslinking *via* a multivalent interaction.

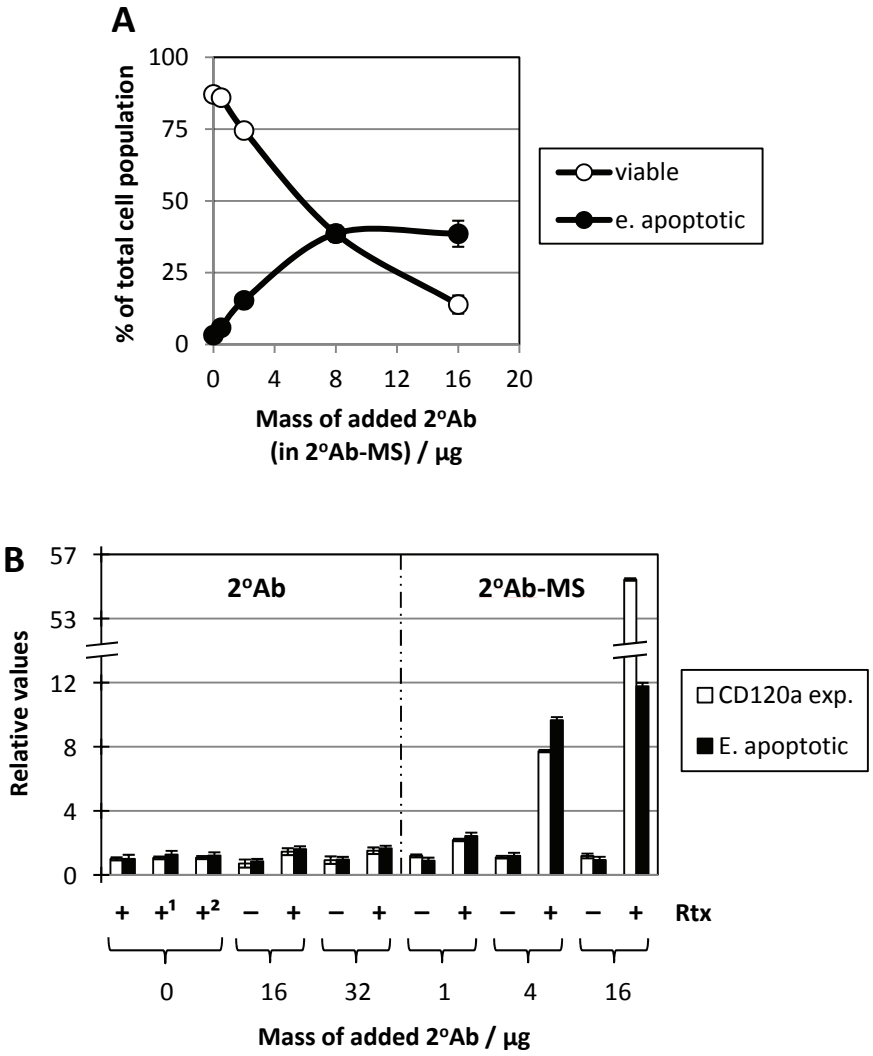

Figure 6.4 A model for the hypercrosslinking of Rtx that occurs *in vivo* by FcγR-bearing effector cells.

(A) The percentages of viable and early apoptotic cells were measured 24 h after subjecting 1.25×10^5 Rtx-presaturated Ramos cells in 250 µL medium to the indicated masses of 2^{o}Ab (in 2^{o}Ab-MS). **(B)** Samples were presaturated with Rtx as in (A), followed by the treatments shown. At 12 h post-treatment, the levels of CD120a in the plasma membrane (*white bars*) and early apoptosis (*black bars*) were measured in each case on cells obtained from the same treated sample. $+^1$ refers to the addition of Rtx-biotin instead of Rtx, and $+^2$ indicates that streptavidin-MS were added together with unbiotinylated Rtx.

Experiments were next carried out to determine whether the apoptosis observed after hypercrosslinking Rtx on Ramos cells occurs alongside upregulated CD120a levels, as was the case with Rtx-LNP and Rtx-MS. A total of 12 h after the addition of different amounts of 2^{o}Ab or 2^{o}Ab-MS to Rtx-presaturated cells, the levels of early apoptosis and plasma-membrane CD120a were measured. The resulting data is summarized in **Figure 6.4B**, which shows that in the absence of Rtx pretreatment, the addition of 2^{o}Ab or 2^{o}Ab-MS on their own at the concentrations tested did not induce apoptosis after 12 h. In contrast, mild increases in apoptosis occurred when 2^{o}Ab was added to Rtx-pretreated cells compared to cells not treated with Rtx; for example, when 32 μg of 2^{o}Ab were added, there was a 1.6-fold increase in CD120a expression in the plasma membrane (MFI after subtracting negative isotype control increased from 20 to 33; $p < 0.005$) and a 1.7-fold increase in early apoptosis (6.9% to 12%; $p < 0.001$) in the presence of Rtx compared to in its absence.

When significantly lower doses of 2^{o}Ab were added as 2^{o}Ab-MS, however, a considerable upregulation of CD120a in the plasma membrane was observed alongside significantly elevated levels of apoptosis, only in the presence of Rtx. For example, when 16 μg of 2^{o}Ab (in 2^{o}Ab-MS) were added, levels of early apoptosis increased 13-fold (3.1% to 39%; $p < 0.0005$) and the MFI observed for CD120a increased by a factor of 46 (from 46 to 2130; $p < 0.0001$) in cells that were pretreated with Rtx compared to cells that were not pretreated. In terms of CD120a upregulation, treatment of presaturated cells with 2^{o}Ab-MS resulted in the highest measured upregulation compared to the other methods of hypercrosslinking studied (Rtx-LNP and Rtx-MS). In the presence of Rtx, apoptosis was 4.9-fold higher (8.0% to 39%; $p < 0.0005$) at 16 μg of added 2^{o}Ab (in 2^{o}Ab-MS) compared to 1 μg, and the MFI corresponding to CD120a expression in the plasma membrane was higher by a factor of 25 (from 84 to 2130; $p < 0.0001$). The controls in Figure 6.4B ($+^{1}$ Rtx-biotin and $+^{2}$ streptavidin-MS +Rtx) indicate that neither Rtx-biotin nor streptavidin-MS on their own were responsible for any observed effects since all measured values were equal to those observed in cells treated only with Rtx ($p > 0.05$ in all cases). These data further support the CD120a-dependent

direct mechanism observed after treatment with Rtx-LNP and Rtx-MS, and they also indicate that the hypercrosslinking of CD20 drives this mechanism of action since different methods of hypercrosslinking produced the same result.

6.4.4 CD120a that is excluded from plasma membrane rafts is colocalized with hypercrosslinked Rtx-enriched patches

To further study the relationship between Rtx/CD20 hypercrosslinking and CD120a upregulation, confocal laser-scanning fluorescence microscopy was employed to investigate the plasma membrane organization of hypercrosslinked Rtx with respect to CD120a and plasma membrane rafts. To visualize Rtx on the cell surface, the Ab was labeled with A568 (Section 6.3.7). It was first verified that A568-Rtx, when hypercrosslinked using 2^{o}Ab-MS, induced apoptosis in the same way as unlabeled Rtx. **Figure 6.5A** shows that after a 24 h incubation, 20 μg of added 2^{o}Ab (in 2^{o}Ab-MS) on its own was not toxic to the cells (top left panel), while a mass of 50 μg resulted in cytotoxic effects in Ramos cells (top right). Treatment with A568-Rtx on its own resulted in low levels of apoptosis (bottom left), while cells presaturated with A568-Rtx and treated with 20 μg of 2^{o}Ab (in 2^{o}Ab-MS) (bottom right) underwent apoptosis at levels consistent with those when using unlabeled Rtx in Figure 6.4A. The data in Figure 6.5A therefore indicate that A568 labeling did not significantly affect the function of Rtx, and they also confirm that 20 μg of 2^{o}Ab (in 2^{o}Ab-MS) is not toxic to Ramos cells under the conditions of these experiments.

To obtain confocal laser-scanning fluorescence microscopy images, Ramos cells were presaturated as in Section 6.4.3 with A568-Rtx instead of Rtx, followed by treatment with 2^{o}Ab-MS or an equivalent volume of HBS. At a time point 12 h after the addition of 2^{o}Ab-MS, cells were stained without permeabilization with A488-CTX (to label plasma membrane rafts) and with A647-CD120a. Representative images are exhibited in **Figure 6.5B & C**. The top two panels in each case show the staining of A647-CD120a (red) and A488-CTX (blue) on their own before being merged in

the third panels from the top. The fourth panel shows staining of A568-Rtx (green) while the bottommost panel contains a merge of all three signals. When comparing cells in the absence of 2°Ab-MS (Figure 6.5B) to those that have been treated with 2°Ab-MS (Figure 6.5C), it is clear that in the absence of 2°Ab-MS, the expression of CD120a is significantly lower and the distributions of A568-Rtx and membrane rafts are more uniform across the surface of the cells.

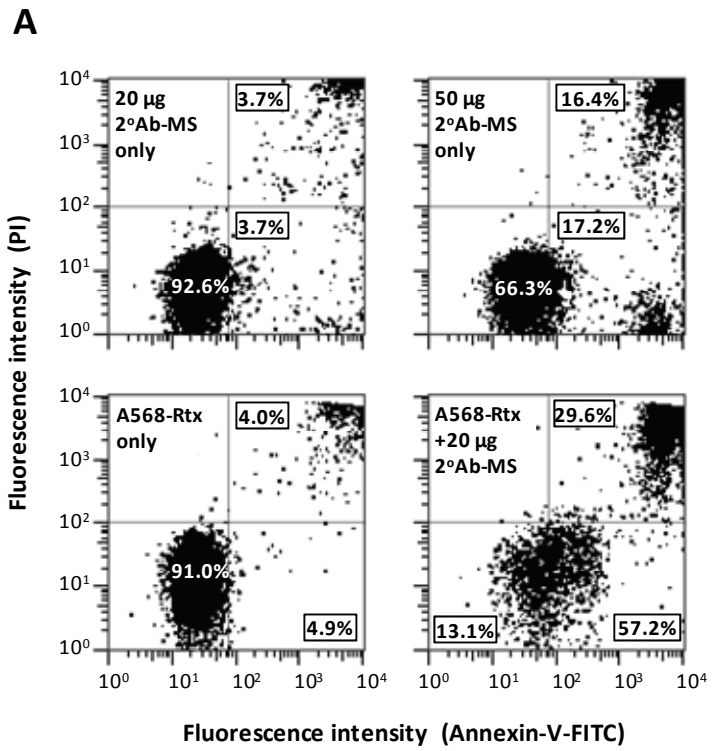

Figure 6.5 Membrane raft-associated CD120a is excluded from regions enriched in hypercrosslinked Rtx/CD20, and non-raft CD120a is colocalized with hypercrosslinked Rtx/CD20.

(A) Verification that labeling of Rtx with A568 did not affect its ability to induce apoptosis in lymphoma cells upon hypercrosslinking with 2°Ab-MS. (Continued on next page.)

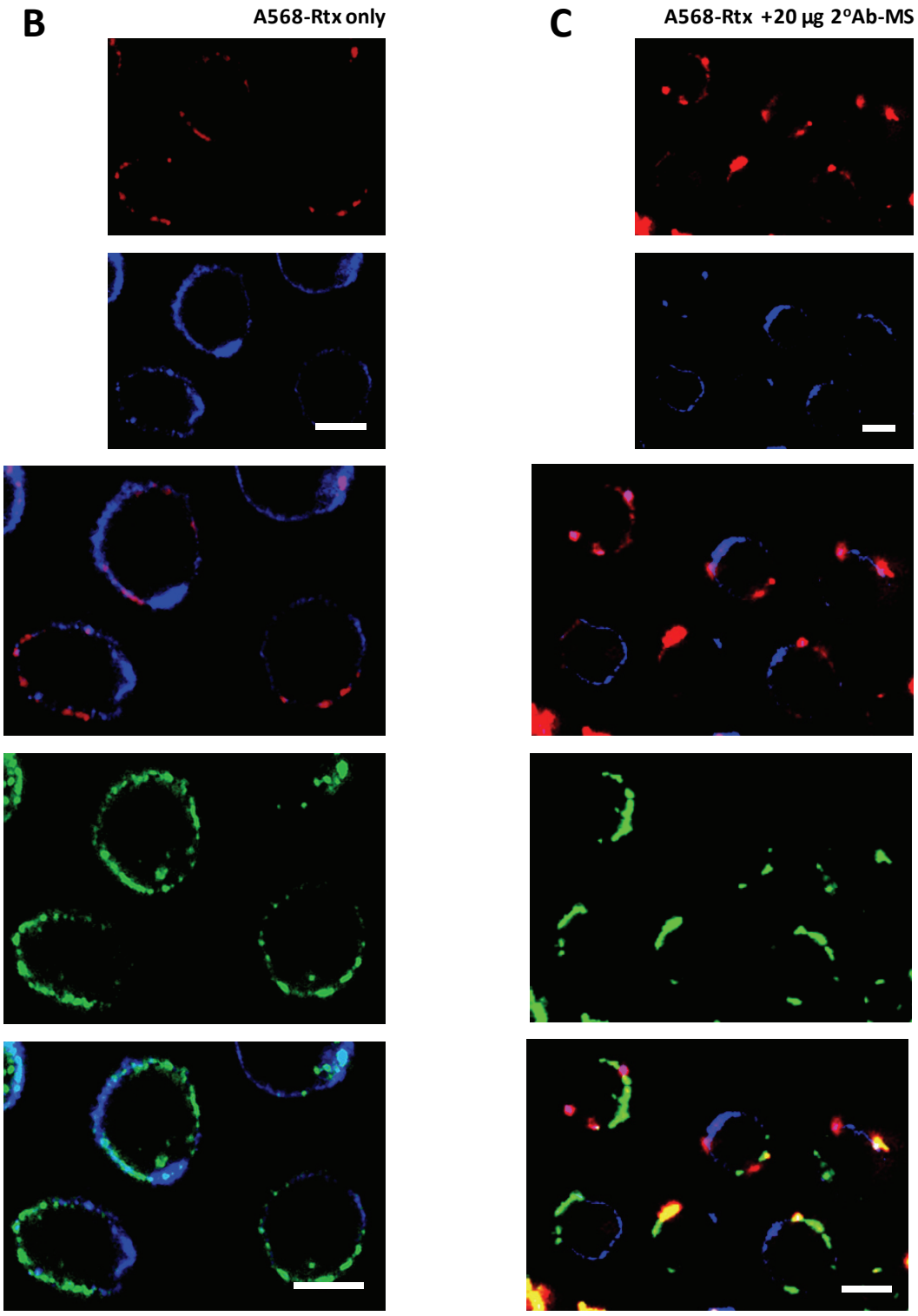

Figure 6.5 (Continued from previous page.) **(B & C)** Confocal laser-scanning fluorescence microscopy images of cells treated with A568-Rtx only **(B)** or A568-Rtx followed by 20 µg of 2°Ab (in 2°Ab-MS) **(C)** for 12 h. A568-Rtx localization is represented by the *green* signal; cells were also stained with A488-CTX to label membrane rafts (*blue*) and A647-CD120a (*red*). In (C), CD120a that is raft-associated (purple regions in the third panel from the top) is excluded from hypercrosslinked Rtx-enriched regions (green), while non-raft associated CD120a is colocalized with Rtx-enriched regions.

The third panels from the top specifically show the regions of CD120a that are associated with plasma membrane rafts (purple) and the regions that are non-raft-associated (red). When examining the distribution of the purple signal compared to that of the green one (A568-Rtx), it is clear in Figure 6.5C that there is low colocalization between the purple and green regions. This implies that raft-associated CD120 does not colocalize with hypercrosslinked Rtx. On the other hand, non-raft CD120a (red signal in the third panel) is almost exclusively colocalized with hypercrosslinked A568-Rtx (green) in Figure 6.5C. In fact, the green and blue signals show a low degree of colocalization, indicating that hypercrosslinked A568-Rtx is excluded from plasma membrane rafts. These same trends were observed across a large number of samples obtained under a variety of conditions.

Together, these data imply that Rtx/CD20, when hypercrosslinked on the cell surface, forms large patches that are excluded from plasma membrane rafts. They also show that CD120a present in the plasma membrane (after upregulation resulting from hypercrosslinked Rtx/CD20) forms different domains, some of which are raft-associated and some of which are not. Raft-associated CD120a is almost exclusively excluded from Rtx-enriched patches, while non-raft-associated CD120a is largely associated with hypercrosslinked Rtx. This suggests that Rtx hypercrosslinking results in the formation of non-raft patches where the proapoptotic form of CD120a is localized following its upregulation.

Figures 6.4 & 6.5, taken together, show that hypercrosslinking Rtx/CD20 using 2^{o}Ab-MS results in significant apoptosis and upregulation of CD120a. Since the use of 2^{o}Ab-MS served as a model for the interaction of effector cells and Rtx-coated lymphoma cells, these data support the hypothesis that this direct mechanism of action occurs *in vivo* after administration of regular bivalent Rtx due to hypercrosslinking of Rtx/CD20 by FcγR-expressing cells.

6.4.5 Effector cells induce elevated apoptosis and CD120a expression only in lymphoma cells treated with Rtx

To determine if effector cells themselves are capable of directly inducing apoptosis in lymphoma cells through a mechanism that depends on CD120a, experiments were carried out where Ramos cells pretreated with either Rtx or HBS were co-incubated with human peripheral blood mononuclear cells (PBMCs) obtained from healthy donors. PBMCs are rich in FcγR-expressing effector cells such as NK cells and monocytes[246] and a subpopulation of these cells would therefore be expected to hypercrosslink Rtx on the surface of treated lymphoma cells in a manner similar to 2^{o}Ab-MS in Sections 6.4.3 and 6.4.4.

A detailed description of the strategies employed to detect expression of CD120a and apoptosis in Ramos cells is provided in Section 6.3.8. After pretreatment with Rtx or HBS, PBMCs were added in different excesses of Ramos cells and coincubation was allowed to proceed for 16 h. Levels of apoptosis and plasma-membrane CD120a were then measured only in the Ramos cells, and the resulting data is shown in **Figure 6.6**. This figure shows that in the absence of Rtx, PBMCs were capable of inducing apoptosis in Ramos cells and the amount of apoptosis depended on the ratio of PBMCs that were added with respect to Rtx. While 8.9% of Ramos cells were in early apoptosis at the 1:1 Ramos:PBMC ratio, this value increased to 43% at the 1:8 ratio ($p < 0.0001$). The data in the absence of Rtx, however, suggest that PBMC-induced apoptosis occurred *via* a mechanism that was CD120a-independent because as the levels of apoptosis increased at ratios of 1:1 and above, the expression of CD120a in the plasma membrane remained constant ($p > 0.05$ between all pairs of treatments).

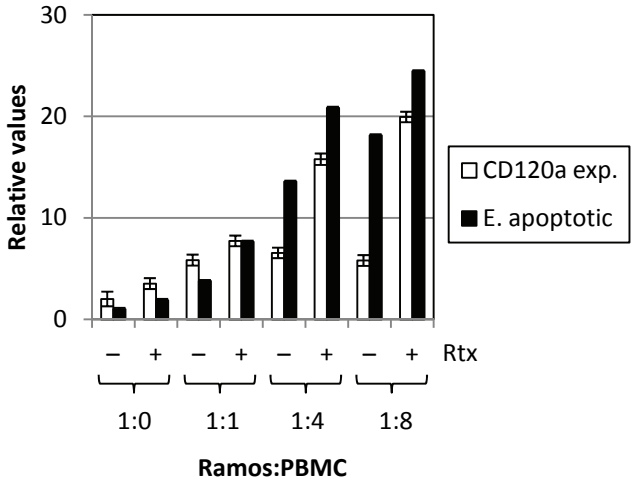

Figure 6.6 Human PBMCs induce significantly higher levels of apoptosis and plasma-membrane CD120a expression in lymphoma cells pretreated with Rtx compared to non-pretreated cells.

PBMCs from healthy donors were coincubated with Ramos cells that were pretreated with either HBS or saturating levels of Rtx. In Ramos cells, both the CD120a expression in the plasma membrane and the level of early apoptosis were measured 16 h after addition of PBMCs.

The most important result in Figure 6.6 is that every ratio tested showed significantly elevated levels of early apoptosis in samples containing Rtx-pretreated Ramos cells compared to cells that were not treated with Rtx. These elevated apoptosis levels were accompanied by yet more pronounced increases in plasma-membrane CD120a expression. For example, at the 1:1 ratio, there was a 2.0-fold increase in early apoptosis (8.9% to 18%; $p < 0.0001$) and a 1.3-fold increase in the MFI of plasma membrane-associated A647-CD120a (203 to 269; $p < 0.01$) in cells treated with Rtx compared to HBS. At the 1:8 ratio, early apoptosis was 1.3-fold higher (43% to 58%; $p < 0.001$) while CD120a levels were 3.4-fold higher (increase in MFI from 202 to 694; $p < 0.0001$).

These experiments therefore confirm that circulating FcγR-expressing effector cells *in vivo* are capable of inducing upregulation of CD120a in the plasma membrane of target lymphoma cells containing bound Rtx, resulting in the direct induction of apoptosis in these cells. These data imply that a direct mechanism of action involving CD120a upregulation occurs *in vivo* after treatment with bivalent Rtx. Others have postulated that a direct mechanism of action may actually be responsible

for a significant fraction of the *in vivo* therapeutic activity observed from Rtx[77], but until now, such a mechanism has been undefined.

6.5 Discussion and conclusions

6.5.1 Discussion

The results from this chapter suggest that a direct mechanism involving upregulation of CD120a followed by apoptosis occurs *in vivo* after normal bivalent Rtx therapy. As stated in Section 5.4.1, the direct mechanism of action of Rtx has not been definitively shown, but here we have demonstrated that Rtx-treated lymphoma cells expressed dramatically elevated levels of CD120a and apoptosis when the Rtx on the cell surface was hypercrosslinked with 2^{o}Ab-MS, compared to only modest increases at higher doses of 2^{o}Ab (Figure 6.4). This hypercrosslinking modeled the multivalent interaction that occurs when Rtx-coated cells interact with FcγR-expressing immune effector cells *in vivo*, lending support to a direct mechanism of action of Rtx involving upregulation of CD120a. We subsequently showed that the same direct mechanism also occurred *in vitro* in Rtx-coated lymphoma cells when they were allowed to interact with human effector cells in PBMC samples from healthy donors (Figure 6.6). This strongly suggests that CD120a-mediated apoptosis is capable of occurring *in vivo* after treatment with bivalent Rtx.

These studies also demonstrate that increasing the concentration of Chol in the plasma membrane of lymphoma cells rescues the cells from apoptosis induced by multivalent Rtx (Figure 6.1). Insertion of Chol resulted in an increase of the DR of CD120a and increased colocalization of CD120a in GM1-positive plasma membrane rafts (Figures 6.1 & 6.2). Depletion of Chol from the plasma membrane resulted in increased detergent solubility of CD120a (Figures 6.1 & 6.3) and sensitized cells to apoptosis induced by multivalent Rtx (Figure 6.3). The level of apoptosis induced by multivalent Rtx is therefore dependent on the concentration of Chol in the plasma membrane.

This is consistent with a CD120a-dependent direct mechanism of action since raft-associated CD120a elicits antiapoptotic signals, as opposed to the non-raft-associated form, which is proapoptotic (Sections 6.2.1 & 6.2.2).

In order to measure the resistance of proteins to solubilization in detergent, a method making use of flow cytometry was employed which allowed for the quantification of DR values (Section 6.3.5). This method is less commonly employed than equilibrium density gradient ultracentrifugation followed by western blotting of fractions along the gradient (described in Section 6.2.3.1). In these experiments, however, employing the traditional ultracentrifugation technique was not possible because of the very large number of cells required for each sample ($1–5 \times 10^8$ cells/sample)[47, 247, 248]. Cells were typically given 40 μg Rtx/10^6 cells to achieve valence-dependent levels of apoptosis (Figure 4.6) and CD120a expression (Figure 5.4); this dose corresponds to at least 4 mg of Rtx (in Rtx-LNP) per ultracentrifugation sample. This is an extremely large amount of Rtx-LNP; it is approximately equal to the total mass of Rtx present in all samples of Rtx-LNP prepared using one iteration of the methodology in Chapter 3. Producing the minimum amount of material necessary for ultracentrifugation experiments using this methodology (or the previous method employed in Section 2.3.2) was therefore not possible in practical terms. Developing a scaled up procedure for preparing precise valences, or an altogether different procedure, would have been required.

The flow cytometry-based method used in this chapter provides a suitable alternative to density gradient ultracentrifugation, and the data was corroborated by confocal laser-scanning fluorescence microscopy images (Figures 6.2 & 6.5). Others have used an identical approach to determine membrane raft affinity when ultracentrifugation is impractical or impossible[249, 250], or to verify western blots obtained from fractions after ultracentrifugation[251].

Simons *et al.* have pointed out that a common feature of density gradient ultracentrifugation DR analyses is variation in results, even between replicates of the same

experiment, and this is a major weakness of the technique[234]. They also point out that DR is only a starting point for studying raft association, and that changes in DR in response to biological stimuli are the most useful indicators of membrane raft involvement in the response. For example, strong DR of a protein in itself does not provide much information pertaining to raft association, but if a stimulus causes the protein to undergo a decrease in DR, a movement out of plasma membrane rafts due to the stimulus could be assigned[234]. The data in Figures 6.1 & 6.3 employ this differential approach to the treatment of DR data, and the changes in DR measured in response to the different treatments are supported by the confocal fluorescence microscopy images in Figures 6.2 and 6.5.

The results in this chapter deviate from those reported by many other groups that show that CD20 is found outside of plasma membrane rafts in different lymphoma cell lines, but upon treatment with Rtx, CD20 translocates to membrane rafts[74, 168, 169]. Using the same approach to quantify DR as in Figures 6.1 & 6.3, we employed A647-pCD20 (Section 4.3.6) to measure the DR of CD20, and we found no changes in DR values for CD20 (~0.6) before and after treatment with Rtx and Rtx-LNP (data not shown). Confocal fluorescence microscopy images such as those shown in Figures 6.5 also indicate that the majority of Rtx (and therefore CD20) does not colocalize with GM1, a membrane raft marker. Most of the studies indicating increased raft association of CD20 after Rtx treatment employed density gradient ultracentrifugation and western blotting, which may explain the difference in part due the variability of such results, as described above. The differences may also be due to the fact that most previous studies have employed a 2^{o}Ab, which results in moderate crosslinking of Rtx/CD20, as opposed to the more substantial hypercrosslinking provided by the multivalent constructs used here. Different degrees of hypercrosslinking would be expected to modulate raft behavior to different extents (Section 6.2.2).

One study in particular showed that by depleting Chol using MBCD concentrations similar to those employed in this chapter, levels of apoptosis induced by Rtx and a 2^{o}Ab decreased as the MBCD concentration was increased[74]. Our results, on the other hand, show that insertion of

additional Chol into the plasma membrane using MBCD/Chol abolishes apoptosis, while Chol depletion using MBCD, and particularly simvastatin, sensitize cells to apoptosis induced by multivalent Rtx. One possibility for the different results may be that MBCD interfered with the ability of the 2^{o}Ab to hypercrosslink Rtx in the study of Janas *et al.*, an event that is required for apoptosis (Sections 1.4.3 and 1.6.1).

One other way that the results here differ from those in other reports is that apoptotic CD120a signaling is generally considered to require internalization of activated CD120a-containing Complex II by clathrin-dependent endocytosis (see Section 6.2.1). Our results show no evidence of CD120a internalization preceding apoptosis, including confocal fluorescence microscopy images that were obtained where CD120a staining occurred after permeabilization of the plasma membrane (not shown). Moreover, we employed chlorpromazine treatment, which inhibits clathrin-dependent apoptosis, at subcytotoxic doses in conjunction with Rtx and Rtx-LNP, and we found no differences in the levels of apoptosis that were induced in the absence of chlorpromazine (data not shown). The requirement for endocytosis may not be universal to all cell types[175], so apoptosis *via* Complex II may not be required in Ramos cells. Other death receptors, such as DR4 and DR5, have also been shown to not require endocytosis before initiating apoptosis[87].

The results in this chapter have demonstrated that a CD120a-dependent mechanism of action is capable of occurring *in vivo* after normal Rtx therapy as a result of hypercrosslinking of Rtx by FcγR-expressing cells. They also showed that increased cellular Chol content abolished multivalent Rtx-induced apoptosis, while lower levels sensitized cells to apoptosis. The synthesis of these two results suggests that improvements in the *in vivo* efficacy of bivalent Rtx therapy may be achieved with concurrent Chol-lowering therapies such as simvastatin or other statins. The utility of such an approach can be investigated using *in vivo* lymphoma xenograft models to study the efficacy of such treatment strategies and to further investigate the role of CD120a in the direct mechanism of action of Rtx, as described in Section 7.4.

6.5.2 Conclusions

Our results have shown that multivalent Rtx serves to upregulate CD120a to the plasma membrane, where it elicits proapoptotic signaling when localized outside of plasma membrane rafts. Insertion of additional Chol into the plasma membrane resulted in the translocation of CD120a to rafts and abolishment of multivalent Rtx-induced apoptosis, while depletion of Chol sensitized cells to apoptosis, indicating that apoptosis induced by multivalent Rtx is Chol-dependent.

To model the interaction of FcγR-expressing effector cells with Ab-coated tumor cells, Fc region-specific 2^{o}Ab-MS induced significantly elevated apoptosis and upregulation of CD120a only when the cells were pretreated with Rtx. The same effect was observed when Ramos cells were cocultured with samples of PBMCs, which contain effector cells that express FcγRs. This suggests that FcγR-expressing effector cells are capable of hypercrosslinking Rtx on the surface of lymphoma cells *in vivo*, and that increased apoptosis resulting from CD120a upregulation may constitute a novel direct mechanism of action of Rtx that occurs upon regular Rtx therapy. Together, this data suggests that Rtx efficacy could be improved through concurrent treatment with Chol-lowering agents such as statins.

7 Discussion and conclusions: Antibody-lipid nanoparticles as a promising tool in cancer drug development

7.1 Recapitulation

The work described in this dissertation outlines a complete methodology that can be used to discover new drugs based on therapeutic monoclonal Abs and develop such therapies to an advanced preclinical stage, including an elucidation of their mechanism of action. The methodology makes use of Ab-LNPs, a type of multivalent therapeutic Ab construct that employs a liposome as a nanoscale scaffold for bridging many Ab molecules together. Therapeutic Abs that show minimal activity as bivalent molecules may show enhanced therapeutic activity as multivalent constructs, enabling their further development as multivalent Abs of defined (optimal) valence, rather than bivalent Abs. The proof of this concept was illustrated using the therapeutic Ab Rtx.

As is the case with other types of multivalent Abs directed against different targets, Rtx-LNPs exhibited enhanced activity compared to bivalent Rtx; as shown in Chapter 2, Rtx-LNPs induced higher levels of apoptosis, ADCC, and CDC compared to equal doses of bivalent Rtx. In order to further understand the direct mechanism of action of Ab-LNPs, a new Ab-LNP preparation methodology was developed in Chapter 3 which allowed for the creation of many valences of Ab-LNP from the same Ab. Using Rtx-LNPs prepared with this methodology, Chapter 4 showed that the levels of apoptosis induced by Rtx-LNPs depended on their valence, and that Rtx-LNPs exhibited unique biological properties consistent with the notion that the higher valences can hypercrosslink CD20 in the plasma membrane more appreciably and form Rtx/CD20 clusters that may play a role in apoptosis.

The improved methodology was used to study the direct mechanism of action of Rtx-LNPs in Chapter 5, which uncovered a mechanism of action of Rtx-LNP involving the valence-dependent upregulation of CD120a and subsequent activation of caspase-8, resulting in apoptosis. Moreover, this chapter showed that Rtx-MS, which do not contain liposomes, also induce apoptosis through a

CD120a-dependent mechanism of action, illustrating that the liposome is not responsible for the apoptosis induced by Rtx-LNP. Chapter 6 showed that the induction of apoptosis of multivalent Rtx was Chol-dependent, with lower levels promoting apoptosis and higher levels inhibiting it, consistent with the known Chol dependence of CD120a signaling. This final chapter also showed that hypercrosslinking of Rtx on lymphoma cells by FcγR-expressing immune effector cells is sufficient to upregulate CD120a and induce apoptosis, suggesting that a CD120a-dependent direct mechanism of action occurs *in vivo* after normal bivalent Rtx therapy. This constitutes a novel direct mechanism of action of Rtx, which so far has been undefined.

7.2 Discussion concerning Ab-LNPs and other multivalent Ab constructs

7.2.1 Strengths and weaknesses of Ab-LNPs as a tool for developing new drugs

The use of Ab-LNPs as liposomal multivalent Ab constructs is a unique approach to using a liposome to enhance the activity of a drug that is present on the outside, rather than the inside, of the liposome. This is one feature that distinguishes Ab-LNPs from immunoliposomes, as discussed in Section 1.2. However, the most important difference between Ab-LNPs and immunoliposomes, the evidence for which is provided in this dissertation, is that while immunoliposomes are the final drug product themselves, Ab-LNPs are not; instead, Ab-LNPs are a tool for optimizing and studying the mechanism of action of multivalent therapeutic Abs. Their use would be particularly advantageous when it is not straightforward to prepare many valences using other types of formulations, as is the case with gold nanoparticles for example[96], or when the multivalent Ab is to be included in more complex systems such as multifunctional therapeutic nanoparticles[167], where it would be desirable to study Ab multivalency separately from the rest of the system.

Another strength of Ab-LNPs is that valences as high as 250 have been reproducibly prepared using the methodology in Chapter 3. Although other studies have probably employed

valences in this range as described in Section 1.6, the actual valences were never defined, possibly because the valence was heterogeneous, suitable assays were not available, or it was not necessary to measure the valence. In studies where the valence has been defined for a multivalent Ab construct, it generally has not exceeded 10 (Section 1.6.3). A range of specific valences up to 250 can now be reproducibly prepared with high start-to-finish yields of coupled Ab (80%).

The principal weakness of Ab-LNPs is that the constructs resulting from the methodology in Chapter 3 are likely not suitable for *in vivo* studies. This is because the Neut molecules used in the coupling process are proteins and there therefore potentially antigenic. The information obtained using these Ab-LNPs (optimal valence and mechanism of action), however, can be translated into a variety of other types of constructs[92-96, 167]. If it should be desirable to study a liposomal multivalent Ab construct *in vivo*, an alternative method of preparing Ab-LNPs would have to be employed, such as that used in Chapter 2 which uses covalent coupling. Section 3.2.1 described the difficulties in terms of yield, reproducibility, and control over the valence of such methods, so they would not be suitable for studies on multivalency from the outset, but they may potentially be used to prepare a single valence for *in vivo* studies.

7.2.2 The use of whole Abs in Ab-LNPs versus Ab fragments

If hypercrosslinking of the target on the surface of the cancer cell is responsible for the improved therapeutic effects, then it may appear advantageous to employ Ab fragments (such as Fab regions) rather than the whole IgG. In this way, defined chemical species could more easily be prepared which could then be coupled to liposomes; this is the approach used by Nellis *et al.* for preparing anti-ErbB2 immunoliposomes[252, 253]. Using Fab fragments for preparing multivalent Abs, however, would completely eliminate the indirect mechanisms of action of the Abs (ADCC and CDC), which are important in the overall efficacy of therapeutic Abs (Section 1.4). Chapter 2 showed that the indirect mechanisms were not only preserved in Rtx-LNP, but enhanced. This was explained by

the fact that the processes of ADCC and CDC themselves result from multivalent interactions involving the Fc region; these interactions are facilitated when the Ab is multivalent. ADCC and CDC are common mechanisms to all therapeutic Abs (Sections 1.4.1 & 1.4.2), so the augmentation of the indirect mechanisms would be expected to be observed using other Abs.

The methodology in Chapter 3 utilizes biotinylation on a NIMAC column, and under the conditions that were employed, between one and two biotin groups were added per Ab. The site of biotinylation on the Ab, however, is not homogeneous. On some Ab molecules, it may be present on the Fab region, which may negatively affect binding to target and therefore the direct mechanism; on other molecules, a site on the Fc region may be biotinylated, which may affect the indirect mechanisms. The nonhomogeneous biotinylation constitutes a significant advantage when considering that the overall mechanism of action consists of a combination of direct and indirect factors; one could imagine that a single biotinylation site on either the Fab or Fc would reduce or eliminate one of the contributing mechanisms.

This appears to have occurred, for example, with a multivalent Ab that uses a specific configuration of six Fab regions and one Fc region. This configuration resulted in complete abolition of all CDC activity, possibly due to the point of attachment on the Fc region interfering with CDC processes such as C1q binding[90]. By having many different biotinylation sites in the Ab molecules in Ab-LNP, some individual molecules may show decreased binding to target (biotinylation in Fab region) or decreases ADCC or CDC (Fc region); these processes, however, rely on multivalent interactions that can be facilitated by the neighboring Abs in Ab-LNP, resulting not only in compensation but improvement in therapeutic responses.

For example, Section 1.4.1 described how C1q is a hexavalent ligand requiring the binding of several Fc regions in order to initiate CDC; if the Fc region of one Ab in Ab-LNP is unable to bind C1q due to interference from a specific biotinylation site, a significant number of other unaffected Abs would be expected to be close by for binding, allowing CDC to progress. It therefore appears that

having many sites of biotinylation in Rtx-LNP is advantageous to preserving all the mechanisms of action of therapeutic Abs in the multivalent construct.

7.2.3 Relevance of the direct mechanism of action of therapeutic Abs studied *in vitro* in the absence of hypercrosslinking

Different strategies for creating multivalent Rtx were employed in this dissertation, including the use of Rtx-LNP, Rtx-MS, Rtx + 2^{o}Ab, and Rtx + 2^{o}Ab-MS. The treatment that provided maximum therapeutic efficacy (levels of plasma-membrane CD120a and apoptosis) was hypercrosslinking with 2^{o}Ab-MS following Rtx treatment (Figure 6.4B). These levels were higher than those observed after treatment with Rtx-LNP of high valence (above 100; Figure 4.6) or Rtx-MS (Figure 5.6), and they were especially higher than cells treated with Rtx followed by 2^{o}Ab (Figure 6.4B). Note that in Figure 6.4A (24 h time point), a significant fraction of cells had become necrotic; Figure 6.4B provides data at 12 h post-treatment, when the necrotic fraction was much lower.

2^{o}Ab-MS acted on cells that were already saturated with Rtx, but Figure 4.1 shows that saturating cells with Rtx-LNP still resulted in significant unbound CD20 as well as a large fraction of Rtx that was not bound to CD20. The lack of saturation of CD20 could be due to a steric effect where the liposomal component of Rtx-LNP takes up too much space to allow sufficient Rtx to saturate all CD20 on the cell surface. However, because 2^{o}Ab-MS acted on Rtx-saturated cells, higher levels of hypercrosslinked CD20 could be achieved in the plasma membrane, resulting in more significant CD120a upregulation and apoptosis compared to Rtx-LNP treatment. The saturation of cells with Rtx, which allows for high levels of clustered CD20, can also be used to explain why the hypercrosslinking induced by effector cells can produce a strong apoptotic signal (Figure 6.6).

Importantly, although use of a 2^{o}Ab is a common method to assess the effects of crosslinking a therapeutic Ab *in vitro*[7, 74-76], Figure 6.4B showed that 2^{o}Ab-MS but not 2^{o}Ab alone was

able to provide a multivalent interaction that resulted in sufficient hypercrosslinking to induce elevated levels of apoptosis. This suggests that when testing the crosslinking of therapeutic Abs, using a 2^{o}Ab may not provide the necessary degree of crosslinking to induce meaningful therapeutic effects, and a multivalent 2^{o}Ab construct may be more appropriate.

It is known that ADCC occurs as a result of the binding of therapeutic Abs like Rtx to activating FcγRs on effector cells of the immune system. This binding of the therapeutic Ab causes hypercrosslinking of the activating FcγR on the effector cell, which triggers the ADCC response (Section 1.4.2). With the results in Chapter 6, it can be argued that it is not necessarily the Ab which causes hypercrosslinking of FcγR, but that the Ab and the FcγR mutually hypercrosslink each other, which in terms of Rtx would result not only in ADCC but also in the direct induction of apoptosis *in vivo*.

Moreover, as discussed in Section 1.4.2, NK cells and granulocytes express only activating FcγRs, while other effector cells including macrophages also express inhibitory FcγRs, which upon hypercrosslinking, negatively regulate ADCC. We demonstrated in Chapter 6 that 2^{o}Ab-MS and effector cells had similar effects on Rtx-treated lymphoma cells in terms of a CD120a upregulation and induction of apoptosis, indicating that the method of Rtx hypercrosslinking does not influence the therapeutic response. This implies that *in vivo*, the direct induction of apoptosis resulting from hypercrosslinking should not depend on whether the particular FcγR that is hypercrosslinked is an activating or inhibitory receptor, because Rtx would be hypercrosslinked as a result. Inhibitory FcγRs could therefore be responsible for inducing direct apoptosis as well as activating FcγRs. It is also conceivable that responses of bivalent Rtx and possibly other Abs that were thought to be entirely the result of ADCC (such as those in Figure 2.3C & D) could have actually been due, at least in part, to the direct mechanism of action.

7.2.4 The nature of the interaction between Ab-LNPs and the surface of target cells

In Ab-LNPs, as in immunoliposomes, the Ab molecules are not rigidly held in place, but diffuse around the liposome[254]. This property may be particularly advantageous to the therapeutic efficacy of Ab-LNPs because it has been shown that rigid multivalent constructs exhibit variable activation or inhibition against targets depending on the spacing between the different binding sites on the multivalent ligand[102]. This suggests that by being allowed to diffuse, the Ab molecules can arrange in lowest-energy (most stable) configuration of the multivalent Ab/target complex.

On the other hand, since Figure 4.1 showed that not all Ab is bound to the target in these multivalent complexes, an even more efficient use of Ab may be a near-planar nanometer-scale configuration with Ab only on one side of the plane. After treatment of target cells, no unbound Ab would be present, allowing all Ab to be engaged in hypercrosslinking. It would be possible to synthesize different sizes and intermolecular spacings of such constructs[102], or possibly create constructs where the Ab is not rigidly held in place using PEG linkers such as those used in Rtx-LNPs. Although the direct mechanism of action of such a construct would be expected to be enhanced, it is unclear how this would affect the indirect mechanisms. To preserve all mechanisms of action, whole IgG would be required (not fragments) and variation in the point of attachment of the linker would also be necessary, as discussed in the previous section.

In terms of the dynamics of the association of Rtx-LNP with target cells, there may be parallels between with other types of multivalent ligands in nature such as carbohydrates and DNA. As outlined in Section 1.6, multivalent ligands show decreased dissociation rates from receptors compared to univalent ones due to recapture of the ligand before complete dissociation of the ligand-receptor complex. Evidence suggests that some DNA regulatory proteins bind to DNA at nonspecific base pair sites and then through Brownian motion diffuse along the backbone until they

reach a high-affinity site. This "bind and slide" mechanism has also been observed in the interaction between multivalent carbohydrates and lectins[100].

It can be hypothesized that after the initial univalent interaction between an Ab molecule in Ab-LNP and the surface of the target cell, the cell "recaptures" another Ab molecule before (or during) dissociation of the first molecule. This constant association and dissociation allows the Ab-LNP to essentially roll across the surface of the cell until a higher-affinity interaction is formed, such as a cluster of target in the plasma membrane on a length scale similar to the diameter of the Ab-LNP. These more stable multivalent interactions may be responsible for inducing the therapeutic effects of multivalent Abs, such as those illustrated in Figure 6.5 where hypercrosslinked Rtx colocalized with CD120a outside of plasma membrane rafts.

7.3 Discussion on the mechanism of action of Rtx

7.3.1 The issue of rapid clearance of multivalent Rtx remains unresolved

In Chapter 2, it was shown that even though Rtx-LNPs showed significantly higher *in vitro* apoptosis, ADCC, and CDC, the *in vivo* efficacy of Rtx and Rtx-LNP were equivalent (Figure 2.5). This was explained by pharmacokinetic studies in Figure 2.6 that showed rapid clearance of Rtx-LNP from the circulation. Efficacy and pharmacokinetics studies have been performed on other types of multivalent anti-CD20 Abs, including a hexavalent construct based on veltuzumab (a humanized anti-CD20 Ab)[90]. Compared to veltuzumab, the hexavalent Ab induced higher apoptosis and similar levels of ADCC, but the CDC of the hexavalent Ab was completely abolished. This contrasts to Rtx-LNP, which showed enhanced CDC compared with Rtx, and which may have resulted from the intact Fc regions in Rtx-LNP enabling multivalent C1q binding. This highlights the advantage of using entire IgG molecules in multivalent therapeutic Ab constructs in order to preserve the favorable effects of the indirect mechanisms of action *in vivo*. The efficacy of the hexavalent Ab was not found to be

superior to that of veltuzumab except at very high doses, and this effect was attributed to the fact that it was cleared from the circulation at least 4.5 times faster than the bivalent Ab. These data mirror those in the current study, where in both cases the enhanced effects from multivalency observed *in vitro* are countered by decreases in circulation lifetime.

On the other hand, Zhang *et al*. have demonstrated more favorable pharmacokinetics and efficacy of a Rtx polymer with a valence of ~10 (ref. 75). Although they did not examine ADCC or CDC, they found that decavalent Rtx induced apoptosis more effectively in ten different $CD20^+$ cell lines, and also exhibited a half-life if 144 h, compared to 96 h for free Rtx. The decavalent construct also exhibited superior efficacy in Raji tumor-bearing nude mice. The reasons for the increase in circulation lifetime of decavalent Rtx versus the decrease for Rtx-LNP are unclear, but one reason may be that the coupling method used may affect pharmacokinetic characteristics and, obviously, the size of the multivalent constructs are remarkably different. This study, however, suggests that if the pharmacokinetics of Rtx-LNP can be improved, the enhanced effects from both indirect and direct factors could be manifested *in vivo*. Importantly, the fact that Rtx-LNP exhibits such a short residence time in the circulation yet exhibit an efficacy that is equivalent to free Rtx reflects the enhanced potency of Rtx-LNP.

The rapid clearance of Rtx-LNP was surprising because previous studies on Trz-LNP showed improvements in circulation lifetime and other pharmacokinetic parameters (Table 1.1). The results using Rtx-LNP imply that the rapid clearance may be due to the Ab employed rather than the size of the constructs or the liposomal component of the formulation. It may still be possible, however, to improve the pharmacokinetics of multivalent Rtx-LNP by employing a non-liposomal construct. Chapters 5 & 6 showed that the enhanced efficacy of Rtx-LNP is not due to a contribution from the liposome, because other means of achieving multivalency (Rtx-MS, 2^oAb-MS) resulted in therapeutic effects through the same CD120a-dependent mechanism of action. Different types of constructs that could be explored include polymeric nanoparticles[93], rotaxanes[92], gold nanoparticles[96],

dendrimers[94, 95], or multifunctional nanoparticles[167]. The issue of rapid clearance may also be resolved through the selection of an alternative anti-CD20 Ab such as those listed in Table 1.2, but an alternative Ab would be expected to possess a different direct mechanism of action and different relative contributions of the direct and indirect mechanisms, as discussed in Section 1.4. An alternative anti-CD20 Ab would therefore require re-initiation of mechanistic studies.

7.3.2 Local concentrations of CD20 in the plasma membrane, and not the number of Rtx-CD20 interactions, determine the level of apoptosis induced by multivalent Rtx

Section 7.2.3 described how the various types of multivalent Rtx employed in this dissertation resulted in different levels of CD120a upregulation and apoptosis in lymphoma cells. Bivalent Rtx showed the lowest efficacy *in vitro* although it saturated all CD20 molecules on the cell surface, while Rtx-LNP bound only to a fraction of surface CD20, formed domains, and showed much higher efficacy (Figures 4.1, 4.2, & 4.6). Rtx-LNP treatment also resulted in a fraction of Rtx molecules that were not bound to CD20, but remained associated to the cell because other Rtx molecules in the same Rtx-LNP were bound to CD20 (Figure 4.1). Together, this indicates that it is not the direct binding of Rtx to CD20 that causes apoptosis; otherwise Rtx would have exhibited higher efficacy than Rtx-LNP. Rather, high local CD20 densities in the plasma membrane, induced through hypercrosslinking by the multivalent construct, appear to be responsible for the increased efficacies.

This is supported by the valence-dependent levels of apoptosis shown in Figure 4.6. The higher valences of Rtx-LNP are capable of more substantial hypercrosslinking of CD20 within the same area of the plasma membrane, resulting in greater local CD20 concentrations. This also explains why CD20 expression has been observed to be independent of sensitivity to Rtx therapy[255]; higher levels of bound Rtx are not necessarily related to greater Rtx sensitivity. A better indicator of

sensitivity to Rtx treatment may be an assessment of the ability of Rtx/CD20 to undergo hypercrosslinking (discussed further in Section 7.3.4). By applying the methodology to other Abs, particularly those against targets known to function through hypercrosslinking, it will become clear whether this same phenomenon occurs with other Abs (Section 7.4).

It should be noted that one potential weakness in Figure 4.1 may be with respect to the Abs that were employed. Based on the discussion in Section 7.2.4, if the interaction between Rtx-LNP and the cell surface is highly dynamic with Rtx-LNP translocating across the surface of the cell, the binding of A647-mCD20 on unoccupied CD20 molecules at any instant could cause those molecules to be unavailable for further interactions with Rtx-LNP. This may eventually cause more staining of unbound CD20 then was actually present at any instantaneous time point. The results would still indicate that Rtx-LNP does not occupy all available CD20 on the cell surface, consistent with the current interpretation of this data, but the levels of unoccupied CD20 would be overestimated.

7.3.3 The direct mechanism of action of Rtx may not exclusively involve CD120a, but also other death receptors and signaling molecules

Cell signaling, in a general sense, encompasses greater complexities than linear transduction pathways with clearly defined endpoints[256]. Rather, a cell contains a network of signaling cascades that can be envisaged as a spider web, where plucking one fiber results in small reverberations at distant sites which determine different biological outcomes[256, 257]. In this sense, it is important to note that CD120a upregulation and activation of the extrinsic apoptosis pathway (Figure 5.1) likely cannot explain the direct mechanism of action of Rtx in itself. This may be particularly true in light of the fact that essentially all death receptors showed elevated expression after Rtx-LNP treatment, particularly CD95 and DR5 in addition to CD120a (Section 5.4.2). The direct induction of apoptosis by hypercrosslinked Rtx therefore appears to involve a coordinated network of many death receptors that ultimately induce apoptosis in target cells, and from the experiments described in this

dissertation, CD120a appears to be the major player in this network. It remains to be seen if this is the case in cell lines other than those employed here, or in primary cells from xenograft models or from humans.

In spite of the strong evidence in support of a CD120a-dependent mechanism at the beginning of Section 5.5.1, a knockdown approach or a CD120a-specific antagonistic antibody[258] may further yield results on the overall dependence of CD120a on apoptosis. CD120a is nearly always expressed at very low levels[174], so strategies aimed at inhibiting its upregulation by Rtx-LNP may yield important information on whether CD120a is necessary in the direct mechanism of action of Rtx, and also whether the other death receptors can compensate for CD120a in its absence.

7.3.4 CD120a expression levels or mutation status as predictive markers for Rtx response

There is significant interest in identifying molecular markers that are predictive of response to Rtx because resistance to Rtx therapy is not well understood[139, 140]. As mentioned in the previous section, CD120a is normally expressed at constitutively low levels in all cells in the human body[174, 177]. In the direct mechanism of action of Rtx, it appears that the ability of multivalent Rtx to upregulate CD120a is responsible for the enhanced therapeutic effects. Specifically, as illustrated in Figures 6.1, 6.2, & 6.5, the majority of upregulated CD120a is localized outside of plasma membrane rafts. This constitutes the apoptosis-inducing form of CD120a, as opposed to the antiapoptotic form, which involves association of CD120a with rafts (Section 6.2.1).

It would be expected that oncogenic cells, in order to survive, would express the raft-associated, NF-κB-activating form of CD120a. In this sense, measuring CD120a expression may not be a good predictive marker for Rtx response because our results suggest that the upregulation of non-raft-associated CD120a drives the direct induction of apoptosis. The results in Chapter 6 (particularly Figure 6.3), however, suggest that if lymphoma cells express high levels of CD120a,

which would be expected to be raft-associated, that the patient may show response to Chol depletion therapy such as statin treatment. Such a strategy may lower the levels of plasma-membrane Chol in lymphoma cells and cause CD120a to translocate outside of plasma membrane rafts, which would be expected to induce apoptosis in these cells. Section 7.3.5 discusses statin treatment in conjunction with Rtx therapy.

Since total CD120a levels do not appear to be a good marker for response to Rtx, there is also the possibility of assessing the mutation status of CD120a. Mutations may influence the ability of CD120a to induce apoptosis, affecting the response to Rtx treatment. The most common mutations in the gene encoding CD120a occur in a group of autoinflammatory disorders called TNFR-associated periodic syndrome (TRAPS)[259, 260]. Symptoms of TRAPS consist of seemingly unprovoked inflammatory attacks due to impaired control of the innate immune system, but autoantibodies or antigen-specific T-cells (the usual markers of autoimmune disease) are absent[261]. Mutations in CD120a that cause TRAPS occur in the extracellular domain, and it has been shown that these mutations do not cause constitutive or enhanced CD120a activation, but they may result in defective apoptosis, allowing increased survival of proinflammatory cells[262].

Apart from those that are associated with TRAPS, however, CD120a mutations are relatively rare, including in cancer[263]; this is in contrast to CD95, DR4, and DR5, where mutations have been identified in many cancer types including different lymphomas[262, 264]. In an effort to identify novel lymphoma-associated mutations in CD120a, its mutation status was queried in a database of hundreds of diffuse large B-cell lymphoma (DLBCL) biopsies which underwent genome sequencing (Dr. Randy Gascoyne, personal communication). This analysis yielded the result that no specific mutations in CD120a were found across a statistically significant number of samples, confirming the lack of CD120a mutations observed in cancer and in diseases other than TRAPS. Like CD120a expression levels, therefore, CD120a expression status does not appear to be a good marker for clinical Rtx response.

It may be more promising to look beyond CD120a to other proteins that interact with it; for example, mutations in proteins that associate with CD120a and which may contribute to oncogenesis have been identified, such as mutations in TRADD, which forms the DISC with CD120a[265, 266]. Another possibility would be to assess the ability of healthy FcγR-expressing effector cells in a patient to engage in hypercrosslinking, because hypercrosslinking was shown to be important in the direct mechanism of action of Rtx (Figures 6.4–6.6). This can be assessed not only by the expression levels of FcγRs on effector cells, but also by the total counts of FcγR-expressing cells; both higher average expression and higher total cell counts would be expected to produce enhanced Rtx hypercrosslinking. Another possibility may be to develop an assay to measure the affinity of FcγRs to the Fc region of therapeutic Abs. This is in light of studies that have shown that certain FcγR dimorphisms result in greater affinity interaction between FcγR and the Fc region of IgG (Section 2.2.2); greater-affinity FcγR–Fc interactions would result in more stable hypercrosslinked Rtx/CD20 clusters and may result in enhanced efficacy due to the CD120a-dependent direct mechanism of action described in Chapters 5 & 6 (refs. 122, 123).

7.3.5 Statins in combination with Rtx therapy

Chapter 6 shows that the hypercrosslinking provided by immune effector cells is sufficient to induce CD120a upregulation and apoptosis. This is strong evidence that CD120a-mediated cell death occurs as a direct mechanism of action of regular bivalent Rtx therapy *in vivo*. The final chapter also examines the Chol dependence of Rtx-LNP induced apoptosis in light of this mechanism since CD120a has been shown to produce proapoptotic signals under conditions of reduced plasma membrane Chol (Sections 6.2.1 & 6.2.2). It was shown in Figures 6.1 & 6.2 that Rtx-LNP increased the detergent solubility of CD120a, but when Chol was reinserted in the plasma membrane using MBCD/Chol, the DR and raft association of CD120a increased, and cells were rescued from apoptosis. Simvastatin treatment also decreased the DR of CD120a and sensitized lymphoma cells

to Rtx-LNP-induced apoptosis (Figure 6.3). Along with the PBMC experiments in Figure 6.6 which supported an *in vivo* CD120a-dependent mechanism, these data suggest that concurrent statin treatment with Rtx therapy may increase the efficacy of Rtx due to the dual raft-dependent nature of CD120a signaling.

Statins have shown anticancer activity in leukemia, lymphoma, colorectal cancer, breast cancer, lung cancer, prostate cancer, and pancreatic cancer[267]. Many mechanisms of action responsible for the therapeutic effects have been described, including the ability of statins to inhibit antiapoptotic NF-κB signaling. Reduced activation of NF-κB resulting from simvastatin treatment has been demonstrated in Epstein-Barr virus-associated lymphomas[268] and cancer-associated osteoclastogenesis[269], and it occurred alongside increased apoptosis in human myeloid leukemia cells[270] and breast cancer cells, where the apoptosis was induced in response to TNF-α[271]. Statins have also been shown to induce apoptosis in ovarian cancer cells[272], to inhibit the cell growth, migration, and invasion of melanoma cells[273], and to help overcome drug resistance in refractory multiple myeloma in a Phase II trial[274]. Finally, many studies have associated statin use with reduced risk of cancer. For example, a European case-control study across 22 centers demonstrated an odds ratio of 0.61 for regular statin use with respect to non-use, representing a significant reduction in overall lymphoma risk associated with statin treatment[275].

There is some evidence that statin use may directly inhibit Rtx binding to CD20 and, therefore, the efficacy of Rtx. Inhibition was shown to be related to conformational changes in the CD20 molecule during statin treatment, and B cells obtained from patients on Rtx therapy showed lower levels of Rtx binding[276]. Although these studies raised concerns on the use of statins during Rtx treatment, there is no consensus on whether or not to stop statin treatment at the initiation of lymphoma therapy containing Rtx[277]. One study that addressed this issue examined Rtx efficacy with respect to statin use on the outcome of a cohort of prospectively observed patients with newly diagnosed DLBCL and follicular lymphoma (FL). It was shown that statin use had no impact on the

overall response rate, overall survival, or event-free survival in patients with DLBCL, but statin use at diagnosis was associated with improved event-free survival in patients with FL, including subgroups treated with a Rtx-containing regimen. Statins therefore did not adversely affect outcome in DLBCL and FL, and the apparent benefit of statin therapy on FL outcome requires further studies[277].

At least in some cases, the anticancer effect of statins is related to lowering the area of the plasma membrane covered with plasma membrane rafts[267]. For example, Chol targeting has been shown to alter lipid raft composition and cell survival in prostate cancer cells and xenografts. Both *in vitro* and *in vivo* experiments showed that simvastatin induced apoptosis in prostate cancer cells by inhibiting Akt pathway signaling, and replenishing cell membranes with Chol reversed these inhibitory and apoptotic effects[243]. This large body of evidence concerning statin use in cancer treatment lends credibility to future studies on the ability of statins to improve the *in vivo* therapeutic efficacy of Rtx through a mechanism that involves CD120a.

7.4 Future work

In an effort to further understand the direct mechanism of action of Rtx, the results from Chapter 6 suggest that an *in vivo* study in lymphoma xenograft models should be carried out in order to determine whether changes in CD120a expression levels in lymphoma cells are observed before and after treatment with Rtx. The same two models as used in Figure 2.1B & C could be employed; the JVM2 model was Rtx-insensitive while the Z138 model was Rtx-sensitive. Based on the results in Chapter 6, it should be established that the animals have functioning FcγR-expressing effector cells in order for hypercrosslinking to occur. These experiments could be carried out alongside a study which examines the efficacy of Rtx in conjunction with statin therapy, and if possible, differences in efficacy could be examined alongside CD120a expression to support or discredit the hypothesis regarding a CD120a-dependent direct mechanism of action of Rtx.

In terms of the Ab-LNP methodology presented in this dissertation, the most important future work involves its application to other therapeutic Abs in an effort to discover new multivalent drugs. In industrial settings, a large number of potential therapeutic Ab candidates do not progress past initial stages of development due to their marginal activity as bivalent molecules. It is possible, however, that creating multivalent constructs from these Abs could lead to the discovery of new responses that were not observed when the Ab was bivalent, as was the case with Rtx. The new drugs could then be developed as multivalent, rather than bivalent, Abs.

To work toward a system for applying the methodology in this dissertation to other Abs, the creation of a business plan has been underway with two partners, Joel Jaffe and Meir Deutsch, under the auspices of the British Columbia Innovation Council. The process would involve partnering with academic laboratories or companies engaged in therapeutic antibody development, who would provide "discarded" Abs for testing. Besides showing low bivalent activity, the Abs to be studied should be at an early stage of development and they should ideally have a target that is known to produce therapeutic responses through clustering. Such a strategy would expand the proof-of-concept provided using Rtx-LNPs and may lead to the generation of new cancer medicines.

7.5 Conclusions

This proof-of-concept has established that the methodology outlined in this dissertation, in its application to other Abs in the context of drug development, can serve to:

(1) Identify therapeutic Abs that show enhanced activities when multivalent rather than bivalent (Chapter 2);

(2) Determine the optimal valence of Abs that benefit from multivalency (Chapter 4);

(3) Decipher the mechanism of action of the new multivalent drug (Chapters 2, 4, 5, & 6);

(4) Use the above information to develop non-liposomal formulations of the multivalent Ab, if required (Chapters 5 & 6).

Although the valence of all approved therapeutic Abs is currently two, the results in this dissertation suggest that every therapeutic Ab may have a different valence where it shows its highest activity. This new concept should be included in the toolbox for creating therapeutic Abs for treating cancer.

References

1. Weiner LM, Surana R, Wang S. Monoclonal antibodies: Versatile platforms for cancer immunotherapy. Nat Rev Immunol 2010 May;10(5):317-27.

2. Harris M. Monoclonal antibodies as therapeutic agents for cancer. Lancet Oncol 2004 May;5(5):292-302.

3. Allen TM, Cullis PR. Drug delivery systems: Entering the mainstream. Science 2004 Mar 19;303(5665):1818-22.

4. Heath TD, Fraley RT, Papahdjopoulos D. Antibody targeting of liposomes: Cell specificity obtained by conjugation of F(ab')2 to vesicle surface. Science 1980 Oct 31;210(4469):539-41.

5. Zhang L, Gu FX, Chan JM, Wang AZ, Langer RS, Farokhzad OC. Nanoparticles in medicine: Therapeutic applications and developments. Clin Pharmacol Ther 2008 May;83(5):761-9.

6. Park JW, Benz CC, Martin FJ. Future directions of liposome- and immunoliposome-based cancer therapeutics. Semin Oncol 2004 Dec;31(6 Suppl 13):196-205.

7. Chiu GN, Edwards LA, Kapanen AI, Malinen MM, Dragowska WH, Warburton C, Chikh GG, Fang KY, Tan S, Sy J, *et al*. Modulation of cancer cell survival pathways using multivalent liposomal therapeutic antibody constructs. Mol Cancer Ther 2007 Mar;6(3):844-55.

8. Drummond DC, Noble CO, Hayes ME, Park JW, Kirpotin DB. Pharmacokinetics and in vivo drug release rates in liposomal nanocarrier development. J Pharm Sci 2008 Nov;97(11):4696-740.

9. Slingerland M, Guchelaar H, Gelderblom H. Liposomal drug formulations in cancer therapy: 15 years along the road. Drug Discov Today 2012 Feb;17(3-4):160-6.

10. Heidel JD, Davis ME. Clinical developments in nanotechnology for cancer therapy. Pharm Res 2011 Feb;28(2):187-99.

11. Park JW, Hong K, Kirpotin DB, Colbern G, Shalaby R, Baselga J, Shao Y, Nielsen UB, Marks JD, Moore D, *et al*. Anti-HER2 immunoliposomes: Enhanced efficacy attributable to targeted delivery. Clin Cancer Res 2002 Apr;8(4):1172-81.

12. Mamot C, Drummond DC, Noble CO, Kallab V, Guo Z, Hong K, Kirpotin DB, Park JW. Epidermal growth factor receptor-targeted immunoliposomes significantly enhance the efficacy of multiple anticancer drugs in vivo. Cancer Res 2005 Dec 15;65(24):11631-8.

13. Kirpotin D, Park JW, Hong K, Zalipsky S, Li WL, Carter P, Benz CC, Papahadjopoulos D. Sterically stabilized anti-HER2 immunoliposomes: Design and targeting to human breast cancer cells in vitro. Biochemistry 1997 Jan 7;36(1):66-75.

14. Omelyanenko V, Kopeckova P, Gentry C, Shiah JG, Kopecek J. HPMA copolymer-anticancer drug-OV-TL16 antibody conjugates. 1. Influence of the method of synthesis on the binding affinity to OVCAR-3 ovarian carcinoma cells in vitro. J Drug Target 1996;3(5):357-73.

15. Johnson RN, Kopeckova P, Kopecek J. Synthesis and evaluation of multivalent branched HPMA copolymer-fab' conjugates targeted to the B-cell antigen CD20. Bioconjug Chem 2009 Jan;20(1):129-37.

16. Popov J, Kapanen AI, Turner C, Ng R, Tucker C, Chiu G, Klasa R, Bally MB, Chikh G. Multivalent rituximab lipid nanoparticles as improved lymphoma therapies: Indirect mechanisms of action and in vivo activity. Nanomedicine 2011 Nov;6(9):1575-91.

17. Mufamadi MS, Pillay V, Choonara YE, Du Toit LC, Modi G, Naidoo D, Ndesendo VMK. A review on composite liposomal technologies for specialized drug delivery. J Drug Deliv 2011 Feb 8;2011(Article ID 939851):19 pgs.

18. Lian T, Ho RJ. Trends and developments in liposome drug delivery systems. J Pharm Sci 2001 Jun;90(6):667-80.

19. Chonn A, Semple SC, Cullis PR. Association of blood proteins with large unilamellar liposomes in vivo. Relation to circulation lifetimes. J Biol Chem 1992 Sep 15;267(26):18759-65.

20. Strebhardt K, Ullrich A. Paul ehrlich's magic bullet concept: 100 years of progress. Nat Rev Cancer 2008 Jun;8(6):473-80.

21. Kohler G, Milstein C. Continuous cultures of fused cells secreting antibody of predefined specificity. Nature 1975 Aug 7;256(5517):495-7.

22. Boulianne GL, Hozumi N, Shulman MJ. Production of functional chimaeric mouse/human antibody. Nature 1984 Dec 13-19;312(5995):643-6.

23. Riechmann L, Clark M, Waldmann H, Winter G. Reshaping human antibodies for therapy. Nature 1988 Mar 24;332(6162):323-7.

24. Weiner LM, Belldegrun AS, Crawford J, Tolcher AW, Lockbaum P, Arends RH, Navale L, Amado RG, Schwab G, Figlin RA. Dose and schedule study of panitumumab monotherapy in patients with advanced solid malignancies. Clin Cancer Res 2008 Jan 15;14(2):502-8.

25. Hagenbeek A, Gadeberg O, Johnson P, Møller Pedersen L, Walewski J, Hellmann A, Link BK, Robak T, Wojtukiewicz M, Pfreundschuh M, *et al*. First clinical use of ofatumumab, a novel fully human anti-CD20 monoclonal antibody in relapsed or refractory follicular lymphoma: Results of a phase 1/2 trial. Blood 2008 June 15;111(12):5486-95.

26. Burtrum D, Zhu Z, Lu D, Anderson DM, Prewett M, Pereira DS, Bassi R, Abdullah R, Hooper AT, Koo H, *et al*. A fully human monoclonal antibody to the insulin-like growth factor I receptor blocks ligand-dependent signaling and inhibits human tumor growth in vivo. Cancer Res 2003 Dec 15;63(24):8912-21.

27. Coiffier B, Lepage E, Briere J, Herbrecht R, Tilly H, Bouabdallah R, Morel P, Van Den Neste E, Salles G, Gaulard P, *et al*. CHOP chemotherapy plus rituximab compared with CHOP alone in elderly patients with diffuse large-B-cell lymphoma. N Engl J Med 2002 Jan 24;346(4):235-42.

28. McLaughlin P, Grillo-Lopez AJ, Link BK, Levy R, Czuczman MS, Williams ME, Heyman MR, Bence-Bruckler I, White CA, Cabanillas F, *et al*. Rituximab chimeric anti-CD20 monoclonal antibody

therapy for relapsed indolent lymphoma: Half of patients respond to a four-dose treatment program. J Clin Oncol 1998 Aug;16(8):2825-33.

29. Leavy O. Therapeutic antibodies: Past, present and future. Nat Rev Immunol 2010 May;10(5):297.

30. Aggarwal S. What's fueling the biotech engine--2008. Nat Biotechnol 2009 Nov;27(11):987-93.

31. Beck A, Wurch T, Bailly C, Corvaia N. Strategies and challenges for the next generation of therapeutic antibodies. Nat Rev Immunol 2010 May;10(5):345-52.

32. Cobleigh MA, Vogel CL, Tripathy D, Robert NJ, Scholl S, Fehrenbacher L, Wolter JM, Paton V, Shak S, Lieberman G, *et al*. Multinational study of the efficacy and safety of humanized anti-HER2 monoclonal antibody in women who have HER2-overexpressing metastatic breast cancer that has progressed after chemotherapy for metastatic disease. J Clin Oncol 1999 Sep;17(9):2639-48.

33. Slamon DJ, Leyland-Jones B, Shak S, Fuchs H, Paton V, Bajamonde A, Fleming T, Eiermann W, Wolter J, Pegram M, *et al*. Use of chemotherapy plus a monoclonal antibody against HER2 for metastatic breast cancer that overexpresses HER2. N Engl J Med 2001 Mar 15;344(11):783-92.

34. Lundin J, Kimby E, Bjorkholm M, Broliden PA, Celsing F, Hjalmar V, Mollgard L, Rebello P, Hale G, Waldmann H, *et al*. Phase II trial of subcutaneous anti-CD52 monoclonal antibody alemtuzumab (campath-1H) as first-line treatment for patients with B-cell chronic lymphocytic leukemia (B-CLL). Blood 2002 Aug 1;100(3):768-73.

35. Van Cutsem E, Kohne CH, Hitre E, Zaluski J, Chang Chien CR, Makhson A, D'Haens G, Pinter T, Lim R, Bodoky G, *et al*. Cetuximab and chemotherapy as initial treatment for metastatic colorectal cancer. N Engl J Med 2009 Apr 2;360(14):1408-17.

36. Hurwitz H, Fehrenbacher L, Novotny W, Cartwright T, Hainsworth J, Heim W, Berlin J, Baron A, Griffing S, Holmgren E, *et al*. Bevacizumab plus irinotecan, fluorouracil, and leucovorin for metastatic colorectal cancer. N Engl J Med 2004 Jun 3;350(23):2335-42.

37. Wierda WG, Kipps TJ, Mayer J, Stilgenbauer S, Williams CD, Hellmann A, Robak T, Furman RR, Hillmen P, Trneny M, *et al*. Ofatumumab as single-agent CD20 immunotherapy in fludarabine-refractory chronic lymphocytic leukemia. J Clin Oncol 2010 Apr 1;28(10):1749-55.

38. Baselga J, Gelmon KA, Verma S, Wardley A, Conte P, Miles D, Bianchi G, Cortes J, McNally VA, Ross GA, *et al*. Phase II trial of pertuzumab and trastuzumab in patients with human epidermal growth factor receptor 2–Positive metastatic breast cancer that progressed during prior trastuzumab therapy. J Clin Oncol 2010 Mar 1;28(7):1138-44.

39. Baselga J, Swain SM. CLEOPATRA: A phase III evaluation of pertuzumab and trastuzumab for HER2-positive metastatic breast cancer. Clin Breast Cancer 2010 Dec 1;10(6):489-91.

40. Goldenberg DM, Morschhauser F, Wegener WA. Veltuzumab (humanized anti-CD20 monoclonal antibody): Characterization, current clinical results, and future prospects. Leuk Lymphoma 2010 May;51(5):747-55.

41. Morschhauser F, Leonard JP, Fayad L, Coiffier B, Petillon MO, Coleman M, Schuster SJ, Dyer MJ, Horne H, Teoh N, *et al*. Humanized anti-CD20 antibody, veltuzumab, in refractory/recurrent non-hodgkin's lymphoma: Phase I/II results. J Clin Oncol 2009 Jul 10;27(20):3346-53.

42. Clark MR. IgG effector mechanisms. Chem Immunol 1997;65:88-110.

43. Natsume A, Niwa R, Satoh M. Improving effector functions of antibodies for cancer treatment: Enhancing ADCC and CDC. Drug Des Devel Ther 2009 Sep 21;3:7-16.

44. Lim SH, Beers SA, French RR, Johnson PW, Glennie MJ, Cragg MS. Anti-CD20 monoclonal antibodies: Historical and future perspectives. Haematologica 2010 Jan;95(1):135-43.

45. Deans JP, Li H, Polyak MJ. CD20-mediated apoptosis: Signalling through lipid rafts. Immunology 2002 Oct;107(2):176-82.

46. Golay J, Zaffaroni L, Vaccari T, Lazzari M, Borleri GM, Bernasconi S, Tedesco F, Rambaldi A, Introna M. Biologic response of B lymphoma cells to anti-CD20 monoclonal antibody rituximab in vitro: CD55 and CD59 regulate complement-mediated cell lysis. Blood 2000 Jun 15;95(12):3900-8.

47. Polyak MJ, Li H, Shariat N, Deans JP. CD20 homo-oligomers physically associate with the B cell antigen receptor: Dissociation upon receptor engagement and recruitment of phosphoproteins and calmodulin-binding proteins. J Biol Chem 2008 Jul 4;283(27):18545-52.

48. Jefferis R, Lund J. Interaction sites on human IgG-fc for FcγR: Current models. Immunol Lett 2002 Jun 3;82(1-2):57-65.

49. Jazirehi AR, Bonavida B. Cellular and molecular signal transduction pathways modulated by rituximab (rituxan, anti-CD20 mAb) in non-hodgkin's lymphoma: Implications in chemosensitization and therapeutic intervention. Oncogene 2005 Mar 24;24(13):2121-43.

50. Cartron G, Watier H, Golay J, Solal-Celigny P. From the bench to the bedside: Ways to improve rituximab efficacy. Blood 2004 Nov 1;104(9):2635-42.

51. Stolz C, Schuler M. Molecular mechanisms of resistance to rituximab and pharmacologic strategies for its circumvention. Leuk Lymphoma 2009 Jun;50(6):873-85.

52. Walport MJ. Complement. N Engl J Med 2001 Apr 5;344(14):1058-66.

53. Zhou X, Hu W, Qin X. The role of complement in the mechanism of action of rituximab for B-cell lymphoma: Implications for therapy. The Oncologist 2008 September 01;13(9):954-66.

54. Wang SY, Weiner G. Complement and cellular cytotoxicity in antibody therapy of cancer. Expert Opin Biol Ther 2008 Jun;8(6):759-68.

55. Dall'Acqua WF, Cook KE, Damschroder MM, Woods RM, Wu H. Modulation of the effector functions of a human IgG1 through engineering of its hinge region. J Immunol 2006 Jul 15;177(2):1129-38.

56. Idusogie EE, Wong PY, Presta LG, Gazzano-Santoro H, Totpal K, Ultsch M, Mulkerrin MG. Engineered antibodies with increased activity to recruit complement. J Immunol 2001 Feb 15;166(4):2571-5.

57. Natsume A, In M, Takamura H, Nakagawa T, Shimizu Y, Kitajima K, Wakitani M, Ohta S, Satoh M, Shitara K, *et al*. Engineered antibodies of IgG1/IgG3 mixed isotype with enhanced cytotoxic activities. Cancer Res 2008 May 15;68(10):3863-72.

58. Satoh M, Iida S, Shitara K. Non-fucosylated therapeutic antibodies as next-generation therapeutic antibodies. Expert Opin Biol Ther 2006 Nov;6(11):1161-73.

59. Weitzman J, Betancur M, Boissel L, Rabinowitz AP, Klein A, Klingemann H. Variable contribution of monoclonal antibodies to ADCC in patients with chronic lymphocytic leukemia. Leuk Lymphoma 2009 Aug;50(8):1361-8.

60. Shields RL, Lai J, Keck R, O'Connell LY, Hong K, Meng YG, Weikert SHA, Presta LG. Lack of fucose on human IgG1 N-linked oligosaccharide improves binding to human FcγRIII and antibody-dependent cellular toxicity. J Biol Chem 2002 July 26;277(30):26733-40.

61. Kanda Y, Yamada T, Mori K, Okazaki A, Inoue M, Kitajima-Miyama K, Kuni-Kamochi R, Nakano R, Yano K, Kakita S, *et al*. Comparison of biological activity among nonfucosylated therapeutic IgG1 antibodies with three different N-linked fc oligosaccharides: The high-mannose, hybrid, and complex types. Glycobiology 2007 Jan 1;17(1):104-18.

62. Oganesyan V, Damschroder MM, Leach W, Wu H, Dall'Acqua WF. Structural characterization of a mutated, ADCC-enhanced human fc fragment. Mol Immunol 2008 4;45(7):1872-82.

63. Shields RL, Namenuk AK, Hong K, Meng YG, Rae J, Briggs J, Xie D, Lai J, Stadlen A, Li B, *et al*. High resolution mapping of the binding site on human IgG1 for FcγRI, FcγRII, FcγRIII, and FcRn and design of IgG1 variants with improved binding to the FcγR. J Biol Chem 2001 Mar 2;276(9):6591-604.

64. Lazar GA, Dang W, Karki S, Vafa O, Peng JS, Hyun L, Chan C, Chung HS, Eivazi A, Yoder SC, *et al*. Engineered antibody fc variants with enhanced effector function. P Natl Acad Sci USA 2006 Mar 14;103(11):4005-10.

65. Agus DB, Gordon MS, Taylor C, Natale RB, Karlan B, Mendelson DS, Press MF, Allison DE, Sliwkowski MX, Lieberman G, *et al*. Phase I clinical study of pertuzumab, a novel HER dimerization inhibitor, in patients with advanced cancer. J Clin Oncol 2005 Apr 10;23(11):2534-43.

66. Hall PS, Cameron DA. Current perspective – trastuzumab. Eur J Cancer 2009 1;45(1):12-8.

67. Yarden Y, Sliwkowski MX. Untangling the ErbB signalling network. Nat Rev Mol Cell Biol 2001 Feb;2(2):127-37.

68. Sliwkowski MX, Lofgren JA, Lewis GD, Hotaling TE, Fendly BM, Fox JA. Nonclinical studies addressing the mechanism of action of trastuzumab (herceptin). Semin Oncol 1999 Aug;26(4 Suppl 12):60-70.

69. Valabrega G, Montemurro F, Aglietta M. Trastuzumab: Mechanism of action, resistance and future perspectives in HER2-overexpressing breast cancer. Ann Oncol 2007 Jun 1;18(6):977-84.

70. Hudis CA. Trastuzumab — mechanism of action and use in clinical practice. N Engl J Med 2007 Jul 5;357(1):39-51.

71. DeGrendele H, Jain VK. The anti-HER2 monoclonal antibody pertuzumab may be effective in androgen-independent prostate cancer. Clin Genitourin Canc 2003;2(3):143-5.

72. Nahta R, Hung M, Esteva FJ. The HER-2-targeting antibodies trastuzumab and pertuzumab synergistically inhibit the survival of breast cancer cells. Cancer Res 2004 Apr 1;64(7):2343-6.

73. Scheuer W, Friess T, Burtscher H, Bossenmaier B, Endl J, Hasmann M. Strongly enhanced antitumor activity of trastuzumab and pertuzumab combination treatment on HER2-positive human xenograft tumor models. Cancer Res 2009 Dec 15;69(24):9330-6.

74. Janas E, Priest R, Wilde JI, White JH, Malhotra R. Rituxan (anti-CD20 antibody)-induced translocation of CD20 into lipid rafts is crucial for calcium influx and apoptosis. Clin Exp Immunol 2005 Mar;139(3):439-46.

75. Zhang N, Khawli LA, Hu P, Epstein AL. Generation of rituximab polymer may cause hyper-cross-linking-induced apoptosis in non-hodgkin's lymphomas. Clin Cancer Res 2005 Aug 15;11(16):5971-80.

76. Pedersen IM, Buhl AM, Klausen P, Geisler CH, Jurlander J. The chimeric anti-CD20 antibody rituximab induces apoptosis in B-cell chronic lymphocytic leukemia cells through a p38 mitogen activated protein-kinase-dependent mechanism. Blood 2002 Feb 15;99(4):1314-9.

77. Shan D, Ledbetter JA, Press OW. Apoptosis of malignant human B cells by ligation of CD20 with monoclonal antibodies. Blood 1998 Mar 1;91(5):1644-52.

78. Hanahan D, Weinberg RA. The hallmarks of cancer. Cell 2000 Jan 7;100(1):57-70.

79. Pennarun B, Meijer A, de Vries EG, Kleibeuker JH, Kruyt F, de Jong S. Playing the DISC: Turning on TRAIL death receptor-mediated apoptosis in cancer. Biochim Biophys Acta 2010 Apr;1805(2):123-40.

80. Cotter TG. Apoptosis and cancer: The genesis of a research field. Nat Rev Cancer 2009 Jul;9(7):501-7.

81. Ghavami S, Hashemi M, Ande SR, Yeganeh B, Xiao W, Eshraghi M, Bus CJ, Kadkhoda K, Wiechec E, Halayko AJ, *et al*. Apoptosis and cancer: Mutations within caspase genes. J Med Genet 2009 Aug;46(8):497-510.

82. Ashkenazi A. Targeting death and decoy receptors of the tumour-necrosis factor superfamily. Nat Rev Cancer 2002 Jun;2(6):420-30.

83. Danial NN, Korsmeyer SJ. Cell death: Critical control points. Cell 2004 Jan 23;116(2):205-19.

84. Vermes I, Haanen C, Steffens-Nakken H, Reutellingsperger C. A novel assay for apoptosis flow cytometric detection of phosphatidylserine expression on early apoptotic cells using fluorescein labelled annexin V. J Immunol Methods 1995 Jul 17;184(1):39-51.

85. Koopman G, Reutelingsperger C, Kuijten G, Keehnen R, Pals S, van Oers M. Annexin V for flow cytometric detection of phosphatidylserine expression on B cells undergoing apoptosis. Blood 1994 Sept 1;84(5):1415-20.

86. Strasser A. The role of BH3-only proteins in the immune system. Nat Rev Immunol 2005 Mar;5(3):189-200.

87. Kohlhaas SL, Craxton A, Sun XM, Pinkoski MJ, Cohen GM. Receptor-mediated endocytosis is not required for tumor necrosis factor-related apoptosis-inducing ligand (TRAIL)-induced apoptosis. J Biol Chem 2007 Apr 27;282(17):12831-41.

88. Ghetie MA, Bright H, Vitetta ES. Homodimers but not monomers of rituxan (chimeric anti-CD20) induce apoptosis in human B-lymphoma cells and synergize with a chemotherapeutic agent and an immunotoxin. Blood 2001 Mar 1;97(5):1392-8.

89. Miller K, Meng G, Liu J, Hurst A, Hsei V, Wong WL, Ekert R, Lawrence D, Sherwood S, DeForge L, *et al*. Design, construction, and in vitro analyses of multivalent antibodies. J Immunol 2003 May 1;170(9):4854-61.

90. Rossi EA, Goldenberg DM, Cardillo TM, Stein R, Wang Y, Chang CH. Novel designs of multivalent anti-CD20 humanized antibodies as improved lymphoma therapeutics. Cancer Res 2008 Oct 15;68(20):8384-92.

91. Deyev SM, Lebedenko EN. Multivalency: The hallmark of antibodies used for optimization of tumor targeting by design. Bioessays 2008 Sep;30(9):904-18.

92. Martos V, Castreño P, Valero J, de Mendoza J. Binding to protein surfaces by supramolecular multivalent scaffolds. Curr Opin Chem Biol 2008 12;12(6):698-706.

93. Kitov PI, Mulvey GL, Griener TP, Lipinski T, Solomon D, Paszkiewicz E, Jacobson JM, Sadowska JM, Suzuki M, Yamamura K, *et al*. In vivo supramolecular templating enhances the activity of multivalent ligands: A potential therapeutic against the escherichia coli O157 AB5 toxins. P Natl Acad Sci USA 2008 Nov 4;105(44):16837-42.

94. Patri AK, Majoros IJ, Baker JR. Dendritic polymer macromolecular carriers for drug delivery. Curr Opin Chem Biol 2002 Aug;6(4):466-71.

95. Patri AK, Myc A, Beals J, Thomas TP, Bander NH, Baker JR. Synthesis and in vitro testing of J591 antibody-dendrimer conjugates for targeted prostate cancer therapy. Bioconjug Chem 2004 Nov;15(6):1174-81.

96. Weiss A, Preston TC, Popov J, Li Q, Wu S, Chou KC, Burt HM, Bally MB, Signorell R. Selective recognition of rituximab-functionalized gold nanoparticles by lymphoma cells studied with 3D imaging. J Phys Chem C 2009 Oct 21;113(47):20252-8.

97. Cuesta AM, Sainz-Pastor N, Bonet J, Oliva B, Alvarez-Vallina L. Multivalent antibodies: When design surpasses evolution. Trends Biotechnol 2010 Jul;28(7):355-62.

98. Coloma MJ, Clift A, Wims L, Morrison SL. The role of carbohydrate in the assembly and function of polymeric IgG. Mol Immunol 2000 Dec;37(18):1081-90.

99. Mammen M, Choi SK, Whitesides GM. Polyvalent interactions in biological systems: Implications for design and use of multivalent ligands and inhibitors. Angew Chem Int Edit 1998;37:2754-94.

100. Dam TK, Brewer CF. Effects of clustered epitopes in multivalent ligand-receptor interactions. Biochemistry 2008 Aug 19;47(33):8470-6.

101. Martos V, Castreno P, Valero J, de Mendoza J. Binding to protein surfaces by supramolecular multivalent scaffolds. Curr Opin Chem Biol 2008 Dec;12(6):698-706.

102. Gestwicki JE, Cairo CW, Strong LE, Oetjen KA, Kiessling LL. Influencing receptor-ligand binding mechanisms with multivalent ligand architecture. J Am Chem Soc 2002 Dec 18;124(50):14922-33.

103. Rinker S, Ke Y, Liu Y, Chhabra R, Yan H. Self-assembled DNA nanostructures for distance-dependent multivalent ligand-protein binding. Nat Nanotechnol 2008 Jul;3(7):418-22.

104. Diestler DJ, Knapp EW. Statistical thermodynamics of the stability of multivalent ligand-receptor complexes. Phys Rev Lett 2008 May 2;100(17):178101.

105. Feng JQ, Mozdzanowska K, Gerhard W. Complement component C1q enhances the biological activity of influenza virus hemagglutinin-specific antibodies depending on their fine antigen specificity and heavy-chain isotype. J Virol 2002 Feb;76(3):1369-78.

106. Schumaker VN, Zavodszky P, Poon PH. Activation of the first component of complement. Annu Rev Immunol 1987;5:21-42.

107. George SR, O'Dowd BF, Lee SP. G-protein-coupled receptor oligomerization and its potential for drug discovery. Nat Rev Drug Discov 2002 Oct;1(10):808-20.

108. Simons K, Toomre D. Lipid rafts and signal transduction. Nat Rev Mol Cell Biol 2000 Oct;1(1):31-9.

109. Hommelgaard AM, Lerdrup M, van Deurs B. Association with membrane protrusions makes ErbB2 an internalization-resistant receptor. Mol Biol Cell 2004 Apr;15(4):1557-67.

110. Friedlander E, Arndt-Jovin DJ, Nagy P, Jovin TM, Szollosi J, Vereb G. Signal transduction of erbB receptors in trastuzumab (herceptin) sensitive and resistant cell lines: Local stimulation using magnetic microspheres as assessed by quantitative digital microscopy. Cytom Part A 2005 Oct;67(2):161-71.

111. Nagy P, Vereb G, Sebestyen Z, Horvath G, Lockett SJ, Damjanovich S, Park JW, Jovin TM, Szollosi J. Lipid rafts and the local density of ErbB proteins influence the biological role of homo- and heteroassociations of ErbB2. J Cell Sci 2002 Nov 15;115(Pt 22):4251-62.

112. Ghatak S, Misra S, Toole BP. Hyaluronan constitutively regulates ErbB2 phosphorylation and signaling complex formation in carcinoma cells. J Biol Chem 2005 Mar 11;280(10):8875-83.

113. Misra S, Ghatak S, Toole BP. Regulation of MDR1 expression and drug resistance by a positive feedback loop involving hyaluronan, phosphoinositide 3-kinase, and ErbB2. J Biol Chem 2005 May 27;280(21):20310-5.

114. Oliveira S, Schiffelers RM, van der Veeken J, van der Meel R, Vongpromek R, van Bergen En Henegouwen PM, Storm G, Roovers RC. Downregulation of EGFR by a novel multivalent nanobody-liposome platform. J Control Release 2010 Jul 14;145(2):165-75.

115. Reff ME, Carner K, Chambers KS, Chinn PC, Leonard JE, Raab R, Newman RA, Hanna N, Anderson DR. Depletion of B cells in vivo by a chimeric mouse human monoclonal antibody to CD20. Blood 1994 Jan 15;83(2):435-45.

116. Gancz D, Fishelson Z. Cancer resistance to complement-dependent cytotoxicity (CDC): Problem-oriented research and development. Mol Immunol 2009 Sep;46(14):2794-800.

117. Flieger D, Renoth S, Beier I, Sauerbruch T, Schmidt-Wolf I. Mechanism of cytotoxicity induced by chimeric mouse human monoclonal antibody IDEC-C2B8 in CD20-expressing lymphoma cell lines. Cell Immunol 2000 Aug 25;204(1):55-63.

118. Di Gaetano N, Cittera E, Nota R, Vecchi A, Grieco V, Scanziani E, Botto M, Introna M, Golay J. Complement activation determines the therapeutic activity of rituximab in vivo. J Immunol 2003 Aug 1;171(3):1581-7.

119. Kennedy AD, Beum PV, Solga MD, DiLillo DJ, Lindorfer MA, Hess CE, Densmore JJ, Williams ME, Taylor RP. Rituximab infusion promotes rapid complement depletion and acute CD20 loss in chronic lymphocytic leukemia. J Immunol 2004 Mar 1;172(5):3280-8.

120. Guo B, Ma ZW, Li H, Xu GL, Zheng P, Zhu B, Wu YZ, Zou Q. Mapping of binding epitopes of a human decay-accelerating factor monoclonal antibody capable of enhancing rituximab-mediated complement-dependent cytotoxicity. Clin Immunol 2008 Aug;128(2):155-63.

121. Clynes RA, Towers TL, Presta LG, Ravetch JV. Inhibitory fc receptors modulate in vivo cytoxicity against tumor targets. Nat Med 2000 Apr;6(4):443-6.

122. Koene HR, Kleijer M, Algra J, Roos D, von dem Borne AE, de Haas M. Fc gammaRIIIa-158V/F polymorphism influences the binding of IgG by natural killer cell fc gammaRIIIa, independently of the fc gammaRIIIa-48L/R/H phenotype. Blood 1997 Aug 1;90(3):1109-14.

123. Cartron G, Dacheux L, Salles G, Solal-Celigny P, Bardos P, Colombat P, Watier H. Therapeutic activity of humanized anti-CD20 monoclonal antibody and polymorphism in IgG fc receptor FcgammaRIIIa gene. Blood 2002 Feb 1;99(3):754-8.

124. Inagaki A, Ishida T, Yano H, Ishii T, Kusumoto S, Ito A, Ri M, Mori F, Ding J, Komatsu H, *et al*. Expression of the ULBP ligands for NKG2D by B-NHL cells plays an important role in determining their susceptibility to rituximab-induced ADCC. Int J Cancer 2009 Jul 1;125(1):212-21.

125. Carbone E, Ruggiero G, Terrazzano G, Palomba C, Manzo C, Fontana S, Spits H, Karre K, Zappacosta S. A new mechanism of NK cell cytotoxicity activation: The CD40-CD40 ligand interaction. J Exp Med 1997 Jun 16;185(12):2053-60.

126. Wilson JL, Charo J, Martin-Fontecha A, Dellabona P, Casorati G, Chambers BJ, Kiessling R, Bejarano MT, Ljunggren HG. NK cell triggering by the human costimulatory molecules CD80 and CD86. J Immunol 1999 Oct 15;163(8):4207-12.

127. Tucker CA, Bebb G, Klasa RJ, Chhanabhai M, Lestou V, Horsman DE, Gascoyne RD, Wiestner A, Masin D, Bally M, *et al*. Four human t(11;14)(q13;q32)-containing cell lines having classic and variant features of mantle cell lymphoma. Leuk Res 2006 Apr;30(4):449-57.

128. Hope MJ, Bally MB, Webb G, Cullis PR. Production of large unilamellar vesicles by a rapid extrusion procedure. Characterization of size distribution, trapped volume and ability to maintain a membrane potential. BBA-Biomembranes 1985;812(1):55-65.

129. Mayer LD, Hope MJ, Cullis PR. Vesicles of variable sizes produced by a rapid extrusion procedure. Biochim Biophys Acta 1986 Jun 13;858(1):161-8.

130. Chiu GN, Bally MB, Mayer LD. Targeting of antibody conjugated, phosphatidylserine-containing liposomes to vascular cell adhesion molecule 1 for controlled thrombogenesis. Biochim Biophys Acta 2003 Jun 27;1613(1-2):115-21.

131. Gomez-Roman VR, Florese RH, Patterson LJ, Peng B, Venzon D, Aldrich K, Robert-Guroff M. A simplified method for the rapid fluorometric assessment of antibody-dependent cell-mediated cytotoxicity. J Immunol Methods 2006 Jan 20;308(1-2):53-67.

132. Estrov Z, Talpaz M, Ku S, Harris D, Van Q, Beran M, Hirsch-Ginsberg C, Huh Y, Yee G, Kurzrock R. Z-138: A new mature B-cell acute lymphoblastic leukemia cell line from a patient with transformed chronic lymphocytic leukemia. Leuk Res 1998 Apr;22(4):341-53.

133. Melo JV, Foroni L, Brito-Babapulle V, Luzzatto L, Catovsky D. The establishment of cell lines from chronic B cell leukaemias: Evidence of leukaemic origin by karyotypic abnormalities and ig gene rearrangement. Clin Exp Immunol 1988 Jul;73(1):23-8.

134. Bowles JA, Weiner GJ. CD16 polymorphisms and NK activation induced by monoclonal antibody-coated target cells. J Immunol Methods 2005 Sep;304(1-2):88-99.

135. Welsh RM, Brubaker JO, Vargas-Cortes M, O'Donnell CL. Natural killer (NK) cell response to virus infections in mice with severe combined immunodeficiency. the stimulation of NK cells and the NK cell-dependent control of virus infections occur independently of T and B cell function. J Exp Med 1991 May 1;173(5):1053-63.

136. Dayde D, Ternant D, Ohresser M, Lerondel S, Pesnel S, Watier H, Le Pape A, Bardos P, Paintaud G, Cartron G. Tumor burden influences exposure and response to rituximab: Pharmacokinetic-pharmacodynamic modeling using a syngeneic bioluminescent murine model expressing human CD20. Blood 2009 Apr 16;113(16):3765-72.

137. Sofou S. Surface-active liposomes for targeted cancer therapy. Nanomedicine 2007 Oct;2(5):711-24.

138. Young LS, Rickinson AB. Epstein-barr virus: 40 years on. Nat Rev Cancer 2004 Oct;4(10):757-68.

139. Howard OM, Gribben JG, Neuberg DS, Grossbard M, Poor C, Janicek MJ, Shipp MA. Rituximab and CHOP induction therapy for newly diagnosed mantle-cell lymphoma: Molecular complete responses are not predictive of progression-free survival. J Clin Oncol 2002 Mar 1;20(5):1288-94.

140. Cheson BD, Leonard JP. Monoclonal antibody therapy for B-cell non-hodgkin's lymphoma. N Engl J Med 2008 Aug 7;359(6):613-26.

141. Allen TM, Brandeis E, Hansen CB, Kao GY, Zalipsky S. A new strategy for attachment of antibodies to sterically stabilized liposomes resulting in efficient targeting to cancer cells. Biochim Biophys Acta 1995 Jul 26;1237(2):99-108.

142. Ishida T, Iden DL, Allen TM. A combinatorial approach to producing sterically stabilized (stealth) immunoliposomal drugs. FEBS Lett 1999 Oct 22;460(1):129-33.

143. Karve S, Alaouie A, Zhou Y, Rotolo J, Sofou S. The use of pH-triggered leaky heterogeneities on rigid lipid bilayers to improve intracellular trafficking and therapeutic potential of targeted liposomal immunochemotherapy. Biomaterials 2009 10;30(30):6055-64.

144. Hansen CB, Kao GY, Moase EH, Zalipsky S, Allen TM. Attachment of antibodies to sterically stabilized liposomes: Evaluation, comparison and optimization of coupling procedures. BBA-Biomembranes 1995;1239(2):133-44.

145. Moreira JN, Ishida T, Gaspar R, Allen TM. Use of the post-insertion technique to insert peptide ligands into pre-formed stealth liposomes with retention of binding activity and cytotoxicity. Pharm Res 2002 Mar;19(3):265-9.

146. Loughrey HC, Choi LS, Wong KF, Cullis PR, Bally MB. Preparation of streptavidin-liposomes for use in ligand-specific targeting applications. In: Gregory Gregoriadis, editor. Liposome technology: Vol. 3: Interactions of liposomes with the biological milieu. 2nd ed. Boca Raton, Fla.: CRC Press; 1993.

147. Wen H, DeCory TR, Borejsza-Wysocki W, Durst RA. Investigation of NeutrAvidin-tagged liposomal nanovesicles as universal detection reagents for bioanalytical assays. Talanta, 2006 Feb 15;68(4):1264-72.

148. Ke S, Wright JC, Kwon GS. Intermolecular interaction of avidin and PEGylated biotin. Bioconjug Chem 2007;18(6):2109-14.

149. Strachan E, Mallia AK, Cox JM, Antharavally B, Desai S, Sykaluk L, O'Sullivan V, Bell PA. Solid-phase biotinylation of antibodies. J Mol Recognit 2004 May-Jun;17(3):268-76.

150. You WW, Haugland RP, Ryan DK, Haugland RP. 3-(4-carboxybenzoyl)quinoline-2-carboxaldehyde, a reagent with broad dynamic range for the assay of proteins and lipoproteins in solution. Anal Biochem 1997 Jan 15;244(2):277-82.

151. Nag A, Mitra G, Ghosh PC. A colorimetric assay for estimation of polyethylene glycol and polyethylene glycolated protein using ammonium ferrothiocyanate. Anal Biochem 1996 Jun 1;237(2):224-31.

152. Lawrence MJ, Barlow DJ, Harvey RD, Heenan RK. Development of non-ionic surfactant vesicles as drug delivery vehicles. In: B. H. Robinson, editor. Self-assembly. Amsterdam: IOS Press; 2003.

153. Moghimi SM, Hunter AC, Murray JC. Long-circulating and target-specific nanoparticles: Theory to practice. Pharmacol Rev 2001 Jun 1;53(2):283-318.

154. Ying X, Wen H, Lu W, Du J, Guo J, Tian W, Men Y, Zhang Y, Li R, Yang T, *et al*. Dual-targeting daunorubicin liposomes improve the therapeutic efficacy of brain glioma in animals. J Control Release 2010 Jan 25;141(2):183-92.

155. Yang T, Choi MK, Cui FD, Kim JS, Chung SJ, Shim CK, Kim DD. Preparation and evaluation of paclitaxel-loaded PEGylated immunoliposome. J Control Release 2007 Jul 31;120(3):169-77.

156. Epstein H, Gutman D, Cohen-Sela E, Haber E, Elmalak O, Koroukhov N, Danenberg HD, Golomb G. Preparation of alendronate liposomes for enhanced stability and bioactivity: In vitro and in vivo characterization. AAPS J 2008 Dec;10(4):505-15.

157. Morton RE, Evans TA. Modification of the bicinchoninic acid protein assay to eliminate lipid interference in determining lipoprotein protein content. Anal Biochem 1992;204(2):332-4.

158. Hale JE, Beidler DE. Purification of humanized murine and murine monoclonal antibodies using immobilized metal-affinity chromatography. Anal Biochem 1994 10;222(1):29-33.

159. Gaberc-Porekar V, Menart V. Perspectives of immobilized-metal affinity chromatography. J Biochem Biophys Methods 2001 Oct 30;49(1-3):335-60.

160. Denkhaus E, Salnikow K. Nickel essentiality, toxicity, and carcinogenicity. Crit Rev Oncol 2002 4;42(1):35-56.

161. Hiller Y, Gershoni JM, Bayer EA, Wilchek M. Biotin binding to avidin. Oligosaccharide side chain not required for ligand association. Biochem J 1987 Nov 15;248(1):167-71.

162. Loughrey H, Bally MB, Cullis PR. A non-covalent method of attaching antibodies to liposomes. Biochim Biophys Acta 1987 Jul 10;901(1):157-60.

163. Loughrey HC, Choi LS, Cullis PR, Bally MB. Optimized procedures for the coupling of proteins to liposomes. J Immunol Methods 1990 Aug 28;132(1):25-35.

164. Jue R, Lambert JM, Pierce LR, Traut RR. Addition of sulfhydryl groups of escherichia coli ribosomes by protein modification with 2-iminothiolane (methyl 4-mercaptobutyrimidate). Biochemistry 1978;17(25):5399-406.

165. Wong SS. Chemistry of protein conjugation and cross-linking. Boca Raton, Fla.: CRC Press; 1991.

166. Wang X, Yang L, Chen Z, Shin DM. Application of nanotechnology in cancer therapy and imaging. CA-Cancer J Clin 2008 Mar 1;58(2):97-110.

167. Sanvicens N, Marco MP. Multifunctional nanoparticles – properties and prospects for their use in human medicine. Trends Biotechnol 2008 8;26(8):425-33.

168. Bezombes C, Grazide S, Garret C, Fabre C, Quillet-Mary A, Muller S, Jaffrezou JP, Laurent G. Rituximab antiproliferative effect in B-lymphoma cells is associated with acid-sphingomyelinase activation in raft microdomains. Blood 2004 Aug 15;104(4):1166-73.

169. Semac I, Palomba C, Kulangara K, Klages N, van Echten-Deckert G, Borisch B, Hoessli DC. Anti-CD20 therapeutic antibody rituximab modifies the functional organization of rafts/microdomains of B lymphoma cells. Cancer Res 2003 Jan 15;63(2):534-40.

170. Cillessen SA, Hess CJ, Hooijberg E, Castricum KC, Kortman P, Denkers F, Vos W, van de Wiel MA, Schuurhuis GJ, Ossenkoppele GJ, *et al*. Inhibition of the intrinsic apoptosis pathway downstream of caspase-9 activation causes chemotherapy resistance in diffuse large B-cell lymphoma. Clin Cancer Res 2007 Dec 1;13(23):7012-21.

171. Peter ME, Krammer PH. The CD95(APO-1/Fas) DISC and beyond. Cell Death Differ 2003 Jan;10(1):26-35.

172. Hehlgans T, Pfeffer K. The intriguing biology of the tumour necrosis factor/tumour necrosis factor receptor superfamily: Players, rules and the games. Immunology 2005 May;115(1):1-20.

173. Carswell EA, Old LJ, Kassel RL, Green S, Fiore N, Williamson B. An endotoxin-induced serum factor that causes necrosis of tumors. P Natl Acad Sci USA 1975 Sep;72(9):3666-70.

174. Guicciardi ME, Gores GJ. Life and death by death receptors. FASEB J 2009 Jun;23(6):1625-37.

175. Schutze S, Tchikov V, Schneider-Brachert W. Regulation of TNFR1 and CD95 signalling by receptor compartmentalization. Nat Rev Mol Cell Biol 2008 Aug;9(8):655-62.

176. Gonzalvez F, Ashkenazi A. New insights into apoptosis signaling by Apo2L/TRAIL. Oncogene 2010 Aug 26;29(34):4752-65.

177. Aggarwal BB. Signalling pathways of the TNF superfamily: A double-edged sword. Nat Rev Immunol 2003 Sep;3(9):745-56.

178. Wajant H. Death receptors. Essays Biochem 2003;39:53-71.

179. Chan KF, Siegel MR, Lenardo JM. Signaling by the TNF receptor superfamily and T cell homeostasis. Immunity 2000 Oct;13(4):419-22.

180. Chan FK, Chun HJ, Zheng L, Siegel RM, Bui KL, Lenardo MJ. A domain in TNF receptors that mediates ligand-independent receptor assembly and signaling. Science 2000 Jun 30;288(5475):2351-4.

181. Beltinger C, Fulda S, Kammertoens T, Meyer E, Uckert W, Debatin KM. Herpes simplex virus thymidine kinase/ganciclovir-induced apoptosis involves ligand-independent death receptor aggregation and activation of caspases. P Natl Acad Sci USA 1999 Jul 20;96(15):8699-704.

182. Ozsoy HZ, Sivasubramanian N, Wieder ED, Pedersen S, Mann DL. Oxidative stress promotes ligand-independent and enhanced ligand-dependent tumor necrosis factor receptor signaling. J Biol Chem 2008 Aug 22;283(34):23419-28.

183. Yi JS, Choo HJ, Cho BR, Kim HM, Kim YN, Ham YM, Ko YG. Ginsenoside Rh2 induces ligand-independent fas activation via lipid raft disruption. Biochem Biophys Res Commun 2009 Jul 24;385(2):154-9.

184. Day TW, Huang S, Safa AR. c-FLIP knockdown induces ligand-independent DR5-, FADD-, caspase-8-, and caspase-9-dependent apoptosis in breast cancer cells. Biochem Pharmacol 2008 Dec 15;76(12):1694-704.

185. Sheikh MS, Antinore MJ, Huang Y, Fornace AJ,Jr. Ultraviolet-irradiation-induced apoptosis is mediated via ligand independent activation of tumor necrosis factor receptor 1. Oncogene 1998 Nov 19;17(20):2555-63.

186. Muppidi JR, Siegel RM. Ligand-independent redistribution of fas (CD95) into lipid rafts mediates clonotypic T cell death. Nat Immunol 2004 Feb;5(2):182-9.

187. Hsiang Y, Lihou MG, Liu LF. Arrest of replication forks by drug-stabilized topoisomerase I-DNA cleavable complexes as a mechanism of cell killing by camptothecin. Cancer Res 1989 Sep 15;49(18):5077-82.

188. Gao X, Picchi A, Zhang C. Upregulation of TNF-alpha and receptors contribute to endothelial dysfunction in zucker diabetic rats. Am J Biomed Sci 2010;2(1):1-12.

189. Cook EB, Stahl JL, Graziano FM, Barney NP. Regulation of the receptor for TNFalpha, TNFR1, in human conjunctival epithelial cells. Invest Ophthalmol Vis Sci 2008 Sep;49(9):3992-8.

190. Cubillas R, Kintner K, Phillips F, Karandikar NJ, Thiele DL, Brown GR. Tumor necrosis factor receptor 1 expression is upregulated in dendritic cells in patients with chronic HCV who respond to therapy. Hepat Res Treat 2010;2010:429243.

191. Rahman MM, McFadden G. Modulation of tumor necrosis factor by microbial pathogens. PLoS Pathog 2006 Feb;2(2):e4.

192. Deb S, Amin S, Imir AG, Yilmaz MB, Suzuki T, Sasano H, Bulun SE. Estrogen regulates expression of tumor necrosis factor receptors in breast adipose fibroblasts. J Clin Endocrinol Metab 2004 Aug;89(8):4018-24.

193. Berger AC, Alexander HR, Wu PC, Tang G, Gnant MF, Mixon A, Turner ES, Libutti SK. Tumour necrosis factor receptor I (p55) is upregulated on endothelial cells by exposure to the tumour-derived cytokine endothelial monocyte- activating polypeptide II (EMAP-II). Cytokine 2000 Jul;12(7):992-1000.

194. de Totero D, Tazzari PL, Capaia M, Montera MP, Clavio M, Balleari E, Foa R, Gobbi M. CD40 triggering enhances fludarabine-induced apoptosis of chronic lymphocytic leukemia B-cells through autocrine release of tumor necrosis factor-alpha and interferon-gama and tumor necrosis factor receptor-I-II upregulation. Haematologica 2003 Feb;88(2):148-58.

195. Grell M, Douni E, Wajant H, Löhden M, Clauss M, Maxeiner B, Georgopoulos S, Lesslauer W, Kollias G, Pfizenmaier K, *et al*. The transmembrane form of tumor necrosis factor is the prime activating ligand of the 80 kDa tumor necrosis factor receptor. Cell 1995;83(5):793-802.

196. Muppidi JR, Tschopp J, Siegel RM. Life and death decisions: Secondary complexes and lipid rafts in TNF receptor family signal transduction. Immunity 2004 Oct;21(4):461-5.

197. Micheau O, Tschopp J. Induction of TNF receptor I-mediated apoptosis via two sequential signaling complexes. Cell 2003 Jul 25;114(2):181-90.

198. Legler DF, Micheau O, Doucey MA, Tschopp J, Bron C. Recruitment of TNF receptor 1 to lipid rafts is essential for TNFalpha-mediated NF-kappaB activation. Immunity 2003 May;18(5):655-64.

199. Singer SJ, Nicolson GL. The fluid mosaic model of the structure of cell membranes. Science 1972 Feb 18;175(23):720-31.

200. Vereb G, Szollosi J, Matko J, Nagy P, Farkas T, Vigh L, Matyus L, Waldmann TA, Damjanovich S. Dynamic, yet structured: The cell membrane three decades after the singer-nicolson model. P Natl Acad Sci USA 2003 Jul 8;100(14):8053-8.

201. Simons K, Ehehalt R. Cholesterol, lipid rafts, and disease. J Clin Invest 2002 Sep;110(5):597-603.

202. Carver LA, Schnitzer JE, Anderson RG, Mohla S. Role of caveolae and lipid rafts in cancer: Workshop summary and future needs. Cancer Res 2003 Oct 15;63(20):6571-4.

203. Li YC, Park MJ, Ye SK, Kim CW, Kim YN. Elevated levels of cholesterol-rich lipid rafts in cancer cells are correlated with apoptosis sensitivity induced by cholesterol-depleting agents. Am J Pathol 2006 Apr;168(4):1107-18.

204. Zhuang L, Lin J, Lu ML, Solomon KR, Freeman MR. Cholesterol-rich lipid rafts mediate akt-regulated survival in prostate cancer cells. Cancer Res 2002 Apr 15;62(8):2227-31.

205. Lajoie P, Partridge EA, Guay G, Goetz JG, Pawling J, Lagana A, Joshi B, Dennis JW, Nabi IR. Plasma membrane domain organization regulates EGFR signaling in tumor cells. J Cell Biol 2007 Oct 22;179(2):341-56.

206. Pike LJ. Rafts defined: A report on the keystone symposium on lipid rafts and cell function. J Lipid Res 2006 Jul;47(7):1597-8.

207. Hancock JF. Lipid rafts: Contentious only from simplistic standpoints. Nat Rev Mol Cell Biol 2006 Jun;7(6):456-62.

208. Simons K, Ikonen E. Functional rafts in cell membranes. Nature 1997 Jun 5;387(6633):569-72.

209. Brown DA, London E. Structure and function of sphingolipid- and cholesterol-rich membrane rafts. J Biol Chem 2000 Jun 9;275(23):17221-4.

210. Edidin M. The state of lipid rafts: From model membranes to cells. Annu Rev Biophys Biomol Struct 2003;32:257-83.

211. Brown DA, London E. Functions of lipid rafts in biological membranes. Annu Rev Cell Dev Biol 1998;14:111-36.

212. Stauffer TP, Meyer T. Compartmentalized IgE receptor-mediated signal transduction in living cells. J Cell Biol 1997 Dec 15;139(6):1447-54.

213. Matko J, Szollosi J. Landing of immune receptors and signal proteins on lipid rafts: A safe way to be spatio-temporally coordinated? Immunol Lett 2002 Jun 3;82(1-2):3-15.

214. Kenworthy AK, Nichols BJ, Remmert CL, Hendrix GM, Kumar M, Zimmerberg J, Lippincott-Schwartz J. Dynamics of putative raft-associated proteins at the cell surface. J Cell Biol 2004 Jun 7;165(5):735-46.

215. Foster LJ, De Hoog CL, Mann M. Unbiased quantitative proteomics of lipid rafts reveals high specificity for signaling factors. P Natl Acad Sci USA 2003 May 13;100(10):5813-8.

216. Magee AI, Parmryd I. Detergent-resistant membranes and the protein composition of lipid rafts. Genome Biol 2003;4(11):234.

217. Rajendran L, Simons K. Lipid rafts and membrane dynamics. J Cell Sci 2005 Mar 15;118(Pt 6):1099-102.

218. Silvius JR. Partitioning of membrane molecules between raft and non-raft domains: Insights from model-membrane studies. Biochim Biophys Acta 2005 Dec 30;1746(3):193-202.

219. Simons K, Vaz WL. Model systems, lipid rafts, and cell membranes. Annu Rev Biophys Biomol Struct 2004;33:269-95.

220. London E. How principles of domain formation in model membranes may explain ambiguities concerning lipid raft formation in cells. Biochim Biophys Acta 2005 Dec 30;1746(3):203-20.

221. Dietrich C, Volovyk ZN, Levi M, Thompson NL, Jacobson K. Partitioning of thy-1, GM1, and cross-linked phospholipid analogs into lipid rafts reconstituted in supported model membrane monolayers. P Natl Acad Sci USA 2001 Sep 11;98(19):10642-7.

222. Kahya N, Brown DA, Schwille P. Raft partitioning and dynamic behavior of human placental alkaline phosphatase in giant unilamellar vesicles. Biochemistry 2005 May 24;44(20):7479-89.

223. Harder T, Engelhardt KR. Membrane domains in lymphocytes - from lipid rafts to protein scaffolds. Traffic 2004 Apr;5(4):265-75.

224. Harder T, Scheiffele P, Verkade P, Simons K. Lipid domain structure of the plasma membrane revealed by patching of membrane components. J Cell Biol 1998 May 18;141(4):929-42.

225. Brown DA, Rose JK. Sorting of GPI-anchored proteins to glycolipid-enriched membrane subdomains during transport to the apical cell surface. Cell 1992 Feb 7;68(3):533-44.

226. Schroeder R, London E, Brown D. Interactions between saturated acyl chains confer detergent resistance on lipids and glycosylphosphatidylinositol (GPI)-anchored proteins: GPI-anchored

proteins in liposomes and cells show similar behavior. P Natl Acad Sci USA 1994 Dec 6;91(25):12130-4.

227. Kurzchalia TV, Hartmann E, Dupree P. Guilty by insolubility--does a protein's detergent insolubility reflect a caveolar location? Trends Cell Biol 1995 May;5(5):187-9.

228. Lichtenberg D, Goni FM, Heerklotz H. Detergent-resistant membranes should not be identified with membrane rafts. Trends Biochem Sci 2005 Aug;30(8):430-6.

229. Brown DA. Lipid rafts, detergent-resistant membranes, and raft targeting signals. Physiology 2006 Dec;21:430-9.

230. Ahmed SN, Brown DA, London E. On the origin of sphingolipid/cholesterol-rich detergent-insoluble cell membranes: Physiological concentrations of cholesterol and sphingolipid induce formation of a detergent-insoluble, liquid-ordered lipid phase in model membranes. Biochemistry 1997 Sep 9;36(36):10944-53.

231. Dietrich C, Bagatolli LA, Volovyk ZN, Thompson NL, Levi M, Jacobson K, Gratton E. Lipid rafts reconstituted in model membranes. Biophys J 2001 3;80(3):1417-28.

232. H. H. Triton promotes domain formation in lipid raft mixtures. Biophys J 2002 11;83(5):2693-701.

233. Schuck S, Honsho M, Ekroos K, Shevchenko A, Simons K. Resistance of cell membranes to different detergents. P Natl Acad Sci USA 2003 May 13;100(10):5795-800.

234. Lingwood D, Simons K. Detergent resistance as a tool in membrane research. Nat Protoc 2007;2(9):2159-65.

235. Field KA, Holowka D, Baird B. Fc epsilon RI-mediated recruitment of p53/56lyn to detergent-resistant membrane domains accompanies cellular signaling. P Natl Acad Sci USA 1995 Sep 26;92(20):9201-5.

236. Gombos I, Bacso Z, Detre C, Nagy H, Goda K, Andrasfalvy M, Szabo G, Matko J. Cholesterol sensitivity of detergent resistance: A rapid flow cytometric test for detecting constitutive or induced raft association of membrane proteins. Cytom Part A 2004 Oct;61(2):117-26.

237. Macdonald JL, Pike LJ. A simplified method for the preparation of detergent-free lipid rafts. J Lipid Res 2005 May 01;46(5):1061-7.

238. Simons K, Ikonen E. How cells handle cholesterol. Science 2000 December 01;290(5497):1721-6.

239. Christian AE, Haynes MP, Phillips MC, Rothblat GH. Use of cyclodextrins for manipulating cellular cholesterol content. J Lipid Res 1997 Nov;38(11):2264-72.

240. Drake DR, Braciale TJ. Cutting edge: Lipid raft integrity affects the efficiency of MHC class I tetramer binding and cell surface TCR arrangement on CD8+ T cells. J Immunol 2001 Jun 15;166(12):7009-13.

241. Pyörälä K, Pedersen TR, Kjekshus J, Faergeman O, Olsson AG, Thorgeirsson G, The Scandinavian Simvastatin Survival Study (4S) Group. Cholesterol lowering with simvastatin improves prognosis of diabetic patients with coronary heart disease: A subgroup analysis of the scandinavian simvastatin survival study (4S). Diabetes Care 1997 April 01;20(4):614-20.

242. Ponce J, de la Ossa NP, Hurtado O, Millan M, Arenillas JF, Dávalos A, Gasull T. Simvastatin reduces the association of NMDA receptors to lipid rafts. Stroke 2008 April 01;39(4):1269-75.

243. Zhuang L, Kim J, Adam RM, Solomon KR, Freeman MR. Cholesterol targeting alters lipid raft composition and cell survival in prostate cancer cells and xenografts. J Clin Invest 2005 Apr;115(4):959-68.

244. Algeciras-Schimnich A, Shen L, Barnhart BC, Murmann AE, Burkhardt JK, Peter ME. Molecular ordering of the initial signaling events of CD95. Mol Cell Biol 2002 Jan;22(1):207-20.

245. Brown BK, Song W. The actin cytoskeleton is required for the trafficking of the B cell antigen receptor to the late endosomes. Traffic 2001 Jun;2(6):414-27.

246. Beum PV, Lindorfer MA, Taylor RP. Within peripheral blood mononuclear cells, antibody-dependent cellular cytotoxicity of rituximab-opsonized daudi cells is promoted by NK cells and inhibited by monocytes due to shaving. J Immunol 2008 Aug 15;181(4):2916-24.

247. Radeva G, Sharom FJ. Isolation and characterization of lipid rafts with different properties from RBL-2H3 (rat basophilic leukaemia) cells. Biochem J 2004 May 15;380(Pt 1):219-30.

248. Mitchell JS, Kanca O, McIntyre BW. Lipid microdomain clustering induces a redistribution of antigen recognition and adhesion molecules on human T lymphocytes. J Immunol 2002 Mar 15;168(6):2737-44.

249. Im JS, Arora P, Bricard G, Molano A, Venkataswamy MM, Baine I, Jerud ES, Goldberg MF, Baena A, Yu KO, *et al*. Kinetics and cellular site of glycolipid loading control the outcome of natural killer T cell activation. Immunity 2009 Jun 19;30(6):888-98.

250. Wolf Z, Orso E, Werner T, Klunemann HH, Schmitz G. Monocyte cholesterol homeostasis correlates with the presence of detergent resistant membrane microdomains. Cytom Part A 2007 Jul;71(7):486-94.

251. Calzolari A, Raggi C, Deaglio S, Sposi NM, Stafsnes M, Fecchi K, Parolini I, Malavasi F, Peschle C, Sargiacomo M, *et al*. TfR2 localizes in lipid raft domains and is released in exosomes to activate signal transduction along the MAPK pathway. J Cell Sci 2006 Nov 1;119(Pt 21):4486-98.

252. Nellis DF, Ekstrom DL, Kirpotin DB, Zhu J, Andersson R, Broadt TL, Ouellette TF, Perkins SC, Roach JM, Drummond DC, *et al*. Preclinical manufacture of an anti-HER2 scFv-PEG-DSPE, liposome-inserting conjugate. 1. Gram-scale production and purification. Biotechnol Prog 2005 Jan-Feb;21(1):205-20.

253. Nellis DF, Giardina SL, Janini GM, Shenoy SR, Marks JD, Tsai R, Drummond DC, Hong K, Park JW, Ouellette TF, *et al*. Preclinical manufacture of anti-HER2 liposome-inserting, scFv-PEG-lipid conjugate. 2. Conjugate micelle identity, purity, stability, and potency analysis. Biotechnol Prog 2005 Jan-Feb;21(1):221-32.

254. Smith LM, Parce JW, Smith BA, McConnell HM. Antibodies bound to lipid haptens in model membranes diffuse as rapidly as the lipids themselves. P Natl Acad Sci USA 1979 Sep;76(9):4177-9.

255. Smith MR. Rituximab (monoclonal anti-CD20 antibody): Mechanisms of action and resistance. Oncogene 2003 Oct 20;22(47):7359-68.

256. Kolch W, Calder M, Gilbert D. When kinases meet mathematics: The systems biology of MAPK signalling. FEBS Lett 2005 Mar 21;579(8):1891-5.

257. Kholodenko BN. Cell-signalling dynamics in time and space. Nat Rev Mol Cell Biol 2006 Mar;7(3):165-76.

258. Kontermann RE, Munkel S, Neumeyer J, Muller D, Branschadel M, Scheurich P, Pfizenmaier K. A humanized tumor necrosis factor receptor 1 (TNFR1)-specific antagonistic antibody for selective inhibition of tumor necrosis factor (TNF) action. J Immunother 2008 Apr;31(3):225-34.

259. McDermott MF, Aksentijevich I, Galon J, McDermott EM, Ogunkolade BW, Centola M, Mansfield E, Gadina M, Karenko L, Pettersson T, *et al*. Germline mutations in the extracellular domains of the 55 kDa TNF receptor, TNFR1, define a family of dominantly inherited autoinflammatory syndromes. Cell 1999 Apr 2;97(1):133-44.

260. Ryan JG, Aksentijevich I. Tumor necrosis factor receptor-associated periodic syndrome: Toward a molecular understanding of the systemic autoinflammatory diseases. Arthritis Rheum 2009 Jan;60(1):8-11.

261. Kimberley FC, Lobito AA, Siegel RM, Screaton GR. Falling into TRAPS--receptor misfolding in the TNF receptor 1-associated periodic fever syndrome. Arthritis Res Ther 2007;9(4):217.

262. Lobito AA, Gabriel TL, Medema JP, Kimberley FC. Disease causing mutations in the TNF and TNFR superfamilies: Focus on molecular mechanisms driving disease. Trends Mol Med 2011 Sep;17(9):494-505.

263. Vogelstein B, Kinzler KW. Cancer genes and the pathways they control. Nat Med 2004 Aug;10(8):789-99.

264. Dechant MJ, Fellenberg J, Scheuerpflug CG, Ewerbeck V, Debatin KM. Mutation analysis of the apoptotic "death-receptors" and the adaptors TRADD and FADD/MORT-1 in osteosarcoma tumor samples and osteosarcoma cell lines. Int J Cancer 2004 May 1;109(5):661-7.

265. Park A, Baichwal VR. Systematic mutational analysis of the death domain of the tumor necrosis factor receptor 1-associated protein TRADD. J Biol Chem 1996 Apr 19;271(16):9858-62.

266. Dechant MJ, Scheuerpflug CG, Pauly E, van der Werff Ten Bosch,J., Debatin KM, Fellenberg J. Screening, identification, and functional analysis of three novel missense mutations in the TRADD gene in children with ALL and ALPS. Pediatr Blood Cancer 2008 Nov;51(5):616-20.

267. Sassano A, Platanias LC. Statins in tumor suppression. Cancer Lett 2008 Feb 18;260(1-2):11-9.

268. Katano H, Pesnicak L, Cohen JI. Simvastatin induces apoptosis of epstein-barr virus (EBV)-transformed lymphoblastoid cell lines and delays development of EBV lymphomas. P Natl Acad Sci USA 2004 Apr 6;101(14):4960-5.

269. Ahn KS, Sethi G, Chaturvedi MM, Aggarwal BB. Simvastatin, 3-hydroxy-3-methylglutaryl coenzyme A reductase inhibitor, suppresses osteoclastogenesis induced by receptor activator of nuclear factor-kappaB ligand through modulation of NF-kappaB pathway. Int J Cancer 2008 Oct 15;123(8):1733-40.

270. Ahn KS, Sethi G, Aggarwal BB. Reversal of chemoresistance and enhancement of apoptosis by statins through down-regulation of the NF-kappaB pathway. Biochem Pharmacol 2008 Feb 15;75(4):907-13.

271. Aberg M, Wickstrom M, Siegbahn A. Simvastatin induces apoptosis in human breast cancer cells in a NFkappaB-dependent manner and abolishes the anti-apoptotic signaling of TF/FVIIa and TF/FVIIa/FXa. Thromb Res 2008;122(2):191-202.

272. Martirosyan A, Clendening J, Goard C, Penn L. Lovastatin induces apoptosis of ovarian cancer cells and synergizes with doxorubicin: Potential therapeutic relevance. BMC Cancer 2010;10(1):103.

273. Glynn SA, O'Sullivan D, Eustace AJ, Clynes M, O'Donovan N. The 3-hydroxy-3-methylglutaryl-coenzyme A reductase inhibitors, simvastatin, lovastatin and mevastatin inhibit proliferation and invasion of melanoma cells. BMC Cancer 2008 Jan 16;8:9.

274. Schmidmaier R, Baumann P, Bumeder I, Meinhardt G, Straka C, Emmerich B. First clinical experience with simvastatin to overcome drug resistance in refractory multiple myeloma. Eur J Haematol 2007 Sep;79(3):240-3.

275. Fortuny J, de Sanjose S, Becker N, Maynadie M, Cocco PL, Staines A, Foretova L, Vornanen M, Brennan P, Nieters A, *et al*. Statin use and risk of lymphoid neoplasms: Results from the european case-control study EPILYMPH. Cancer Epidemiol Biomarkers Prev 2006 May;15(5):921-5.

276. Winiarska M, Bil J, Wilczek E, Wilczynski GM, Lekka M, Engelberts PJ, Mackus WJ, Gorska E, Bojarski L, Stoklosa T, *et al*. Statins impair antitumor effects of rituximab by inducing conformational changes of CD20. PLoS Med 2008 Mar 25;5(3):e64.

277. Nowakowski GS, Maurer MJ, Habermann TM, Ansell SM, Macon WR, Ristow KM, Allmer C, Slager SL, Witzig TE, Cerhan JR. Statin use and prognosis in patients with diffuse large B-cell lymphoma and follicular lymphoma in the rituximab era. J Clin Oncol 2010 Jan 20;28(3):412-7.